ALMA MATER STUDIORUM - UNIVERSITÀ DI BOLOGNA

FACOLTA' DI INGEGNERIA

CORSO DI LAUREA IN INGEGNERIA MECCANICA

DIPARTIMENTO

DIEM-MACCHINE

TESI DI LAUREA

In

Protocolli di gestione dei motori a combustione interna LS

DESIGN OF ALTERNATIVE ENERGY STORAGE SYSTEMS FOR HYBRID VEHICLES BASED ON STATISTICAL PROCESSING OF DRIVING CYCLES INFORMATION

CANDIDATO:

Bolletta Alberto

RELATORE:

Chiar.mo Prof. Cavina Nicolò

CORRELATORI:
Chiar.mo Prof. Rizzoni Giorgio
Chiar.mo Prof. Canova Marcello
Ill.mo Dott. Ing. Chiara Fabio

Anno Accademico 2009/2010

Sessione III

Acknowledgments

This thesis was elaborated and developed while I was visiting scholar at the Center of Automotive Research (CAR) of The Ohio State University. I wish to thank the director of this center of research, Prof. Giorgio Rizzoni. He gave me the great opportunity to spend almost eight months in this center where he formed a fantastic team that he leads with his wide knowledge and managerial capability.

I want to thank my two advisors at CAR, Dott. Fabio Chiara and Prof. Marcello Canova. They gave me a fundamental help during the entire working experience. For me it has been a pleasure working with them.
I want to thank my advisor in Bologna, Prof. Cavina, who taught the two most interesting classes during my academic career, and who gave me the opportunity to work on my thesis at CAR.

A special thank to my friends met during this wonderful experience. They made me enjoy every day of stay and they became a kind of family. I met wonderful funny people and each one brought something extraordinary into this experience. I hope I will have the chance to meet them again. I hope that both the distance and time will not ruin our friendships.

Another special thank to friends that have characterized my life in Bologna until now. Each of them has participated to an episode of my life, adding brilliant memories to my existence. They are a large and important part of life.

The most important thank to my family. Their never ending love, support and encouragement have been essential during my life and academic career.

Summary

Acknowledgments 2

Abstract 8

1. Introduction 10

1.1 Hybrid Electric Vehicles 11

a) Series Hybrid Electric Vehicle 12

b) Parallel Hybrid Electric Vehicle 13

c) Power-split Hybrid Electric Vehicle 13

1.2 Non-electric Hybrid Vehicles 14

1.2.1 Energy Storage Systems for HV 14

1.2.2 Short-term Energy Storage System 15

2. Literature Review 18

2.1 Energy Storage System Design Methodologies 18

2.2 Driving Cycles Analysis Methodologies 23

2.2.1 Principle of Machine Components Design 31

2.3 Overview of Modeling Approach for ESS 33

2.3.2. Operation of Short-term ESS 37

2.3.3. Hydraulic ESS Literature Review 39

2.4 Introduction to the Work 41

3. Driving Cycle Analysis Methodology 43

3.1 Development of a Driving Cycles Analysis Tool 45

3.1.1. Driving Cycles 45

a) Regulatory Cycles 45

b) Real-world Driving Cycles 46

3.1.2. Driving Cycles Analysis 48

3.1.2.1. Vehicle Longitudinal Dynamic 49

3.1.2.2. Creation of Event ID 54
3.1.2.3. Events Clustering Process 56
3.1.2.4. Braking Events Analysis 57
3.1.2.5. Traction Events Analysis 60
3.1.2.6. Coasting Phase 62
3.1.2.7. Synthetic Cycle Statistically Relevant Events 64
3.2 Vehicle Mass Sensitivity Study 67
3.2.1. Vehicle Mass Sensitivity Study on US06 Driving Cycle 67
3.2.1.1 First Case Analysis 69
3.2.1.2 Second Case Analysis 86
3.2.1.3 Analysis of “Real-world” Driving Cycles 100
3.3 Representative Cycles Analysis 112
3.3.1. User I 112
3.3.2. User II 113
3.3.3. User III 114
4. Design Procedure for Alternative Energy Storage Systems 117
4.1 Definition of Design Inputs for the AESS 118
4.2 Definition of the Design Targets of the AESS 119
4.2.1. From Design Inputs to Design Targets 119
4.3 Definition of Design Constraints for the AES Systems 120
4.4 Determination of the Relationships between Design Targets and Design Parameters of the AESS 121
4.5 Definition of the attributes of the selected design solution 123
a) Pump Mass and Volume 124
b) Accumulator Mass and Volume 124
c) Fluid and Reservoir Mass and Volume 126
4.6 Design evaluation 126

5. Results 128
5.1 Definition of Real-world Driving Cycle for System Sizing 128
5.1 Application of the Design Procedure 129
5.2.1. Hydraulic Energy Storage System Design 135
5.3 Definition of Real-world Driving Cycles for Design Validation 138
5.3.1. Cycle-A 138
5.3.2. Cycle-B 142
5.4 Definition of Simulation Methodology 145
5.4.1. Methodology to Determine Testing Events 145
5.4.2. Methodology to Simulate the Short-Term ESS Use 148
5.4.3. Simulation Model 150
5.4.4. Definition of AESS Efficiency 151
5.5 Evaluation of Energy Storage System Performances by Simulation 152
5.5.1. Sizing Results 152
5.5.2. Simulation Results 155
5.5.3. Comparison of Designs Efficiency over the Tested Cycles 181
6. Conclusions 185
Bibliography 188

Abstract

Hybrid vehicles represent the future for automakers, since they allow to improve the fuel economy and to reduce the pollutant emissions. A key component of the hybrid powertrain is the Energy Storage System, that determines the ability of the vehicle to store and reuse energy. Though electrified Energy Storage Systems (ESS), based on batteries and ultracapacitors, are a proven technology, Alternative Energy Storage Systems (AESS), based on mechanical, hydraulic and pneumatic devices, are gaining interest because they give the possibility of realizing low-cost mild-hybrid vehicles. Currently, most literature of design methodologies focuses on electric ESS, which are not suitable for AESS design. In this contest, The Ohio State University has developed an Alternative Energy Storage System design methodology.

This work focuses on the development of driving cycle analysis methodology that is a key component of Alternative Energy Storage System design procedure. The proposed methodology is based on a statistical approach to analyzing driving schedules that represent the vehicle typical use. Driving data are broken up into power events sequence, namely traction and braking events, and for each of them, energy-related and dynamic metrics are calculated. By means of a clustering process and statistical synthesis methods, statistically-relevant metrics are determined. These metrics define cycle representative braking events. By using these events as inputs for the Alternative Energy Storage System design methodology, different system designs are obtained. Each of them is characterized by attributes, namely system volume and weight. In the last part the work, the designs are evaluated in simulation by introducing and calculating a metric related to the energy conversion efficiency. Finally, the designs are compared accounting for attributes and efficiency values. In order to automate the driving data extraction and synthesis process, a specific script Matlab based has been developed.

Results show that the driving cycle analysis methodology, based on the statistical approach, allows to extract and synthesize cycle representative data. The designs based on cycle statistically-relevant metrics are properly sized and have satisfying efficiency values with respect to the expectations. An exception is the design based on the cycle worst-case scenario, corresponding to same approach adopted by the conventional electric ESS design methodologies. In this case, a heavy system with poor efficiency is produced. The proposed new methodology seems to be a valid and consistent support for Alternative Energy Storage System design.

1. Introduction

The development of vehicles that have greater fuel efficiency and produce lower emissions has become a priority for the automotive industry due to government demands as well as the recent energy crisis. In principle, Battery Electric Vehicles (BEVs) are considered by many as the solution of choice for personal mobility with reduced environmental impact. However, despite of the continuous technological research, the energy storage density of electric batteries remains very low, compared with that of hydrocarbon fuels [1].

For this reason, the use of BEVs is today limited to applications characterized by short driving distance and allowing for long recharging times, such as delivery trucks.

In the last decades, the automakers have introduced to the market several hybrid electric vehicles, which have the potential of utilizing two distinct energy sources to provide motion to the vehicle. A hybrid vehicle is based on a complex drivetrain that accommodates a primary energy converter (generally, an internal combustion engine) and a secondary energy converter and storage system, such as a combination of electric motors and batteries. These additional components enable different engineering solutions that contribute in decreasing considerably the vehicle energy consumption and, consequently, CO_2 emissions.

In general, two main categories of hybrid vehicles can be identified, depending on the components installed:

- *Hybrid Electric Vehicle(HEV)*: also defined as long-term energy storage systems vehicles. These are characterized by two or more prime movers and power sources. The vehicles design combines a primary energy converter, as an internal combustion engine or a fuel cell, and an electrified secondary energy converter, such as an electric motor. Plug-in hybrid electric vehicles (PHEVs) are part of this group and are basically HEV with the ability to recharge the energy storage system by connecting the vehicle to the electric grid.
- *Non-Electric Hybrid Vehicle*: also defined as short-term energy storage systems vehicles. These vehicles mainly differ from the HEV because of the presence of non-electrified secondary energy converter, such as mechanical, hydraulic and pneumatic energy storage systems.

1.1 Hybrid Electric Vehicles

In general, hybrid electric vehicles include a primary energy converter and an electrified secondary energy converter [1] . The primary energy converter can be an internal combustion engine or, in innovative power train designs, a fuel cell. The secondary energy converter is an electric motor. Different types of motors are used depending on the powertrain design (standard DC, induction AC, brushless DC, etc.). In some configurations, two electric machines are included in the powertrain, one of them acts primarily as a generator. A fundamental component of hybrid electric vehicles is the energy storage system. In the most common vehicles configurations, electrochemical batteries are used. Batteries are devices that convert chemical energy into electric energy and vice versa. Due to their relatively high energy density and low power density [1], electrochemical batteries are suitable for long-term energy storage.

Depending on their specific powertrain configuration, HEVs give the possibility to combine the advantages of the purely electric vehicles, in particular zero local emissions, with the advantages of ICE-based vehicles, namely performance and range. Respect to conventional vehicles based on internal combustion engines, HEVs can profit from various opportunities to improve the fuel economy [2].

In principle, it is possible to:

- recover energy during deceleration instead of dissipating it in friction braking;
- downsize the engine;
- regulate and optimize the energy distribution between the prime movers through advanced control strategies;
- eliminate the idle fuel consumption by turning off the engine if the conditions allow for.

Depending on the configuration of the powertrain components, it is possible to identify three categories of HEVs:

a. *Series hybrid*: the electric motor alone drives the vehicle and the electricity can be provided either by the engine or by the batteries or by an engine-driven generator;
b. *Parallel hybrid*: both prime movers operate on the same drive shaft. They can drive the vehicle individually or simultaneously;

c. *Power-split hybrid:* it is an intermediate solution between series and parallel configurations.

A brief description of these configurations is proposed as follows.

a) Series Hybrid Electric Vehicle

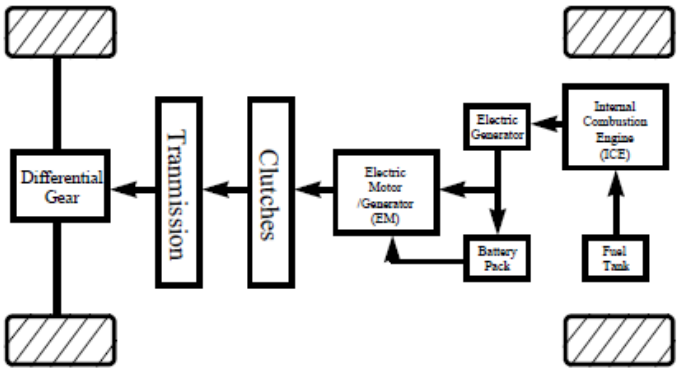

Fig 1.1: Series hybrid configuration [3]

Series hybrid propulsion systems utilize the internal combustion engine as an auxiliary power unit to extend the driving range of a purely electric vehicle [1]. The engine is not directly coupled to the wheels. Its torque output is converted into electricity through a generator that can either directly supply the motor or charge the battery.

One of the main advantages of this configuration is the possibility to size the engine to operate at a point with optimal efficiency, since it is not related to the required driving load. However, a series hybrid configuration needs three machines, namely the engine, the electric generator and the electric traction motor. The presence of three interconnected energy converters limits the overall powertrain efficiency. Furthermore, since the traction motor has to be sized based on the maximum power requirements, the vehicle weight may increase considerably. For the above reasons, series HEVs are today limited to few platforms (SUVs, trucks) and heavy-duty vehicles.

b) Parallel Hybrid Electric Vehicle

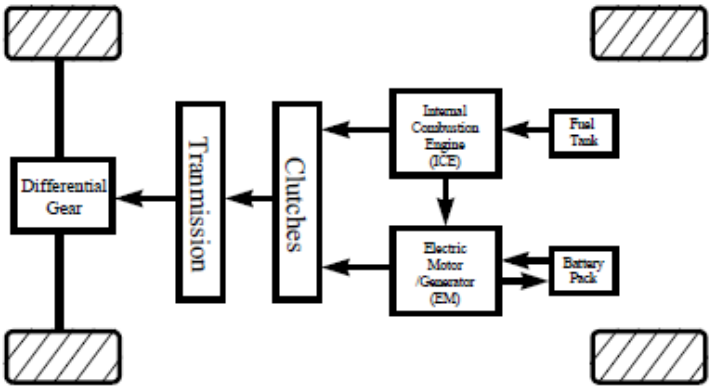

Fig 1.2: Parallel hybrid configuration [3]

In parallel hybrid electric vehicles both the engine and electric motor can supply the traction power, either individually or in combination, creating an additional degree of freedom in fulfilling the power requirements of the vehicle. For this reason, the supervisory powertrain control strategy is very important to optimize the power distribution between the energy conversion systems. With parallel HEV configurations, the engine can be turned off at idle and the electric motor can be used to assist accelerations and, in general, high power demand conditions. Both machines can therefore be sized for a fraction of the maximum power.

One of the main disadvantages is the design complexity that is caused by the fact that both the machines are mechanically linked to the drive train, requiring clutches and transmission components to best optimize energy efficiency.

c) Power-split Hybrid Electric Vehicle

This configuration can be considered a combination of a parallel hybrid and a series hybrid configuration. Both mechanical and electric links are present with two distinct electric machines: one is used as a prime mover while other machine works like a generator and it is used to charge the battery via the engine.

1.2 Non-electric Hybrid Vehicles

Non-electric hybrid vehicles have a non-electrified secondary energy converter. The majority of such systems are based on mechanical energy storage devices (flywheels) or hydraulic accumulators, which are characterized by low energy and high power density. For this reason, they are also defined as short-term energy storage systems.
Non-electrified HV can accomplish several functions, such as:

- recovering and storing part of the energy made available by the vehicle's braking phase and releasing it during the following traction phase. This energy recovery strategy is named regenerative braking;
- allowing for engine torque assist, start/stop strategies and vehicle launch operations.

1.2.1 Energy Storage Systems for HV

Several design solutions have been proposed for energy storage on hybrid vehicles. In general, ESS are characterized by two main parameters, namely specific power and specific energy. The first is directly related to the capability of the system to recuperate high quantities of energy in a limited amount of time, while the second parameter is a measure of the total amount of energy that can be stored in the device. A comparison of the most common energy storage devices are reported in the Ragone plot in Fig 1.3.

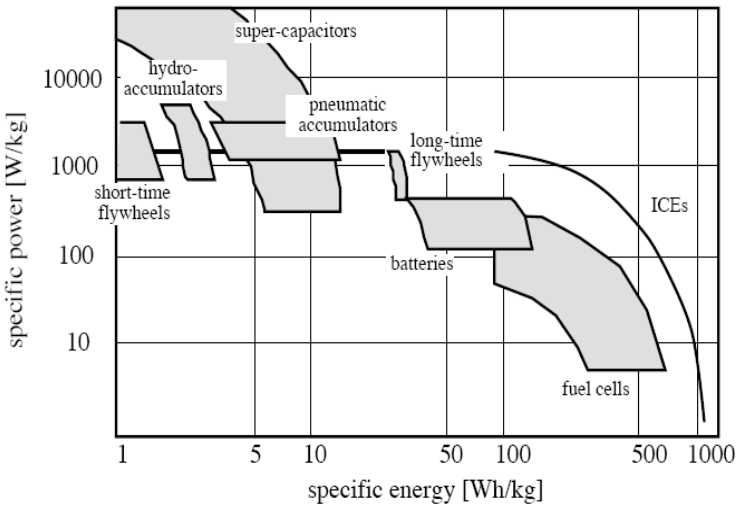

Fig 1.3: Ragone plot with energy storage devices comparison [1]

In Fig 1.3, the most common energy storage devices are shown. It is possible to group them in two distinct categories depending on the function in the power train configuration. The long-term energy storage devices are characterized by high specific energy values and moderate specific power values. In fact their primary function is to provide energy to the system during long time periods. Due to the component characteristics also the energy storing phase occurs on extended period. The short-term energy storage devices are characterized by high specific power values instead. The target storing and release phase duration is therefore much shorter than for the previous devices, making them effective for regenerative braking strategies.

1.2.2 Short-term Energy Storage System

Fig 1.3 presents a comparison of ESS depending on the specific power and specific energy characteristics. Long-term energy storage system components have high specific energy and moderate specific power, and the electrochemical battery is the most common representative unit of this category. Long-term ESS are key components in hybrid electric vehicles. On the other hand, short-term energy storage systems components have high specific power and moderate specific energy. Hydraulic systems, mechanical systems and pneumatic systems belong to this category. Short-term ESS are gaining substantial interest during the last years from the automotive companies, due to the opportunity for low-cost hybridization. Though electric hybrids are a proven technology, with several models in production and advanced development phase, prototypes have been designed and tested by well-know companies adopting flywheel based ESS [5] . Similarly hydraulic energy storage systems have been tested as part of an hydraulic powertrain that substitutes the classical mechanical power train [6] These vehicles show that it is possible to have several advantages realizing low-cost mild-hybrid vehicles. In fact, short-term ESS allows the vehicle recovery braking energy through regenerative braking. In order to maximize energy recovery, high power density is required. The energy recovery allows to considerably improving the fuel consumption, particularly in urban driving. Another advantage of these systems it is the potential low-costs and the opportunity of moderate weight addition, especially for ESS.

a) Mechanical Energy Storage Systems

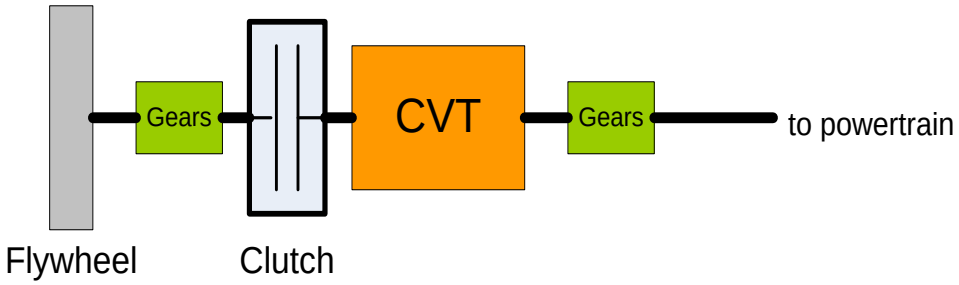

Fig 1.4: Conceptual scheme of a mechanical ESS

A typical configuration of a mechanical energy storage system is composed by a flywheel, CVT (continuously variable transmission) and clutch. Fig 1.4 shows a simplified scheme of a mechanical energy storage system. A continuously variable transmission (CVT) system with a wide range is necessary between the flywheel shaft and the drive train [4].

In mechanical energy storage systems the main storing component is the flywheel which accumulates energy in kinetic form. The flywheel is generally placed inside a vacuum containment system to reduce the windage losses due to the air viscosity, and it is supported by low-friction bearings. We can distinguish mainly the typologies of applications: low speed flywheels (up to 20,000 r/min) or high speed (up to 70,000 r/min) . The kinetic energy E stored in the flywheel depends on the inertia I and on the angular velocity w by means of the formula:

$$E = \frac{1}{2} * I * w^2 \tag{1.1}$$

For mobile applications, it would be better to reduce as much as possible the volume and mass of the components, hence using high rotating speeds. However, flywheels are limited to a maximum speed due to limits of material strength. In detail the radial tensile strength on the flywheel structure is mainly due to the centrifugal force due to the rotation of the flywheel around its axis [7]:

$$\sigma_r = \iiint \rho(\vec{r}) * |\vec{r}| * \omega^2 * d^3 * \vec{r} \tag{1.2}$$

where $\vec{r}$ is the radius vector of the generic infinitesimal portion of the body with respect to the axis of rotation, $\rho(\vec{r})$ is the mass density at the same point and ω is the flywheel velocity. The maximum radial tensile strength of the flywheel depends upon the geometry of the flywheel and the physical structure of the material.

b) Hydraulic Energy Storage Systems

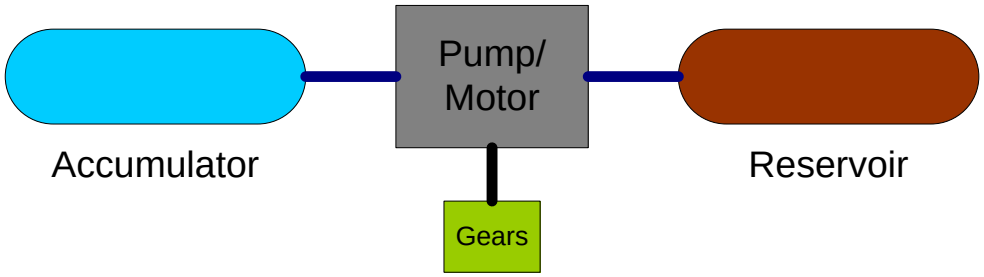

Fig 1.5: Conceptual scheme of an hydraulic ESS

All types of hybrid-hydraulic propulsion systems include a high-pressure accumulator and a low-pressure reservoir. The accumulator contains the hydraulic fluid and a gas such as nitrogen (N_2) or methane (CH_4), separated by a membrane. When the hydraulic fluid flows in, the gas is compressed. During the discharge phase, the fluid flows out through the motor and then into the reservoir. The hydraulic motor converts pressure energy of a fluid into mechanical energy available at the motor shaft. Conversely, the machine can operate as a pump, converting mechanical energy back into hydraulic energy. The accumulator potential energy can be expressed by the formula [4] :

$$E_{accumulator} = P_0 \int_{V_{min}}^{V_{max}} \left(1 - \frac{V}{V_{acc}}\right)^{-\gamma} dV \tag{1.3}$$

Where $E_{accumulator}$ is the accumulator potential energy, P_o is the accumulator pre-charge pressure, V_{min}, V_{max} and V_{acc} are the initial volume, the final volume and the total volume of the accumulator, V is the fluid volume in the accumulator and γ is the specific heat ratio of the pre-charge gas. Where $P_{acc,max}$ is the maximum accumulator pressure

2. Literature Review

The previous chapter introduced the most important concepts on hybrid vehicles and energy storage systems. In particular, short-term energy storage systems have been introduced, pointing out their suitability for regenerative braking application, vehicle launch and torque assist. In this chapter, a literature review concerning energy storage system design procedures for ESS, driving cycle analysis methodologies and ESS modeling approaches is presented. This review is aimed at giving a general picture about the state of the art regarding the above topics. In particular it gives a prospective of the contest in which this work brings his contribution.

2.1 Energy Storage System Design Methodologies

The design of energy storage systems for hybrid vehicles is a topic on which engineers have been focusing for several years, since the idea to recover energy form regenerative braking and utilize it to reduce fuel consumption is a key to a more sustainable transportation. In the first treated paper [8] both mechanical and hydraulic energy storage systems were analyzed to obtain minimum sizing of the components.

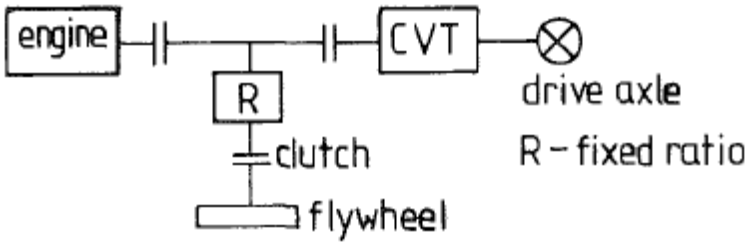

Fig 2.6: Example of internal combustion engine—flywheel hybrid vehicle powertrain

In Fig 2.6 a flywheel concepts is illustrated. In this configuration the CVT between the flywheel and drive axle allows the flywheel and vehicle speed to be matched under all driving condition. When the engine is operated along the specified power line, its speed and power are directly governed by the flywheel speed except when the flywheel clutch is disengaged.

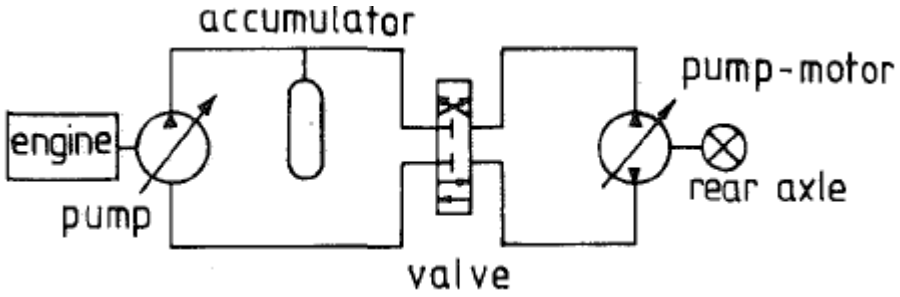

Fig 2.7:Example of Internal combustion engine—accumulator hybrid vehicle powertrain

In Fig 2.7 a hydraulic concept is illustrated. It uses two variable displacement hydrostatic units. The unit attached to the engine operates only as a pump, but the other unit will alternate between being a pump and a motor, depending upon whether the vehicle is being driven with positive torque or being retarded by regenerative braking. The hydraulic energy from the engine-driven pump is either put into storage in the hydraulic accumulator, or is used to drive the car directly through the final drive pump/motor unit. During regenerative braking, the energy developed by the pump/motor unit is stored in the accumulator.

The studies are based on a 1360 kg vehicle and the implementation of these systems allows the engine to operate close to condition of maximum efficiency or to be turned off during some intervals of the duty cycle. This sizing methodology is based on simulations using different energy storage systems capacities on three driving cycles: Federal Urban Driving cycle, New York City cycle and EPA Highway cycle. Moreover an effect of hill terrains have been proposed introducing constant slopes of -4, -2, +2, +4 percent. From the definition of engine and storage systems control strategies, the performances of the components are evaluated. Also engine on-off cycling have been considered, since it can affect temperature variations in many components. Analyzing Table 2.1 it is possible to notice that as the energy accumulator component increase the size, the frequency of engine on-off decreases and the intervals become longer because a bigger amount of energy is stored.

In this study there is no reference to fuel economy and the only point of reference to evaluate the performances of the systems is the “Friction brake loss” that is related to energy lost and it indicates the amount of energy that could be saved with a larger energy accumulator. The design methodology is simply based on several accumulators dimensions comparison, but there is no consideration about costs and weights of the installed components.

Table 2.1: Accumulator and flywheel car operating characteristics

	Grade	ESU capac. (MJ)	No. of engine cycles	Max. eng. on (sec)	Min. eng. on (sec)	Max. eng. off (sec)	Min. eng. off (sec)	Frict. brake loss (MJ)	Approx. cycle energy (MJ)
A. Federal Urban Driving Cycles (1372 sec, 92 km/h max. speed, 31.5 km/h ave. speed)									
ACCUMULATOR	0	.45	6	132	66	236	106	0.00	4.22
		.30	10	107	33	168	51	0.00	
		.15	22	109	9	75	8	0.13	
		.10	26	109	5	74	7	0.48	
	-2%	.45	3	65	44	539	155	0.089	0.74
		.30	4	52	12	516	23	0.082	
		.15	6	59	9	309	23	0.379	
		.10	13	58	7	267	13	0.959	
	-4%	.45	1	53	53	1319*	1319*	2.32	-2.38
		.30	1	38	38	1334*	1334*	2.35	
		.15	2	22	13	1161*	176	2.51	
		.10	5	15	6	904*	37	2.78	
	+2%	.45	7	224	72	105	43	0.00	7.90
		.30	9	227	34	92	31	0.00	
		.15	18	138	17	58	12	0.00	
		.10	24	118	8	52	5	0.12	
	+4%	.45	3	635	102*	106	78	0.00	11.7
		.30	8	369	42	55	15	0.00	
		.15	16	251	22	46	10	0.00	
		.10	19	181	12	51	11	0.016	
FLYWHEEL	0	.30	14	70	7	145	7	0.00	4.22
		.15	28	37	5	83	5	0.10	
	-2%	.30	5	19	12	555*	9	0.09	0.74
		.15	7	19	6	585*	10	0.38	
	-4%	.30	1	16	16	1356*	1356*	2.38	-2.38
		.15	2	10	10	1164*	188	2.52	
	+2%	.30	16	116	14	118	29	0.00	7.90
		.15	32	99	5	53	5	0.007	
	+4%	.30	16	124	15	78	21	0.00	11.7
		.15	27	118	7	53	6	0.00	
B. EPA Highway Cycle (764 sec, 96.4 km/h max. speed, 77.6 km/h ave. speed)									
ACCUMULATOR	0	.30	3	335	93	24*	8	0.00	7.88
		.15	5	336	35	24*	6	0.13	
	-2%	.15	15	63	7	55	7	0.31	2.70
	-4%	.15	2	25	18	416*	395	2.00	-1.83
	+2%	.15	2	446	288	18*	12	0.06	13.2
	+4%	.15	1	747	747	17*	17*	0.003	18.5
FLYWHEEL	0	.30	8	297	18	42*	8	0.00	7.88
		.15	14	255	5	42*	6	0.07	
C. New York City Cycle (598 sec, 44.6 km/h max. speed, 11.4 km/h ave. speed)									
ACCUMULATOR	0	.30	3	41	36	294	170	0.00	0.62
		.15	5	23	15	177	36	0.00	
FLYWHEEL	0	.30	3	17	12	322	196	0.00	0.62
		.15	6	9	5	215	36	0.00	

* at end of cycle.

The definition of a methodology to determine the requirements for hybrid vehicles does not involve just mechanical and hydraulic storage systems. In fact plug in hybrid vehicles (PHEV) and fuel cell hybrid vehicles have been subject of a large number of studies and researches. About energy storage systems for fuel cell vehicles the following paper treats [10]. In this study an hybrid mid-size SUV and an hybrid mid-size car were considered, both with primary power source and secondary power source: respectively a fuel cell power unit and an electrochemical energy storage unit. In this case the battery pack sizing is based on several power and energy requirements. These requirements are determined on the vehicles use on representative driving cycles: the regulatory cycles US06, 2UDDS and HWFET. In this analysis the fuel cell unit power

is determined. Starting from that, the secondary storage system has to be properly sized to provide the necessary power and energy for the following predetermined events: startup, power driving cycle, regenerative braking phases, acceleration phases, driving on hilling path phase (gradeability performance) and electrical components loads.

For each event above, the power and energy requirements have been evaluated for all the aforementioned driving cycles. Within the determined power and energy requirements, it is possible to identify the limit requirements that are related to the most energy and power requiring cases. In Table 2.2, for each aforementioned event, energy and power values related to limit requirements are reported considering the mid-size SUV hybrid vehicle.

Table 2.2: Summary of Energy Storage Requirements for SUV With a 100 kW Fuel Cell System

	Event Description	Peak Power (kW)	Duration (s)	Cumulative Energy (kWh)	Comments
A	Startup Traction Loads	46.4	<11	0.15	50% rated power,120s warm-up over 2UDDS, HWFET, & US06
B	Power-assist (response)	70.0	<3	0.08	2 second 10%-90% FC response (ramp) rate (during 2UDDS, HWFET, & US06)
C	Power-assist (downsize)	43.3	<3	0.05	During 2UDDS, HWFET, & US06. US06 is limiting case
D	Gradeability (see Table 2)	0.0	1200	0.00	81.4 kW sustained load for 1200s
E	Acceleration	40.0	20	0.22	140 kW sustained load for 20s
F	Accessory Loads	1.5	600-2800	0.10	US06 peak power, energy is for US06 4 min, or FTP 8 min
G	Fuel Cell Shutdown	N/A	N/A	N/A	-
H	Regenerative Braking	70.0	<30	1.50	Pmax is during US06, energy is FTP cycle max

In order to size the total energy storage system to meet the energy requirements, this method considers the greatest of four cases: (1) If any energy storage power is required to sustain the grade test at the specified fuel cell size, the energy required to sustain this power plus a 750W accessory power for 20 minutes; (2) The energy required to sustain the energy storage power requirement over six consecutive acceleration tests; (3) The energy required to sustain the Highway or FTP accessory load for eight minutes, or the US06 accessory load for 4 minutes; or (4) The summation of the energies in A, B, and C.

In the following paper [9] a study to optimize the main components of an hybrid electric vehicle is proposed. In particular the extent is the sizing of an internal combustion engine, electric motor and energy storage system based on the demand of different driving cycles. Using this methodology the authors want to determine the peak power capacity of both engine and motor, and the energy capacity of the battery pack for each considered driving cycles.

In order to achieve these targets the total power P demanded by the vehicle is calculated through the following equation:

$$P = \frac{V * (f * M * g + \frac{1}{2} * C_d * A_f * \rho * V^2 + M\delta \frac{dV}{dt})}{\eta_t} + P_{aux} \quad (2.1)$$

where, P is the vehicle power demand in Watts, V is the velocity of the vehicle in m / s , f is the coefficient of rolling resistance, M is the vehicle weight in kg, g is the acceleration of gravity in $m / (s^2)$, ρ is the air density in $kg / (m^3)$, C_d is the coefficient of air drag, A_f is the frontal area of the vehicle in m^2, δ is the mass factor which includes the effect of rotational inertia, η_t is the transmission efficiency and P_{aux} is the power required to drive the ancillary loads in watts.

The basic sizing concept is that the steady portion of the driving power is provided by the engine, while the transient portion by the motor. Therefore the expression (2.1) can be divided in two terms

$$P_{engine} = \frac{V * (f * M * g + \frac{1}{2} * C_d * A_f * \rho * V^2)}{\eta_t} + P_{aux} \quad (2.2)$$

and

$$P_{motor} = \frac{M * \delta * \frac{dV}{dt} * V}{\eta_t} \quad (2.3)$$

Where P_{engine} is the power provided by the engine and P_{motor} is the power provided by the motor. From the equations (2.2) and (2.3) the maximum power requirements are determined by the peak velocity v_{max} and the motor power rating by the maximum of $\frac{dV}{dt} * V$ of the specific driving cycle.

To properly size the energy storage unit, in this case the battery pack, the capability to deliver the motor peak power is required. Since during positive motor power demand the power is delivered by the battery, it is possible to express the battery power in watts P_b by means of the following equation

$$P_b = \frac{P_{motor}}{\eta_{batt} * \eta_{motor}} \quad (2.4)$$

where η_{batt} is battery discharging efficiency and η_{motor} is motor efficiency.
Using the sizing criteria above, in Table 2.3 are reported the powers values of the system components for some exemplary driving cycles.

Table 2.3 Determination of ICE, EM and battery power for different driving cycles

Drive Cycles	v_{max} km/h	K_{max} m^2/s^3	P_{ICE} kW	P_{motor} kW	P_b kW
EPA 75	91.2	20	17.53	38.25	50
AU	107.5	33.5	22.8	64	82
ECE 15	120	9.5	27.8	18	23.5
M10-15	70	10.7	12.55	20.5	26.8
BJ-11	40	4	8	7.65	10

2.2 Driving Cycles Analysis Methodologies

In the previous paragraph, different design methodologies have been presented for the energy storage system of H.V., showing that each methodology determines the energy and power requirements for the vehicle components starting from the analysis of driving cycles data. Each methodology uses a different process and different starting inputs to size the components. These inputs derive from an analysis process that extracts and synthesizes specific information from the driving cycles. Each sizing methodology adopts a unique process to analyze driving patterns and to obtain the required inputs for the subsequent hybrid vehicle components sizing process.
The driving cycle analysis can be processed mainly in two steps, depending on the information to extract. The preliminary analysis of driving cycles permits to extract kinematic and statistic driving data considering just the cycle velocity profile versus time, allowing one to obtain information concerning time, distances, number of stops, velocity and acceleration. A more thorough analysis is based on the longitudinal vehicle dynamic equation introduced referring to a set of vehicle parameters. The information that can be extracted regards the energy and power data related to the driving cycle and to the vehicle parameters.

In [10], the main goal is to determine the desirable characteristics of an energy storage system for two vehicles, mid-size SUV and midcar, using three typical driving cycles: 2UDDS, HWFET and US06. In this case the driving patterns have been analyzed to extract the cumulative traction energy and the cumulative available braking energy. For each vehicle and for a specific cycle, the total energy required to move the vehicle and the total energy required to brake. The latter is the energy that can be theoretically recovered through an energy storage system. These aforementioned data are reported in Fig2.8 and Fig 2.9. It is worth noting how the amount of the available braking energy depends on each specific driving cycle, increasing the complexity of energy storage system design.

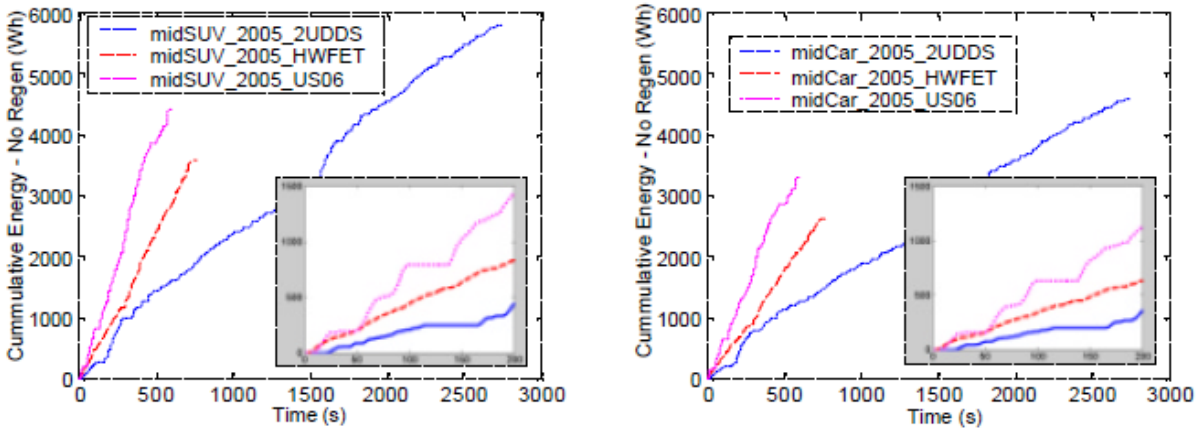

Fig2.8 cumulative traction energy is shown, that is the energy required to complete the patterns.

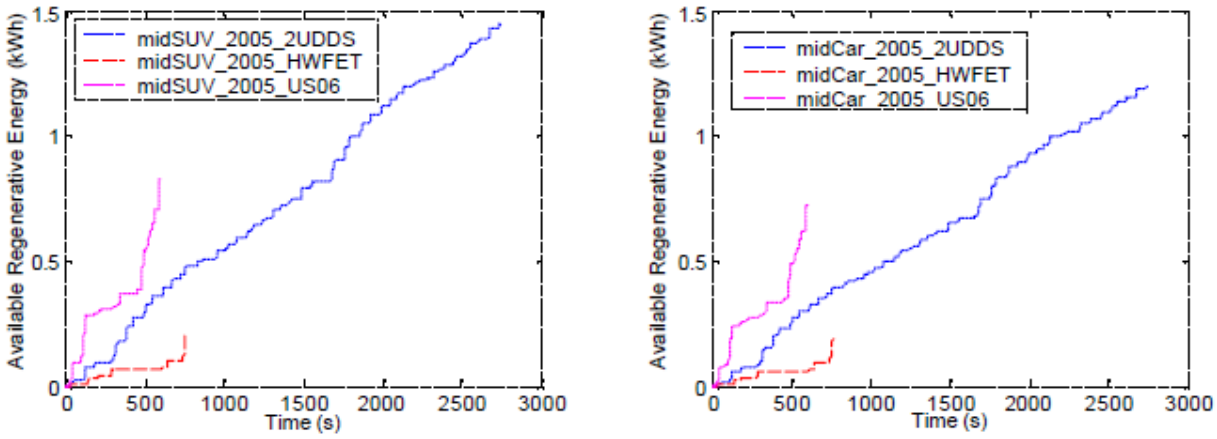

Fig 2.9 the available braking energy that is dissipate during braking phases.

Analyzing every driving cycle profile it is possible to identify the traction phases, during which the powertrain provides traction power for vehicle motion, and the braking phases, during which the braking force is applied to decelerate the vehicle. The latter ones are also named braking events, where regenerative braking occurs. Each

braking event is characterized by a unique duration, power profile and available energy, as shown in Fig 2.10.

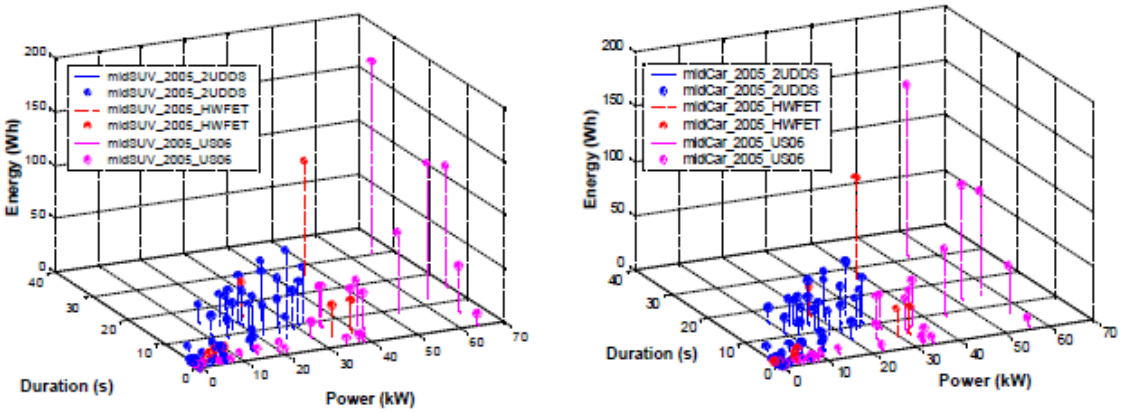

Fig 2.10 regenerative braking events analysis for SUV and car [10]

Despite of the fact that the biggest amount of total available braking energy is in 2UDDS driving cycle, the braking events with the highest energy and power peaks are in US06 cycle for both the vehicles. Since the power and energy capacity of the energy storage system has to be determined during design phase, these figures above are fundamental to determine the size of the battery pack that better fits the driving cycles characteristics.

As mentioned before, the braking phase analysis has a critical role. In the next paper [11] the braking energy characteristics on the vehicle speed and braking power in typical urban cycle have been investigated. After the determination of the test vehicle parameters, reported in Table 2.4, the driving power is calculated by means of

$$P = \frac{V}{1000} * (M * g * f - \frac{1}{2} * C_d * A_f * \rho * V^2 - M\delta \frac{dV}{dt}) \tag{2.4}$$

The power $P > 0$ for traction phases, whereas $P < 0$ for braking phases. By integrating equation (2.4) it is possible to obtain the braking energy and traction energy profiles during any driving cycle. In this case the power profile has been obtained for the FTP75 urban driving cycle. This profile, along with the velocity profile, is reported in Fig 2.11.

Table 2.4: vehicle parameters

Item	Symbol	Unit	Value
Vehicle mass ,	M	kg	1500 (Fully loaded) 1250 (Unloaded)
Rolling resist. coeffi.	f_r		0.01
Aerodynamic drag coeffi.	C_D		0.3
Front area	A	m^2	2.2
Wheel base	L	m	2.7
Distance form gravity center to front wheel center	a	m	1.08 (Fully Loaded) 0.81 (full loaded)
Gravity center height	h_g	m	0.6 (fully loaded) 0.5 (unloaded)

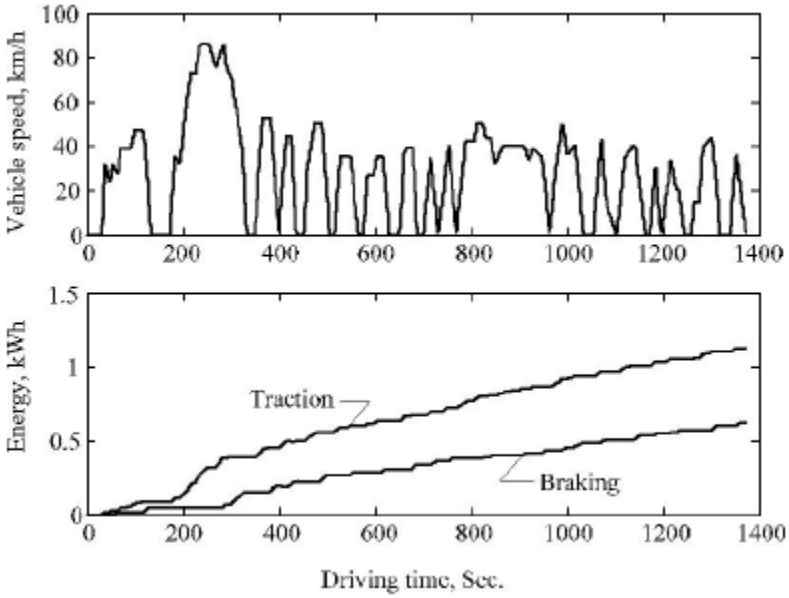

Fig 2.11 FTP75 urban driving cycle, [10]

.

In this analysis of driving cycles, every braking event has been characterized by means of the quantification of energy and vehicle speed at which the phase started. This can be helpful for optimal design and control of braking system As result, the Fig 2.12 has been obtained for the FTP75 urban driving cycle.

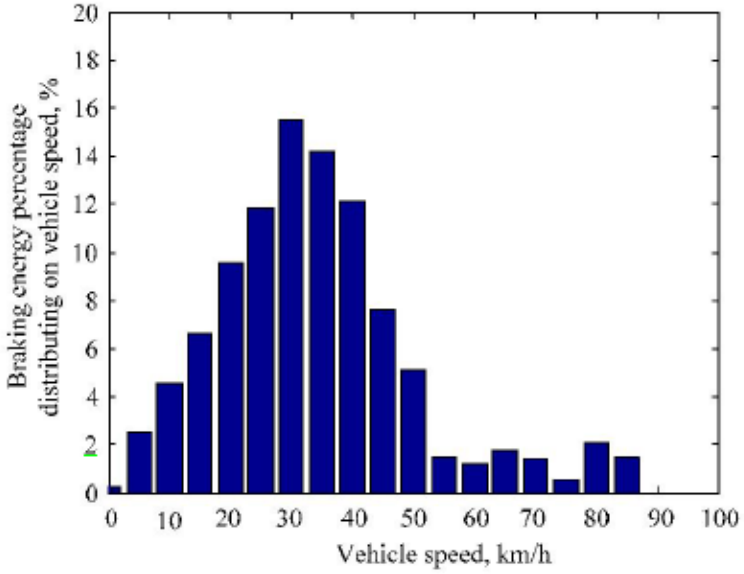

Fig 2.12 Braking energy distribution on vehicle speed in FTP75 urban driving cycle

Moreover, by means of every single braking event analysis, the braking energy distribution versus braking power over all the driving cycle has be evaluated. This approach can be helpful for power capacity design of the storage system. In Fig 2.13 the braking energy percentage versus braking power is reported for US-FTP75 driving cycle. It shows that using a 15 kW storage system, it is possible to recovery about 85% of available braking energy in all driving cycle. In Table 2.5 the same analysis is reported for different driving cycles.

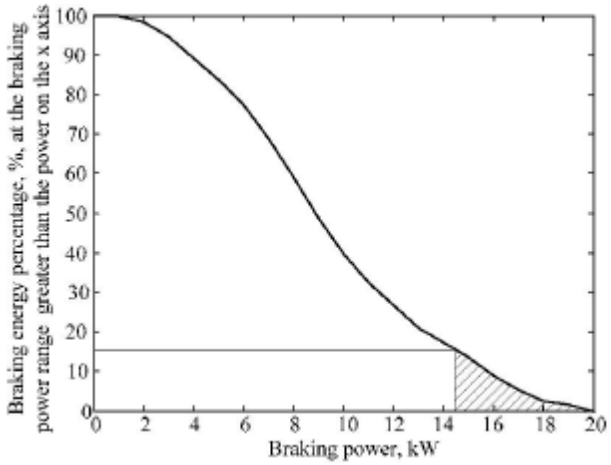

Fig 2.13 The braking energy percentage at the braking power range that are greater than the power shown in the horizontal axis for FTP75

Table 2.5:relation between ESS power and recoverable energy depending on driving cycle

	FTP 75 urban	LA92	US06	New York	ECE-15
Power range in which 85% of total energy is consumed	0–14.4	0–44.5	0–46.5	0–18.5	0–33.5

The determination of an energy storage system design methodology implies that the way to analyze the input data to obtain the system optimal design is set, but the results strictly depend on the driving cycle that represents the typical vehicle use. In [12], the impact of several driving cycles in the definition of hybrid plug-in vehicle requirements has been shown. After the vehicle main design methodology definition, several driving cycles have been considered to size the components: Japan1015, Highway EPA Cycle (HWFET), New European Drive Cycle (NEDC), SC03, LA92, and US06. In Fig 2. 14 and Fig 2.15 the main kinematic characteristics of driving cycles are shown: the average and maximum values of velocity and acceleration.

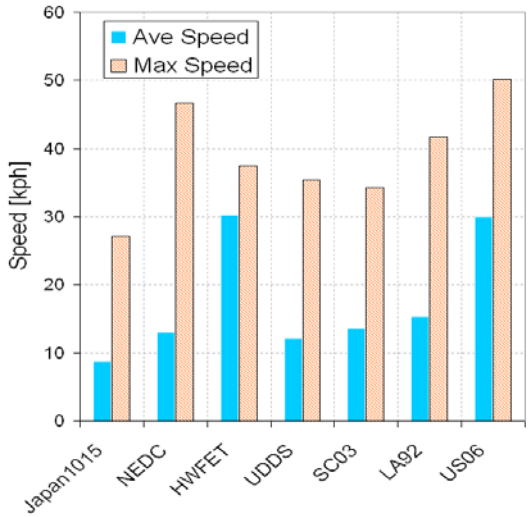

Fig 2. 14:average and maximum velocity over several driving cycle profiles

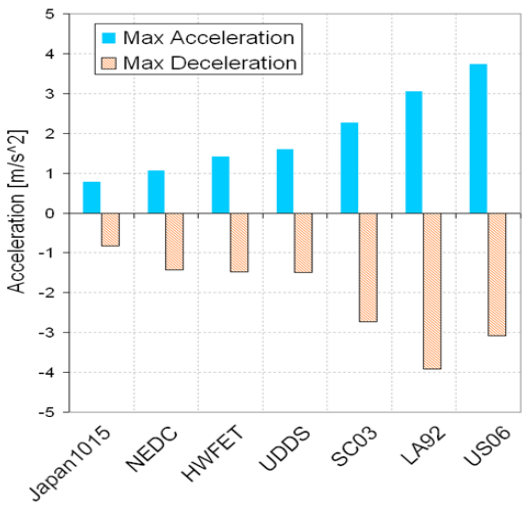

Fig 2.15: average and maximum velocity over several driving cycle profiles

The vehicle components sizing process is realized for the mentioned driving cycles considering the 10 AER (all electric range) criteria: it means that the hybrid vehicle should be able to drive in all electric mode for a range of 10 miles before the operating mode change and engine turns on. In Fig 2.16 the components size over several driving cycles are reported. From that figure, it is worth to notice:

- the engine power is almost constant since it is only sized to meet gradeability requirements (6% grade at 65 mph).
- electric motor and energy storage system sizes fluctuate a lot because the power capabilities are meant to match the maximum power requirements of the driving cycles.

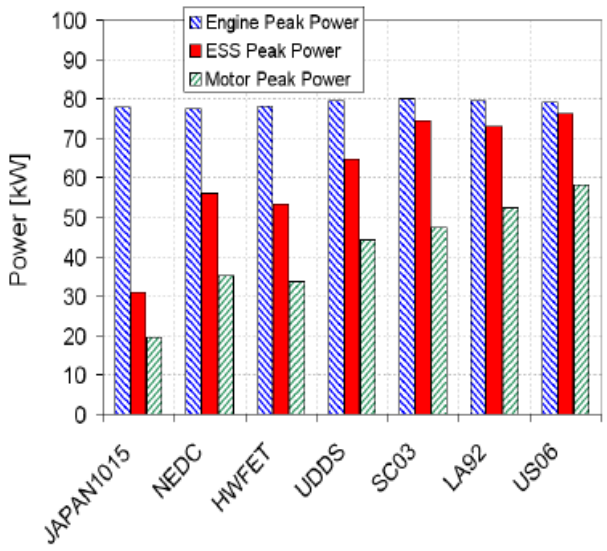

Fig 2.16: components size over several driving cycles expressed as maximum power

In [13], the energy storage system for an hybrid vehicle is investigated. A comparison between a battery based storage system and a mechanical storage system is proposed. In order to do it the US-FTP75 driving cycle is analyzed to extract energy-related information. The driving cycle velocity profile versus time is reported in Fig 2.17.

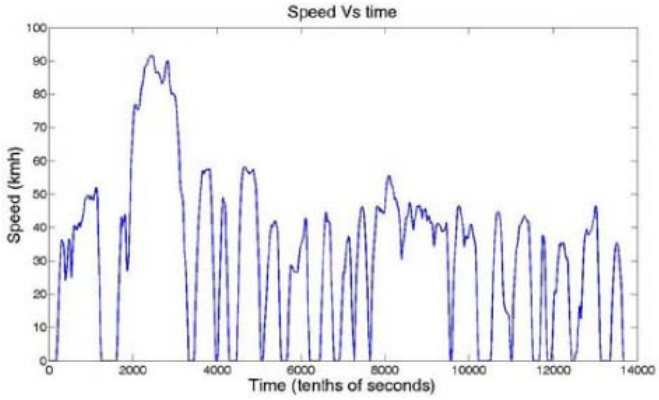

Fig 2.17: US-FTP75velocity profile

In the US-FTP75 driving cycle, the braking events have been identified. Adopting an exemplary typical vehicle mass of 1900 Kg, the amount of energy lost during each braking phase has been evaluated. Then the distribution of energy over the cycle is obtained as in Fig 2.18: for each considered energy interval, the events occurrences are calculated. As it is possible to notice, in this cycle this biggest part of braking events has a small amount of energy.

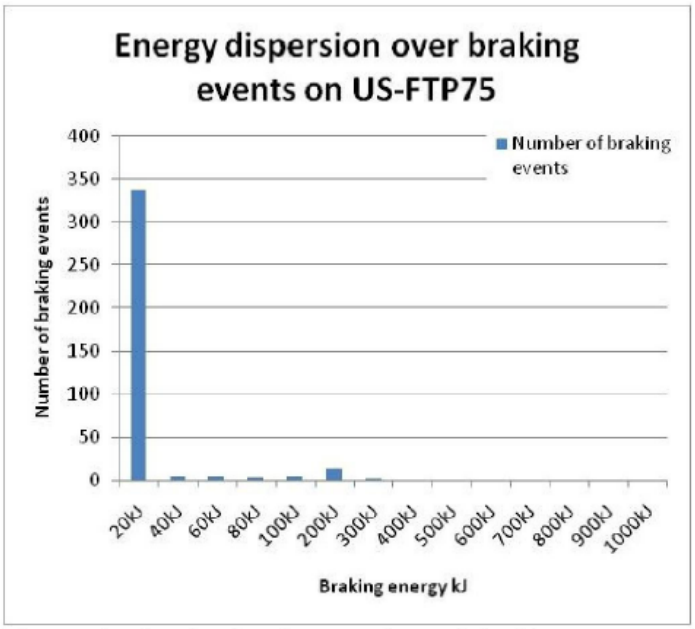

Fig 2.18:Energy distribution

The same analysis based on braking events energy determination and classification is done for a representative real world driving cycle in Fig 2.19. The data marked as "Delta KE" represent the change of kinetic energy of the vehicle in each braking event. But this energy evaluation does not take into account the losses caused by: aero drag, rolling resistance and efficiency of energy storing components. The data marked as "Recoverable" take these factors into account causing energy distribution changes.

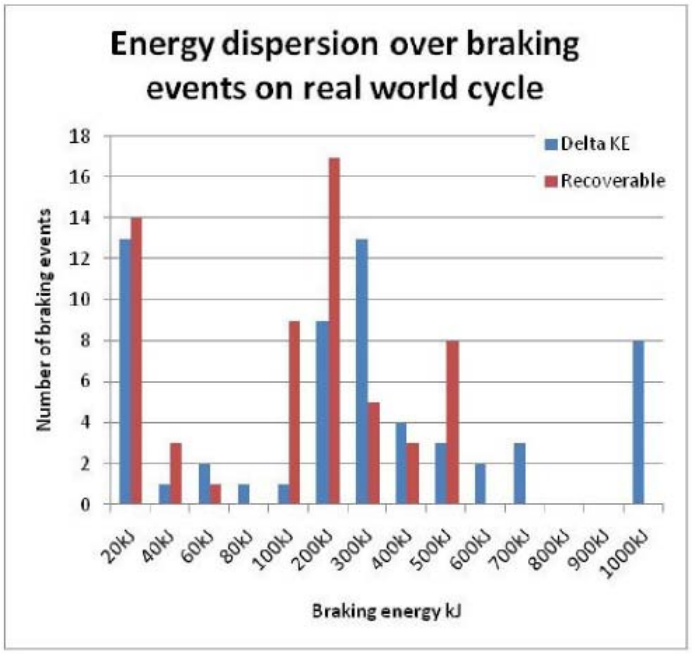

Fig 2.19: Energy distribution in real world driving cycle

2.2.1 Principle of Machine Components Design

The energy storage system design methodology needs inputs representing the right typical use of the vehicle to properly size the components. In the same way, machines mechanical components design is based on possible load profiles determination. Machines are composed by multiple components and each of them, during duty cycles, is subject to different stresses that can be static or dynamically variable. The components design is essentially based on a criteria that takes into account the expected stresses and experimental test results. Experimental tests are an essential part in the design process, since from them it is possible to obtain materials characterization caused by several possible uses and working conditions. It was proven that a machine part can withstand static stresses of high magnitude but it can fail if these stresses fluctuate. The safe limits in design analysis of a machine part subject to fluctuating load must be below static loading limits: this discovery prompted the definition of a new property called the fatigue limit.

In design of machine components subject to fluctuating load, the first step is the determination of its life span. In fact, it can withstand the load for an infinite fatigue life span or for a finite number of cycles. Then, the main concern is the typical loading profile definition that represents the target use. Every mechanical component design starts from the foreseen use of it, indeed.

In [14], the authors deal with the necessity of pursuing fatigue reliability to the design of machine tools components. Machine-tools components are subject to variable loads and a design based just on maximum static loads is not sufficient. It is then necessary to base the design on a typical use.

First of all, by means of a large numbers of experimental tests using specimens at each stress level in a planned sequence, the curves R-S-N with constant reliability are obtained. In Fig 2.20 such exemplary curves are shown.

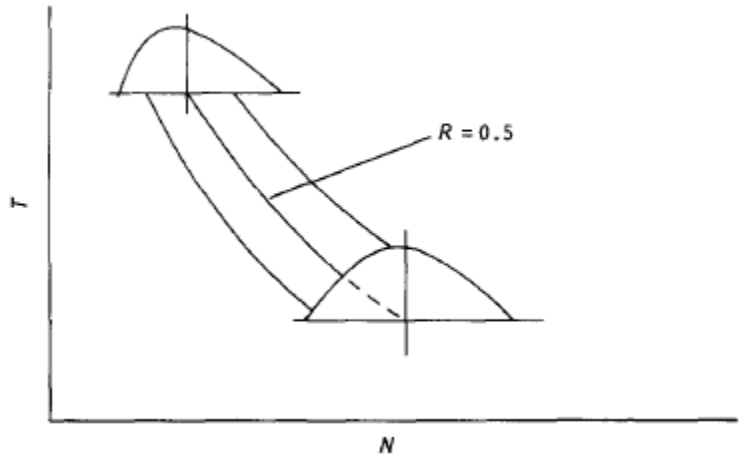

Fig 2.20 Exemplary R-S-N curves, where T is load and N cycles to failure

In the machine tools operating process the shear stress, work speed and loading change. By means of the use of a large quantity of tests and data, the loading spectrum and speed spectrum are obtained in Fig 2.21 and in Fig 2.22.

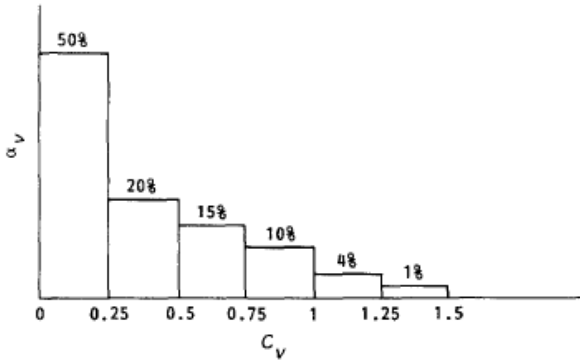

Fig 2.21 Power spectrum, α_v, operation time ratio;C_v, power utilization ratio

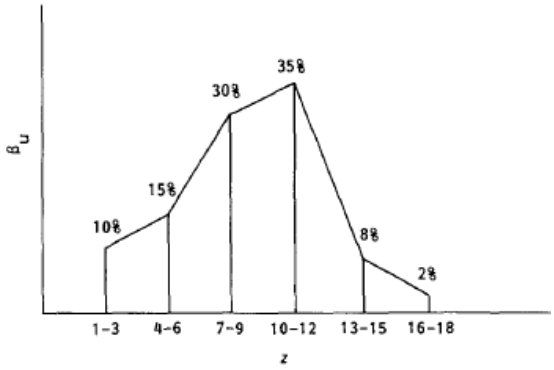

Fig 2.22 Speed spectrum. β_u., operation time ratio; z, speed step

By means of the knowledge of the characteristic fatigue loading spectrum and the R-S-N curves in Fig 2.23, the reliability analysis is done according to the Palmgren-Miner rule of linear cumulative damage :

$$\sum_{i=1}^{N} {}^{C_i}/_{N_{iR}} = 1 \qquad (2.5)$$

where C_i is the actual number of cycles of the load T_i and N_{iR} is the number of cycles to failure with a specified reliability R at the load T_i.

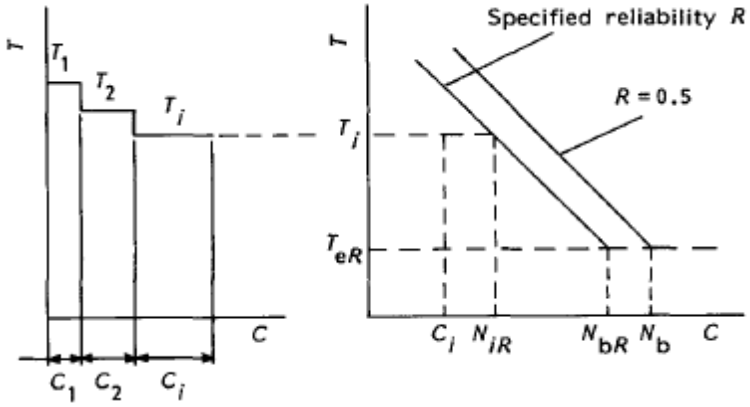

Fig 2.23 Loading spectrum and fatigue damage. T, load; C, number of cycles

The design for reliability methodology starts from the knowledge of loadings that can be obtained by means of statistical data or by means of experiments to properly size machine components.

2.3 Overview of Modeling Approach for ESS

In the previous sections, an overview about energy storage system methodologies design and driving cycles analysis methodologies have been presented. In this paragraph a modeling approach overview for ESS is treated. In particular it focuses on hydraulic energy storage system and main components modeling. This system modeling is the base for the simulations processed in the following chapters of this work.

The energy storage systems is implemented in the vehicle power train to allow for a dynamic energy buffer that can be used to optimize the energy flows on board and, ultimately, the fuel efficiency of the vehicle [15]. From a system standpoint, power and energy flows through the energy storage system can be represented by means of some fundamental system components:

- *Power connection node*: this element, physically represented by a clutch/transmission component, allows one to physically connect the ESS to the vehicle powertrain, enabling for a bi-directional flow of power.
- *Energy converter*: this element converts the power flows at the summation node into a suitable form of energy that can be stored. The conversion process occurs with energy losses, which must be correctly accounted for in order to conduct energy analysis.

- *Energy storage*: this element is able to store energy and release it when required by the control system. From a dynamic system standpoint, the amount of energy stored at a given time represents the state variable of the system.

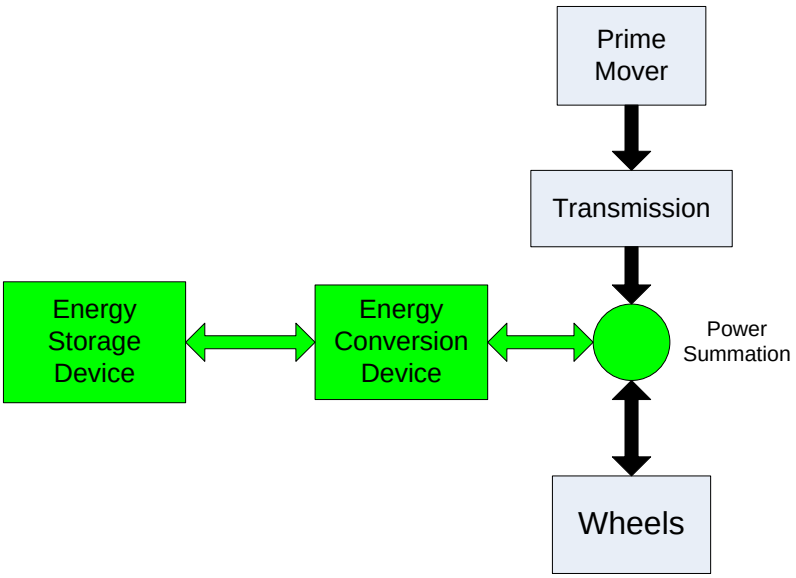

Fig 2.24: Energy flow scheme

2.3.1. Hydraulic Energy Storage System Model Components Description

In this section an overview of the main subsystem models of an hydraulic energy storage system is presented.

a) Hydraulic Pump/Motor

The pump/motor has the main function to provide the requested torque by moving the fluid from the reservoir to the accumulator, working as a pump, or from the accumulator to the reservoir, working as motor. The variable displacement pump/motor was modeled by means of using technical data and information available from manufacturers. In this model the flow rates are based upon the speed and displacement of the pump. The block diagram is shown in Fig 2.25.

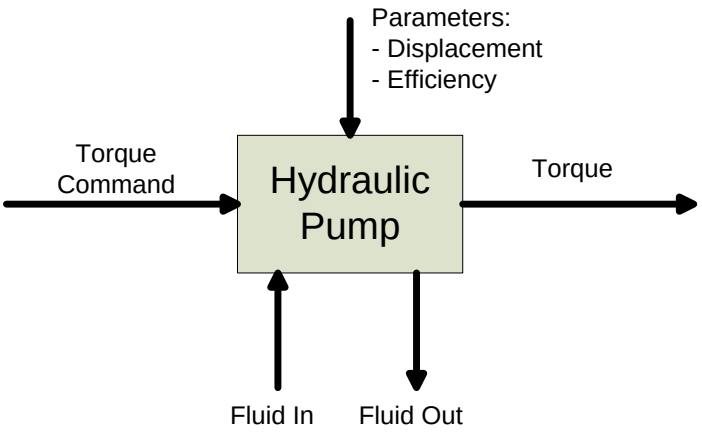

Fig 2.25: hydraulic pump model

The mathematical formulations of the model are

$$T = D_{pump} * \Delta P * \eta_{pump} \tag{2.6}$$

$$Q = D_{pump} * \omega_{pump} - k_{leak} * \Delta P \tag{2.7}$$

where

$$\eta_{pump} = f(T, w_{pump}) \tag{2.8}$$

In the above equations D_{pump} is the pump displacement, ΔP is the pressure difference between pump outlet and inlet, η_{pump} is the pump efficiency, $w_{pump}$is the pump speed, $k_{leak}$is a coefficient that considers the leaks, Q is the pump flow and T is the torque.

The overall efficiency is based on a lookup table from published pump data from Parker-Hannifin. Since pump efficiency data is only published for maximum displacement, an adjustment in efficiency must be made for cases where the pump displacement is reduced. The approach used refers to a common industry practice: pump leakage is assumed to be constant for a given pressure and pump speed, regardless of displacement. The leakage can be calculated for maximum displacement and applied to all other displacement settings. The resultant reduction in volumetric efficiency for non-maximum displacement conditions can be calculated.

b) Accumulator/Reservoir

The accumulator/reservoir stores energy in the form of pressurized hydraulic fluid. The model of this component operates by means of integrating the volumetric flow rate to determine the change in fluid volume. The resulting pressure is calculated based on the initial volume, total volume, pre-charge pressure, and ratio of specific heats. The model block is reported in Fig 2.26.

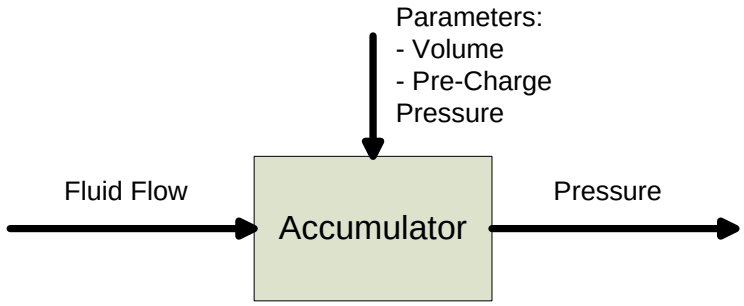

Fig 2.26: hydraulic accumulator model

The mathematical formulations of the model are:

$$p_1 * v_1^{\gamma} = p_2 * v_2^{\gamma} \tag{2.9}$$

The previous equation can be transformed to a more useful form in the following way:

$$V_f = V_A * (1 - (\frac{p_{pr}}{p})^{\frac{1}{k}}) \tag{2.10}$$

Where V_f is the fluid volume, V_A is the accumulator capacity, p is the inlet gauge pressure, p_{pr} is the pre-charge pressure and k is the ratio of specific heats.

c) Hydraulic Valve (Flow Restriction)

Since the flow changes direction because of the pump/motor working mode changes, the hydraulic valve is necessary. It is modeled as a flow restriction causing a pressure drop depending on the flow rate. The magnitude of the pressure drop is found via lookup table for a given valve. Data published by Parker-Hannifin for an appropriately sized valve was used in the model. The model block is reported in Fig 2.27.

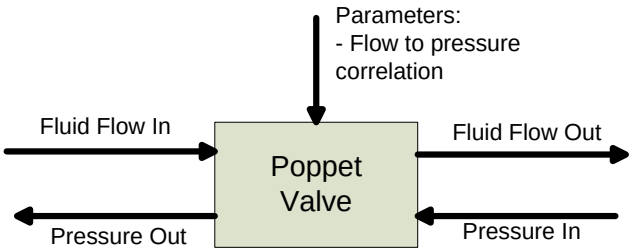

Fig 2.27: poppet valve model

After the models overview, the powertrain layout of the hydraulic hybrid simulator is reported in Fig 2.28 . In this configuration the energy storage system is installed in a parallel configuration. The pump is coupled to the powertrain shaft of the transmission.

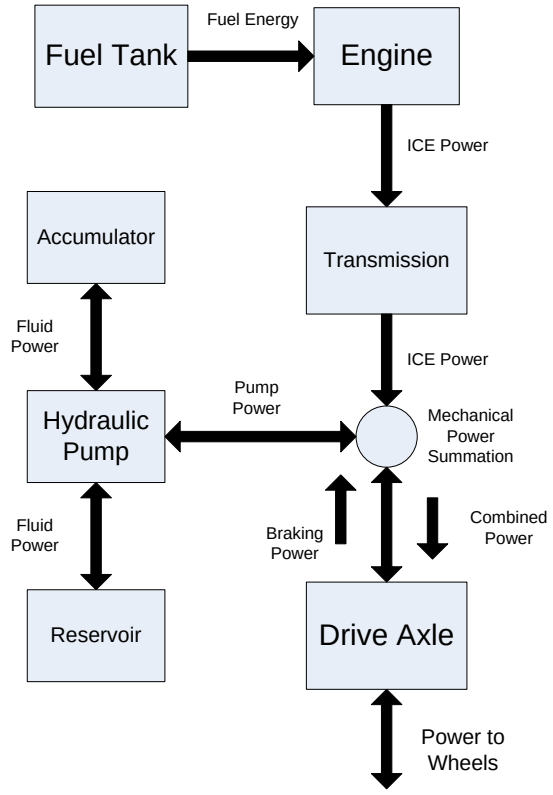

Fig 2.28: Hydraulic Hybrid Powertrain Layout

2.3.2. Operation of Short-term ESS

In the previous section the hydraulic energy storage system modeling overview has been presented. These models are used to perform simulations over tested driving cycles considering a regenerative braking strategy. The goal is to evaluate the energy and power flow between the storage system and the power train. This flow is bi-directional,

depending on the vehicle phase over the cycle: during braking phases, the energy flow is directed towards the storage system, while during the traction phases the energy flows towards the power train to provide torque to the wheels. The target use of the short-term ESS involves storing energy during the braking phase and the complete energy release during the following traction phase.

An exemplary operation of the hydraulic ESS use is shown in the figures below. In Fig 2.29 an exemplary driving cycle, US-FTP, is considered and the power profile for a generic mid-size SUV is obtained.

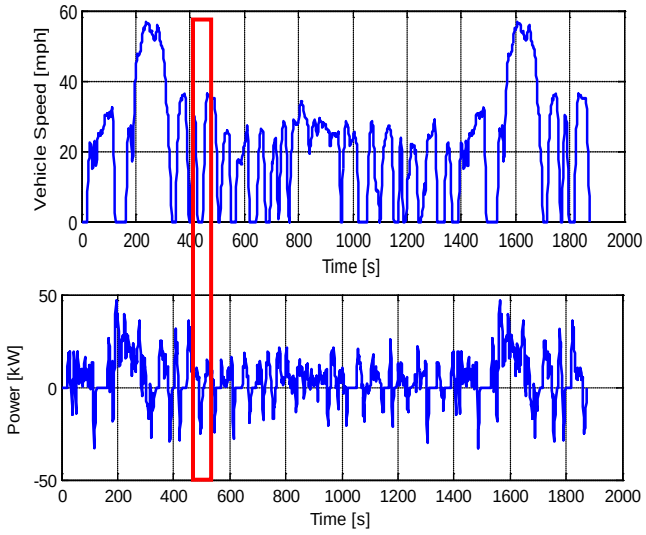

Fig 2.29: US-FTP driving cycle velocity profile and power profile for the

From these profiles it is possible to individuate a typical braking phase followed by a traction phase can be considered as reported in Fig 2.30 and highlighted by a red line. Both driving cycle velocity profile and power profile are reported. It possible to notice the decelerating phase followed by a vehicle rest and then an accelerating phase.

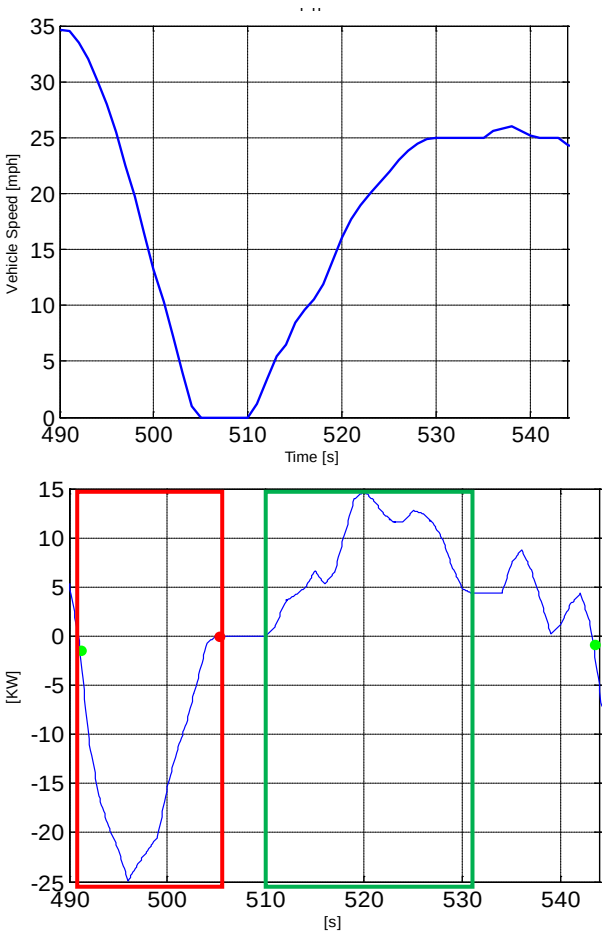

Fig 2.30: typical braking and traction phase velocity and power profiles

In the first phase, highlighted by a red line, the energy flows from the power train to the accumulator. The hydraulic pump coupled to the power train transforms mechanical energy into pressure energy moving the fluid from the reservoir to the accumulator. In the following traction phase, highlighted by a green line, the fluid flows from the accumulator to the reservoir. The torque is provided to wheels by means of the pump working in this phase as motor.

2.3.3. Hydraulic ESS Literature Review

In the previous section the model of a hydraulic ESS and the main use in a regenerative braking strategy have been shown. In literature a lot of papers treat the hydro accumulator modeling. Hydraulic regeneration systems have been considered by the automotive industry for implementation in hybrid vehicles for a number of years. A seminal study on this subject is presented in [16], describing an analytical model of a

hydraulic regeneration system consisting of an accumulator, an oil reservoir, a variable-displacement pump/motor and connecting lines. The modeling approach adopted allows for determining several variables, including accumulator pressure and temperature, pump/motor torque and efficiencies, pressure losses, and flywheel speed. Power losses and round-trip efficiencies are also determined. The results are indicative that improvements are needed to increase the energy density of hydraulic accumulators in many applications where space, weight, and power are critical.

The University of Michigan has developed various prototypes of hydraulic hybrid, using models and HIL (Hardware In the Loop) systems for experimental and prototyping studies. Recently published are [16] [17] focus on the modeling, simulation, design optimization and control of a series hydraulic hybrid (SHH) propulsion system. The study is performed in simulation, considering a series hybrid propulsion system of a four-wheel drive off-road downsized Diesel truck. In the SHH, the engine is directly coupled to a hydraulic pump/motor. Traction pump/motors are connected to the wheels to provide propulsion, and a hydraulic accumulator allows energy storage (max. operating pressure of 35-45 MPa). A low-pressure is also present in the system, primarily to enable transfer of fluid to-and-from the accumulator. The energy storage model is largely based on the energy-based model developed in [16]. In order to operate such system, a thermostatic controller was implemented. The simulation studies presented compare the SHH to the conventional vehicle, showing an overall fuel economy improvement of about 50% on the FUDS cycle.

The Center for Compact and Efficient Fluid Power (CCEFP) at the University of Minnesota works on light-duty hybrid vehicles. In [19] an attempt at improving the energy density of hydraulic accumulators is made. Conventional accumulators operate as closed systems, where the gas enclosed in the chamber is alternatively compressed and expanded. As the system must contain the expanded gas and the hydraulic oil displaced, the optimal energy density occurs at a modest expansion ratio, resulting in a small energy density. By adopting an open accumulator approach, allowing intake and exhaust of compressed and expanded air from and to the atmosphere, a potential increase in energy density is available. The paper reports analysis and simulation results to illustrate the advantages and challenges of such system.

A different approach to hybrid hydraulic systems is proposed in [20], where a Hydraulic Launch Assist (HLA) system is illustrated. Similarly to the starter/alternator technology of mild hybrids, the HLA captures energy during vehicle deceleration by compressing fluid in a hydraulic accumulator system. The hydraulic accumulator system can then be

used to provide torque at a subsequent vehicle launch. The HLA system is connected to the driveline with a clutch. The paper focuses on the implementation of such system (normally designed for heavy-duty applications) to small road vehicles in urban driving conditions. Simulation results show fuel economy savings in the order of 7-10% in standard urban driving cycles.

A similar approach is presented in [21], where a Hydraulic assist power system (HAPS) concept uses the existing hydraulic pump of the transmission unit as the motor/pump set directly. This solution leads to reduced size, lower weight and less cost of a conventional hydraulic system, and enables for vehicle energy recovery, engine restart, and hill-holding.

2.4 Introduction to the Work

In this literature review some energy storage systems design methodologies have been presented in order to give a design approaches overview. It is possible to affirm that the most of the design procedures focuses on electric hybrid vehicle and plug-in hybrid vehicles. They mainly treat issues related to the electric components requirements determination. Each of them has a specific method to analyze driving cycles that are considered to represent a typical system use and to extract information. Their common design approach is to seek in the driving cycle the most extreme energy-related conditions and to match the system requirements to them. So the design is realized with the goal to match the cycle maximum power requirements or to match the power requirements of the worst pre-defined events. In other terms they base the energy storage system design worst-case scenario over the cycle. This approach is suitable for long-term energy ES but are not for short-term ES systems. A short-term ESS based on this criterion would bring to system components oversized respect to the real requirements. Although it could be useful to store big amounts of energy it would have great drawbacks. The determination of the energy storage system components has to consider physical and practical aspects as components masses and volumes indeed. The maximization of main storing units, as the flywheel for the mechanical system or the accumulator for the hydraulic system, implies masses and volumes increase. If on the hand these increases give the chance to store more energy and then to theoretically reduce the fuel consumption, on the other hand they can increase the expenses to carry

on the project and they can bring disadvantage in fuel economy because of the increased weight of the vehicle.

The work developed in this thesis proposes a design methodology for short-term energy storage systems, such as mechanical, hydraulic and pneumatic systems. The procedure starts from the extraction of statistical information from the driving cycle adopting several criteria. Then, using these information as design inputs, several system designs are obtained.

This thesis focuses specifically the driving cycle analysis methodology. This is the first part of the short-term ES system design procedure and it synthesizes the design inputs of the design procedure. Despite of the presence of several driving cycles analysis methodologies shown in the literature review, it was necessary to create a new one suitable for this design procedure. The driving cycle analysis is a key element in the design approach and it diverges from the other approaches. In fact, as explained in the following chapter 3, it presents an innovative way to analyze the cycle and to synthesize the cycle information. In chapter 4, the complete short-term ESS design methodology is explained and applied to an exemplary hydraulic system. In chapter 5, by means of using the complete design procedure applied to the hydraulic energy storage system, the design procedure is validated. Since from the design procedure several system designs can be obtained, a final system designs comparison is done considering efficiency values over testing driving cycles.

3. Driving Cycle Analysis Methodology

The literature review chapter has outlined several design methodologies for energy storage system. Most of the approaches presented consider design metrics based on driving cycles information, from which a “worst-case” scenario is defined to determine the system design specifications. Such methods are suitable for long-term energy storage systems but not for short-term systems, since the use of the two systems is different.

The Ohio State University has developed a design methodology to target short-term energy storage systems, in particular mechanical and hydraulic systems.

This design approach, shown in detail in Fig 3.1, is based on:

- Application of data analysis and clustering techniques to identify characteristic driving events;
- Utilize characteristic events to set design targets and constraints;
- Using parametric models of ESS to determine design attributes;
- Evaluate design on energy-based hybrid vehicle model.

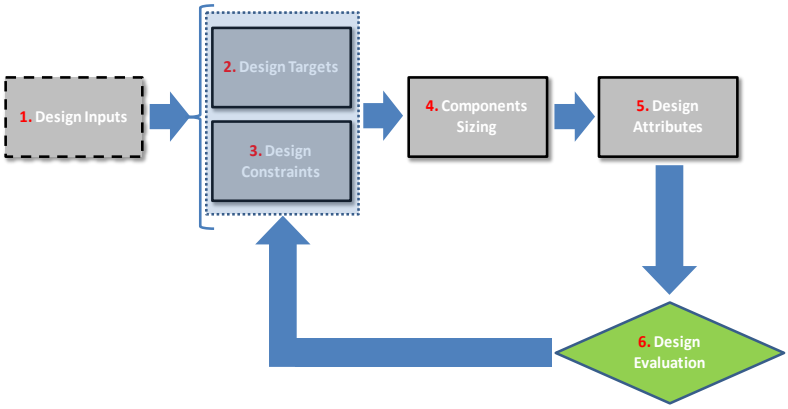

Fig 3.31: ESS design methodology flow chart

The preliminary phase of the design methodology is the driving cycle analysis, which defines the ESS design specifications in terms of energy and power requirements. In this chapter a driving cycle analysis and synthesis methodology is proposed to produce the Design Inputs for the definition of the ESS design parameters. Fig 3.1 shows the flow chart of the design procedure. The innovation of the driving cycle analysis methodology is related to the different way to analyze the cycle and to synthesize the extracted information. At first, the methodology focuses on the braking

and acceleration events of the driving cycle. Then, the extracted driving data are statistically processed to build characteristic stop/start events which define the Design Input for the design process.

In the first part of this chapter, road-load analysis of driving cycles is proposed and illustrated for the US06 cycle. The aim of the procedure is to extract information on the most relevant dynamic and energy-related variables. At the end of this analysis it will be possible to define a “statistically” relevant event that will define the size of the energy storage system.

In the second part, the “statistically” relevant event will be analyzed by means of a sensitivity test varying the vehicle mass and front area values. Then the “statistically” relevant event identification process will be applied to several different driving cycles, although the methodology is completely independent on the nature of the driving cycle.

In the last part, three statistically relevant cycles representative of “real-world” commuting scenarios are presented. The patterns obtained are then processed to define design targets that will be the input of the following part of the design procedure of the energy storage system.

3.1 Development of a Driving Cycles Analysis Tool

In order to define the design requirements for AESS, a tool for the analysis of driving cycles was built. The developed tool allows one to determine the vehicle power and energy demand at the wheel for a prescribed driving profile. Further, a decomposition in events is made to determine the characteristics of deceleration/ acceleration maneuver that is the statistically most representative of the entire driving profile.
The analysis tool includes the following tasks:

- calculation of the traction power at the wheel based upon a simplified model of the longitudinal dynamics of the vehicle;
- identification and classification of the cycle events;
- calculation of the distribution of the dynamic and energy-related variables;
- synthesis of the distributions of such variables to create a statistically representative event of the driving cycle

First of all, a brief introduction to regulatory and "real world" driving cycles is necessary, since they both have been used to test the analysis tool.

3.1.1. Driving Cycles

Driving cycles are generally characterized by a velocity vs. time profile and represent a driving route. These cycles can be modeled on data acquired during real driving experiences or can be synthesized from model. They are usually adopted to perform many different vehicles tests on the dynamometer, where the force at the wheels is chosen to emulate the vehicle energy losses while driving that specific route.

a) Regulatory Cycles

Worldwide vehicles emissions and consumption tests are based on regulatory driving cycles, whose profiles depend on the most common routes characteristics of each specific country. The most common test cycles to determine fuel economy and emission levels are the New European drive Cycle (NEDC),the Japan 10-15 cycle and the U.S. CAFE cycles. Although many others countries use these cycles, each one is designed to represent vehicle velocity profiles characteristic of given country, with different mean

and top velocity, duration, length and stop numbers. In this analysis the considered driving cycles are the US06, FTP-75 and NEDC.

b) Real-world Driving Cycles

In this work, the analysis and synthesis of design requirements has been extended also to "real-world" cycles [23]. Real-world driving data are different from regulatory cycles. Though regulatory cycles are used by national authorities to test and homologate vehicles, "real-world" cycles are more representative of real world driving conditions. They consist of synthetic vehicle velocity segments, generated stochastically on the basis of acquisition of on-road vehicle speed vs. time data during one year period. By means of a clustering process and Markov-chain model application, it is possible to generate stochastic velocity segments. During the generation process, by imposing different boundary conditions (maximum velocity, average velocity and stops per mile), the segments are grouped into three main driving pattern categories: urban, freeway and highway. Moreover, it is possible to represent for each category also traffic and no traffic conditions by means of small variation in the boundary conditions values. The input data were chosen in consideration of typical daily commuting scenarios for urban or sub-urban driving in the United States. Table 3.1 shows the patterns created for this study. Every segment has one mile length.

Table 3.6 Input data to create "real cycles"

Pattern		Average velocity [mph]	Minimum velocity [mph]	Stops per mile
Urban	No traffic (UNT)	15	35	1
	Traffic (UT)	5	20	10
Highway	No traffic (HNT)	40	55	0.5
	Traffic (HT)	20	45	2
Freeway	No traffic (FNT)	50	70	0.1
	Traffic (FT)	30	55	1

Below are some velocity vs. time profiles obtained with the conditions in Table 3.1.

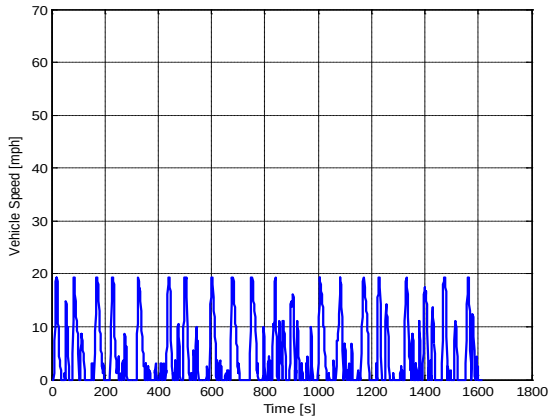

Fig 3.32 Example of custom urban driving cycle with traffic condition

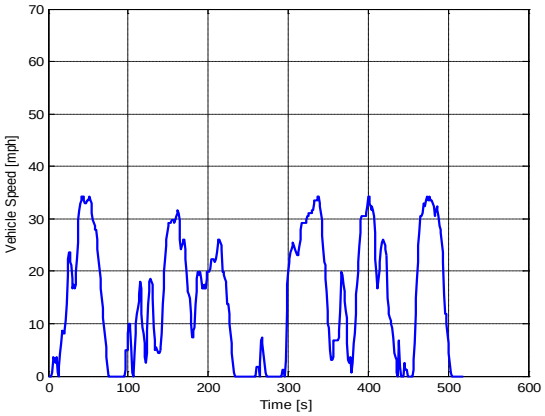

Fig 3.33 Example of custom urban driving cycle with no traffic condition

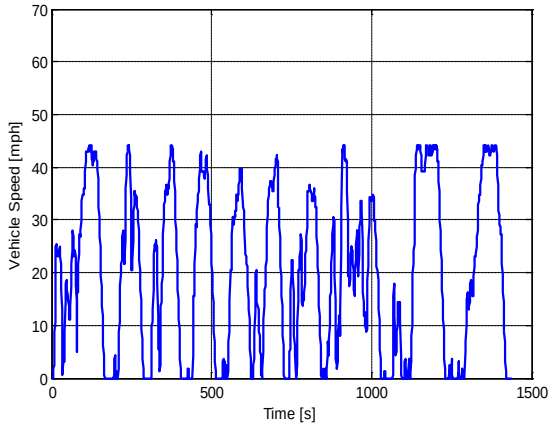

Fig 3.34 Example of custom highway driving cycle with traffic condition

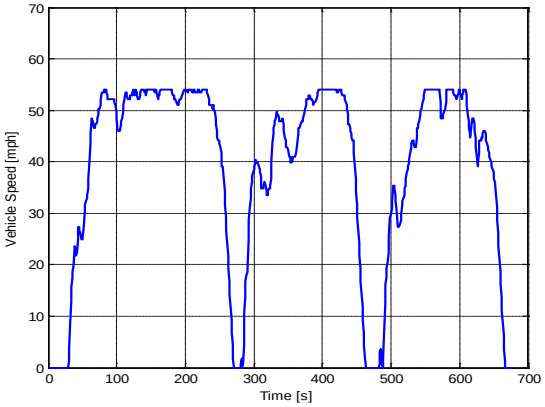

Fig 3.35 Example of custom highway driving cycle with no traffic condition

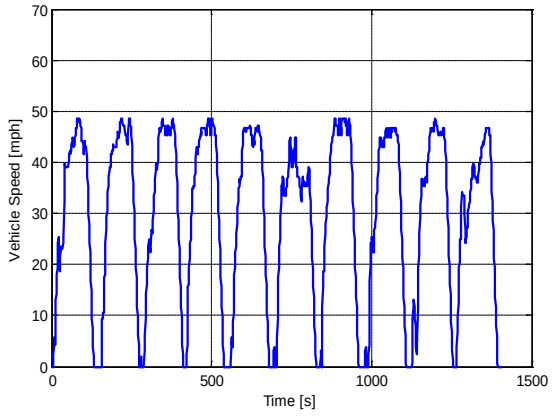

Fig 3.36 Example of custom freeway driving cycle with traffic condition

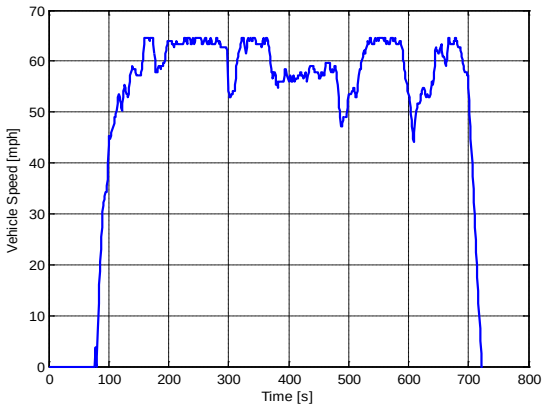

Fig 3.37 Example of custom freeway driving cycle with no traffic condition

In the figures above it is possible to notice the “real-world” segments different characteristics depending on the pattern. In Fig 3.2 the urban cycle with traffic conditions is characterized by low speed and frequent stops, while in Fig 3.7, the freeway cycle with no traffic has high speed and one stop.

3.1.2. Driving Cycles Analysis

A first analysis of the driving data can be made by identifying the average and maximum velocity values, along with the duration, length and number of stops. In particular, the following metrics are computed:

- Average and maximum acceleration;
- Average and maximum deceleration;
- Average and maximum velocity;
- Cycle length;
- Cycle duration;
- Stop number (not accounting the final vehicle stop);
- Number of stops/km.

Such metrics are reported in Table 3.2 for some important regulatory cycles, such as US06, FTP Highway and FTP Urban.

Table 3.7:velocity metrics for some regulatory driving cycles

	US06	FTP highway	FTP urban
Average velocity [m/s]	21.49	21.58	9.48
Average acceleration [m/s^2]	0.67	0.19	0.51
Average deceleration [m/s^2]	-0.73	-0.22	-0.57
Top speed [m/s]	35.9	26.78	25.35
Maximum acceleration [m/s^2]	3.75	1.43	1.48
Maximum deceleration [m/s^2]	-3.08	-1.21	-1.47
Stop number	4	0	21
Cycle time [s]	600	765	1874
Cycle length [km]	12.88	16.51	17.77
Number of stops/km	0.31	0	1.19

A second step in the analysis consists in the determination of vehicle forces and power requirements. To this extent a vehicle model has to be introduced starting from the elementary equation that describes the longitudinal dynamics of a road vehicle.

3.1.2.1. Vehicle Longitudinal Dynamic

Considering a generic vehicle with velocity V travelling on a road with grade α, the equation that determines the net traction force required at the wheels to propel the vehicle is given by:

$$F_t = \left(F_r + F_g + F_a\right) + m_v * \frac{dV(t)}{dt} \tag{3.1}$$

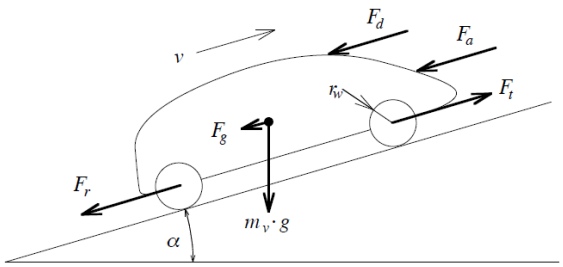

where m_v is the system mass, F_t is the net traction force, F_a is the aerodynamic friction force, F_r the rolling friction force, F_g the force caused by gravity when driving on non-horizontal roads [24].

a) Aerodynamic Friction

The aerodynamic resistance F_a acting on a vehicle in motion is caused on one hand by the viscous friction of the surrounding air on the vehicle surface. For a standard passenger car, the car body causes approximately 65% of the aerodynamic resistance. The rest is due to the wheel housings (20%), the exterior mirrors, eave gutters, window housings, antennas, etc. (approximately 10%), and the engine ventilation (approximately 5%) [25]. The equation generally considered to capture this action is:

$$F_a = \frac{1}{2} * \rho_a * A_f * C_d * V^2 \tag{3.2}$$

where V is the vehicle speed, ρ_a the density of the ambient air, A_f is the vehicle frontal area and the parameter C_d is the aerodynamic friction coefficient, generally estimated using CFD programs or experiments in wind tunnels.

b) Rolling Friction Losses

The rolling friction losses are caused by the tires deformation and rolling friction during vehicle cruise, and are given by [24]:

$$F_r = m_v * C_r * g * \cos(\alpha) \tag{3.3}$$

where m_v is the vehicle mass and g the acceleration due to gravity. The term $\cos(\alpha)$ models the influence of a non-level road.

The rolling friction coefficient C_r depends on many variables. The most important influencing quantities are vehicle velocity V, tire pressure p, and road surface conditions. The influence of the tire pressure is approximately proportional to $1 / \sqrt{p}$. The vehicles peed has a small influence at lower values, but its influence substantially increases when it approaches a critical value where resonance phenomena start. An example of these relationships is shown in

Fig 3.8, where C_r changes with velocity V and tire pressure p. But, when the velocity remains moderate, the coefficient C_r can be considered constant.

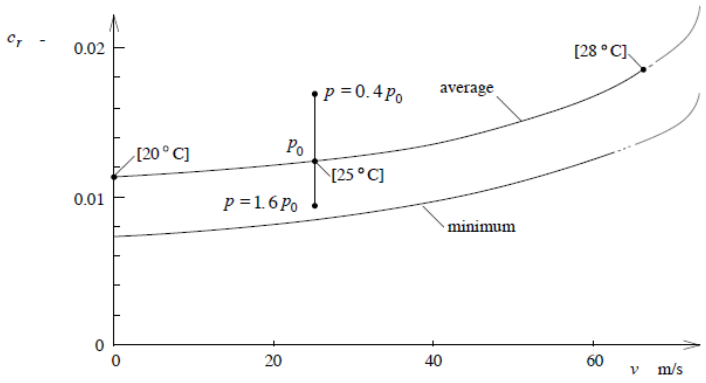

Fig 3.38: Tire friction coefficient as a function of the vehicle speed v and variations of the tire pressure p ,[24]

c) Uphill Driving Force

The force induced by gravity when driving on a non-level road can be modeled by the following equation:

$$F_g = m_v * g * \text{sen}\,(\alpha) \tag{3.4}$$

d) Inertial Forces

The inertial forces are apparent forces caused by the motion of the vehicle mass m_v and by the motion of powertrain rotating components. The inertial force caused by the vehicle mass can be expressed by the following equation:

$$F_i = m_v * \frac{dV(t)}{dt} \tag{3.5}$$

For more precise calculation it is necessary to consider also the wheel inertial mass and powertrain components masses. The inertia torque $T_{m,w}$ of the wheels is given by

$$T_{m,w}(t) = \Theta_w * \frac{d}{dt} w_w(t) \tag{3.6}$$

Θ_w is the inertia of wheels and rotating parts present on that side of the gear box and $w_w$the wheels speed.

This torque acts as additional inertia force expressed by $F_{m,w} = T_{m,w}/r_w$, where r_w is the wheel radius. Then the contribution of wheels to vehicle inertia can be expressed by $m_{r,w} = \Theta_w/{r_w}^2$. The total inertia torque $T_{m,e}$ of the engine is related to engine speed w_e and Θ_e the total moment of inertia of the powertrain. This analysis takes into account a prime mover and a transmission with a total transmission ratio γ. The inertia torque of engine is

$$T_{m,e}(t) = \Theta_e * \frac{d}{dt} w_e(t) \tag{3.7}$$

This torque acts as additional inertia force expressed by $F_{m,e} = T_{m,w}/r_w$.

Considering a constant gear ratio and no mechanical losses, the corresponding additional vehicle mass is

$$m_{r,e} = \Theta_c(\gamma^2/{r_w}^2) \tag{3.8}$$

The equivalent mass of rotating components to add to the vehicle inertial mass is

$$m_r = m_{r,w} + m_{r,e} \tag{3.9}$$

e) Analysis Assumptions

In order to calculate the vehicle traction force, the following parameters are typically required:

- A_f, vehicle frontal area;
- C_d, drag coefficient;
- m_v, vehicle mass;

Some initial assumptions have been made for this analysis:

- The air density ρ_a was assumed to be constant;
- The rolling friction loss was calculated assuming same tyres radius dimensions for all the vehicles and horizontal road without slope.

These assumptions allows one to consider a constant rolling friction coefficient C_r. Furthermore, the following assumptions are made:

- The uphill driving force contribution F_g is neglected;
- In the calculation of inertial forces F_i, the contribution of wheels and rotating masses to vehicle inertia is considered as a constant term, increasing the vehicle effective mass m_v by 10%.

In light of the above assumptions, generic vehicle model in our analysis is simplified by means of the mass, frontal area and drag coefficient parameters. Since this vehicle follows a generic driving cycle velocity profile V, it is possible calculate the traction or braking force F_t with equation (3.1).

The power calculation point-by-point is immediate, by means of the following equation:

$$P = F_t * V \tag{3.10}$$

It is possible to distinguish three conditions based on the sign of the power:

- $P > 0$ is the traction phase, which occurs when a traction power is provided by the powertrain to the vehicle.
- $P < 0$ is the braking phase, which occurs when the vehicle velocity is positive (no change in the direction) and the net force at the wheel is negative.
- $P = 0$, it may occur in two cases:
  - $V = 0$, the car is temporary stopped.
  - $F_t = 0$, coasting phase. During the coasting phase, there is no net traction force delivered by the vehicle propulsion system and no net braking force applied to the vehicle braking system. In this condition, the engine and powertrain rotating parts are dragged by the vehicle decelerating motion caused by the action of the dissipative forces. In this case, the resistance losses of the vehicle are exactly matched by the decrease of its kinetic energy.

In Fig 3.9, the velocity and power profile for the US06 driving cycle are reported. The vehicle model used to determine the power profile is a midsize SUV with the characteristics reported in Table 3.3.

Table 3.8: vehicle parameters

SUV data	
Vehicle mass	1900 Kg
Frontal area	2.86 m^2
Drag coefficient	0.42

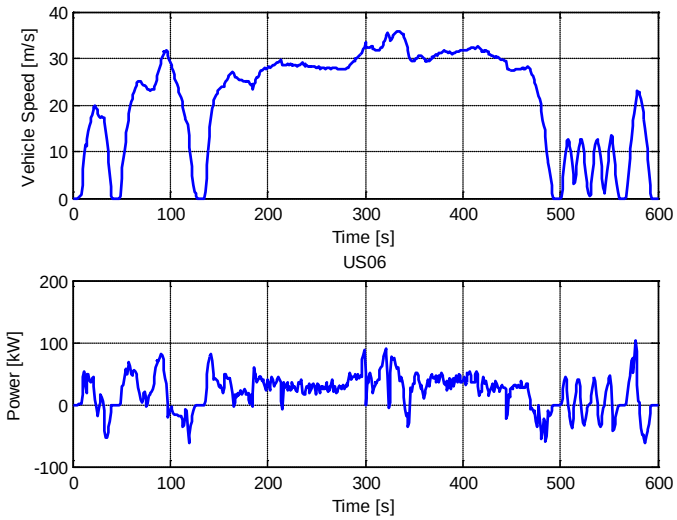

Fig 3.39:Velocity and power profiles for a mid-size SUV on the US06 driving cycle

The main goal of this analysis is to evaluate the energy that is spent to during the active braking phases and that can be in theory recovered for the following acceleration phases. The active braking phases do not include coasting periods, during which no external power is applied to slow down the vehicle and no energy can be recovered.

3.1.2.2. Creation of Event ID

The first step of this analysis is the creation of power vs. time profile: in this way it is possible to determine the total energy at the wheel required by the vehicle and to evaluate how much could be potentially stored by braking energy recovery.

In the literature review chapter, some design methodologies have been proposed, based on driving cycle analysis. The general approach is based on the identification of energy/power-related metrics evaluated along the entire driving cycle. A key element of the proposed methodology is the analysis of each power event within the cycle and the evaluation of all the related characteristic metrics.

A power event is defined as a segment of driving cycle delimited by two consecutive power sign change.

It is possible to define:

- Positive event, starting when the total power sign switches from negative to positive and lasts until the next switch in sign. This corresponds to vehicle traction phase.
- Negative event, starting when the power sign switches from positive to negative and lasts until the next switch in sign. This corresponds to vehicle braking phase.

In Fig 3.10, the power profile of the US06 cycle is reported with the identification of negative events by means of red-green points.

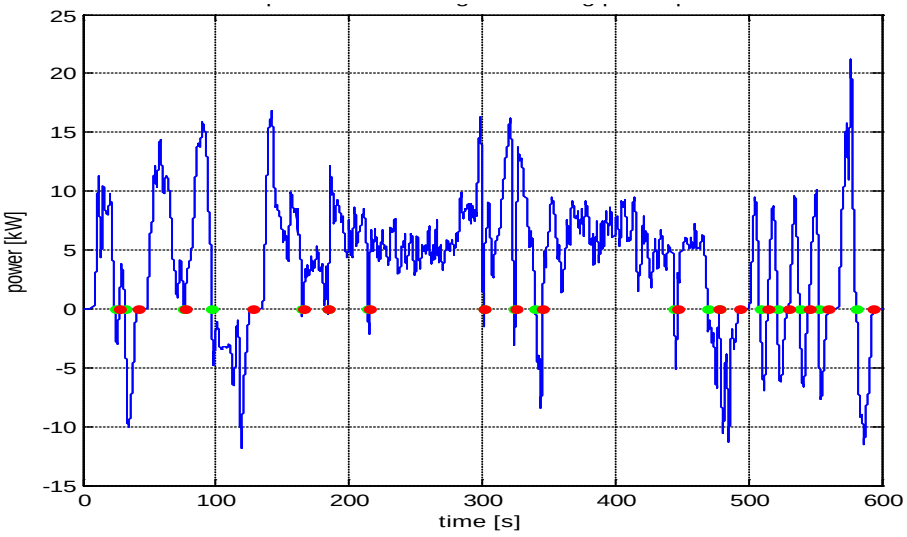

Fig 3.40 Identification of power events on the US06 cycle shown in Fig 3.9 (every negative event is determined by a green-red point).

It is important to study in detail not only the negative power events caused by braking phases, but also the positive ones. This way, a better knowledge of how the stored energy that can be reintroduced into the system is achieved.

Every positive (negative) power event can be characterized by the following metrics:

- Maximum acceleration (deceleration): maximum acceleration (deceleration) value per event;
- Maximum velocity: maximum velocity value per event;
- Maximum power (minimum power): maximum (minimum) power value per event;
- Energy: energy required per event, obtained as the integral of the power in time, between is the event start ($t0$) and the event conclusion ($t1$).

$$E = \int_{to}^{t1} P(t)dt \tag{3.11}$$

Since the vehicle velocity data are typically sampled, hence discrete signals, the above equation becomes

$$E = \sum_{i=1}^{N} P_i * \Delta t \tag{3.12}$$

where Δt is the sampling time. The number of intervals N is obtained as

$$N = \frac{T_{event}}{\Delta t} \tag{3.13}$$

Considering T_{event} as the event duration. Other metrics are obtained as follows:

- Average acceleration (deceleration): the average value of the acceleration (deceleration) per event;
- Average velocity: the average value of the velocity per event;
- Average power: the average value of the power per event. The generic average value of a specific variable $x(t)$, indicated with $\bar{x}(t)$, is calculated as:

$$\bar{x} = \frac{\int_{to}^{t1} x(t)dt}{t_1 - t_0} \cong \frac{\sum_{i=1}^{N} x(t)_i}{N} \tag{3.14}$$

where t_0 and t_1 are the start and the end time of the event, respectively.

The characteristic metrics defined above can be considered over all the cycle. If y is a generic metric, which could be the maximum, the mean or the minimum, it is possible to obtain:

- The average value: if N is the events number and y_i the value for event i , then

$$\bar{y}_{av} = \frac{\sum_{i=1}^{N} y_i}{N} \tag{3.15}$$

- The maximum value: is the maximum value among all the cycle values

3.1.2.3. Events Clustering Process

The presented driving cycle analysis methodology focuses on the identification of braking and traction events. As shown in the literature review chapter, a similar approach was proposed in [26]. While in that study only energy and power metrics for braking phases were calculated, in this work a more detailed analysis is proposed. In fact, both braking and traction events are considered and each of them is analyzed by calculating the metric set mentioned before. This approach allows one to extract

important data that can be used to retrieve statistically relevant cycle information during the data synthesis phase.

In order to statistically analyze the metrics, the events clustering process is applied considering separately positive power events and negative power events. For each metric, the distribution in the cycle can be evaluated. In this distribution is calculated the events frequency corresponding to a metric value normalized to its maximum in the cycle. This methodology allows one to have a statistical representation of the metrics characterizing the cycle events. These distributions are useful tools, since it is possible to individuate which are the metrics values which are the most frequent in the cycle. In other terms, the metrics distributions are fundamental to retrieve synthetic values that can be representative metrics values for the braking/traction phase in the cycle. In this methodology the metrics distributions are used in order to calculate the representative metrics values by means of the weighted average method. The equation to obtain the weighted mean $\bar{y}_{WM}$ of a generic metric y_i is

$$\bar{y}_{WM} = \sum_{i=1}^{N} y_i * f_i \tag{3.16}$$

where the index i is referred to the generic event i and f_i is the considered weight of the variable y in the event i. The weight can be referred to the metric's own distribution.

The metrics distribution has been evaluated for both braking and traction event metrics for US06 cycle and are reported from Fig 3.11 to Fig 3.24. Moreover, the weighted average value for each metric has been calculated and reported.

3.1.2.4. Braking Events Analysis

As an example, Fig 3.11 - Fig 3.17 represent the distributions of negative events of the energy, maximum negative power, average negative power, maximum and average velocity, maximum and average deceleration respectively for the US06 driving cycle. The y-axis reports the frequency of the variable shown in the x-axis as observed in the cycle, normalized with respect to the total number of occurrences per cycle. The normalization values are listed in Table 3.4.

The black line represents the value obtained with the weighted average shown in equation (3.16).

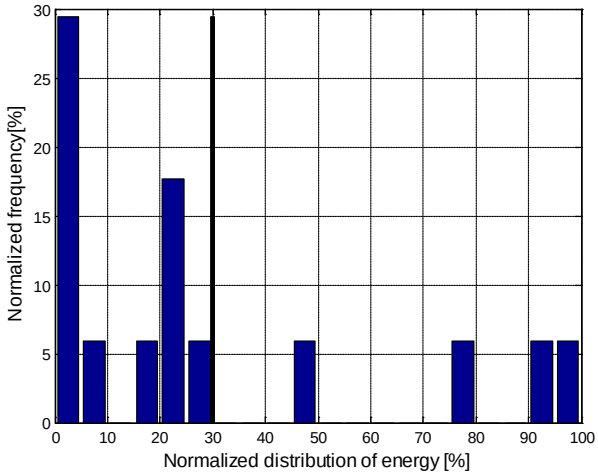

Fig 3.41 Distribution of negative event energy for the US06 cycle

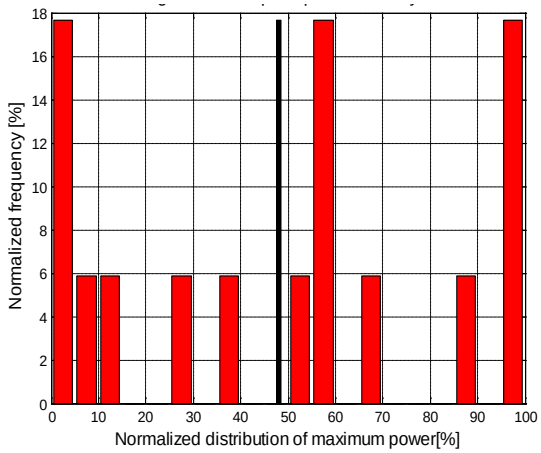

Fig 3.42 Distribution of negative event maximum power for the US06 cycle

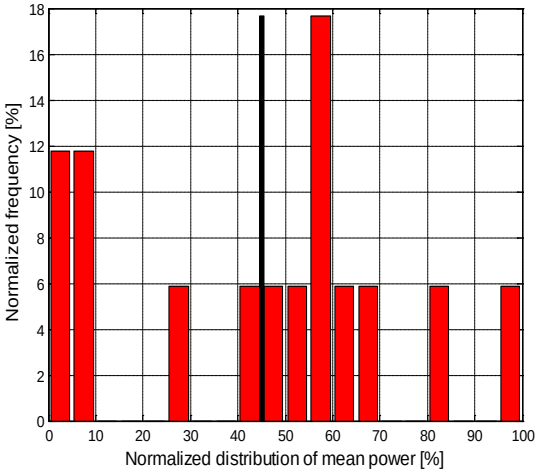

Fig 3.43 Distribution of negative event mean power for the US06 cycle

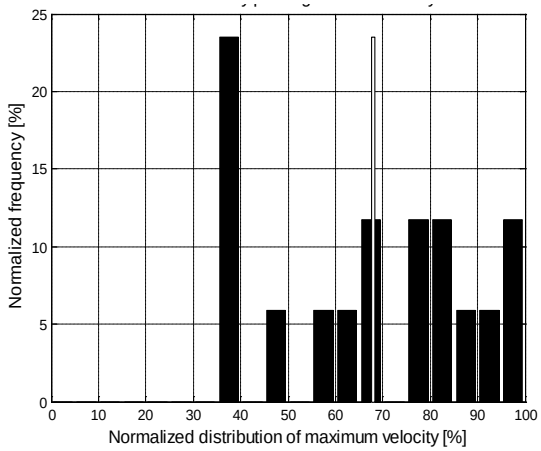

Fig 3.44 Distribution of negative event maximum velocity for the US06 cycle

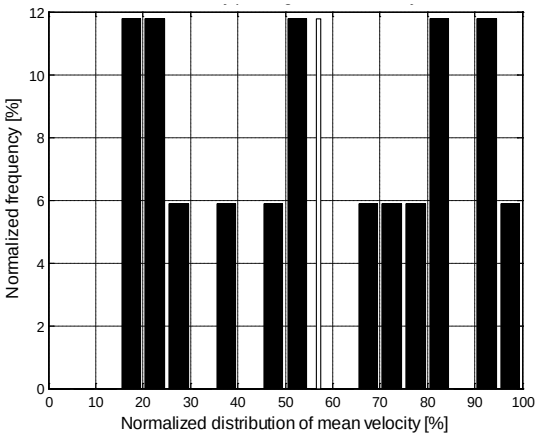

Fig 3.45 Distribution of negative event mean velocity for the US06 cycle

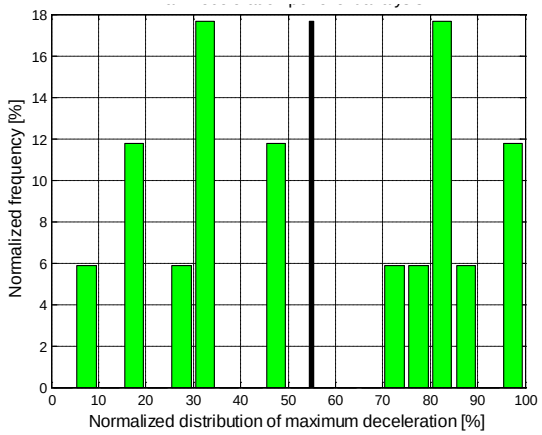

Fig 3.46 Distribution of negative event maximum deceleration for the US06 cycle

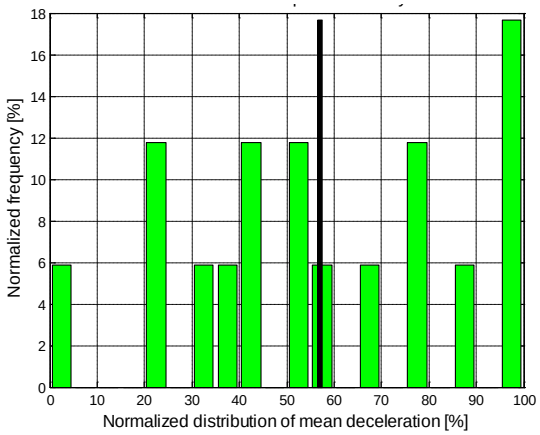

Fig 3.47 Distribution of negative event mean deceleration for the US06 cycle

Table 3.9:Normalization values for negative events distributions

Negative event metric	Normalization value
Energy [kJ]	583.30
Maximum power [kW]	62.63
Mean power [kW]	34.32
Mean velocity [m/s]	34.61
Max velocity [m/s]	34.95
Maximum deceleration [m/s^2]	-3.08
Mean deceleration [m/s^2]	-1.77

Fig 3.11 shows that for the specific driving schedule shown in this example, a large portion of the braking events is characterized by a small amount of braking energy. This is around 30% of the total number of negative events. Only a small percentage is characterized by braking energy close to the maximum available that is around 6%. This information can be coupled with the distributions describing the maximum and average negative power per event in Fig 3.12 and Fig 3.13. The analysis shows a large percentage of the braking events are characterized by a negative maximum and average power widely distributes between the minimum and the maximum values of the related variables. These trends are directly related to dynamic variables shown Fig 3.14, Fig 3.15, Fig 3.16 and Fig 3.17, characterized by a wide distribution between the minimum and the maximum values. An exception for the maximum velocity with an high density of elements close to the variable maximum value.

3.1.2.5. Traction Events Analysis

Besides the determination of the best way to store braking energy, it is important to know how to provide this energy during driving cycle progress. This is related to cycle profile and can be caught with a similar negative events analysis. In this way it is possible to create a target positive energy event with a representative maximum power and required energy. With this goal, the percentage distribution determination of the event characteristics normalized to the cycle maximum value has been obtained.

Fig 3.18 -Fig 3.24 represent the distributions over the US06 exemplary driving schedule for positive events of the energy, average velocity, maximum negative power, average negative power, maximum and average deceleration respectively.

The black line represents the value obtained with the weighted mean process in the equation (3.16)

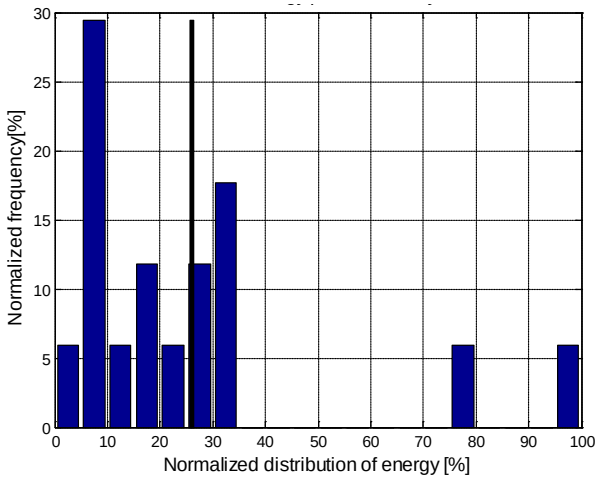

Fig 3.48 Distribution of positive event energy for the US06 cycle

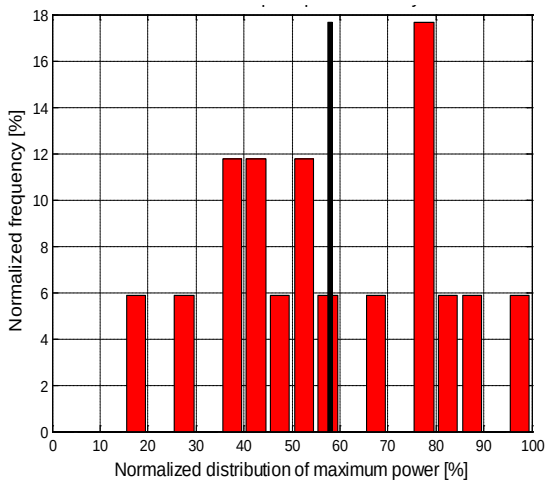

Fig 3.49 Distribution of positive event maximum power for the US06 cycle

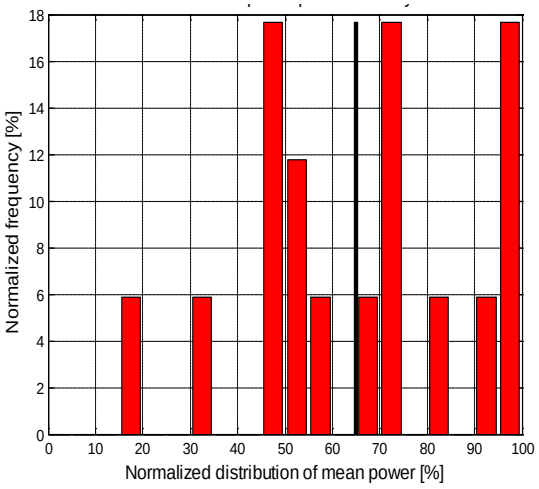

Fig 3. 50 Distribution of positive event mean power for the US06 cycle

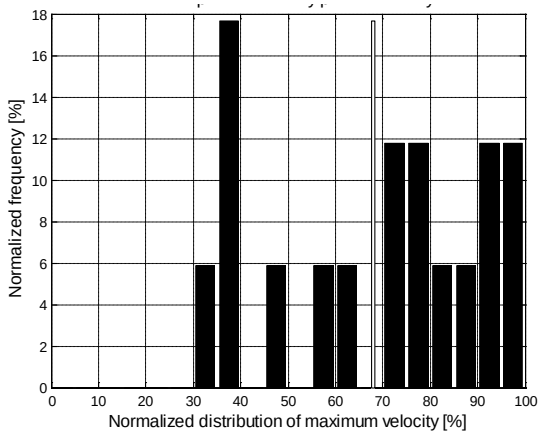

Fig 3.51 Distribution of positive event maximum velocity for the US06 cycle

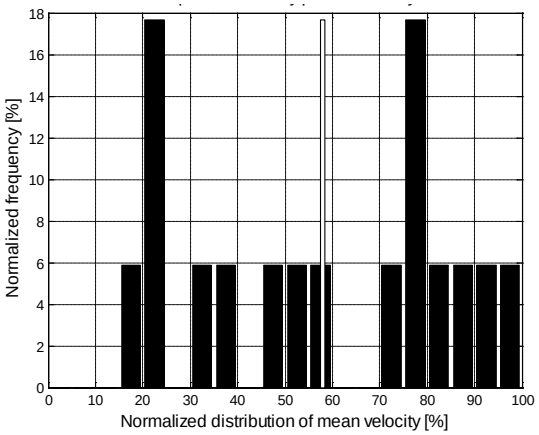

Fig 3.52 Distribution of positive event mean velocity for the US06 cycle

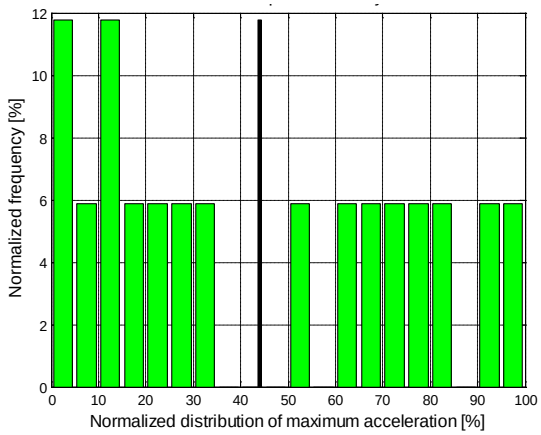

Fig 3.53 Distribution of positive event maximum acceleration for the US06 cycle

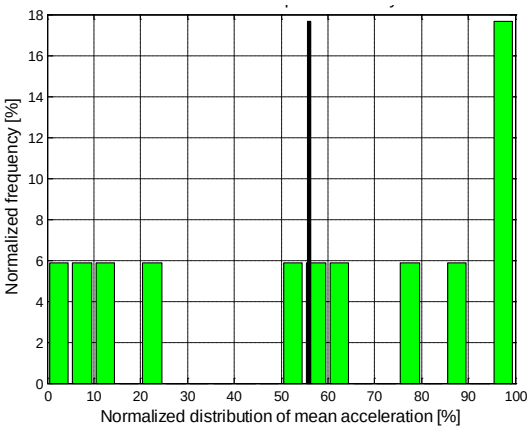

Fig 3.54 Distribution of positive event mean acceleration for the US06 cycle

Table 3.10 Normalization values for positive events distributions

Positive event metric	Normalization value
Energy [kJ]	3452.81
Maximum power [kW]	103.22
Mean power [kW]	48.42
Mean velocity [m/s]	35.11
Max velocity [m/s]	35.89
Maximum acceleration [m/s^2]	3.75
Mean acceleration [m/s^2]	1.60

Fig 3.18 shows that a very large portion of traction events are characterized by a small amount of energy: for almost 90% of events it is below 35% of the maximum energy value. Fig 3.19 - Fig 3.24 present the distribution of the average and maximum power, average and maximum velocity and average and maximum acceleration. It is possible to notice that they are widely distributed between the maximum and minimum values.

3.1.2.6. Coasting Phase

Analyzing the power equation (3.10) it is possible to notice that the power value is zero when the car is stopped or in coasting phase. During the coasting phase no external power is applied and the vehicle is subject just to dissipative forces that depend on vehicle velocity, as the aerodynamic and friction forces. Although the vehicle is decelerating, no braking power is exercised by the driver. Therefore it is not possible to recover energy.

Since the power profile derives from the velocity profile, this process causes the assumption of absence of coasting phases. However these phases must be accounted for in order to get the real amount of recoverable energy.

Since during coasting phase the vehicle naturally decelerates, every non-coasting braking phase can be identified by deceleration values comparison. Using the elementary equation that describes the longitudinal dynamics it is possible to evaluate the coasting deceleration imposing a zero external force, $F_t = 0$.

$$\frac{dV(t)}{dt} = -\frac{\left(F_r + F_g + F_a\right)}{m_v} \tag{3.17}$$

Considering that in this analysis F_g is zero, all the terms in equation (3.17) depend on vehicle velocity. In particular, the aerodynamic force depends on square velocity and the rolling force is linearly dependent to vehicle speed. Hence, this is a non linear

differential equation, whose solution allows one to identify the presence of coasting phases during the cycle. After the identification of vehicle decelerating phases in the cycle, it is possible to compare the cycle vehicle deceleration profiles with the theoretical vehicle coasting deceleration during these phases. The theoretical vehicle coasting deceleration profiles are obtained by solving equation (3.17). The effective vehicle coasting phases during the cycle are individuated when the cycle vehicle deceleration profile is equal to the theoretical coasting deceleration profile.

In the figure below it is possible to notice that excluding the energy related to coasting phase causes a small energy distribution variation and the energy weighted mean value change.

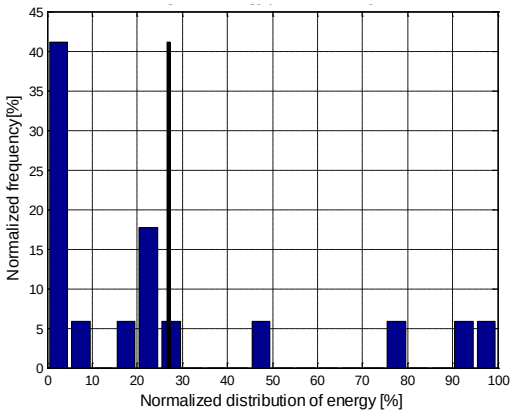

Fig 3.55 Distribution of negative event energy for the US06 cycle

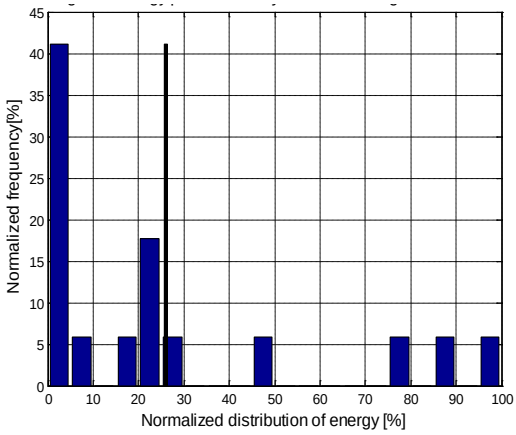

Fig 3.56 Distribution of negative event energy with coasting energy exclusion for the US06 cycle

As it is possible to notice analyzing the graphs above, the braking available energy that can be recovered has a similar trend considering or not the coasting phase. This can be explain because usually the driver alternates acceleration phases with braking phases, and coasting periods are limited. Even if the coasting phases are not so relevant in US06 cycle, it causes an energy weighted mean value change represented by the black vertical bar. The value change is about 2%.

The coasting phases analysis have to be evaluated in several different driving patterns. It is expected that this phase duration changes depending on the vehicle speed and on the traffic conditions. Indeed from these two factors mainly depends the driving style.

The reference value that can be used to evaluate the coasting phase importance is the theoretical recoverable energy. Three different patterns have been analyzed: urban, highway and freeway in traffic and no traffic conditions (Table 3.1). For every case

three random cycles have been chosen from an amount of fifty cycles and below are reported the percent differences of available energy obtained excluding or not the coasting energy phases. In Table 3.6 the results are reported.

Table 3.11 Percent values of available braking energy that has to be excluded because of coasting phase

Urban[%]		**Highway[%]**		**Freeway[%]**	
Traffic	**Non Traffic**	**Traffic**	**Non Traffic**	**Traffic**	**Non Traffic**
1.87	1.48	2.1	4	2.4	3.23
2.18	1.57	2.49	3.90	2.67	4.1
1.94	2.22	2.15	2.85	2.39	6.3
Mean value[%]					
1.99	1.76	2.25	3.58	2.49	4.54

Observing the mean values for every case, the results confirm our expectations. The coasting phases have great variations depending on the pattern and it is possible to identify a trend. In urban conditions the driver mainly alternates braking phases with accelerating phases, then the coasting phases are short and almost not depending on traffic conditions. On highways and freeways coasting periods, the frequencies are higher and the traffic conditions influence is greater because it causes significant velocity variations and driving style variations.

Observing Table 3.6, it is possible to notice that the influence of coasting phase is usually limited and it is possible to account for it during braking energy calculation simply, by introducing an efficiency term.

3.1.2.7. Synthetic Cycle Statistically Relevant Events

The scope of this analysis is the determination of a “statistically” relevant event in order to be able that represent the entire cycle, from the point of view of the energy storage system design. Every event is composed by the representative metrics values: energy, maximum power, mean power, mean deceleration, maximum deceleration and mean velocity.

The most intuitive way to create the target event is to use the mean value of each of the above metrics across all the events with the equation (3.15). On the other hand, a possible target event can be obtained with the maximum values of each metric above

across all the events. This would define a “worst-case” scenario, which is typically adopted when sizing the battery pack of HEVs [22].

A different way to define the representative event is to calculate a weighted average of the variables of each cycle event by using as weights the values of occurrences in the equation (3.16).It is clear that the calculation of the weighted average of the variables can be performed with a different distribution of weights, obtained in a way that is significant for the design. In particular, one could put more emphasis on the distribution of a specific variable of the cycle and use weights from this distribution to calculate also the other representative events. This way it is possible to calculate the weighted average values of the variables by means of weights of the average and the maximum power per event.

The methods used in Table 3.7 to determine a “statistically” relevant event are summarized:

- Mean values method: every value is obtained as the all events values average (equation 3.15);
- Weighted mean method: every value is obtained by means of the weighted mean where the weights are the number of occurrences (equation 3.16);
- Maximum values method: every value is equal to the maximum value among all the events;
- Weighted mean method with Mean Power distribution: the Mean Power distribution is used as weight to calculate the weighted mean for all the quantities (equation 3.16);
- Weighted mean method with Maximum power distribution: the Maximum Power distribution is used as weight to calculate the weighted mean for all the quantities (equation 3.16);

In Table 3.7 the methods above have been used to determine the “statistically” relevant event for the US06 cycle.

Table 3.12:List of "statistically" relevant applied to the US06 cycle

	Weighted mean	Mean values	Maximum values	Weighted mean with Mean Power distribution	Weighted mean with Maximum Power distribution
Energy [KJ]	157.49	133.67	583.30	285.82	265.65
Maximum power [KW]	27.56	26.41	62.63	30.69	27.56
Mean power [KW]	13.90	12.06	28.37	13.90	12.48
Mean deceleration [m/s^2]	-0.95	-0.96	-1.77	-0.86	-0.78
Max deceleration [m/s^2]	-1.63	-1.62	-3.09	-1.51	-1.36
Mean velocity [m/s]	20.08	20.01	34.61	16.96	15.23
Maximum velocity [m/s]	23.07	23.86	34.96	17.13	15.38

Each of the representative events is a potential design input for the sizing of the vehicle energy storage system. Among them, it is possible to notice that the event based on maximum values method represent the worst-case scenario and their values differs substantially from the others representative events values. A design based on a maximum power case is expected to lead to components whose size and weight differ extremely from the designs based on the other statistically relevant events.

3.2 Vehicle Mass Sensitivity Study

In this section, the driving cycle analysis tool is applied to conduct a sensitivity study related to vehicle frontal area and mass. Two testing cases are created: in the first one both frontal area and mass are varied, while in the second one only the mass is subject to variation. The testing cycle is the US06 driving cycle. Then, this sensitivity analysis is extended to more regulatory cycles and to "real world" cycles (Table 3.1).

3.2.1. Vehicle Mass Sensitivity Study on US06 Driving Cycle

The analysis performed in the previous section was relative to a specific vehicle, characterized by three parameters:

- A_f, vehicle frontal area;
- C_v, drag coefficient, a dimensionless quantity that quantify the car drag resistance in air;
- M_v, vehicle mass.

A sensitivity study is useful to observe how a change in the vehicle parameters can influence the analysis results and the representative cycle metrics determination.
This analysis has been done with two different vehicle configurations: in the first case a variation of both frontal area and mass is assumed, in the second just the vehicle mass is changing. For each case five vehicle configurations are considered.

a) Case I

   Vehicle mass: the standard vehicle mass is assumed to be 1900 Kg and the mass variation for the sensitivity study is -15%,-10%, +10%,+15%.

Table3. 13:vehicle mass variations for Case I

Vehicle mass variations					
	-15%	-10%,	Standard mass	+10%	+15%
Vehicle mass [Kg]	1615	1710	1900	2090	2185

Vehicle frontal area A_f: in this case the frontal area value is variable. Using three vehicle models frontal areas and masses as references, reported in Table 3.9, a function is created. In this way it is possible to correlate the previously determined mass values, (Table3. 8) to a realistic frontal area value. Every mass is associated with only one frontal area. The main characteristics of the three vehicles considered for this correlation function are reported in Table 3.9:

Table 3.14: mass and frontal area of vehicle categories for case I

Vehicle categories-Case I			
	City car	**Midsize SUV**	**Truck**
Mass [kg]	900	1900	2800
Frontal area $[m^2]$	1.8	2.86	3.15

The final vehicle configurations for this sensitivity mass study are reported in Table 3.10.

Table 3.15: vehicle configurations for Case I

Vehicle configurations					
Set up #	*1*	*2*	*3*	*4*	*5*
Mass [Kg]	1615	1710	1900	2090	2185
Frontal area [m^2]	2.56	2.66	2.86	2.92	2.95

b) Case II

Vehicle mass: vehicle mass values are the same reported in Table3. 8

Vehicle frontal area A_f: in this case the frontal area value is constant. The vehicle frontal area is assumed to be constant and not changing with the vehicle mass. For this case an average value of the vehicles frontal area considered in Table 3.9 is assumed. The vehicle categories for this analyzed case are reported in Table 3.11

Table 3.16: vehicle configurations for Case II

Vehicle configurations					
Set up #	*1*	*2*	*3*	*4*	*5*
Mass [Kg]	1615	1710	1900	2090	2185
Frontal area [m^2]	2.76	2.76	2.76	2.76	2.76

The drag coefficient was assumed constant and equal to $C_v = 0.42$.

In both cases, the cycle characteristic event for the braking phase is obtained for each vehicle configuration by means of the weighted average method (equation 3.16). In this analysis the weighted average method is used considering three different distributions, namely weighted average method where each variable has his own distribution, weighted average method with maximum power distribution and weighted mean method with mean power distribution.
The results of this analysis reported in table are presented in two ways:

- Absolute values: each event metric is reported in absolute value;
- Sensitivity calculation S_x^y: each event metric value is calculated using the following equation:

$$S_x^y = \frac{\Delta y / y_0}{\Delta x / x_0} \tag{3.18}$$

where x is the vehicle parameter respect which we want to evaluate the sensibility of the metric y. The parameter value x_0 is defined as the standard initial value. The variable y_0 is the value of the considered metric for the parameter value x_0. In this case Δy is the metric value variation expressed as the difference between the value of y and y_0. It is also defined Δx as the difference between a specific value of x and x_0.

3.2.1.1 First Case Analysis

In the case I both vehicle mass and frontal area are changing as reported in Table 3.10. The power profile based on US06 driving cycle changes depending on vehicle mass and frontal area set up. In Fig 3.27 these profiles are shown.

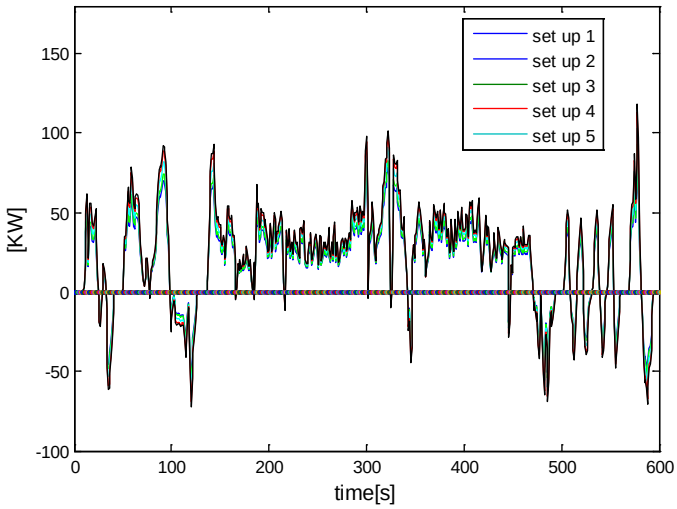

Fig 3.57 Power profiles depending on vehicle mass value for the US06 cycle.

Since the inertial force and rolling resistance force depend on vehicle mass and the aerodynamic force depends on frontal area, the power vs. time profile is different for each case.

a) Braking Phase Relevant Event

In this sensitivity analysis, considering each vehicle mass value, it is possible to obtain cycle representative events by means of the weighted average method (equation 3.16) using three different distributions. In fact each metric value can be obtained using its own distribution, the maximum power distribution and mean power distribution.

For each evaluating method both the metric absolute values and metric values obtained by means of the sensitivity equation (3.18) are reported.

Since the sensitivity study is mainly related to the vehicle mass variation, the sensitivity calculation is done taking into account the event metric values variations in relation with vehicle mass changes. So, considering the aforementioned equation, the vehicle parameter x values are vehicle masses.

In the tables below, the absolute values of the representative events metrics and calculated by means of equations (3.18) are reported for all the aforementioned cycle characteristic events:

- Table 3.12 and Table 3.13: in these charts every value is obtained with the weighted mean method using the own distribution for each metric

Table 3.17: sensitivity analysis results expressed as absolute values (data from the US06 cycle)

Weighted mean method values					
Mass variation	*-15%*	*-10%*	*0% (1900 kg)*	*+10%*	*+15%*
Frontal area [m^2]	*2.56*	*2.66*	*2.86*	*2.92*	*2.95*
Energy [kJ]	130.87	139.70	157.45	165.23	174.93
Maximum power [kW]	23.39	24.78	27.57	31.76	29.62
Mean power [kW]	11.42	12.10	13.90	14.72	15.74
Mean deceleration [m/s^2]	-0.98	-0.96	-0.95	-0.94	-0.97
Max deceleration [m/s^2]	-1.66	-1.63	-1.63	-1.57	-1.57
Mean velocity [m/s]	18.72	20.07	20.07	20.33	20.31
Max velocity [m/s]	22.66	23.36	23.07	23.07	23.42

Table 3.18: sensitivity analysis results expressed as relative variations (data from the US06 cycle)

Weighted mean method values					
Mass variation	*-15%*	*-10%*	*0% (1900 kg)*	*+10%*	*+15%*
Frontal area [m^2]	*2.56*	*2.66*	*2.86*	*2.92*	*2.95*
Energy	1.12	1.12		0.50	0.74
Maximum power	1.01	1.01		1.52	0.50
Mean power	1.19	1.29		0.59	0.88
Mean deceleration	-0.21	-0.10		-0.11	0.14
Max deceleration	-0.12	0.00		-0.37	-0.25
Mean velocity	0.45	0.00		0.13	0.08
Max velocity	0.12	-0.13		0.00	0.10

- Table 3.14 and Table 3.15: in these charts every value is obtained using the weighted average method using as weights the Mean Power distribution

Table 3.19: sensitivity analysis results expressed as absolute values (data from the US06 cycle)

Weighted mean method with Mean Power distribution					
Mass variation	*-15%*	*-10%*	*0% (1900 kg)*	*+10%*	*+15%*
Frontal area [m^2]	*2.56*	*2.66*	*2.86*	*2.92*	*2.95*
Energy [kJ]	227.80	243.19	285.82	310.64	335.87
Maximum power [kW]	24.98	26.46	30.69	32.45	36.68
Mean power [kW]	11.42	12.10	13.90	14.72	15.74
Mean deceleration [m/s^2]	-0.84	-0.84	-0.86	-0.83	-0.85
Max deceleration [m/s^2]	-1.45	-1.45	-1.51	-1.45	-1.48
Mean velocity [m/s]	16.29	16.27	16.96	16.20	16.52
Max velocity [m/s]	16.38	16.38	17.13	16.43	16.53

Table 3.20: sensitivity analysis results expressed as relative variations (data from the US06 cycle)

Weighted mean method with Mean Power distribution					
Mass variation	*-15%*	*-10%*	*0% (1900 kg)*	*+10%*	*+15%*
Frontal area	*2.56*	*2.66*	*2.86*	*2.92*	*2.95*
Energy	1.35	1.49		0.87	1.17
Maximum power	1.24	1.37		0.57	1.30
Mean power	1.19	1.29		0.59	0.88
Mean deceleration	0.15	0.23		-0.35	-0.08
Max deceleration	0.26	0.40		-0.40	-0.13
Mean velocity	0.26	0.41		-0.45	-0.17
Max velocity	0.29	0.44		-0.41	-0.23

- Table 3.16 and Table 3.17 : in these charts every value is obtained using the weighted mean method using as weights the Maximum power distribution

Table 3.21: sensitivity analysis results expressed as absolute values(data from the US06 cycle)

Weighted mean method with Maximum power distribution					
Mass variation	*-15%*	*-10%*	*0% (1900 kg)*	*+10%*	*+15%*
Frontal area [m^2]	*2.56*	*2.66*	*2.86*	*2.92*	*2.95*
Energy [kJ]	213.26	227.66	256.59	304.03	286.88
Maximum power [kW]	23.38	24.78	27.55	31.76	29.62
Mean power [kW]	10.69	11.33	12.48	14.40	13.44
Mean deceleration [m/s^2]	-0.79	-0.79	-0.78	-0.81	-0.72
Max deceleration [m/s^2]	-1.35	-1.36	-1.36	-1.42	-1.26
Mean velocity [m/s]	15.25	15.23	15.23	15.85	14.11
Max velocity [m/s]	15.34	15.34	15.38	16.08	14.33

Table 3.22: sensitivity analysis results expressed as relative variations(data from the US06 cycle)

Weighted mean method with Maximum power distribution					
Mass variation	*-15%*	*-10%*	*0% (1900 kg)*	*+10%*	*+15%*
Frontal area	*2.56*	*2.66*	*2.86*	*2.92*	*2.95*
Energy	1.12	1.12		1.85	0.79
Maximum power	1.01	1.00		1.53	0.50
Mean power	0.96	0.92		1.54	0.51
Mean deceleration	-0.09	-0.13		0.39	-0.51
Max deceleration	0.05	0.00		0.44	-0.49
Mean velocity	-0.01	0.00		0.41	-0.49
Max velocity	0.02	0.03		0.46	-0.46

For every cycle three different methods have been used to evaluate the characteristic quantities values variations depending on vehicle mass. A comparison of the values obtained by means of the three different methods is useful to evaluate their sensibility to mass variation. The values in the charts from Table 3.12 to Table 3.17 are graphically compared from Fig 3.28 to Fig 3.41.

Below, from Fig 3.28 to Fig 3.34 the characteristic events metrics in absolute values have been graphically compared. The reference charts are Table 3.12, Table 3.14 and Table 3.16.

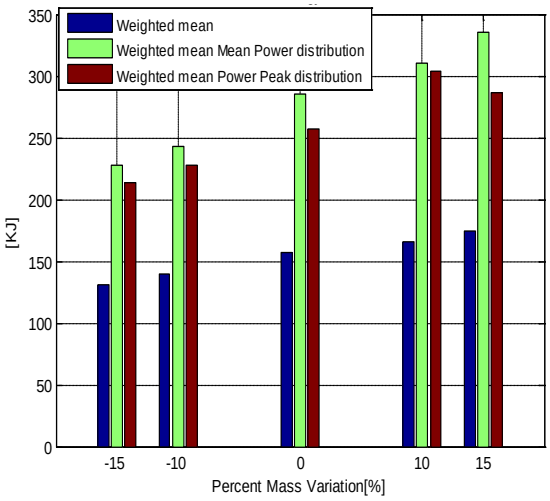

Fig 3.58 Energy values

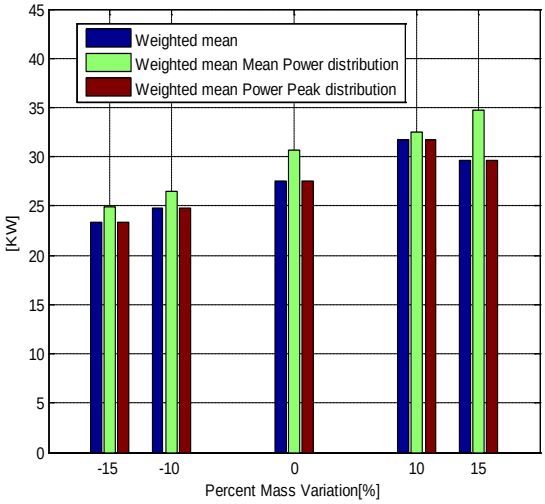

Fig 3.59 Maximum power values

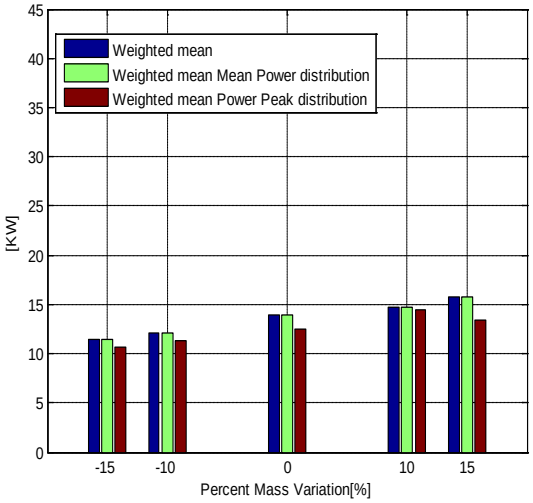

Fig 3.60 Mean power values

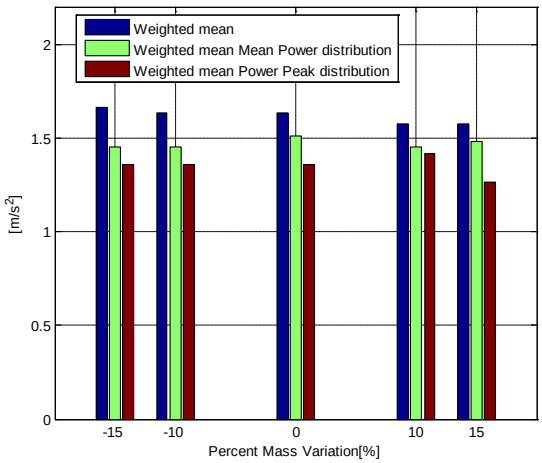

Fig 3.61 Maximum deceleration values

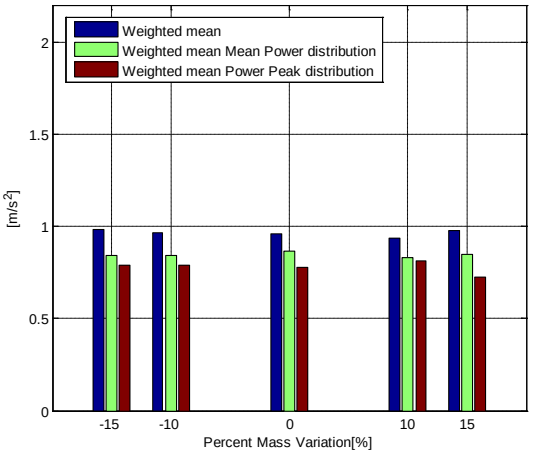

Fig3. 62 Mean deceleration values

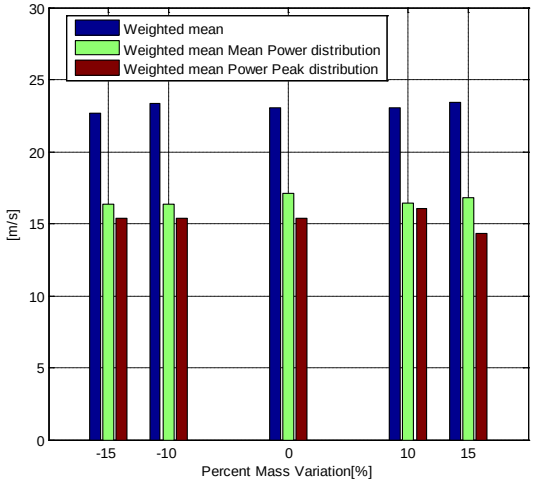

Fig 3.63 Maximum velocity values

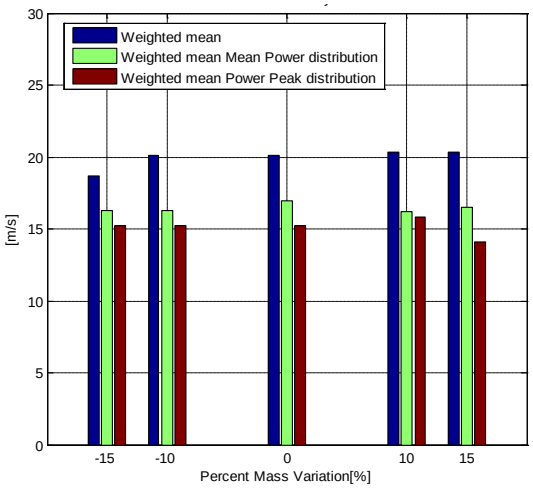

Fig 3.64 Mean velocity values

In the figures above it is possible to notice that the energy, power, velocity and acceleration values depending on vehicle parameters changes. It is possible to notice how these changes have bigger consequences on energy-related metric than the others. This is due to the fact that the analysis begins from a driving cycle profile and the events identification is based on the relative power profile. The vehicle parameters change modifies this power profile, by increasing /decreasing the vehicle net power required to follow the velocity profile, but the velocity profile is always unchanged. The representative values of velocity and acceleration change if the power profile modification causes variation in the events identification. In other terms, if a vehicle traction phase becomes a braking phase or vice versa because of parameters variation.

While energy and power are more affected by small parameters change, from Fig 3.28 to Fig 3.30, velocity and acceleration values are usually slightly affected respect the energy-related metrics variations.

Below, from Fig 3.35 to Fig 3.41 the characteristic events metrics obtained by means of the equation (3.16) have been graphically compared. The reference charts are Table 3.13, Table3.15 and Table 3.17.

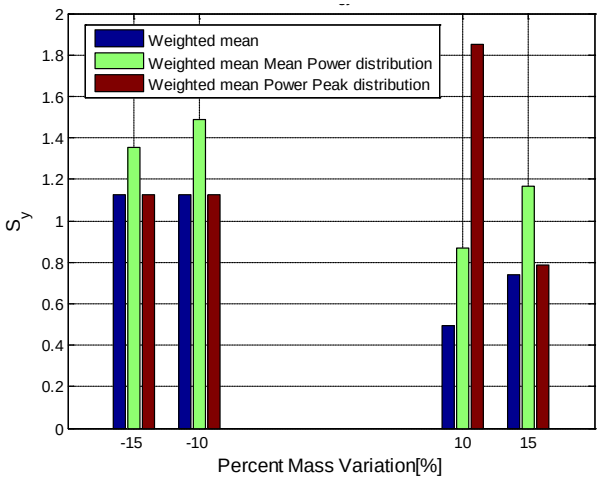

Fig 3.65: Energy values

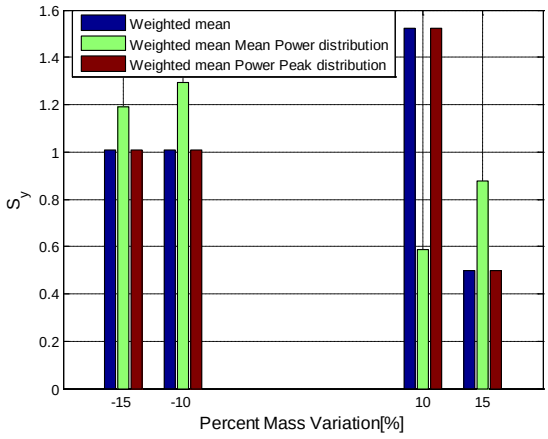

Fig 3.66: Maximum power values

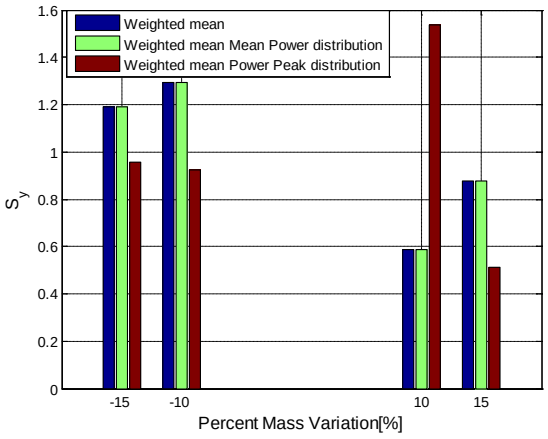

Fig 3.67: Mean power values

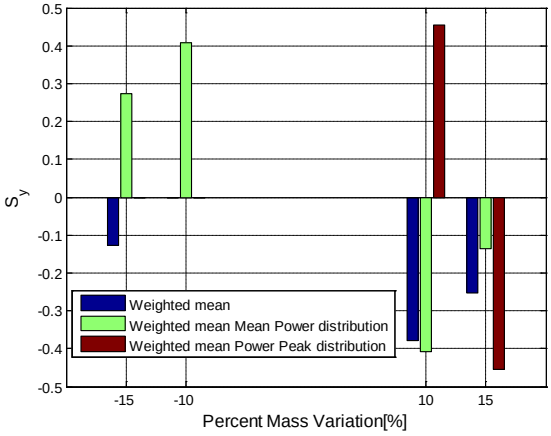

Fig 3.68: Maximum deceleration values

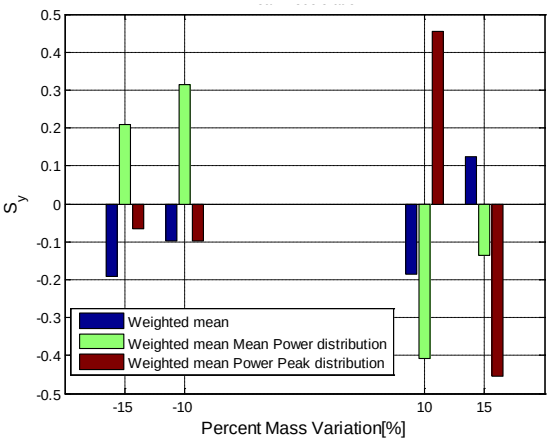

Fig 3.69: Mean deceleration values

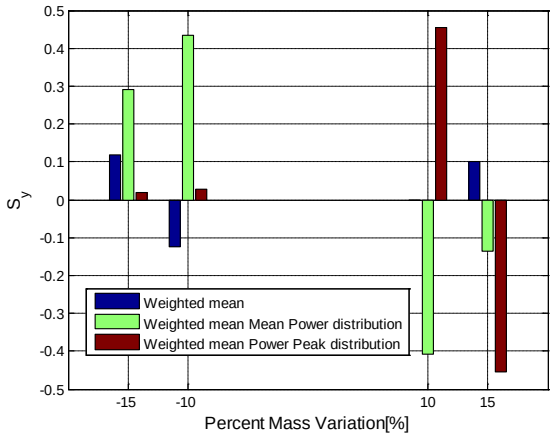

Fig 3.70: Maximum velocity values

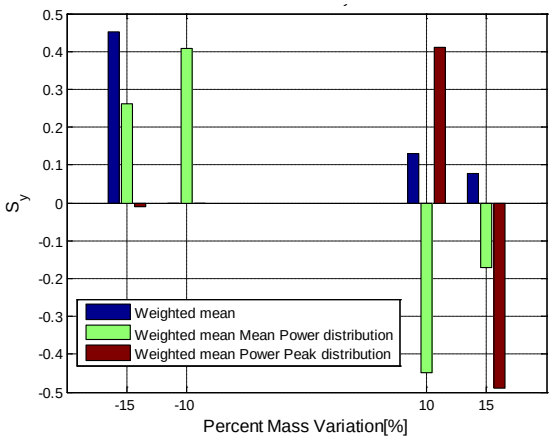

Fig 3.71: Mean velocity values

By analyzing Fig 3.28 and Fig 3.35 it is possible to notice how the vehicle parameters changes influence the energy value. Its weighted average trend is what expected: increasing energy values as mass increases. To evaluate the weighted mean with maximum power distribution and mean power distribution is necessary to refer to weighted mean of maximum power, Fig 3.29 and Fig 3.36 and mean power, Fig 3.30 and Fig 3.37. In fact, during the mass variation from 10% to 15% the maximum power absolute value decreases since the sensitivity to variation is smaller.

b) Power and Energy Data Analysis in the Cycle

By analyzing the power profile in Fig 3.27, it is possible to notice profile variations depending on mass and frontal area values. This is because both inertial force and dissipative forces are related to the vehicle mass and frontal area. The calculation of the requested traction energy and braking energy is obtained respectively as the integral of the positive power and negative power in the cycle. Hence, it is expected that both the cycle total braking energy and the cycle total requested positive energy are subjected to variations if the vehicle parameters change. In the figures below, it is possible to analyze the affect of mass variation and related frontal area on the total braking energy and total traction energy.

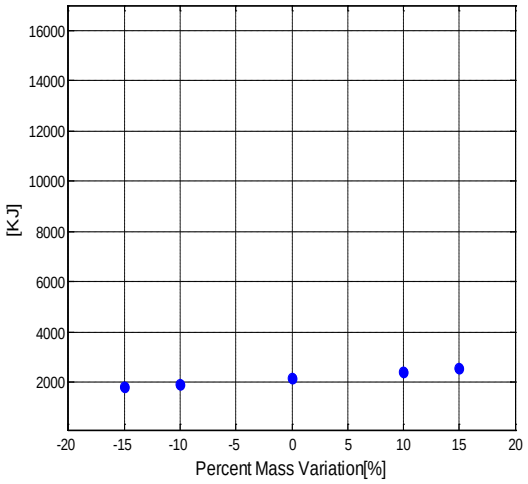

Fig 3.72 Total braking energy trend depending on mass variation and related frontal area

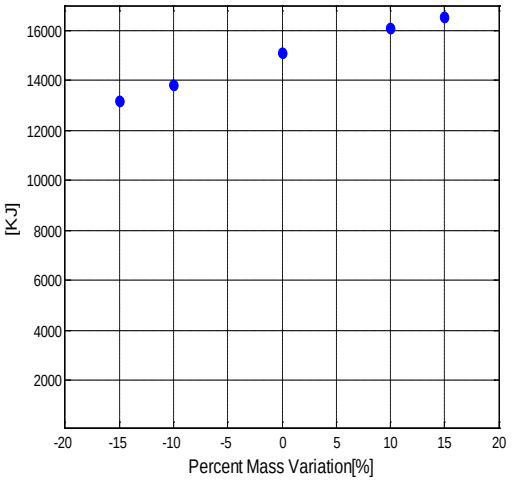

Fig 3.73 Total traction energy trend depending on mass variation and related frontal area

In the figures above, it is shown that as the vehicle mass increases, in a logical way also the cycle total braking power and cycle total requested traction energy increase their values.

- Power terms trend

A change in the vehicle mass M_v or frontal area A_f, directly influences the aerodynamic power(P_a), rolling power(P_r) and inertia power (P_i), according to their definitions, reported below:

$$P_a = \frac{1}{2} A_f \rho_a C_d V^3 \tag{3.19}$$

$$P_r = C_r g M_v \cos(\alpha)\, V \tag{3.20}$$

$$P_i = M_v \frac{dV(t)}{dt} V \tag{3.21}$$

$$P_t = P_i + P_r + P_a \tag{3.22}$$

Using the previous equations, it is possible to verify how the vehicle mass and frontal area changes can influence the P_a, P_r, P_i trends during an exemplary vehicle braking phase. The values of percent mass variation and frontal area values assumed are reported in Table 3.10. For the calculation of the power terms in above equations, it is necessary to set an initial braking phase velocity and deceleration. For this example it is

possible to set these values equal to the weighted mean maximum velocity and maximum deceleration values from Table 3.12. In Table 3.18 the values adopted for this exemplary calculation are listed.

Table 3.23: values adopted for this exemplary braking phase

Weighted mean method values					
Mass variation	*-15%*	*-10%*	*0% (1900 kg)*	*+10%*	*+15%*
Frontal area [m^2]	*2.56*	*2.66*	*2.86*	*2.92*	*2.95*
Max deceleration [m/s^2]	-1.66	-1.63	-1.63	-1.57	-1.57
Max velocity [m/s]	22.66	23.36	23.07	23.07	23.42

In Fig 3.44 each power term trend depending on vehicle configuration is shown.

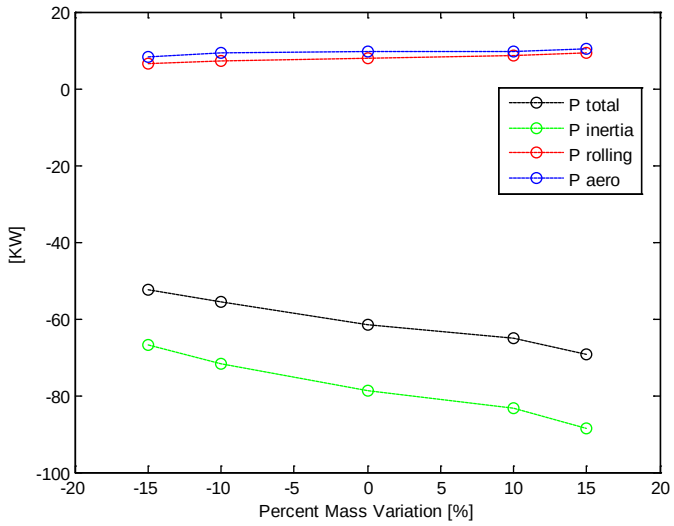

Fig 3.74 Power values varying vehicle mass and frontal area

From the figure above it is possible to notice that P_r and P_i are directly influenced by mass change: as it increase also the inertial power and the rolling power increase.

P_a depends just on frontal area values changes: since they are not big also the power trend is almost constant.

In accordance with these results it is possible to observe in Fig 3.42 that the total braking energy that is theoretically recoverable increases with the weight.

c) Braking Phase

In Fig 3.27 the power profiles variation depending on the vehicles parameters have been shown. Since the braking and traction events identification is based on the power profile, power profile variation directly influences the identification process. Then, also

the event related metrics values are subject to change. The statistically relevant braking events are influence by mass and frontal area variation depending on the synthesis method used (Table 3.12, Table 3.14 and Table 3.16). A useful sensitivity evaluation can be done graphically comparing some characteristic quantities of the braking phase representative events.

The used synthesis methods are: average values method (equation 3.15), weighted average method (equation 3.16), weighted average method with mean power distribution and weighted average method with maximum power distribution. From Fig 3.45 to Fig 3.48 two fundamental data are compared: maximum braking power and braking energy. From Fig 3.49 to Fig 3.52 two metrics are compared: maximum deceleration and maximum braking power. From Fig 3.53 to Fig 3.56 the average velocity and braking energy are compared.

- Mean braking power vs. Braking energy

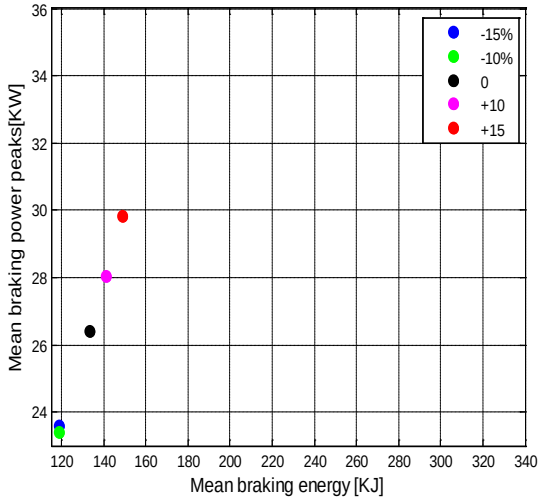

Fig 3.75 Comparison between Mean Maximum braking power and Mean Braking Energy

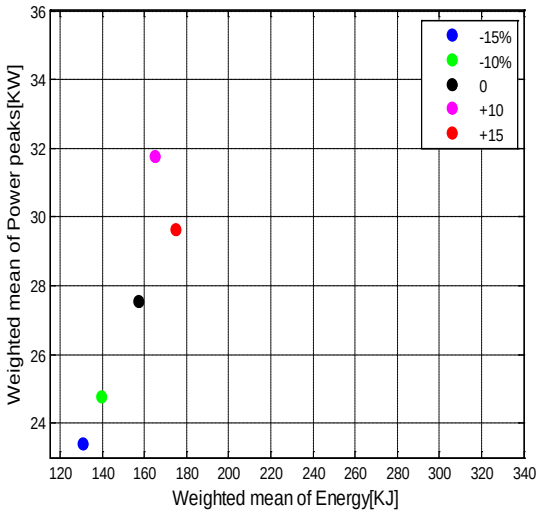

Fig3. 76 Comparison between Weighted mean of Maximum braking power and Weighted mean of Braking Energy

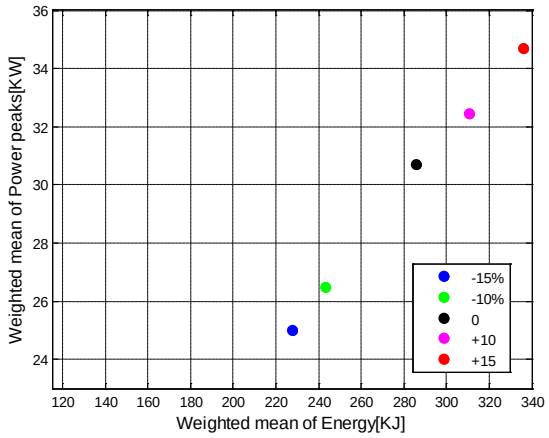

Fig 3.77 Comparison between Weighted mean of Maximum braking power and Weighted mean of Braking Energy with mean power distribution

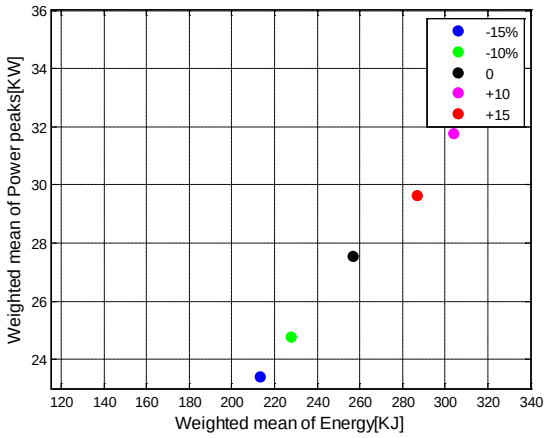

Fig 3.78 Comparison between Weighted mean of Maximum braking power and Weighted mean of Braking Energy with maximum powers distribution

- Maximum deceleration vs. Maximum braking power

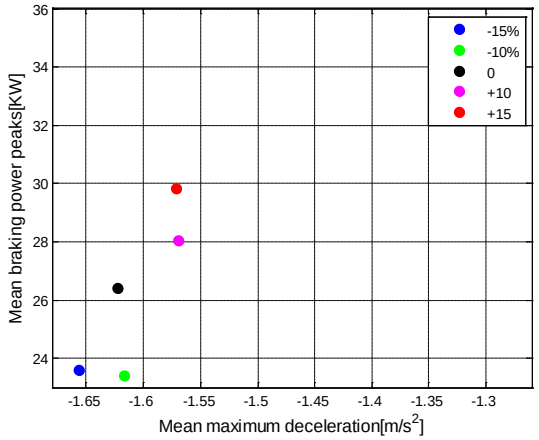

Fig 3.79 Comparison between Mean Maximum deceleration and Mean Maximum braking power

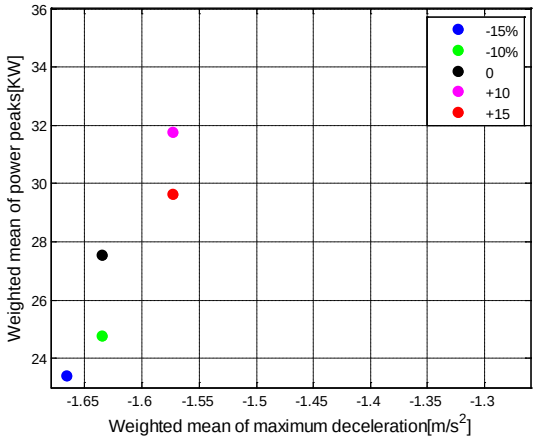

Fig 3.80 Comparison between Weighted mean of Maximum deceleration and Weighted mean of Maximum braking power

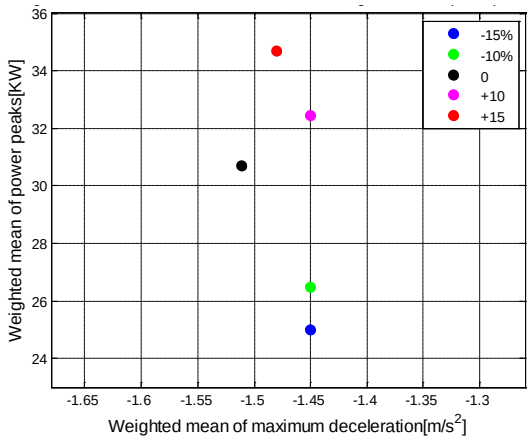

Fig 3.81 Comparison between Weighted mean of

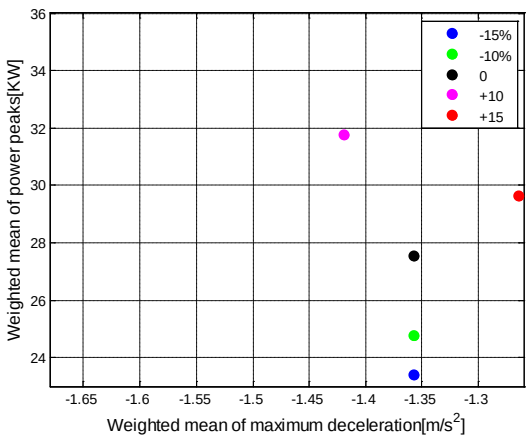

Fig 3.82 Comparison between Weighted mean of

Maximum deceleration and Weighted mean of Maximum braking power with mean power distribution

Maximum deceleration and Weighted mean of Maximum braking power with maximum power distribution

- Average velocity vs. Braking energy

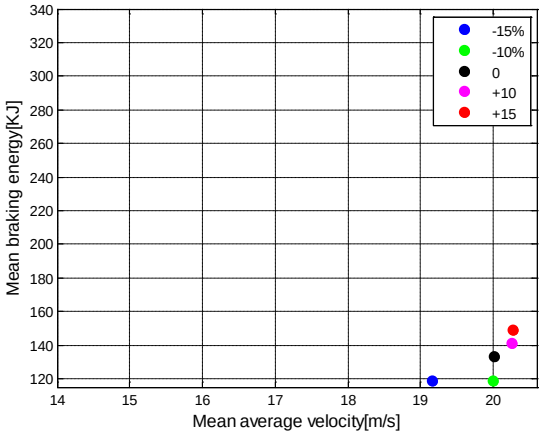

Fig 3.83 Comparison between Mean Average velocity and Mean Braking energy

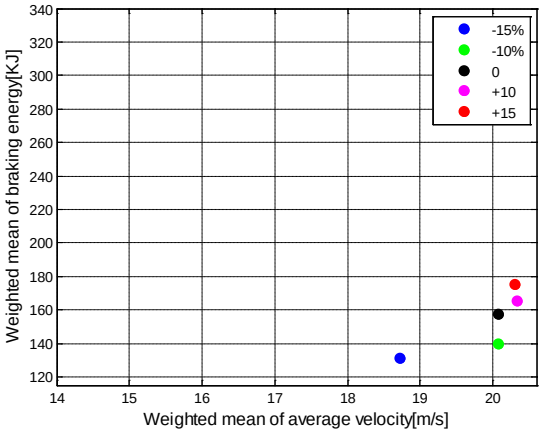

Fig 3.84 Comparison between Weighted mean of Average velocity and Weighted mean of Braking energy

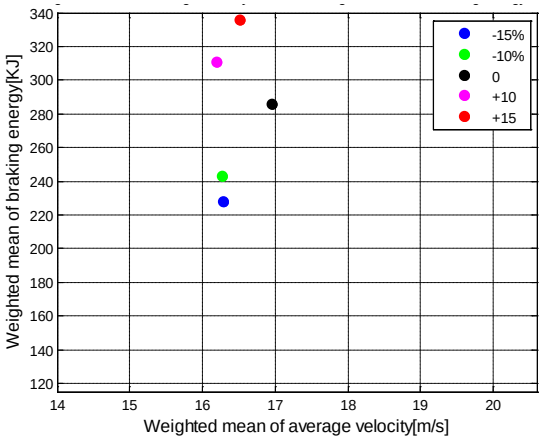

Fig 3.85 Comparison between Weighted mean of Average velocity and Weighted mean of Braking energy with mean power distribution

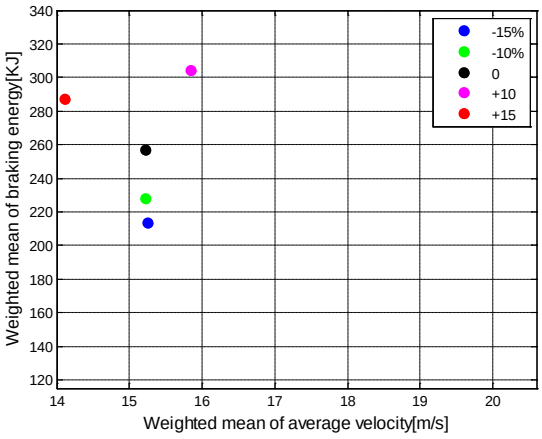

Fig 3.86 Comparison between Weighted mean of Average velocity and Weighted mean of Braking energy with maximum power distribution

d) Traction Phase

In the previous paragraph some important metrics of braking phase representative events have been graphically compared. In this part, the same comparison is done for the cycle traction phase representative event. These events have been defined by means of the same synthesis methods used for the braking phase.

From Fig 3.57 to Fig 3.60 two fundamental metrics are compared: maximum traction power and traction energy. From Fig 3.61 to Fig 3.64 maximum acceleration and maximum traction power are compared. From Fig 3.65 to Fig 3.68 the average velocity and traction energy are compared.

- Mean traction power vs. Traction energy

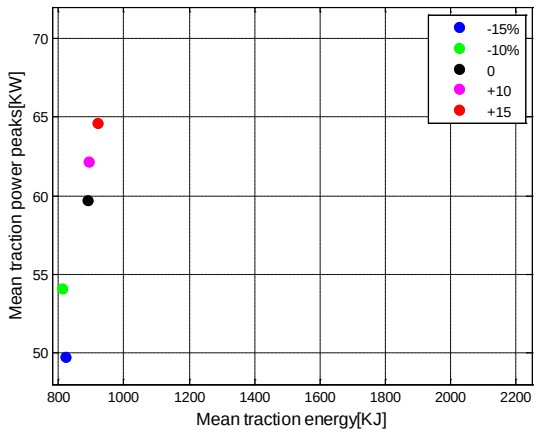

Fig 3.87 Comparison between Mean Maximum traction power and Mean Traction energy

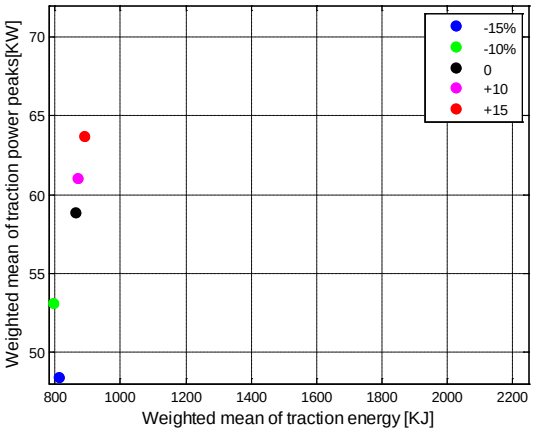

Fig 3.88 Comparison between Weighted mean of Maximum traction power and Weighted mean of Traction energy

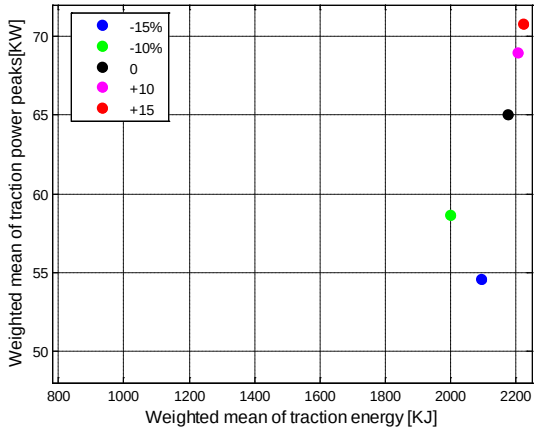

Fig 3.89 Comparison between Weighted mean of Maximum traction power and Weighted mean of Traction energy with mean power distribution

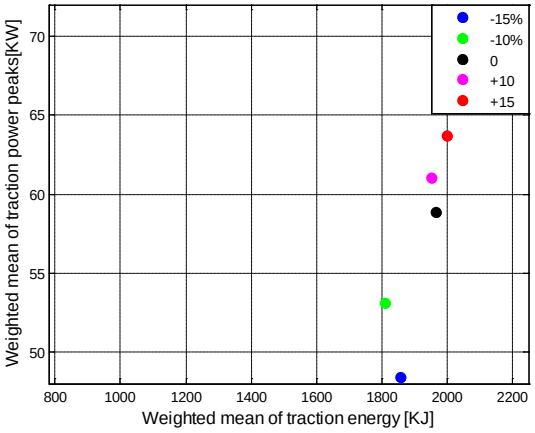

Fig 3.90 Comparison between Weighted mean of Maximum traction power and Weighted mean of Traction energy with maximum power distribution

- Maximum acceleration vs. Maximum traction power

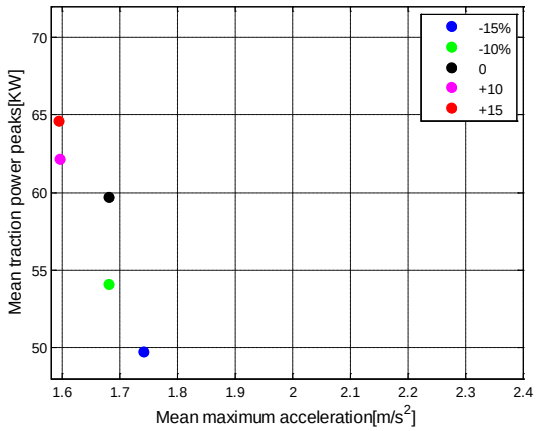

Fig 3.91 Comparison between Mean Maximum acceleration and Mean Maximum traction power

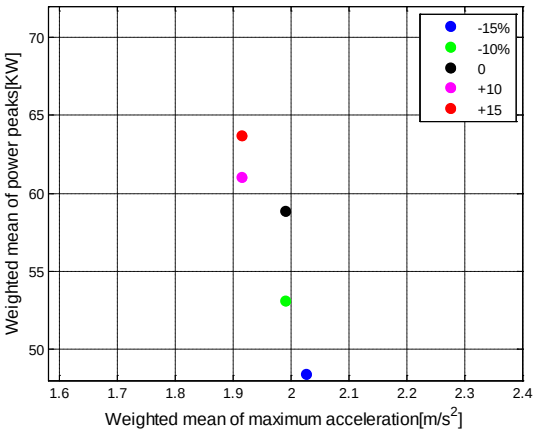

Fig 3. 92 Comparison between Weighted mean of Maximum acceleration and Weighted mean of Maximum traction power

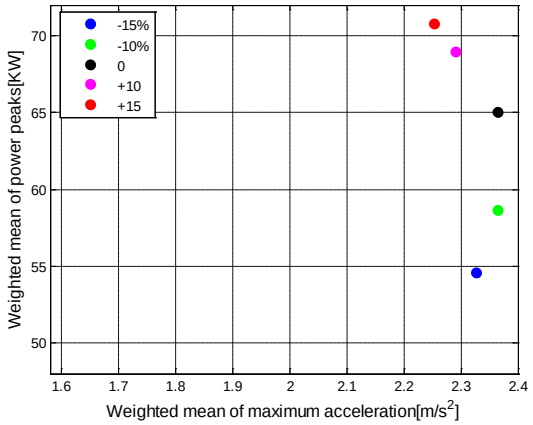

Fig 3.93 Comparison between Weighted mean of Maximum acceleration and Weighted mean of Maximum traction power with mean power distribution

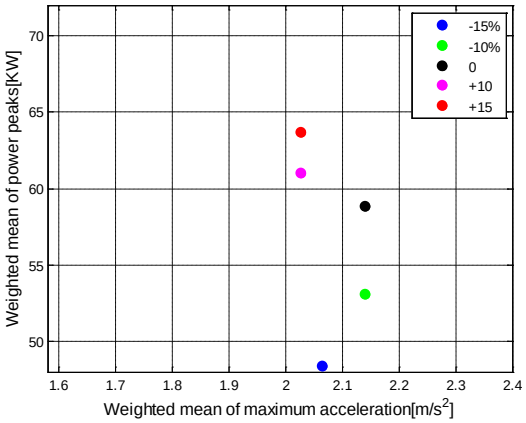

Fig 3.94 Comparison between Weighted mean of Maximum acceleration and Weighted mean of Maximum traction power with maximum power distribution

- Average velocity vs. Traction energy

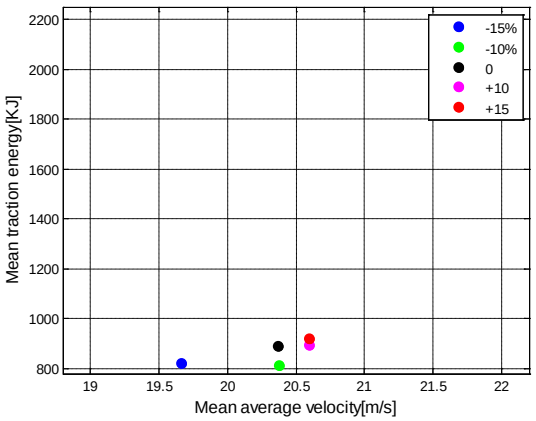

Fig 3.95 Comparison between Mean Average velocity and Mean Traction energy

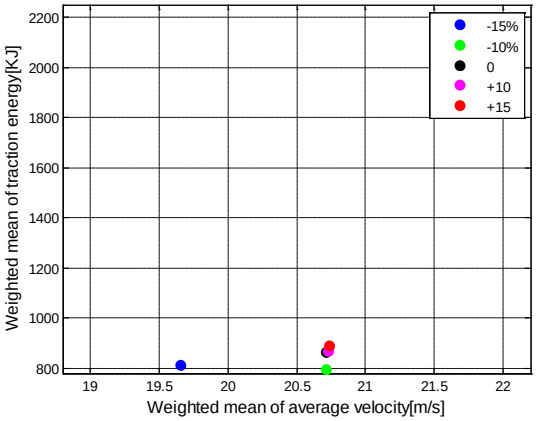

Fig 3.96 Comparison between Weighted mean of Average velocity - Weighted mean of Traction energy

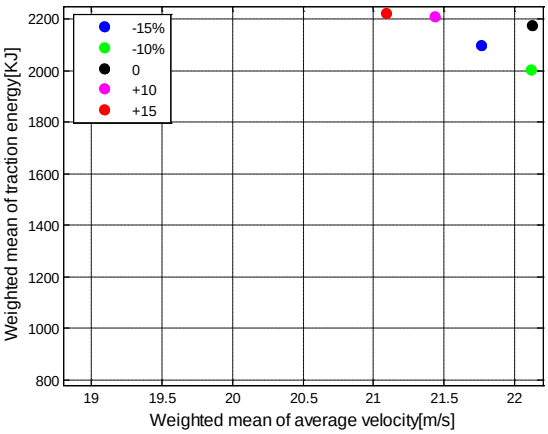

Fig 3.97 Comparison between Weighted mean of Average velocity and Weighted mean of Traction energy with mean power distribution

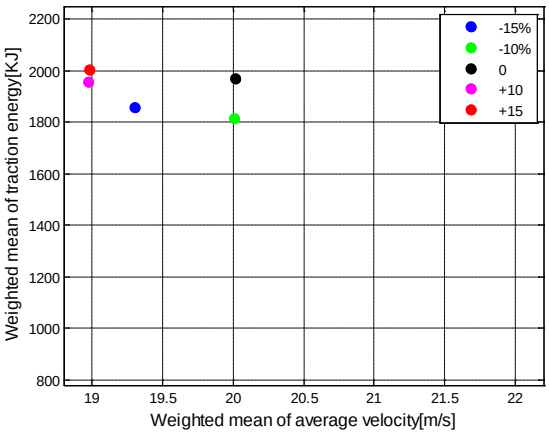

Fig 3.98 Comparison between Weighted mean of Average velocity and Weighted mean of Traction energy with maximum power distribution

a) Tables and Graphics Analysis

In the plots shown from Fig 3.28 to Fig 3.41 the characteristics events metrics in absolute values and in relative variations respect to mass change are reported. From Fig 3.45 to Fig 3.56 a useful sensitivity evaluation is done graphically comparing some characteristic quantities of braking phase and traction phase representative events.
Some observations can be done about the used methodologies:

- The metric value obtained by means of the weighted mean method is the only information related to the metrics trend since refers to its own distribution.
  In Fig 3.46 it is possible to notice that there is unexpected behavior of the Weighted Mean Maximum Braking Power during the mass variation from +10% to +15%. In fact its value in the first vehicle configuration is bigger than for the second vehicle configuration. This is not the only case and similarly it happens for the mean values method. Also in Fig 45 the Mean Braking Maximum power trend has to be analyzed: in fact the value with -15% mass variation is bigger than with -10% mass variation. This is related to the power profile variation with the mass. Since the main process input is the velocity profile, the power to be provided changes. There are points along the power profile where, depending on the mass value, changes sign, meaning that the traction phases become braking phases or vice versa.

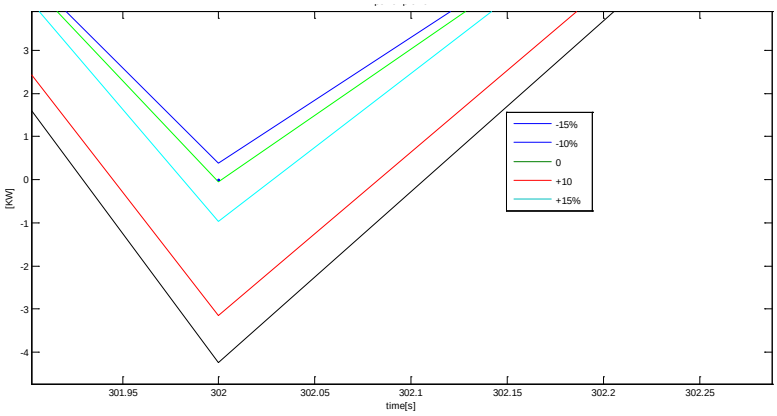

Fig 3.99 Power profiles trend detail varying vehicle mass and frontal area

In Fig 3.69 the power profiles are reported: in this case only the -15% mass variation profile remains in positive phase, whereas the other profiles assume negative values. One positive power event changes in two positive power events and one negative power events. This change influences both braking and traction mean and weighted mean values.

By means of this example it is possible to explain how the traction and braking cycle characteristic events based on mean values and weighted mean values are subject to unexpected trend variations. The same comment is valid also for kinetic metrics. In fact the power profile shift due to vehicle configuration change cause the modification of negative and positive power events and also of the individuation of velocity and acceleration profile segments related to them.

- The metric values obtained by means of the weighted average with mean power and maximum power distribution present different behavior and sensitivity to vehicle configuration variations. This can be noticed as examples in Fig 3.36, Fig 3.37, Fig 3.47 and Fig 3.48. This is because they are strictly depending on maximum power and mean power distributions. As explained before this related to the power profile change depending on the vehicle configuration variation. Although they are both referred to power, the effect of this modification is different on the two metrics. Then the application of these distributions to weighted mean calculation can bring to very different metrics values.

A similar methodologies evaluation about sensitivity to vehicle configuration variations can be done also for the following Case II.

3.2.1.2 Second Case Analysis

In the second case just the vehicle mass is changing and frontal area is kept constant to an average value 2.76 m^2. The vehicle configurations analyzed in this second case are listed in Table 3.11.

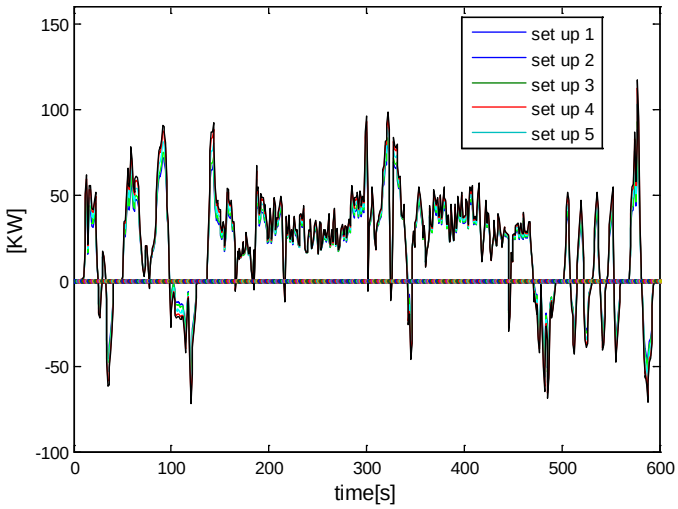

Fig 3.100 Power profiles depending on vehicle mass value

As seen in case I the power vs. time profile in Fig 3.70 changes depending on the on the vehicle configuration. The inertial force and dissipative rolling force depend on vehicle mass but in this case the frontal area has been maintained constant.

a) Braking Phase Relevant Event

- Considering every vehicle mass value, it is possible to obtain cycle representative events by means of the weighted average method using three different distributions. In fact each metric value can be obtained using its own distribution, the maximum power distribution and mean power distribution. In the tables below, from Table 3.19 to Table 24, the representative events metrics absolute values and calculated by means of equation (3.16) are reported for all the aforementioned cycle characteristic events:

- Table 3.19 and Table 3.20: in these charts every value is obtained with the weighted mean method using the own distribution for each metric

Table 3.24: sensitivity analysis results expressed as absolute values

Weighted mean method values					
Mass variation	*-15%*	*-10%*	*0% (1900 kg)*	*+10%*	*+15%*
Frontal area [m^2]	*Constant= 2.76*				

Energy [kJ]	131.01	137.49	153.93	168.72	172.01
Maximum power [kW]	25.98	24.75	27.59	28.35	29.67
Mean power [kW]	13.07	12.08	12.79	15.07	14.79
Mean deceleration [m/s^2]	-0.98	-0.98	-0.96	-0.92	-0.92
Max deceleration [m/s^2]	-1.60	-1.66	-1.63	-1.57	-1.57
Mean velocity [m/s]	19.15	18.72	20.02	20.31	20.31
Max velocity [m/s]	22.31	22.66	23.07	23.42	23.45

Table 3.25: sensitivity analysis results expressed as relative variations

Weighted mean method values					
Mass variation	*-15%*	*-10%*	*0% (1900 kg)*	*+10%*	*+15%*
Frontal area [m^2]	*Constant= 2.76*				
Energy	0.99	1.07		0.96	0.79
Maximum power	0.39	1.03		0.28	0.50
Mean power	-0.15	0.55		1.79	1.05
Mean deceleration	-0.14	-0.21		-0.42	-0.28
Max deceleration	0.12	-0.18		-0.37	-0.25
Mean velocity	0.29	0.65		0.15	0.10
Max velocity	0.22	0.18		0.15	0.11

- Table 3.21 and Table 3.22: in these charts every value is obtained using the weighted mean method using as weights the mean power distribution

Table 3.26: sensitivity analysis results expressed as absolute values

Weighted mean method with Mean Power distribution					
Mass variation	*-15%*	*-10%*	*0% (1900 kg)*	*+10%*	*+15%*
Frontal area [m^2]	*Constant= 2.76*				
Energy [kJ]	252.65	239.33	266.42	323.94	322.52
Maximum power [kW]	28.63	26.43	28.21	33.19	33.57
Mean power [kW]	13.07	12.08	12.79	15.07	14.79
Mean deceleration [m/s^2]	-0.96	-0.84	-0.80	-0.85	-0.80
Max deceleration [m/s^2]	-1.66	-1.45	-1.39	-1.48	-1.39
Mean velocity [m/s]	18.80	16.29	15.53	16.52	15.49
Max velocity [m/s]	18.82	16.38	15.73	16.78	15.75

Table 3.27: sensitivity analysis results expressed as relative variations

Weighted mean method with Mean Power distribution

Mass variation	*-15%*	*-10%*	*0% (1900 kg)*	*+10%*	*+15%*
Frontal area [m^2]	*Constant= 2.76*				
Energy	0.34	1.01		2.16	1.41
Maximum power	-0.10	0.63		1.77	1.27
Mean power	-0.15	0.55		1.79	1.05
Mean deceleration	-1.33	-0.50		0.63	0.00
Max deceleration	-1.29	-0.43		0.65	0.00
Mean velocity	-1.40	-0.49		0.64	-0.02
Max velocity	-1.31	-0.41		0.67	0.01

- Table 3.23 and Table 3.24: in these charts every value is obtained using the weighted mean method using as weights the maximum power distribution

Table 3.28: sensitivity analysis results expressed as absolute values

Weighted mean method with Maximum power distribution					
Mass variation	*-15%*	*-10%*	*0% (1900 kg)*	*+10%*	*+15%*
Frontal area [m^2]	*Constant= 2.76*				
Energy [kJ]	229.25	224.05	260.50	276.70	293.86
Maximum power [kW]	25.98	24.75	27.59	28.35	29.67
Mean power [kW]	11.86	11.31	12.50	12.87	13.48
Mean deceleration [m/s^2]	-0.88	-0.79	-0.78	-0.72	-0.73
Max deceleration [m/s^2]	-1.51	-1.36	-1.36	-1.26	-1.26
Mean velocity [m/s]	17.06	15.25	15.19	14.11	14.11
Max velocity [m/s]	17.08	15.34	15.38	14.33	14.35

Table 3.29: sensitivity analysis results expressed as relative variations

Weighted mean method with Maximum power distribution					
Mass variation	*-15%*	*-10%*	*0% (1900 kg)*	*+10%*	*+15%*
Frontal area [m^2]	*Constant= 2.76*				
Energy	0.80	1.40		0.62	0.86
Maximum power	0.39	1.03		0.28	0.50
Mean power	0.34	0.95		0.30	0.52
Mean deceleration	-0.85	-0.13		-0.77	-0.43
Max deceleration	-0.73	0.00		-0.74	-0.49
Mean velocity	-0.82	-0.04		-0.71	-0.48
Max velocity	-0.74	0.03		-0.68	-0.45

- The same three different methods of Case I have been used to evaluate the characteristic metrics values variations depending on vehicle mass. A comparison of the values obtained by means of the three different methods is

useful to evaluate their sensibility to mass variation. The values in the charts from Table 3.19 to Table 3.24 are graphically compared from Fig 71 to Fig 84.

- Below, from Fig3. 71 to Fig 3.77 the characteristic events metrics in absolute values have been graphically compared. The reference charts are Table 3.19, Table 3.21 and Table 3.23.

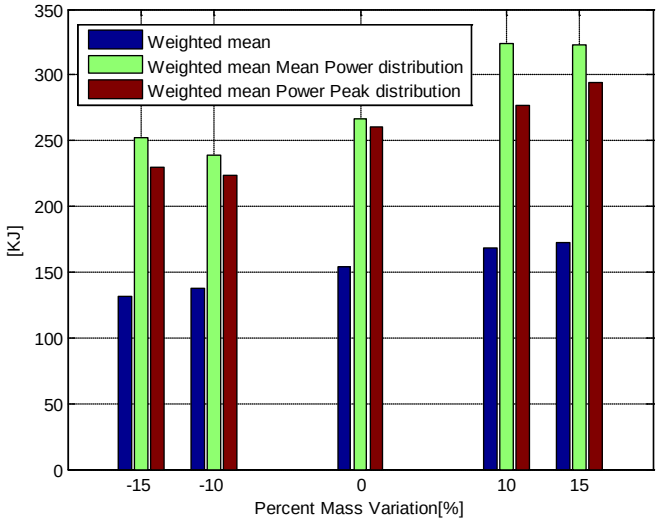

Fig3. 101 Energy values

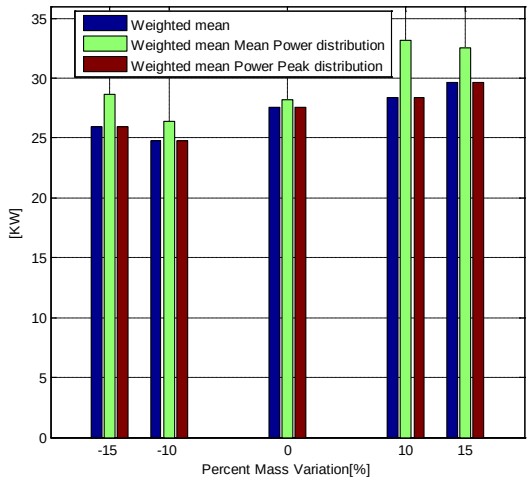

Fig 3.102 Maximum power values

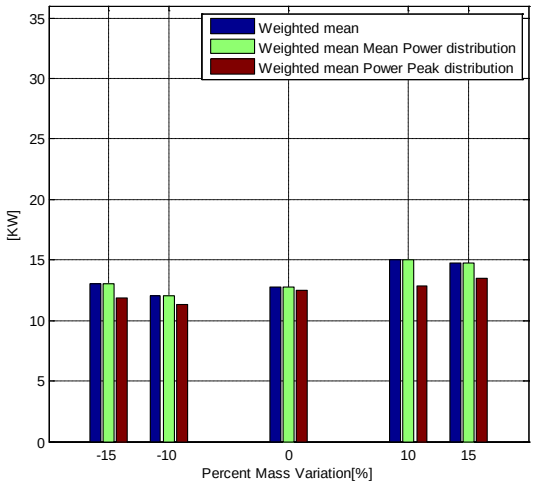

Fig 3.103 Mean power values

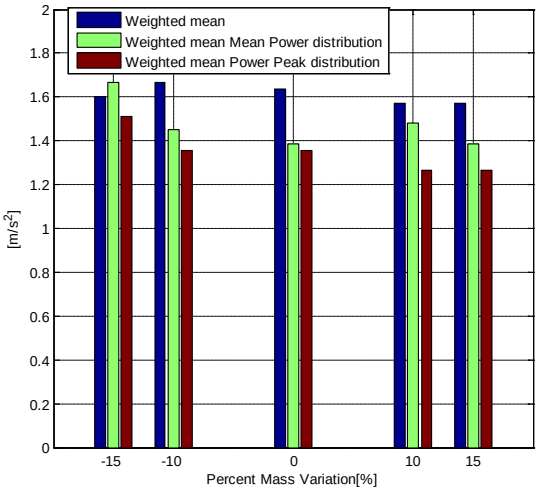

Fig 3.104 Maximum deceleration values

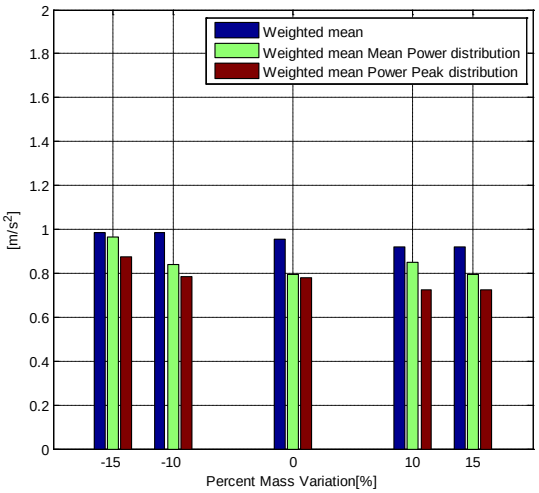

Fig 3.105 Mean deceleration values

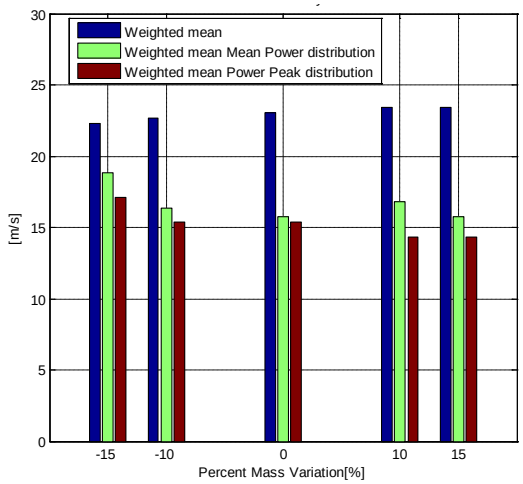

Fig 3.106 Maximum velocity values

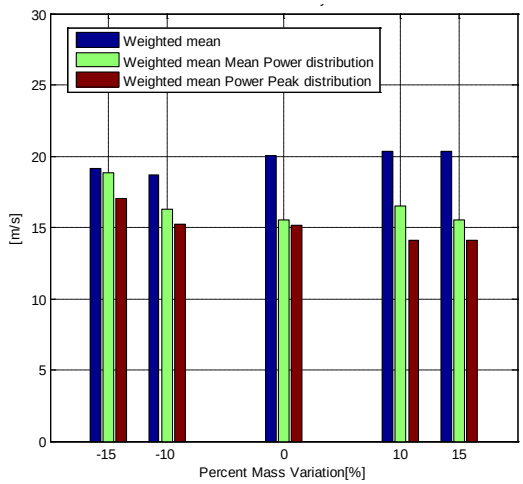

Fig 3.107 Mean velocity values

Below, from Fig3. 71 to Fig 3.84 the characteristic events metrics obtained by means of the equation (3.16) have been graphically compared. The reference charts are Table 3.20, Table 3.22 and Table 3.24.

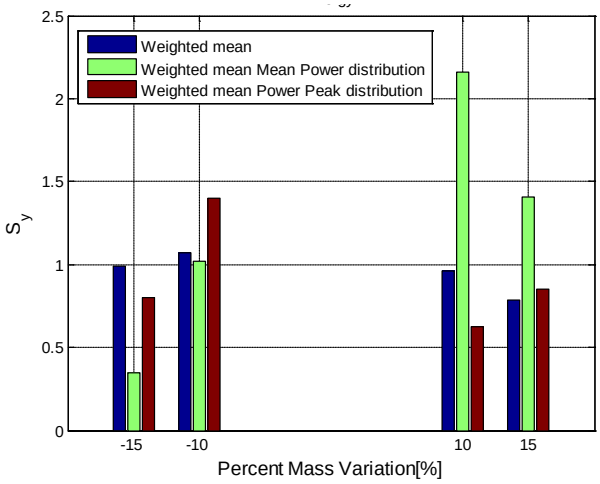

Fig 3.108: Energy values

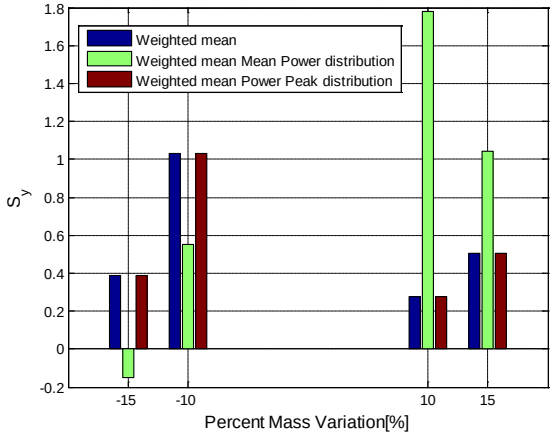

Fig3. 109: Maximum power values

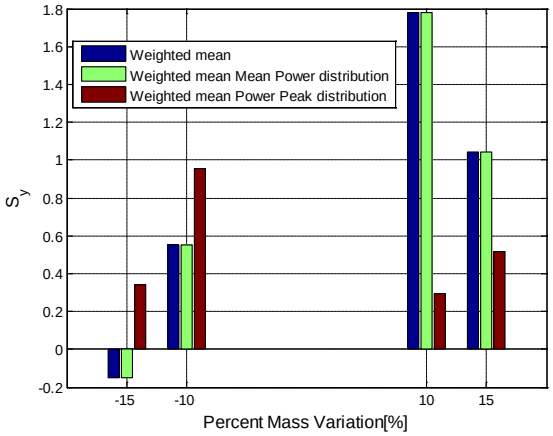

Fig3. 110: Mean power values

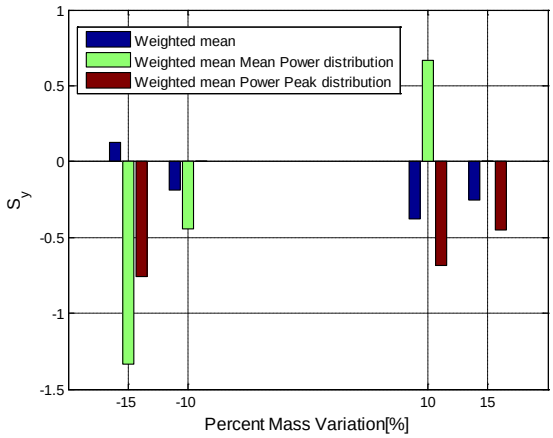

Fig 3.111: Maximum deceleration values

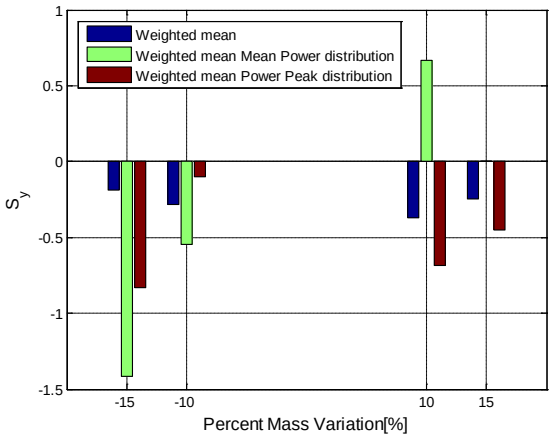

Fig 3.112: Mean deceleration values

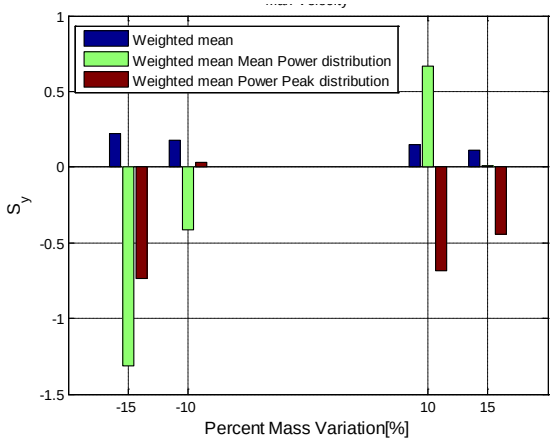

Fig 3.113: Maximum velocity values

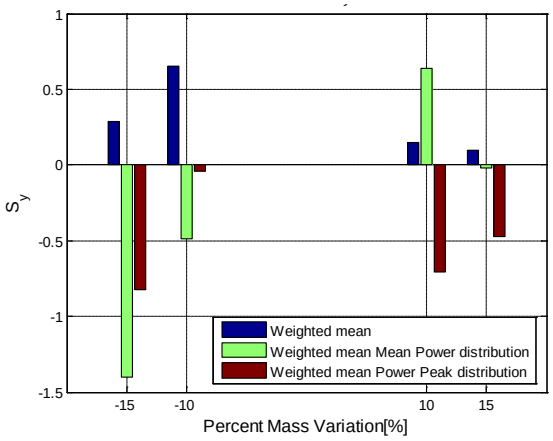

Fig 3.114: Mean velocity values

By analyzing Fig3. 71 and Fig 3.78 it possible to notice that the energy values are increasing with the vehicle mass as expected. In Fig 3.72, Fig 3.73, Fig3. 79 and Fig3. 80 the weighted mean values of mean and maximum power present different trends, in particular the mean power presents a wider variation range. These trends are not directly related to the velocity and deceleration sensitivity. This is because the mass variation does not affect the velocity profile. As mentioned for Case I, the mass change influences the events individuation process since it is based on the power profile. From Fig 3.81 to Fig 3.84 it is possible to notice that the effects of the vehicle parameter change are very small for the weighted means values. The opposite trend is shown by the values based on the power distribution that show big sensibility.

b) Power and energy data analysis in the cycle

- From the previous data tables, from Table 3.19 to Table 3.23, it is possible to define cycle target event values. Considering all the cycle and not just the single events, it is expected that both the total theoretical recoverable braking energy and the total requested traction energy are subjected to change depending on the vehicle set up.

In the figures below, Fig 3.85 and Fig 3.86, it is possible to analyze these data.

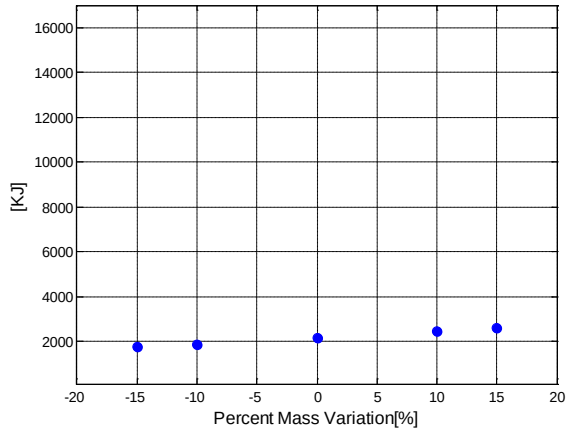

Fig 3.115 Total braking energy trend depending on mass variation and constant area

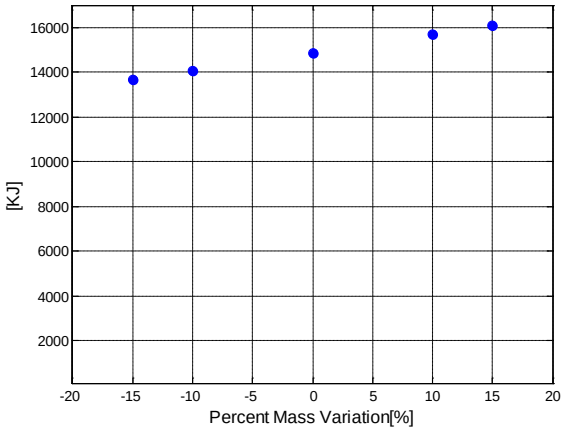

Fig 3.116 Total traction energy trend depending on mass variation and constant area

c) Braking phase

In the previous part, it has been shown that power profile trend changes depending the vehicle configuration (Fig 3.27) and for an exemplary braking phase also power terms change (Fig 3.70). Since the power profile varies, also the metrics values of statistically relevant braking events are influence by mass and frontal area variation depending on the synthesis method used (Table 3.19, Table 3.21 and Table 3.23). An useful sensitivity evaluation can be done graphically comparing some characteristic quantities of the braking phase representative events. These events have been defined by means of the same synthesis methods used for Case I.

From Fig 3.87 to Fig3. 90 two fundamental energetic data are compared: maximum braking power and braking energy. From Fig 3.91 to Fig 3.94 metrics are compared: maximum deceleration and maximum braking power. From Fig 3.95 to Fig 3.98 the average velocity and braking energy are compared.

- Mean braking power vs. Braking energy

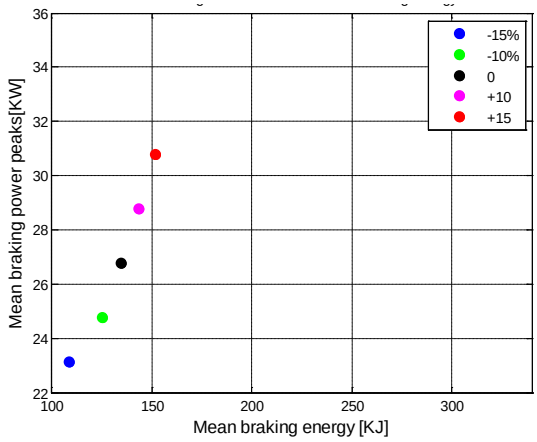

Fig 3.117 Comparison between Mean Maximum braking power and Mean Braking Energy

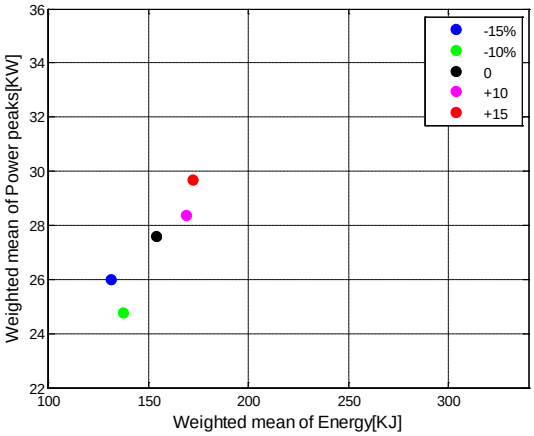

Fig 3.118 Comparison between Weighted mean of Maximum braking power and Weighted mean of Braking Energy

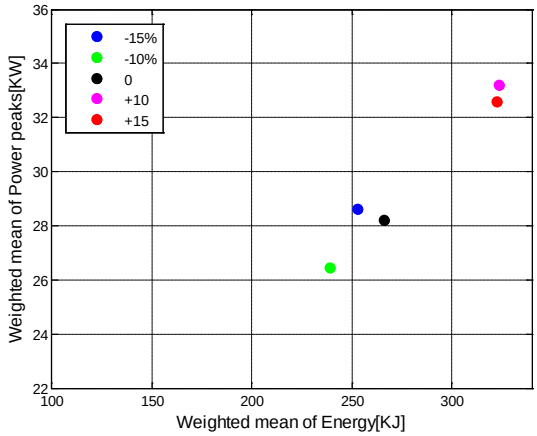

Fig 3.119 Comparison between Weighted mean of Maximum braking power and Weighted mean of Braking Energy with mean power distribution

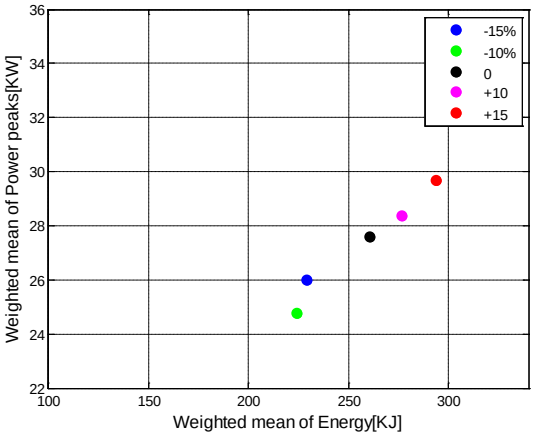

Fig3. 120 Comparison between Weighted mean of Maximum braking power and Weighted mean of Braking Energy with maximum powers distribution

- Maximum deceleration vs. Maximum braking power

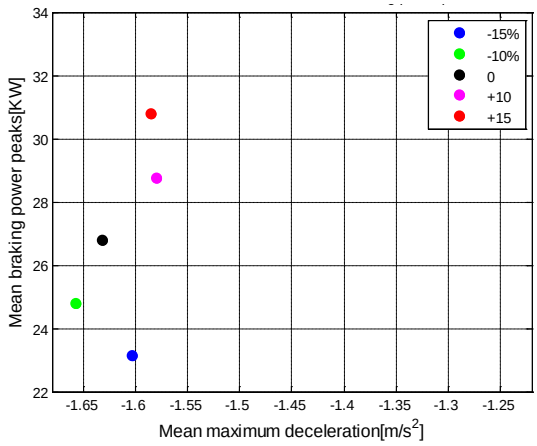

Fig 3.121 Comparison between Mean Maximum deceleration and Mean Maximum braking power

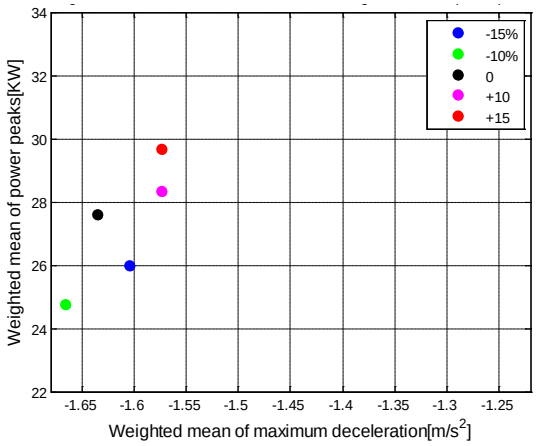

Fig 3.122 Comparison between Weighted mean of Maximum deceleration and Weighted mean of Maximum braking power

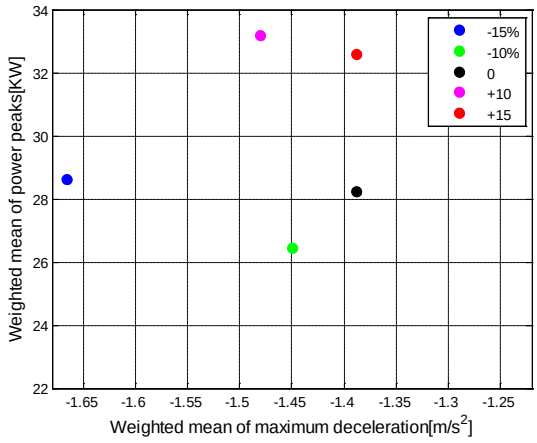

Fig 3.123 Comparison between Weighted mean of Maximum deceleration and Weighted mean of Maximum braking power with mean power distribution

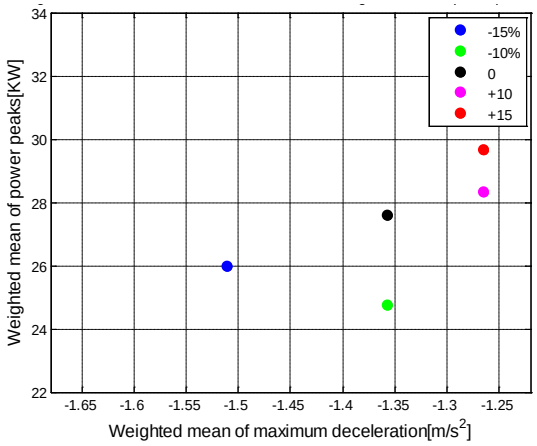

Fig 3.124 Comparison between Weighted mean of Maximum deceleration and Weighted mean of Maximum braking power with maximum power distribution

- Average velocity vs. Braking energy

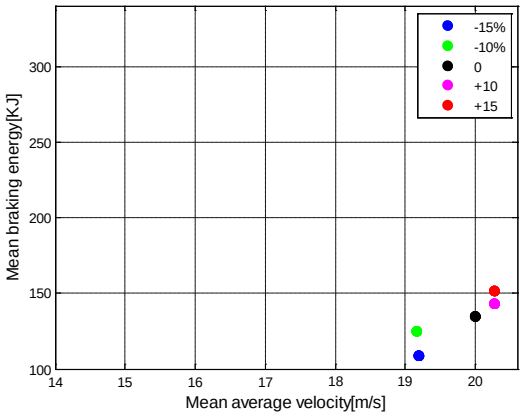

Fig 3.125 Comparison between Mean Average velocity and Mean Braking energy

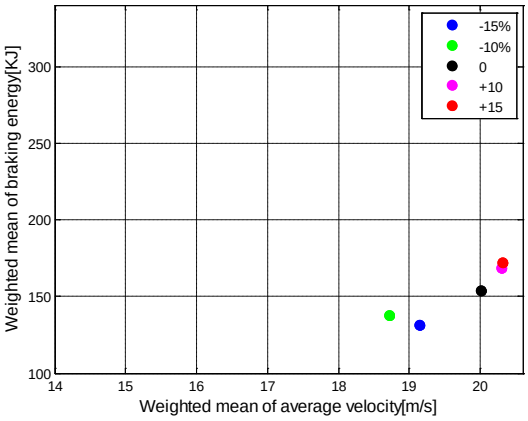

Fig 3.126 Comparison between Weighted mean of Average velocity and Weighted mean of Braking energy

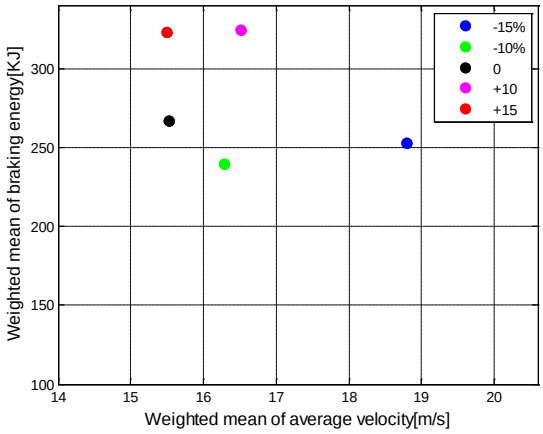

Fig 3.127 Comparison between Weighted mean of Average velocity and Weighted mean of Braking energy with mean power distribution

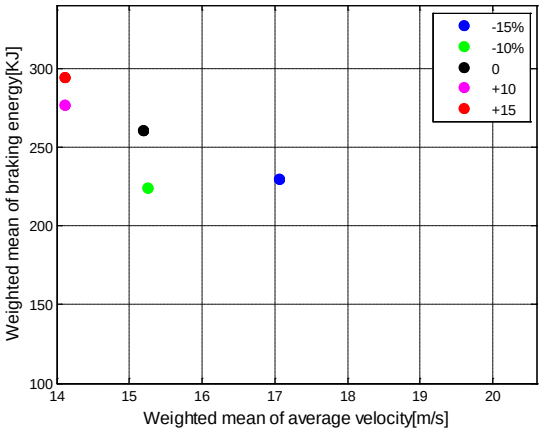

Fig 3.128 Comparison between Weighted mean of Average velocity and Weighted mean of Braking energy with maximum power distribution

d) Traction phase

In the previous paragraph some important metrics of braking phase representative events have been graphically compared. In this part, the same comparison is done for the cycle traction phase representative event. These events have been defined by means of the same synthesis methods used for the braking phase.

From Fig 3.99 to Fig 3.102 two fundamental metrics are compared: maximum traction power and traction energy. From Fig 3.103 to Fig 3.106 maximum acceleration and maximum traction power are compared. From Fig 3.107 to Fig 3.110the average velocity and traction energy are compared.

- Mean traction power vs. Traction energy

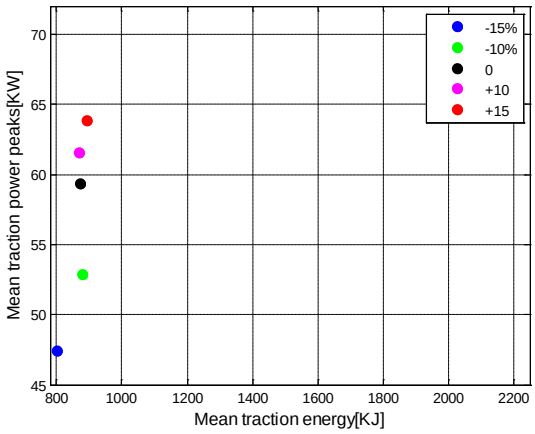

Fig 3.129 Comparison between Mean Maximum traction power and Mean Traction energy

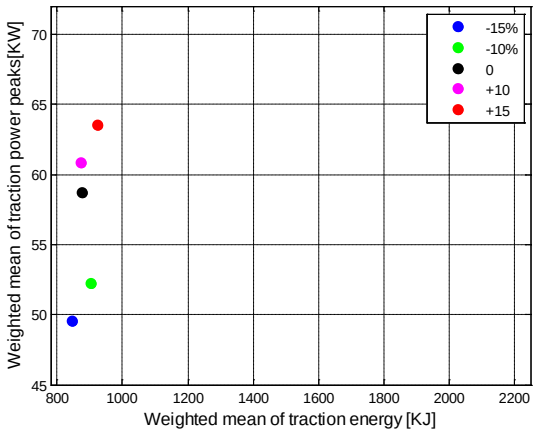

Fig 3.130 Comparison between Weighted mean of Maximum traction power and Weighted mean of Traction energy

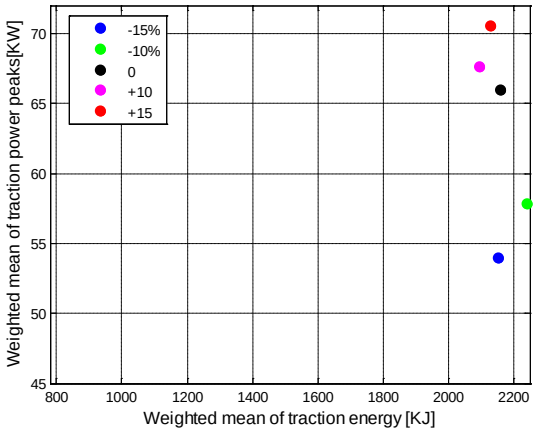

Fig 3.131 Comparison between Weighted mean of Maximum traction power and Weighted mean of Traction energy with mean power distribution

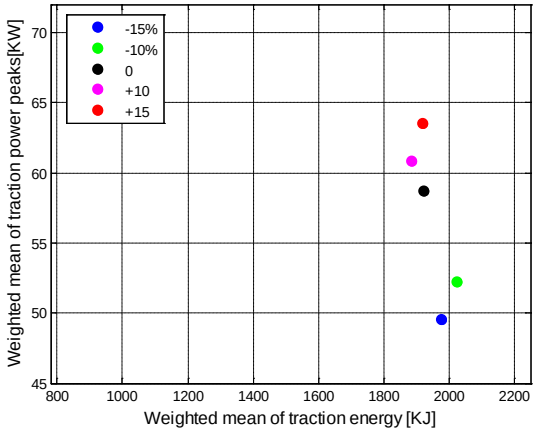

Fig 3.132 Comparison between Weighted mean of Maximum traction power and Weighted mean of Traction energy with maximum power distribution

- Maximum acceleration vs. Maximum traction power

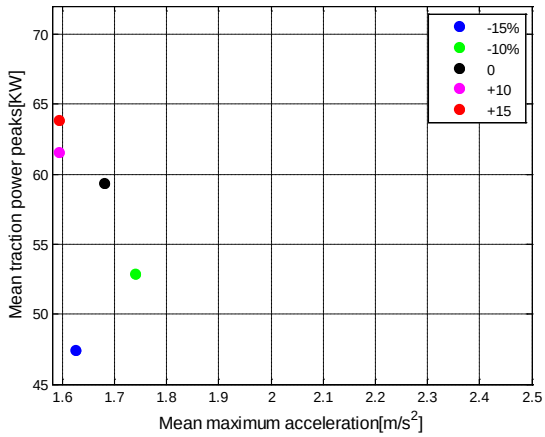

Fig 3.133 Comparison between Mean Maximum acceleration and Mean Maximum traction power

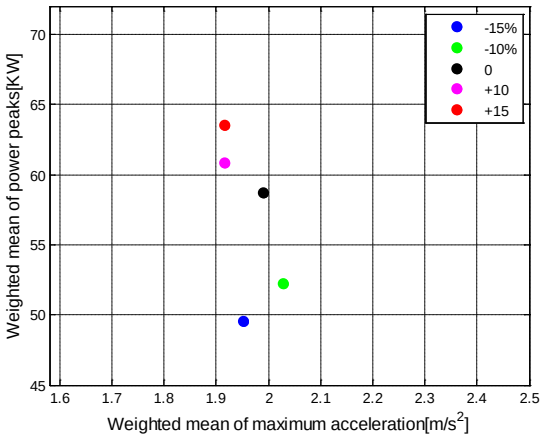

Fig 3.134 Comparison between Weighted mean of Maximum acceleration and Weighted mean of Maximum traction power

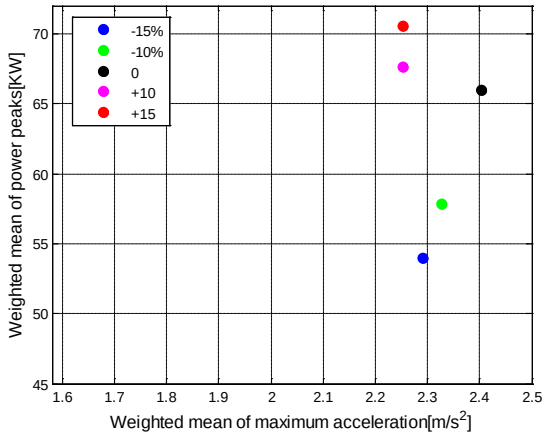

Fig 3.135 Comparison between Weighted mean of Maximum acceleration and Weighted mean of Maximum traction power with mean power distribution

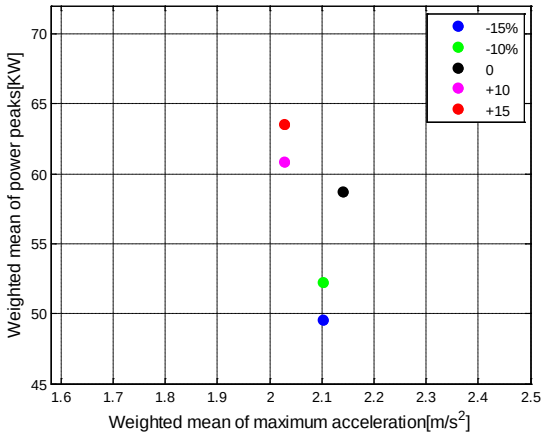

Fig 3.136 Comparison between Weighted mean of Maximum acceleration and Weighted mean of Maximum traction power with maximum power distribution

- Average velocity vs. Traction energy

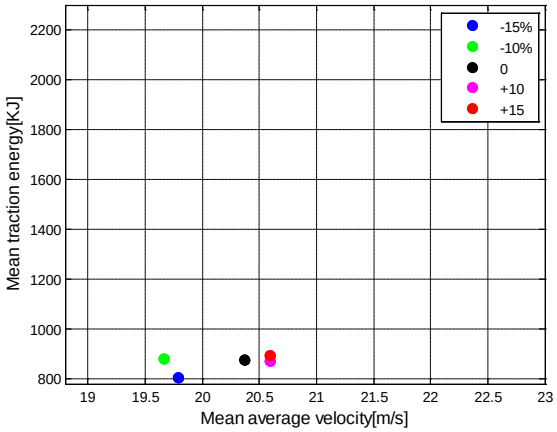

Fig 3.137 Comparison between Mean Average velocity and Mean traction energy

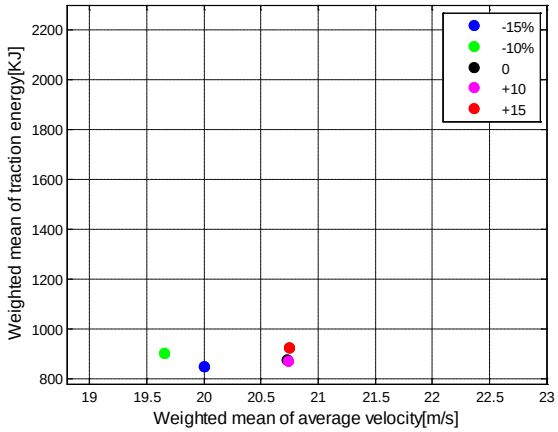

Fig 3.138 Comparison between Weighted mean of Average velocity and Weighted mean of Traction energy

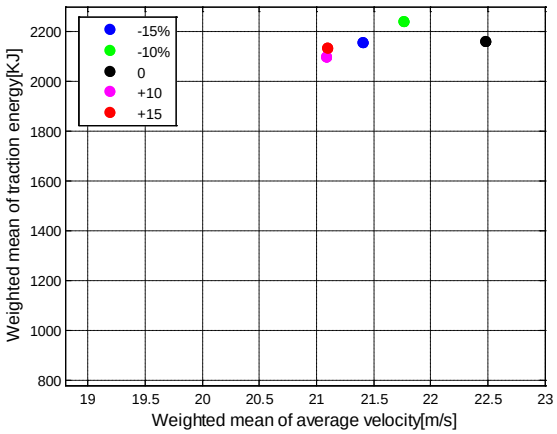

Fig 3.139 Comparison between Weighted mean of Average velocity and Weighted mean of Traction energy with mean power distribution

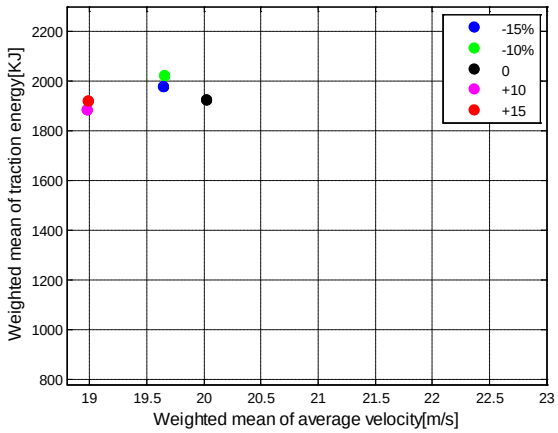

Fig 3.140 Comparison between Weighted mean of Average velocity and Weighted mean of Traction energy with maximum power distribution

3.2.1.3 Analysis of "Real-world" Driving Cycles

The sensitivity study can be applied also to the "real world" cycles obtained by means of the procedure introduced in the first section. In the tables below the analysis has been processed on the three different cycles: urban, highway and freeway (Table 3.1).

For every cycle, the statistically relevant event of the braking phase has been defined by means of the same synthesis methods used for Case I. In these cases it is possible to assume that both vehicle frontal area and mass change. The vehicle configurations are the same as in Case I. They are listed in Table 3.10.

- Urban

The Urban cycle has been created by the union of 50 “Urban Traffic” patterns and 50 “Urban No traffic” patterns. In this way both the driving conditions have considered in the analysis. In the tables below, from Table 3.25 to Fig 3.29, the representative events metrics absolute values and calculated by means of equations (3.16) are reported for all the aforementioned cycle characteristic events:

Table 3.30: sensitivity analysis results expressed as absolute values

Weighted mean method values					
Mass variation	*-15%*	*-10%*	*0% (1900 kg)*	*+10%*	*+15%*
Frontal area [m^2]	*2.56*	*2.66*	*2.86*	*2.92*	*2.95*
Energy [kJ]	21.40	22.68	27.33	30.13	31.54
Maximum power [kW]	6.01	6.37	7.08	7.81	8.17
Mean power [kW]	2.56	2.71	3.02	3.33	3.49
Mean deceleration [m/s^2]	-0.48	-0.48	-0.48	-0.48	-0.48
Max deceleration [m/s^2]	-0.96	-0.96	-0.96	-0.96	-0.96
Mean velocity [m/s]	3.45	3.45	3.45	3.45	3.45
Max velocity [m/s]	4.49	4.49	4.49	4.49	4.49

Table 3.31: sensitivity analysis results expressed as relative variations

Weighted mean method values					
Mass variation	*-15%*	*-10%*	*0% (1900 kg)*	*+10%*	*+15%*
Frontal area [m^2]	*2.56*	*2.66*	*2.86*	*2.92*	*2.95*
Energy	1.45	1.70		1.03	1.03
Maximum power	1.01	1.00		1.03	1.03
Mean power	1.01	1.02		1.03	1.04
Mean deceleration	0.00	0.00		0.00	0.00
Max deceleration	0.00	0.00		0.00	0.00
Mean velocity	0.00	0.00		0.00	0.00
Max velocity	0.00	0.00		0.00	0.00

Table 3.32: sensitivity analysis results expressed as absolute values

Weighted mean method with Mean Power distribution					
Mass variation	*-15%*	*-10%*	*0% (1900 kg)*	*+10%*	*+15%*

Frontal area [m^2]	*2.56*	*2.66*	*2.86*	*2.92*	*2.95*
Energy [kJ]	19.62	20.79	23.12	25.50	26.69
Maximum power [kW]	5.51	5.84	6.49	7.15	7.49
Mean power [kW]	2.56	2.71	3.02	3.33	3.49
Mean deceleration [m/s^2]	-0.20	-0.20	-0.20	-0.20	-0.20
Max deceleration [m/s^2]	-0.46	-0.46	-0.46	-0.46	-0.46
Mean velocity [m/s]	1.65	1.65	1.65	1.65	1.65
Max velocity [m/s]	1.68	1.68	1.68	1.68	1.68

Table 3.33: sensitivity analysis results expressed as relative variations

Weighted mean method with Mean Power distribution					
Mass variation	*-15%*	*-10%*	*0% (1900 kg)*	*+10%*	*+15%*
Frontal area [m^2]	*2.56*	*2.66*	*2.86*	*2.92*	*2.95*
Energy	1.01	1.01		1.03	1.03
Maximum power	1.01	1.00		1.02	1.03
Mean power	1.01	1.02		1.03	1.04
Mean deceleration	0.00	0.00		0.00	0.00
Max deceleration	0.00	0.00		0.00	0.00
Mean velocity	0.00	0.00		0.00	0.00
Max velocity	0.00	0.00		0.00	0.00

Table 3.34: sensitivity analysis results expressed as absolute values

Weighted mean method with Maximum power distribution					
Mass variation	*-15%*	*-10%*	*0% (1900 kg)*	*+10%*	*+15%*
Frontal area [m^2]	*2.56*	*2.66*	*2.86*	*2.92*	*2.95*
Energy [kJ]	21.40	22.68	25.23	27.81	29.11
Maximum power [kW]	6.01	6.37	7.08	7.80	8.17
Mean power [kW]	2.79	2.96	3.29	3.64	3.80
Mean deceleration [m/s^2]	-0.21	-0.21	-0.21	-0.21	-0.21
Max deceleration [m/s^2]	-0.50	-0.50	-0.50	-0.50	-0.50
Mean velocity [m/s]	1.80	1.80	1.80	1.80	1.80
Max velocity [m/s]	1.83	1.83	1.83	1.83	1.83

Table 3.35: sensitivity analysis results expressed as relative variations

Weighted mean method with Maximum power distribution					
Mass variation	*-15%*	*-10%*	*0% (1900 kg)*	*+10%*	*+15%*
Frontal area [m^2]	*2.56*	*2.66*	*2.86*	*2.92*	*2.95*
Energy	1.01	1.01		1.03	1.03
Maximum power	1.01	1.00		1.02	1.03
Mean power	1.01	1.00		1.07	1.04
Mean deceleration	0.00	0.00		0.00	0.00
Max deceleration	0.00	0.00		0.00	0.00
Mean velocity	0.00	0.00		0.00	0.00
Max velocity	0.00	0.00		0.00	0.00

For every cycle the three different methods have been used to evaluate the characteristic metrics values variations depending on vehicle mass. The values in the charts from

Table 3.25 ,Table 3.27 and Table 3.29 are graphically compared from Fig 3.111 to Fig 3.117

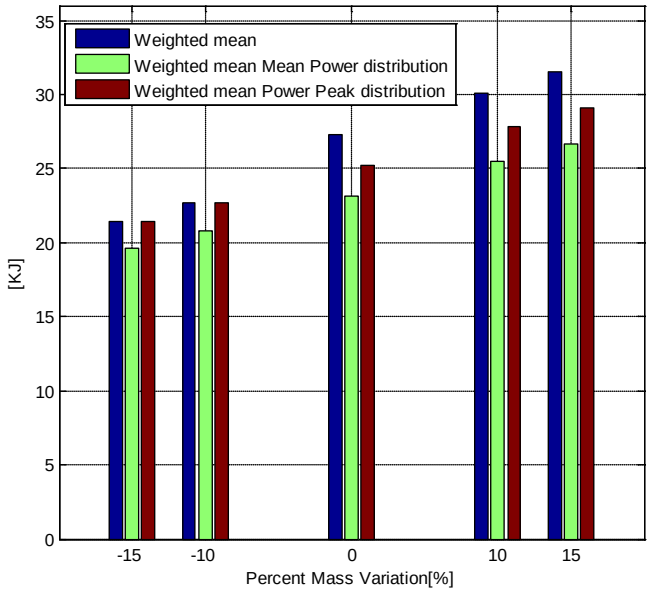

Fig 3.141 Energy values

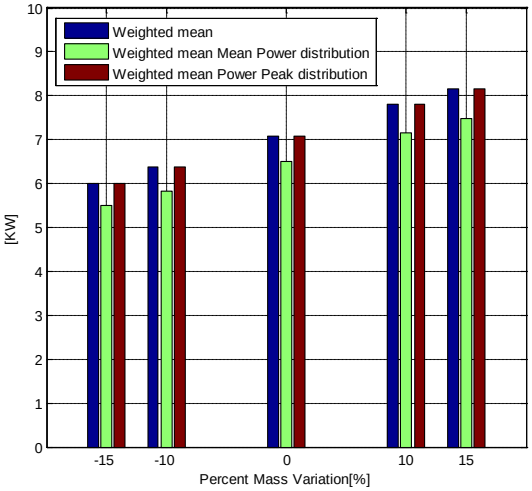

Fig 3.142 Maximum power values

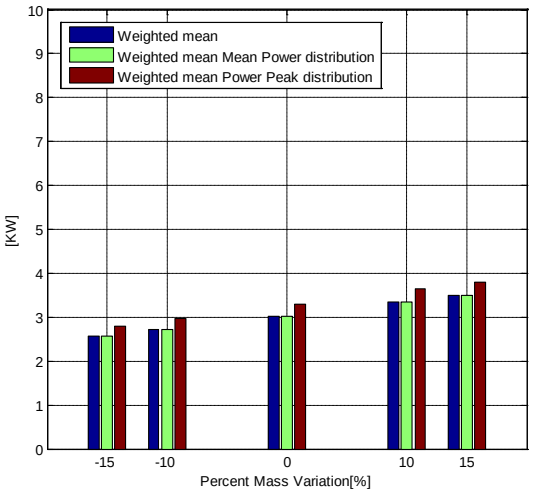

Fig 3.143 Mean power values

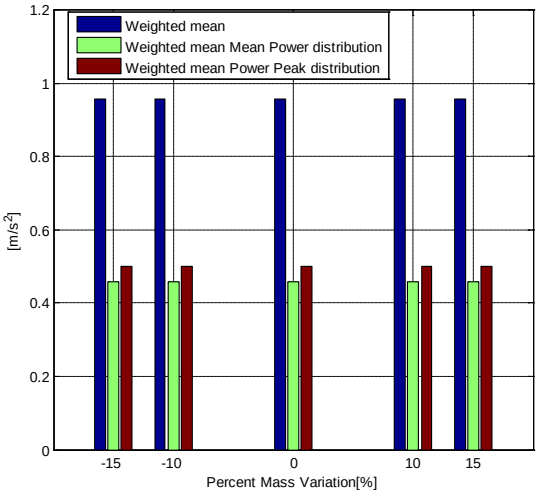

Fig 3.144 Maximum deceleration values

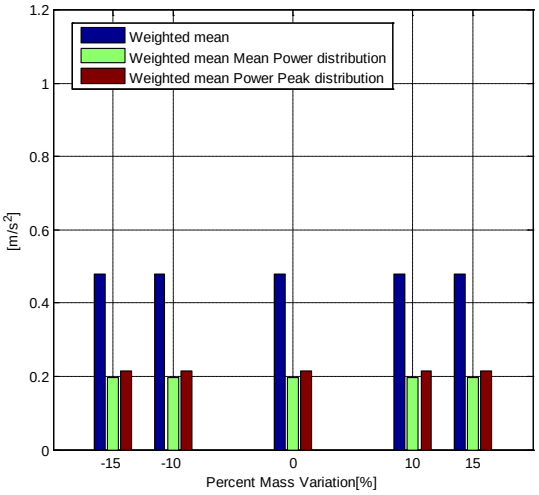

Fig 3.145 Mean deceleration values

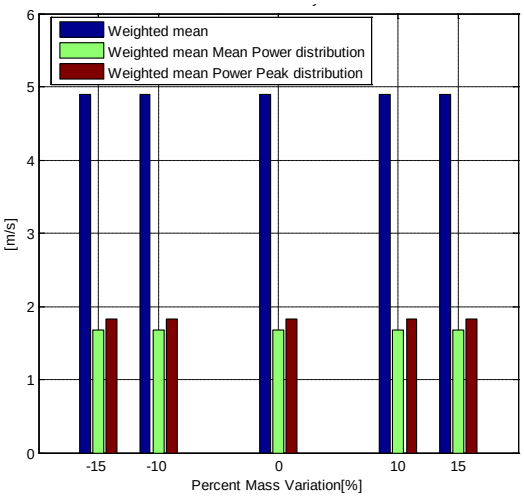

Fig 3.146 Maximum velocity values

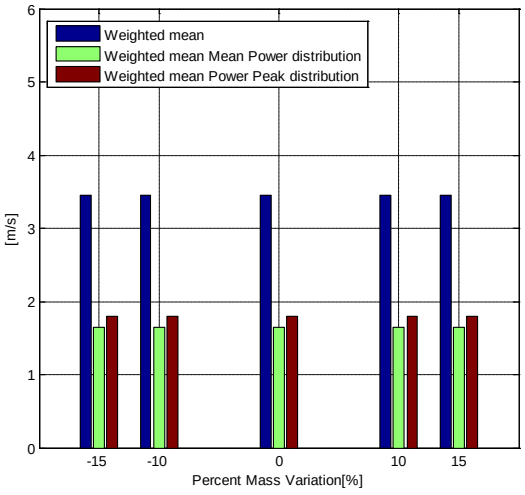

Fig 3.147 Mean velocity values

- Freeway

The Freeway cycle has been created by the union of 50 “Freeway Traffic” patterns and 50 “Freeway No traffic” patterns. In this way both the driving conditions have considered in the analysis.

In the tables below, from Table 31 to Table 36, the representative events metrics absolute values and calculated by means of equations (3.16) are reported for all the aforementioned cycle characteristic events.

Table 3.36: sensitivity analysis results expressed as absolute values

Weighted mean method values					
Mass variation	*-15%*	*-10%*	*0% (1900 kg)*	*+10%*	*+15%*
Frontal area [m^2]	*2.56*	*2.66*	*2.86*	*2.92*	*2.95*
Energy [kJ]	63.70	67.67	75.62	84.22	88.51
Maximum power [kW]	10.67	11.31	12.59	13.92	14.58
Mean power [kW]	5.42	5.75	6.42	7.16	7.48
Mean deceleration [m/s^2]	-0.55	-0.55	-0.55	-0.53	-0.51
Max deceleration [m/s^2]	-0.87	-0.87	-0.87	-0.87	-0.83
Mean velocity [m/s]	15.82	15.82	15.82	16.10	16.37
Max velocity [m/s]	17.95	17.95	17.95	18.28	18.28

Table 3.37: sensitivity analysis results expressed as relative variations

Weighted mean method values					
Mass variation	*-15%*	*-10%*	*0% (1900 kg)*	*+10%*	*+15%*
Frontal area [m^2]	*2.56*	*2.66*	*2.86*	*2.92*	*2.95*
Energy	1.05	1.05		1.14	1.14
Maximum power	1.02	1.01		1.06	1.06
Mean power	1.04	1.04		1.16	1.10
Mean deceleration	0.00	0.00		-0.36	-0.49
Max deceleration	0.00	0.00		0.00	-0.31
Mean velocity	0.00	0.00		0.18	0.23
Max velocity	0.00	0.00		0.18	0.12

Table 3.38: sensitivity analysis results expressed as absolute values

Weighted mean method with Mean Power distribution					
Mass variation	*-15%*	*-10%*	*0% (1900 kg)*	*+10%*	*+15%*
Frontal area [m^2]	*2.56*	*2.66*	*2.86*	*2.92*	*2.95*
Energy [kJ]	63.70	67.67	75.62	84.22	88.51
Maximum power [kW]	10.67	11.31	12.59	13.92	14.58
Mean power [kW]	5.42	5.75	6.42	7.16	7.48
Mean deceleration [m/s^2]	-0.25	-0.25	-0.25	-0.25	-0.25
Max deceleration [m/s^2]	-0.58	-0.58	-0.58	-0.58	-0.58
Mean velocity [m/s]	3.95	3.95	3.95	3.95	3.95
Max velocity [m/s]	3.99	3.99	3.99	3.99	3.99

Table 3.39: sensitivity analysis results expressed as relative variations

Weighted mean method with Mean Power distribution					
Mass variation	*-15%*	*-10%*	*0% (1900 kg)*	*+10%*	*+15%*
Frontal area [m^2]	*2.56*	*2.66*	*2.86*	*2.92*	*2.95*
Energy	1.05	1.05		1.14	1.14
Maximum power	1.02	1.01		1.06	1.06
Mean power	1.04	1.04		1.16	1.10
Mean deceleration	0.00	0.00		0.00	0.00
Max deceleration	0.00	0.00		0.00	0.00
Mean velocity	0.00	0.00		0.00	0.00
Max velocity	0.00	0.00		0.00	0.00

Table 3.40: sensitivity analysis results expressed as absolute values

Weighted mean method with Maximum power distribution					
Mass variation	*-15%*	*-10%*	*0% (1900 kg)*	*+10%*	*+15%*
Frontal area [m^2]	*2.56*	*2.66*	*2.86*	*2.92*	*2.95*
Energy [kJ]	63.70	67.67	75.62	84.22	88.51
Maximum power [kW]	10.67	11.31	12.59	13.92	14.58
Mean power [kW]	5.42	5.75	6.42	7.16	7.48
Mean deceleration [m/s^2]	-0.25	-0.25	-0.25	-0.25	-0.25
Max deceleration [m/s^2]	-0.58	-0.58	-0.58	-0.58	-0.58
Mean velocity [m/s]	3.95	3.95	3.95	3.95	3.95
Max velocity [m/s]	3.99	3.99	3.99	3.99	3.99

Table 3.41: sensitivity analysis results expressed as relative variations

Weighted mean method with Maximum power distribution					
Mass variation	*-15%*	*-10%*	*0% (1900 kg)*	*+10%*	*+15%*
Frontal area [m^2]	*2.56*	*2.66*	*2.86*	*2.92*	*2.95*
Energy	1.05	1.05		1.14	1.14
Maximum power	1.02	1.01		1.06	1.06
Mean power	1.04	1.04		1.16	1.10
Mean deceleration	0.00	0.00		0.00	0.00
Max deceleration	0.00	0.00		0.00	0.00
Mean velocity	0.00	0.00		0.00	0.00
Max velocity	0.00	0.00		0.00	0.00

For every cycle, the characteristic quantities values variations, depending on vehicle mass, have been evaluated. The comparison of the values is in the charts from Table 3.31,Table 3.33 and Table 3.35 are graphically compared from Fig 3.118 to Fig 3.124.

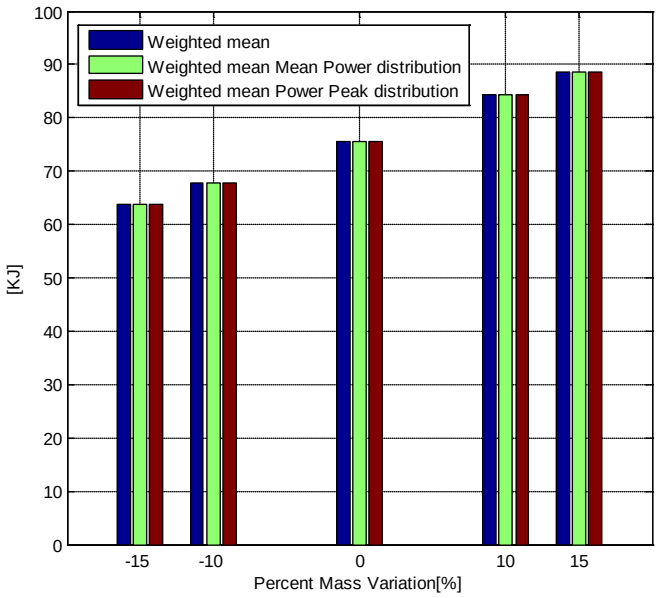

Fig 3.148 Energy values

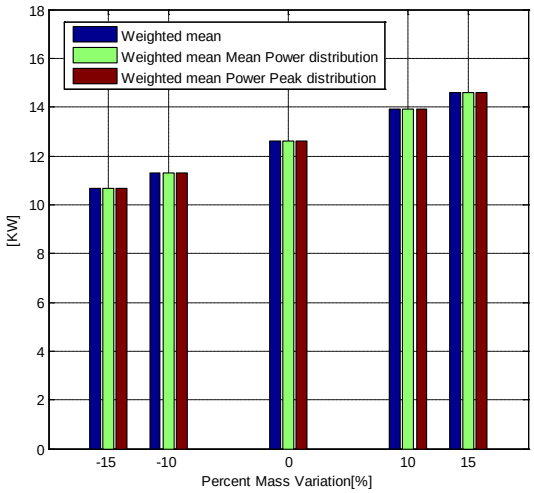

Fig 3.149 Maximum power values

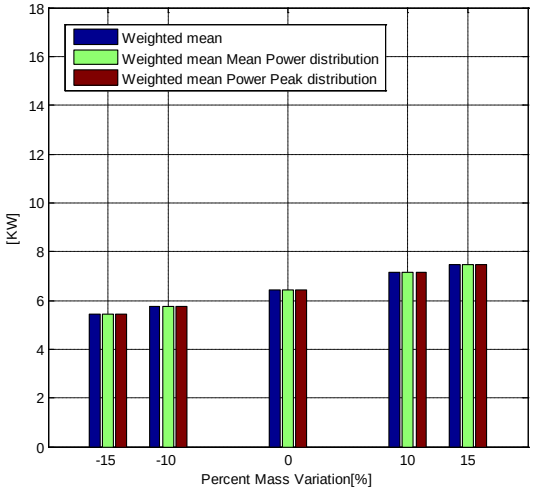

Fig 3.150 Mean power values

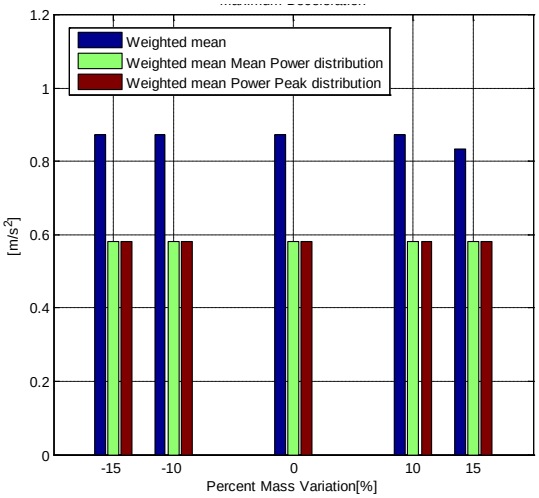

Fig 3.151 Maximum deceleration values

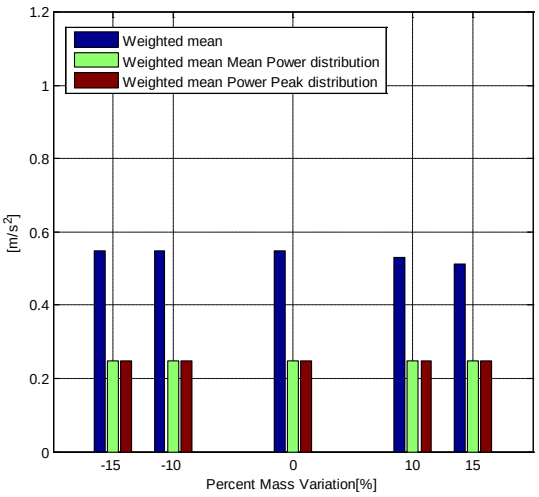

Fig 3.152 Mean deceleration values

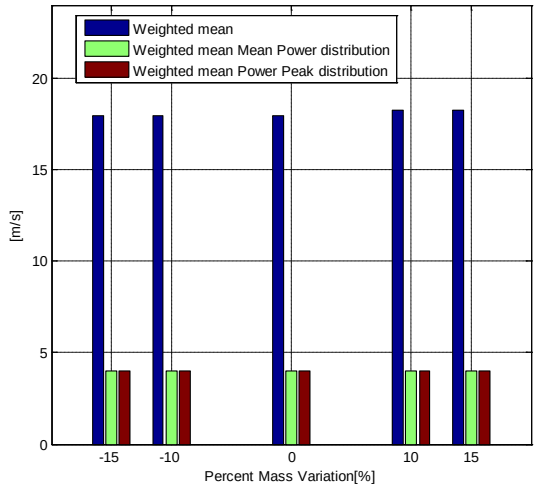

Fig 3.153 Maximum velocity values

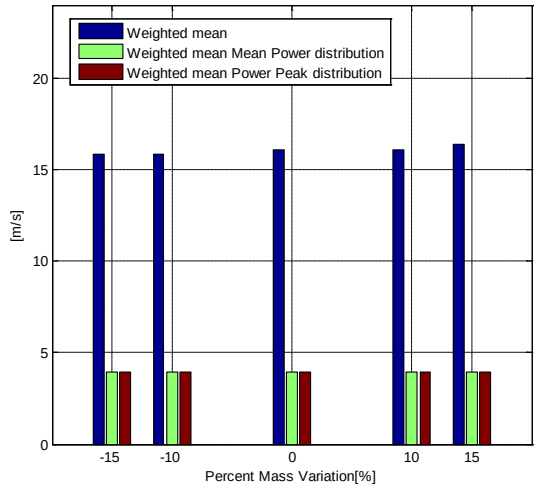

Fig 3.154 Mean velocity values

- Highway

The Highway cycle has been created by the union of 50 “Highway Traffic” patterns and 50 “Highway No traffic” patterns. In this way both the driving conditions have considered in the analysis.

In the tables below, from Table 3.37 to Table 42 the representative events metrics absolute values and calculated by means of equations (3.16) are reported for all the aforementioned cycle characteristic events.

Table 3.42: sensitivity analysis results expressed as absolute values

Weighted mean method values					
Mass variation	*-15%*	*-10%*	*0% (1900 kg)*	*+10%*	*+15%*
Frontal area [m^2]	*2.56*	*2.66*	*2.86*	*2.92*	*2.95*
Energy [KJ]	51.52	54.71	61.06	67.80	71.19
Maximum power [kW]	12.19	12.93	14.39	15.90	16.66
Mean power [kW]	5.91	6.27	7.00	7.77	8.15
Mean deceleration [m/s^2]	-0.56	-0.56	-0.56	-0.56	-0.55
Max deceleration [m/s^2]	-1.04	-1.04	-1.04	-1	-1
Mean velocity [m/s]	11.18	11.18	11.40	11.39	11.40
Max velocity [m/s]	13.29	13.29	13.29	13.29	13.53

Table 3.43: sensitivity analysis results expressed as relative variations

Weighted mean method values					
Mass variation	*-15%*	*-10%*	*0% (1900 kg)*	*+10%*	*+15%*
Frontal area [m^2]	*2.56*	*2.66*	*2.86*	*2.92*	*2.95*
Energy	1.04	1.04		1.11	1.11
Maximum power	1.02	1.01		1.05	1.05
Mean power	1.04	1.04		1.10	1.10
Mean deceleration	0.00	0.00		0.00	-0.12
Max deceleration	0.00	0.00		-0.39	-0.26
Mean velocity	0.13	0.19		-0.01	0.00
Max velocity	0.00	0.00		0.00	0.12

Table 3.44: sensitivity analysis results expressed as absolute values

Weighted mean method with Mean Power distribution					
Mass variation	*-15%*	*-10%*	*0% (1900 kg)*	*+10%*	*+15%*
Frontal area [m^2]	*2.56*	*2.66*	*2.86*	*2.92*	*2.95*
Energy [KJ]	48.09	51.06	56.99	63.28	66.45
Maximum power [kW]	10.67	11.31	12.59	13.92	14.58
Mean power [kW]	5.91	6.27	7.00	7.77	8.15
Mean deceleration [m/s^2]	-0.26	-0.26	-0.26	-0.26	-0.26
Max deceleration [m/s^2]	-0.58	-0.58	-0.58	-0.58	-0.58
Mean velocity [m/s]	3.33	3.32	3.32	3.32	3.32
Max velocity [m/s]	3.38	3.38	3.38	3.38	3.38

Table 3.45: sensitivity analysis results expressed as relative variations

Weighted mean method with Mean Power distribution					
Mass variation	*-15%*	*-10%*	*0% (1900 kg)*	*+10%*	*+15%*
Frontal area [m^2]	*2.56*	*2.66*	*2.86*	*2.92*	*2.95*
Energy	1.04	1.04		1.11	1.11
Maximum power	1.02	1.01		1.06	1.06
Mean power	1.04	1.04		1.10	1.10
Mean deceleration	0.00	0.00		0.00	0.00
Max deceleration	0.00	0.00		0.00	0.00
Mean velocity	-0.02	0.00		0.00	0.00
Max velocity	0.00	0.00		0.00	0.00

Table 3.46: sensitivity analysis results expressed as absolute values

Weighted mean method with Maximum power distribution					
Mass variation	*-15%*	*-10%*	*0% (1900 kg)*	*+10%*	*+15%*
Frontal area [m^2]	*2.56*	*2.66*	*2.86*	*2.92*	*2.95*
Energy [KJ]	54.95	58.36	65.13	72.32	75.94
Maximum power [kW]	12.19	12.92	14.39	15.90	16.66
Mean power [kW]	6.75	7.17	8.00	8.88	9.32
Mean deceleration [m/s^2]	-0.30	-0.30	-0.30	-0.30	-0.30
Max deceleration [m/s^2]	-0.66	-0.66	-0.66	-0.66	-0.66
Mean velocity [m/s]	3.80	3.80	3.80	3.80	3.80
Max velocity [m/s]	3.86	3.86	3.86	3.86	3.86

Table 3.47: sensitivity analysis results expressed as relative variations

Weighted mean method with Maximum power distribution					
Mass variation	*-15%*	*-10%*	*0% (1900 kg)*	*+10%*	*+15%*
Frontal area [m^2]	*2.56*	*2.66*	*2.86*	*2.92*	*2.95*
Energy	1.04	1.04		1.11	1.11
Maximum power	1.02	1.02		1.05	1.05
Mean power	1.04	1.03		1.10	1.10
Mean deceleration	0.00	0.00		0.00	0.00
Max deceleration	0.00	0.00		0.00	0.00
Mean velocity	0.00	0.00		0.00	0.00
Max velocity	0.00	0.00		0.00	0.00

A comparison of the characteristic quantities values variations is in the charts from Table 3.37, Table 3.39 and Table 3.41 are graphically compared from Fig 3.125 to Fig 3.131.

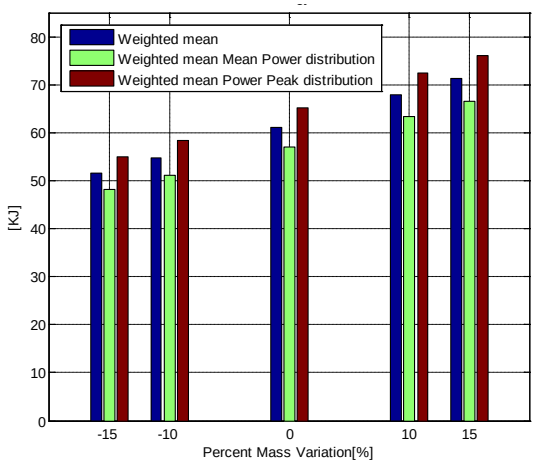

Fig 3.155 Energy values

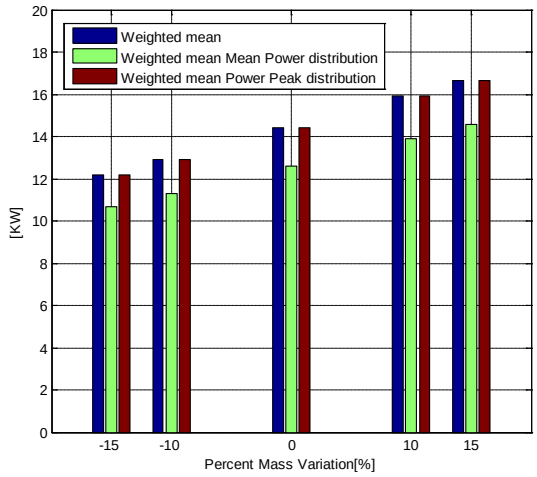

Fig 3.156 Maximum power values

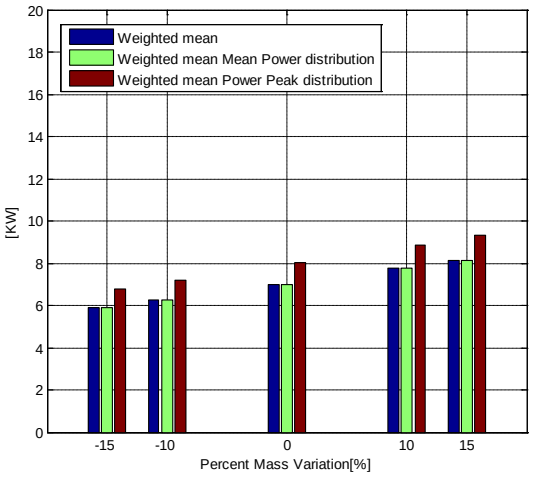

Fig 3.157 Mean power values

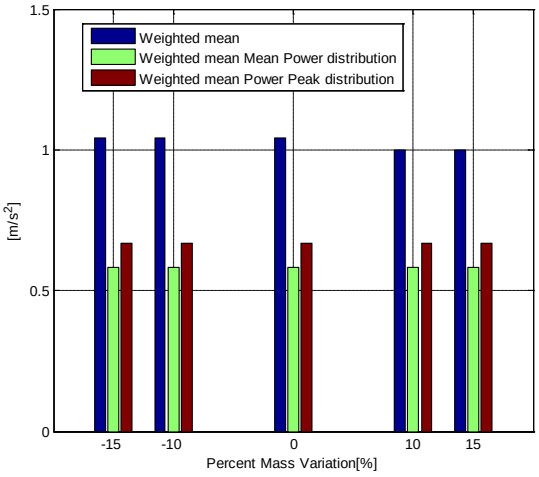

Fig 3.158 Maximum deceleration values

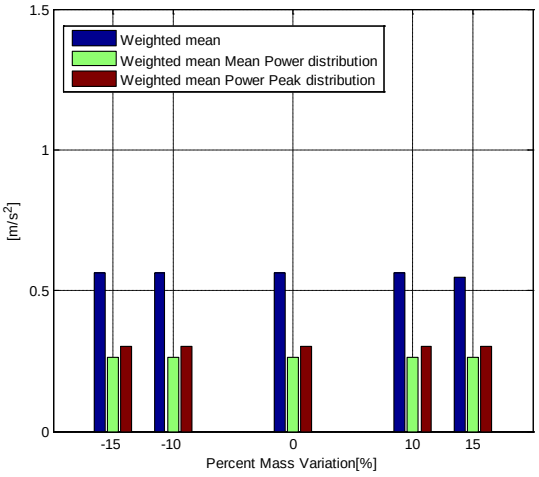

Fig 3.159 Mean deceleration values

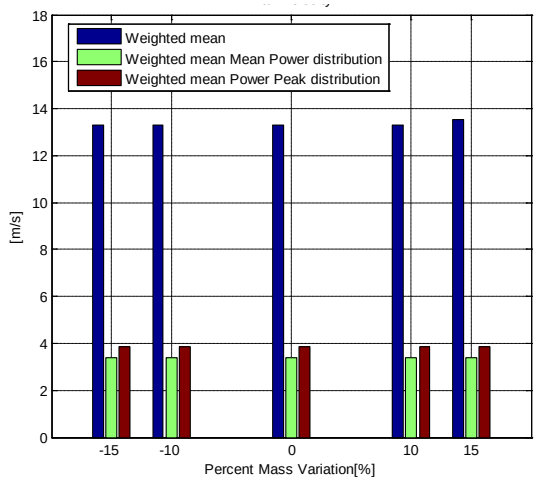

Fig 3.160 Maximum velocity values

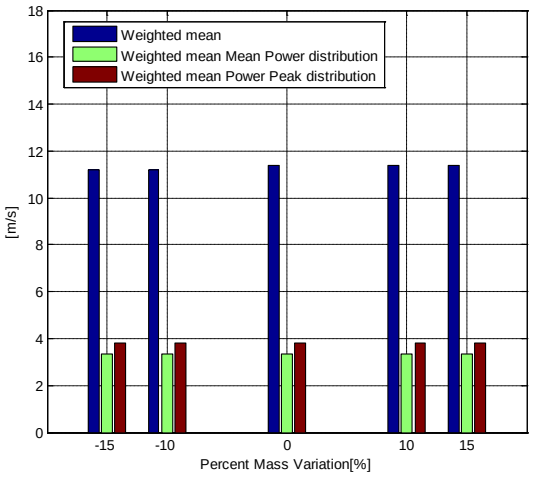

Fig 3.161 Mean velocity values

3.3 Representative Cycles Analysis

In previous section a driving cycles analysis methodology has been proposed and developed. This methodology has been applied to real world cycles, based on data acquired during on road tests, and to some fundamental regulatory cycles usually used adopted for fuel consumption and emission certification of vehicles.
As final step of this analysis it is possible to define statistically relevant cycles that can represent typical commuting scenarios. We can then define three different "users":

Table 3.48 Users scenarios composition

User	Total distance	Composition
I	4 miles	2 UT + 2 UNT
II	10 miles	2 UT + 3 HT + 3 HNT + 2UNT
III	20 miles	2 UT + 3 HT + 3 HNT + 5 FT + 5 FNT + 2 UNT

The cycles that compose the users are referred to Table 3.1. It is important to notice that since it is a statistical analysis there is no relation with the sequence of the basic cycles composing every "user".
For these "users" we are going to elaborate possible representative values with the mean values method, maximum values method, weighted average values method, weighted average values method with mean power distribution and weighted average values method with maximum power distribution as done in Table 3.7.
The considered vehicle is a SUV with the following characteristics:

Table 3.49 Vehicle characteristics

SUV data	
Vehicle mass	1900 Kg
Frontal area	2.86 m^2
Drag coefficient	0.42

3.3.1. User I

The first user represents a typical driving cycle inside a city with variable traffic conditions. In fact there are two urban patterns with traffic and two urban patterns with no traffic conditions assuming a reasonable short driving distance in the city.
In Fig 3.132 the User I vehicle speed profile is reported. It is possible to notice a maximum velocity difference related to the different traffic conditions.

In Table 3.45 the characteristic metrics of statistically relevant event are reported using the five different methods reported above.

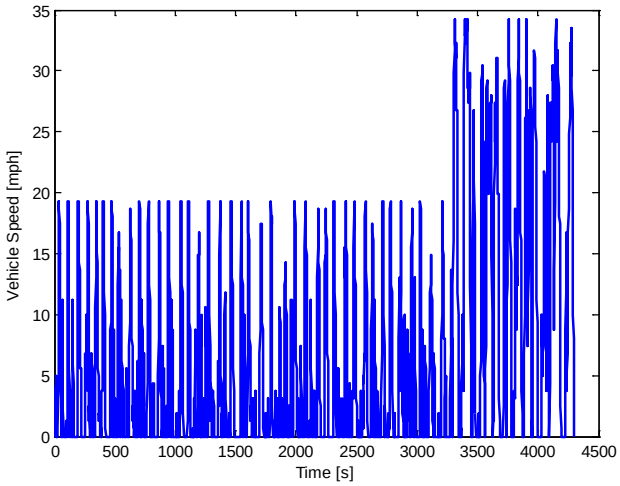

Fig 3.162 User I Vehicle speed vs. time profile

Table 3.50 Representative event values for User I

	Weighted mean method	Mean values method	Maximum values method	Weighted mean method with Mean Power distribution	Weighted mean method with Maximum power distribution
Energy [kJ]	24.59	20.50	189.20	24.59	28.38
Maximum power [kW]	6.46	5.71	43.05	5.59	6.46
Mean power [kW]	2.85	2.47	21.90	2.85	3.28
Mean deceleration [m/s^2]	-0.46	-0.46	-1.48	-0.19	-0.22
Max deceleration [m/s^2]	-0.92	-0.99	-4.16	-0.54	-0.62
Mean velocity [m/s]	3.59	3.54	14.96	1.94	2.24
Maximum velocity [m/s]	5.04	5.09	15.27	1.98	2.29

3.3.2. User II

The second user represents a typical driving cycle inside a city and on highway with variable traffic conditions. In this case the driving distance is supposed to be longer than the previous only city cycle. In Fig 3.133 the User II vehicle speed profile is reported. It is possible to notice a maximum velocity difference related to the different traffic conditions and patterns.

In Table 3.46 the characteristic metrics of statistically relevant event are reported using the five different methods reported above.

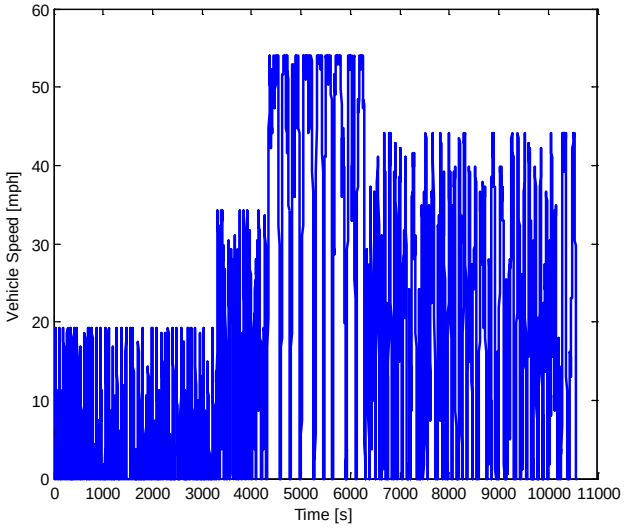

Fig 3.163 User II Vehicle speed vs. time profile

Table 3.51 Representative event values for User II

	Weighted mean method	Mean values method	Maximum values method	Weighted mean method with Mean Power distribution	Weighted mean method with Maximum power distribution
Energy [kJ]	50.93	39.57	363.81	54.57	50.93
Maximum power [kW]	11.37	10.25	81.22	12.18	11.37
Mean power [kW]	5.45	4.67	36.34	5.45	5.09
Mean deceleration [m/s^2]	-0.52	-0.52	-1.48	-0.22	-0.21
Max deceleration [m/s^2]	-1	-1.03	-4.16	-0.62	-0.58
Mean velocity [m/s]	7.83	7.70	23.72	3.56	3.32
Maximum velocity [m/s]	9.66	9.54	24.16	3.62	3.38

3.3.3. User III

The third user represents a typical driving cycle inside a city, on the highway and on the freeway with variable traffic conditions. The driving distance is supposed to be the longest since the cycle includes all the different patterns.

In Fig 3.134 the User III vehicle speed profile is reported. It is possible to notice a maximum velocity difference related to the different traffic conditions and patterns.
In Table 47 the characteristic metrics of statistically relevant event are reported using the five different methods reported above.

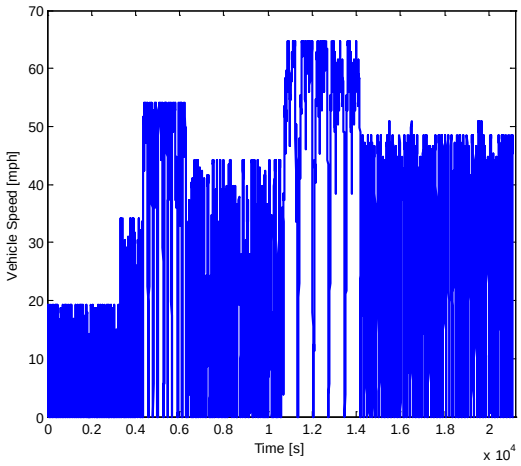

Fig 3.164 User III Vehicle speed vs. time profile

Table 3.52 Representative event values for User III

	Weighted mean method	Mean values method	Maximum values method	Weighted mean method with Mean Power distribution	Weighted mean method with Maximum power distribution
Energy [kJ]	61.54	45.96	512.88	71.80	71.80
Maximum power [KW]	12.59	10.90	89.96	12.59	12.59
Mean power [kW]	6.19	5.24	44.19	6.18	6.18
Mean deceleration [m/s^2]	-0.53	-0.53	-1.52	-0.21	-0.21
Max deceleration [m/s^2]	-0.96	-0.95	-4.16	-0.58	-0.58
Mean velocity [m/s]	11.30	11.09	28.25	3.95	3.95
Maximum velocity [m/s]	13.11	12.97	28.50	3.99	3.99

Above five methods have been used to obtain values that can create target events for every “user”. In Table 3.45, Table 3.46 and Table 3.47 these values are reported. It is possible to notice that the target energy and target power values are bigger as in the driving cycles higher speed driving patterns are introduced, reported in Fig 3.132, Fig

3.133 and Fig 3.134. It seems then that an energy recovering system could be implemented more successfully in a vehicle driving the “III User” pattern than the “ I User” pattern. But, it is important to take in consideration the quantities that characterize all the cycle, as total theoretical recoverable energy and total required energy.

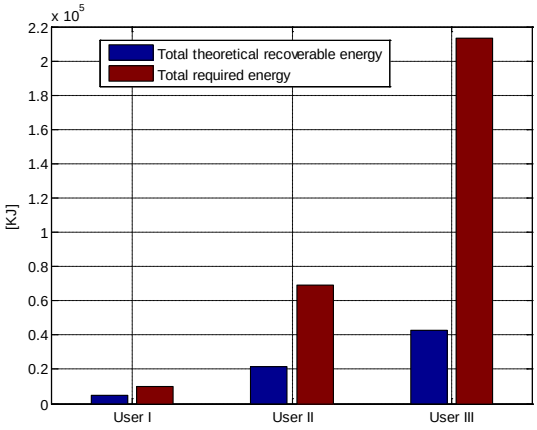

Fig 3.165 Comparison between the total theoretical recoverable energy and the required energy

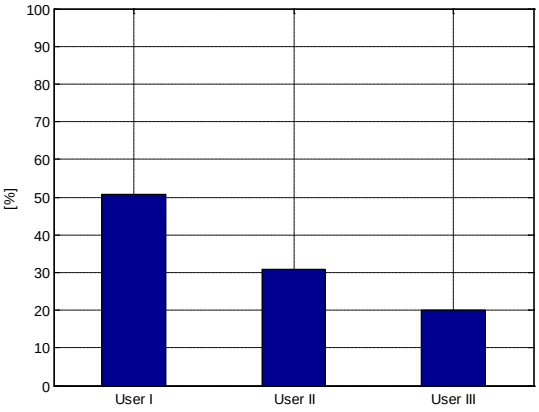

Fig3.166 Percent value of theoretical recoverable energy and required energy rate

In Fig 3.135 these two fundamental quantities are reported. It is possible to notice that as the driving cycle is composed by high speed patterns, the recoverable braking energy increases, but not as much as the energy required moving the vehicle does. In Fig3.136 it is reported the per cent value of recoverable energy and required energy: for “User I”, almost 50% of required energy could be obtained by the energy accumulated during braking phases, whereas for “User III” this values drops to almost 20%.

4. Design Procedure for Alternative Energy Storage Systems

In this chapter the methodology to design an Alternative Energy Storage System (AESS) is presented. The procedure is developed to target *short term* energy storage, with the main goal to recover the maximum amount of energy during a deceleration event and then release it during a following acceleration event.

The literature review about classic design methodologies pointed out the inadequacy of these methodologies for short-term energy storage systems, since the designs are typically based on the worst-case scenario along the entire driving cycle.

The following methodology diverges from this approach in order to be suitable for short-term energy storage systems. In this chapter the design procedure will be shown for an hydraulic energy storage system, although it can be applied also to mechanical energy storage systems.

The procedure for designing the AESS is shown in Fig 4.1. The main steps are:

I. Definition of the design inputs for the AESS;
II. Definition of the design targets as related to the design inputs;
III. Determination of the physical constraints of the system;
IV. Determination of the relationship between design targets and design parameters of the system;
V. Definition of the attributes of the selected design solution;
VI. Design evaluation;

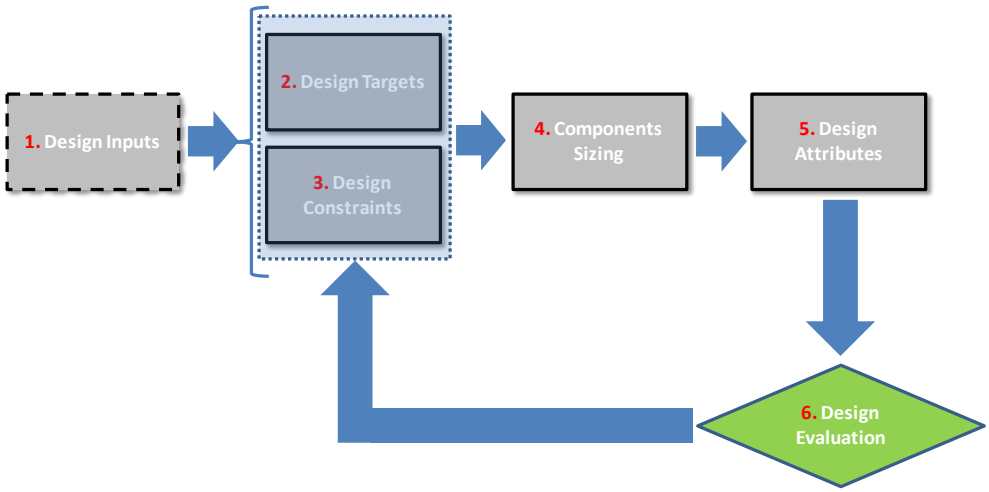

Fig 4.167:design procedure

The first step defines the design inputs by means of the analysis of a driving cycle that represents the use of the AESS. Then, the design inputs are coupled to design targets identifying related values for the metrics of the system. The physical constraints of the system, related to actual limitations of the specific components of the AESS, are the boundaries of the design targets. The following step is components sizing based on the relationships between design parameters of the system and design targets. Finally, after the designs attributes identification, the final system designs obtained by means of this process can be evaluated. If these are not satisfactory, a new iteration is started from point II.

In this case, the only system considered is the hydraulic system, but the same process can be applied for the mechanical one.

4.1 Definition of Design Inputs for the AESS

The first step in the design process is the definition of design inputs from the driving pattern on which the system is intended to be mostly used. This is obtained by means of the extraction and statistical processing of information on the most relevant dynamic and energy-related variables of a driving schedule. The design methodology is based on the driving cycle statistical analysis developed and proposed in Chapter 3.

The steps of the analysis of the driving cycles are summarized below:

I. calculation of the total vehicle traction power based upon a simplified model of the longitudinal dynamics of the vehicle;
II. identification and classification of the cycle events;
III. calculation of the distribution of dynamic and energy-related matrics;
IV. synthesis of the distributions of such variables to create a statistically representative event of the driving cycle.

The driving cycle analysis methodology permits to have several different design inputs depending on the way the statistically representative event is synthesized. Each design set is composed by seven dynamic and energy-related variables, namely energy, maximum and average power, maximum and average deceleration, maximum and average velocity.

4.2 Definition of the Design Targets of the AESS

Each design set, determined in the previous step, can be coupled to the actual design targets, which identify values for the design parameters of the system. The main design targets of an energy storage system are:

- Maximum value of the mechanical energy that can be recovered
- Maximum power at which mechanical energy can be recovered
- Vehicle speed range of operation for the recovery system

4.2.1. From Design Inputs to Design Targets

The design target are listed above and among them it is possible to recognize two energy-related metrics and one velocity metric. In particular the metric, "vehicle speed range", includes implicitly two velocity metrics: the initial vehicle speed and the vehicle deceleration. These four variables are all present in the design inputs. However in order to obtain a small number of inputs to insert in the procedure, it is possible to obtain the velocity metrics from the energy-related ones. The equations to relate the energy E and maximum power P_M to initial vehicle velocity V_i and deceleration a are:

$$E = \frac{1}{2} M_v {V_i}^2 \tag{4.1}$$

$$P_M = M_v V_i a \tag{4.2}$$

Using the equations above, by using only two energy-related design inputs, energy and maximum power, it is possible to obtain also the initial speed and the deceleration. Since the analysis focuses on short-term events, the deceleration is assumed constant.
In the following sections the four aforementioned variables will be linked to the design parameters by means of appropriate mathematical relationships.

4.3 Definition of Design Constraints for the AES Systems

In this step of the design procedure, the physical constraints of the Hydraulic Energy Storage systems are identified and listed, with reference to a parallel hybrid vehicle. A parallel hydraulic energy storage system consists of a hydraulic accumulator, reservoir, pump/motor and gears and it is connected to the vehicle driveline as shown in

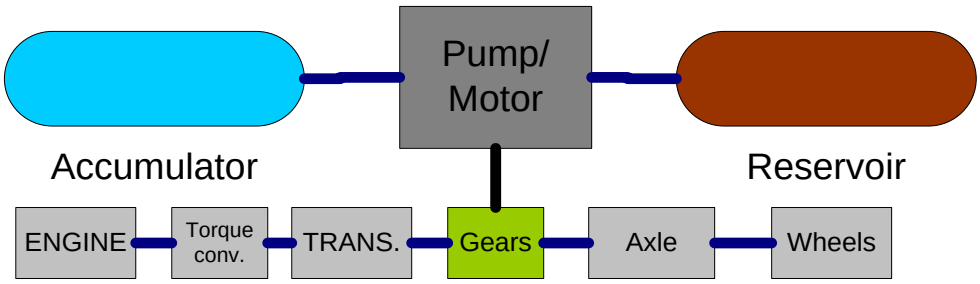

Fig 4.168: Parallel Hybrid Energy Storage System scheme

In this system, the main limitations are imposed by pump and accumulator, and they must be taken into account. The pump is limited to a maximum pressure differential, as well as maximum and minimum speed. The accumulator is limited by the maximum pressure and the ratio between system pressure and pre-charge pressure. In Table 4.1 the constraints are listed.

Table 4.53: hydraulic ESS design constraints

Design Constraints
- Maximum pump pressure
- Maximum pump speed
- Minimum pump speed
- Maximum accumulator pressure
- System pressure to accumulator pre-charge pressure ratio

4.4 Determination of the Relationships between Design Targets and Design Parameters of the AESS

In the section above the design targets have been identified and the main hydraulic system components individuated. Each component can be parameterized and the physical properties connected to the design targets. By establishing a mathematical connection between the two allows one to intuitively optimize the parameters to better meet the targets and goals for the system. In Table 4.2 the hydraulic system design parameters are shown.

Table 4.54: : hydraulic ESS design parameters

Design Parameters			
Accumulator	**Reservoir**	**Pump/Motor**	**Gears**
- Volume - Maximum pressure - Pre-charge pressure	-Volume -Pre-charge pressure	-Maximum displacement -Maximum pressure	-Pump to driveshaft

The effects of the system parameters on the design targets can be calculated referring to the following equations.

a) Desired Energy Storage

The energy storage device in a hydraulic ESS is the accumulator. The potential energy stored in an accumulator can be calculated as the integral of the work done on the gas chamber by the hydraulic fluid. As a first approximation, by neglecting the heat transfer to the surroundings and assuming adiabatic gas compression, the following expression for the energy stored in the accumulator can be derived [28]:

$$E_{accumulator} = p_0 \int_{V_{min}}^{V_{max}} \left(1 - \frac{V}{V_{acc}}\right)^{-\gamma} dV \tag{4.3}$$

Where $E_{accumulator}$ is the accumulator potential energy, p_o is the accumulator pre-charge pressure, V_{min}, V_{max} and V_{acc} are the initial volume, the final volume and the total volume

of the accumulator, V is the fluid volume in the accumulator and γ is the specific heat ratio of the pre-charge gas.

b) **Desired Power Capability**

The power that can be absorbed or provided by the hydraulic system is a function of the hydraulic pump speed, maximum pump displacement, and accumulator pressure. In details:

$$P_{pump,max} = \Delta p_{pump} * D_{pump,max} * \omega_{pump} * \eta_{pump} \tag{4.4}$$

Where $P_{pump,max}$ is the maximum pump power, Δp_{pump} is the pressure differential across the pump, $D_{pump,max}$ is the maximum pump displacement, η_{pump} is the pump efficiency and ω_{pump} is the pump speed. The maximum pump displacement is dependent on the specific pump model chosen.

The pressure differential across the pump is the difference between the accumulator pressure and the reservoir pressure:

$$\Delta p_{pump} = p_{acc} - p_{res} \tag{4.5}$$

The pump speed is a function of the gearing between the pump and the drivetrain and the vehicle speed:

$$\omega_{pump} = \frac{V_{veh}}{r_w} * g_{FD} * g_{pump} \tag{4.6}$$

Where V_{veh} is the vehicle velocity, r_w is the tire radius, g_{FD} is the final drive ratio and g_{pump} is the gear ratio between pump and driveshaft.

For a given vehicle speed, the torque demand on the pump can be found as a function of the desired acceleration of the vehicle according to the following expression:

$$T_{pump,des} = \frac{M_{eff} * \frac{dV_{veh}}{dt} * r_w}{g_{FD} * g_{pump}} \tag{4.7}$$

where M_{eff} is the effective vehicle mass. In this term, the contribution of wheels and rotating masses to vehicle inertia is considered as a constant term, increasing the vehicle

effective mass m_v by 10%. The desired pump torque can be compared to the available pump torque (physical constraint):

$$T_{pump,avail} = \Delta p_{pump} * D_{max,pump} \tag{4.8}$$

If the available torque matches or exceeds the desired pump torque for a given vehicle speed, the target power can be met (assuming pump speed constraint is met).

c) Range of Vehicle Speed Operation

Due to limitations on pump speed, consideration must be given to the desired range of vehicle speed operation for the system. The pump speed is directly related to vehicle speed through the following equation:

$$\omega_{pump} = \frac{V_{veh}}{r_w} * g_{FD} * g_{pump} \tag{4.9}$$

Constraints on maximum and minimum pump speed limit the range of vehicle speed operation for a given gear ratio between the pump and the drivetrain. The pump speed limits are imposed by the manufacturer and they are related to the pump design.

4.5 Definition of the attributes of the selected design solution

In order to close the loop on the design process, correlations must be developed between the components of the hydraulic energy storage system defined by the design parameters in Table 2, and the physical properties. In fact, each component is characterized by a mass and volume, whose values depend on the components sizes. By means of these correlations definition, the attributes for each system design are determined. These attributes are expressed in terms of total mass and volume. This process allows for a more complete comparison of the various system designs and enables more accurate vehicle simulation with the system models implemented.

Since it is not possible to know the exact final mass and volume of all the system components without designing and testing the complete system, estimates for the physical properties are necessary. In order to do it, commercial components have been

used to create system components parametric models to correlate the parameters to attributes values.

For the hydraulic energy storage system, the components considered for the attributes definitions are : the pump, the accumulator, the reservoir, the hydraulic lines and the hydraulic fluid.

a) Pump Mass and Volume

With reference to a production medium duty, variable displacement axial piston pump for mobile applications [29] as the basis for the correlation, pump displacement can be plotted against mass and volume. These correlations are shown in Fig 4.3 and Fig 4.4. The plotted points are related to commercial products physical properties. A linear correlation is extracted correlate the pump displacement value to the component mass and volume.

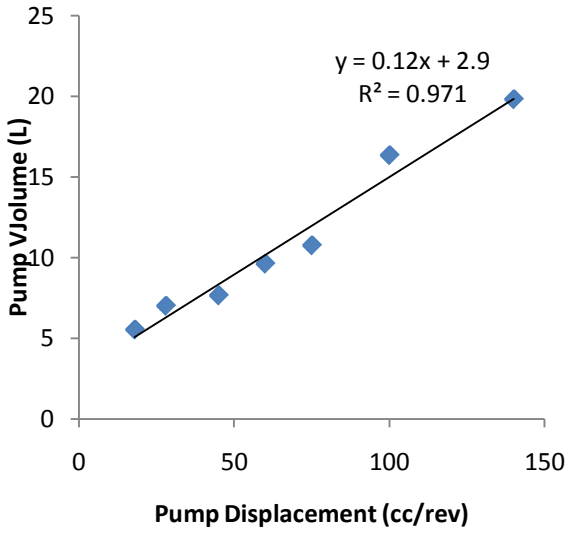

Fig 4.169: Axial Piston Pump Volume Correlation,[29]

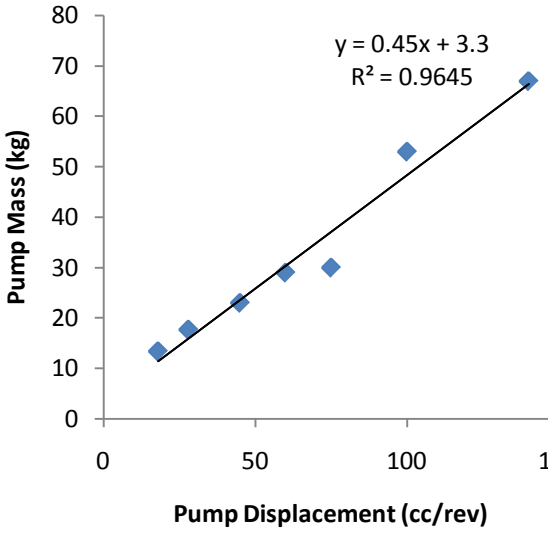

Fig 4.170: Axial Piston Pump Mass Correlation, [29]

b) Accumulator Mass and Volume

The nominal accumulator volume chosen for energy sizing purposes can be used to determine the actual volume occupied by the accumulator as well as the accumulator

dry mass for a given pressure and material [27]. A commercial bladder type accumulator made from steel was used to develop the following relationships. In Fig 4.5 and Fig 4.6 the mass and volume correlation to nominal volume are extracted using commercial products physical properties.

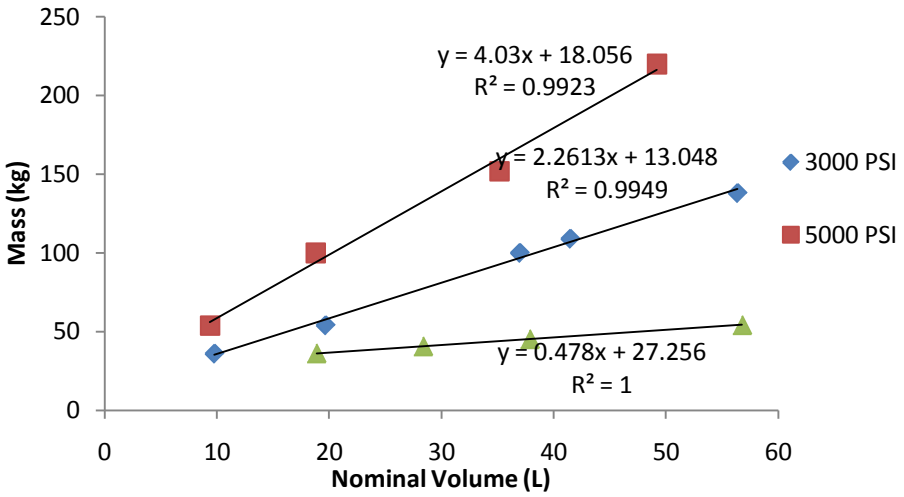

Fig 4.171: Nominal Volume to Mass Correlation, [27]

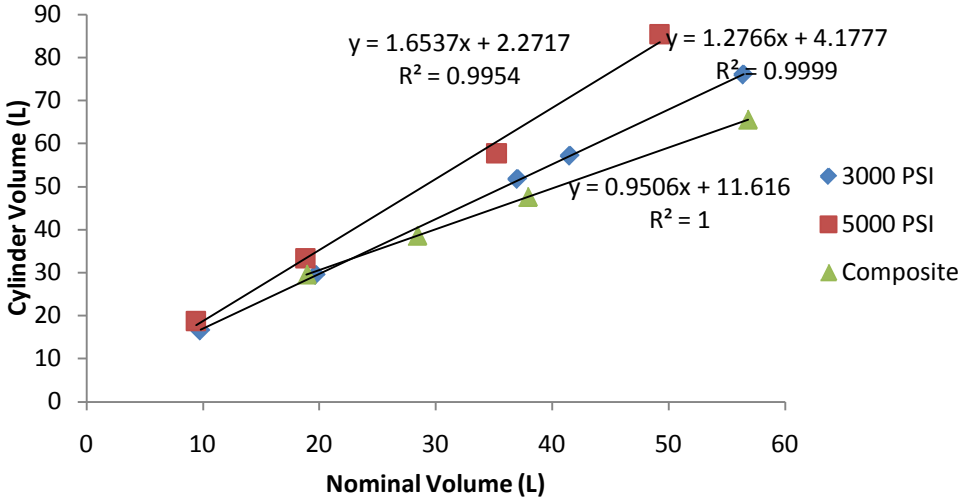

Fig 4.172: Nominal Cylinder to Volume Correlation, [27]

c) Fluid and Reservoir Mass and Volume

The necessary reservoir volume is based on the fluid volume needed to fill the accumulator from empty to maximum pressure. This volume also depends on pre-charge pressure which can vary based on design requirements.

If the pre-charge pressure is assumed to be constant, a correlation between available volume (maximum fluid volume) and nominal accumulator size can be determined, assuming an adiabatic compression. The following equation can be used to calculate the maximum accumulator fluid volume:

$$V_{max} = V_{acc} * \left(1 - \left(\frac{p_{pr}}{p_{max}}\right)^{\frac{1}{k}}\right) \tag{4.10}$$

where V_{max} is the maximum fluid volume, V_{acc} is the nominal accumulator volume, p_{pr} is the pre-charge pressure, and p_{max} is the maximum accumulator pressure. Once the fluid volume is known, fluid density can be used to estimate the mass of the fluid in the system. The reservoir volume can be estimated as the same as the fluid volume for the system. Knowing the volume of the reservoir, an approximate mass for the reservoir can be calculated based on material type, wall thickness, and the cross section.

4.6 Design evaluation

In the previous steps, the short-term energy storage system was sized depending on the design inputs and its attributes were defined. The last step of the procedure concerns the evaluation of the design performance. In order to do so, simulations of the energy storage system use during testing braking events are performed.

The energy storage system design is based on a driving test representing a typical system use. In order to perform the simulations, it is necessary to determine testing driving cycles. These cycles can be similar to the one used to size the system or different to represent other testing scenarios. From these cycles, multiple testing events are extracted by means of a criteria based on the statistical cycles analysis. These events are characterized by stop/start phases to reproduce an ideal short-term energy storage system use characterized by a system energy storing phase and a complete energy releasing phase. Since the vehicle dynamics has to be considered, a simplified inertial mass model is created. For each testing event simulations are run and the system

performance are evaluated by means of efficiency calculations: one way efficiency, η_{1-way}, and two way efficiency, η_{2-way}. The one way efficiency takes into account the effective stored energy, E_{stored} and the event available energy in the braking phase, $E_{available}$. This is the one-way efficiency definition:

$$\eta_{1-way} = \frac{E_{stored}}{E_{available}} * 100 \tag{4.11}$$

The second efficiency calculation is related to the inertial mass initial kinetic energy, E_{veh-i}, and to final kinetic energy, E_{veh-f}. This is defined also as round-trip efficiency or two way efficiency:

$$\eta_{2-way} = \frac{E_{veh-f}}{E_{veh-i}} * 100 \tag{4.12}$$

In order to evaluate the performances of each specific system design on the tested driving cycle, it is necessary to define a meaningful efficiency value. The efficiency values calculated in each testing event have to be related to the events significance in the cycle, in terms of events frequency. It is clear that in the final design performance evaluation, an efficiency value on a testing event that frequently occurs in the cycle has a bigger weight than an efficiency value on an uncommon event. Therefore, the design performance will be evaluated by means of a "statistically representative" efficiency, obtained by applying the weighted average method to the efficiency values. This statistically representative efficiency will be evaluated for both the one way efficiency and the round-trip efficiency. The weights determination process is related to testing events individuation and it will be explained in following chapter.

The final system design evaluation is done considering the aforementioned statistically representative efficiency on the testing cycle, taking into account also the system attributes, mass and volume.

By applying the presented design procedure to the hydraulic energy storage system, it is possible to obtain from each design input a system design. For each design the system components sizes are defined, such as the components weights and volumes. In the next chapter, the designs obtained are evaluated in simulation.

5. Results

In the previous chapters, a design methodology for short-term energy storage system for hybrid vehicles was proposed. This procedure is based on statistically relevant information extracted from a driving schedule representing the typical use of the vehicle. The information becomes the design inputs that determine the components sizing by means of defining a set of design targets and design constraints. Then the system design is evaluated considering the design solution attributes values.
In this chapter the energy storage system designs obtained are evaluated in simulation. The main extent is to provide a design procedure validation and to compare the designs over two driving cycles. In order to achieve these targets, the following steps are considered:

I. Definition of a real-world driving cycle for AESS design;
II. Application of the design procedure to size a hydraulic AESS;
III. Definition of real-world driving cycles for design verification;
IV. Definition of simulation methodology;
V. Evaluation of energy storage system designs in simulation;

5.1 Definition of Real-world Driving Cycle for System Sizing

The driving cycle definition is the preliminary phase to design procedure initialization. Since the energy storage system design depends on the characteristics of this driving cycle, it is important to create a meaningful driving pattern. In fact, it should be intended to represent the typical use of the vehicle. In order to achieve this goal, the "real-world" driving data can be used to create a statistically relevant driving scenario. Real-world driving data are synthetic driving cycles segments based on the acquisition of on-road vehicle speed vs. time data during one year period [23].
In order to initialize the hydraulic energy storage system design procedure it is necessary to create a driving pattern representing a typical use of the system. From this cycle the designs requirements are going to be extracted. As shown above, six different driving segments typologies have been created. The basic criterion is the definition of a commuting scenario with a meaningful patterns distribution and composition. The most meaningful cycle can be obtained, by including all the different driving conditions,

representing a generic trip starting and ending in the city after travelling over highways and freeways. In Table 5.1 this cycle is reported:

Table 5.55: real-world system design driving cycle composition

Total distance	Composition
20 miles	2 UT + 2 UNT+ 3 HT + 3 HNT + 5 FT + 5 FNT

Where:

UT is 1 mile urban driving segment with traffic condition;
UNT is 1 mile urban driving segment with no traffic condition;
HT is 1 mile highway driving segment with traffic condition;
HNT is 1 mile highway driving segment with no traffic condition;
FT is 1 mile freeway driving segment with traffic condition;
FNT is 1 mile freeway driving segment with no traffic condition;

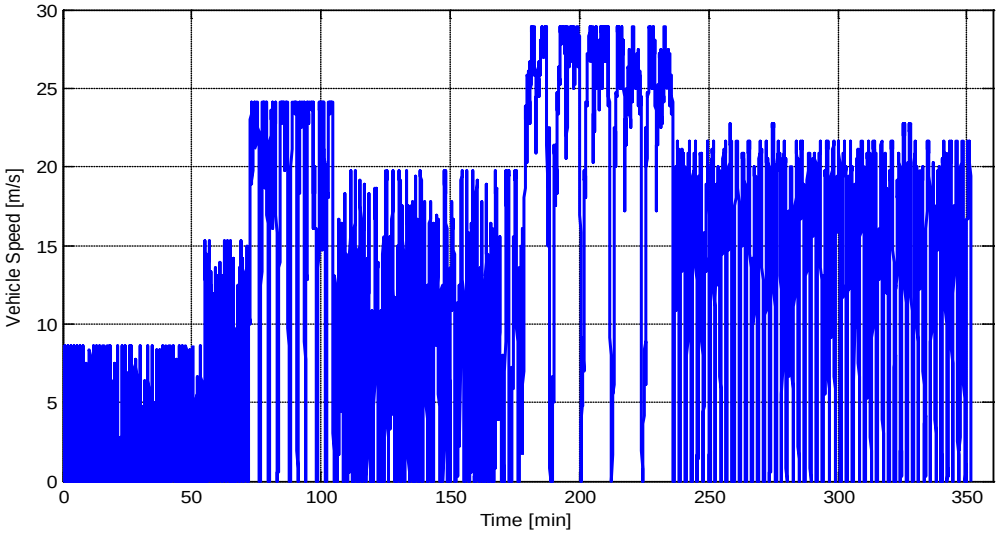

Fig 5.173: velocity profile of the system design driving cycle

It is important to underline that in the statistical analysis it is not important the order in which the analyzed segments are combined, since the procedure decomposes the cycle into events.

This driving data are then processed statistically to define the design requirements, which are the input to the energy storage system design phase.

5.1 Application of the Design Procedure

Using the driving cycle analysis procedure developed in Chapter 3, the design requirements are obtained starting from the vehicle speed data shown in Fig 5.1 and considering a mid-size SUV as in Table 5.2.

Table 5.56: vehicle parameters for the design procedure

Vehicle Parameters	
Effective mass	1900 kg
Frontal area	2.86 m^2
Drag coefficient	0.42

The total power can be calculated based on equations (3.11):

$$P = F_t V = \left[\left(F_r + F_g + F_a\right) + m_v \frac{dV(t)}{dt}\right] V \tag{5.1}$$

The total power for the system design real-world driving cycle is represented below.

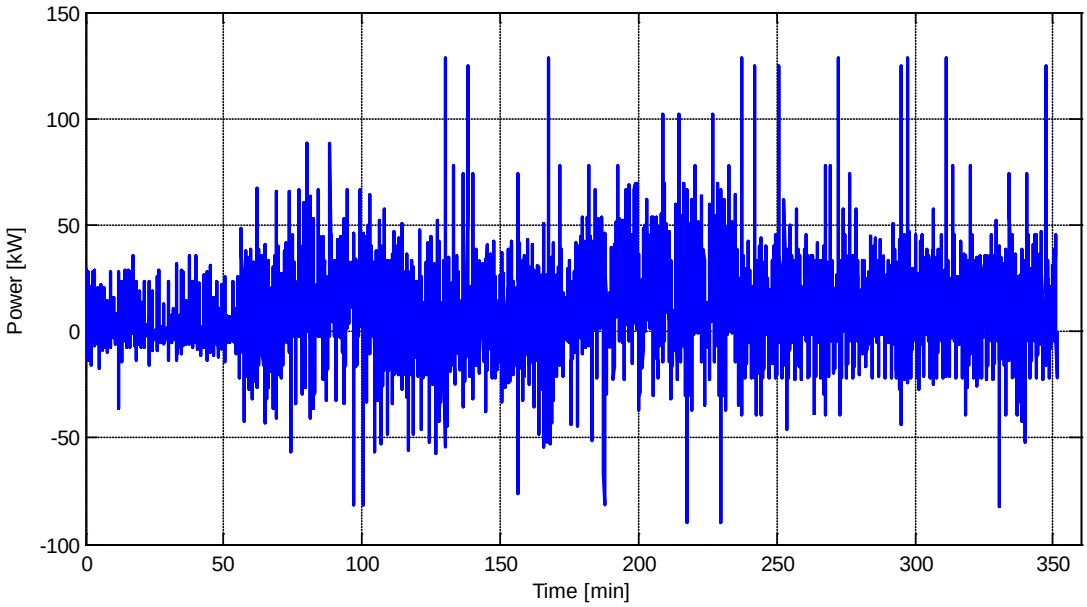

Fig 5.174: vehicle power demand at the wheel of the system design driving cycle

It is possible notice that the power profile oscillations amplitude has great variations because during the driving cycle the maximum speed values change depending on the distribution of driving segments. The maximum positive values are about 130kW, while the maximum absolute negative values are about 70 kW.

The next phase concerns the positive and negative power events identification: negative power events are relative to vehicle braking phases while positive power events are relative vehicle traction phases. As example, Fig 5.3 shows two events identified in the cycle.

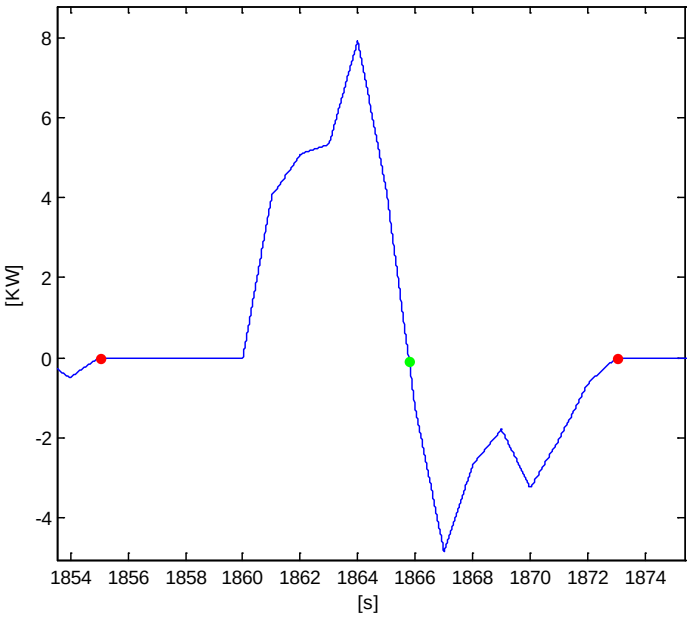

Fig 5.175: Example of events identification in a cycle profile segment

For each power event, a set of characteristic metrics is evaluated: total energy, maximum power, average power, maximum deceleration/acceleration, maximum deceleration/acceleration, maximum velocity and average velocity.

By means of these metrics, positive and negative power events are classified with the aim to develop detailed distributions of each of them. From Fig 5.4 to Fig 5.8 the distributions in the driving cycle of the variables above are shown for negative power events. The y-axis shows the frequency of the variable in the x-axis as observed in the cycle, normalized with respect to the total number of occurrences per cycle. The normalization values are listed in Table 5.3.

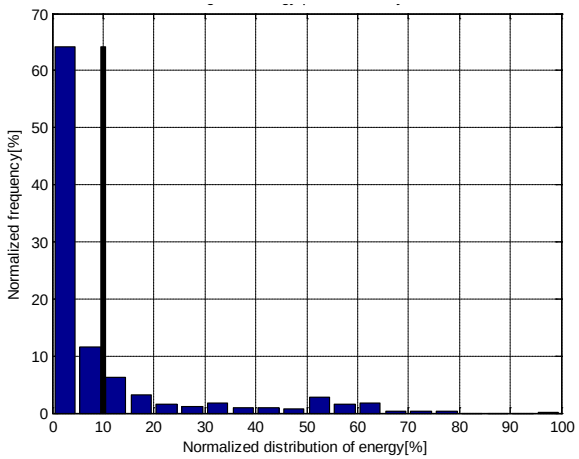

Fig 5.176: Energy distribution for driving cycle shown in Fig 5.1

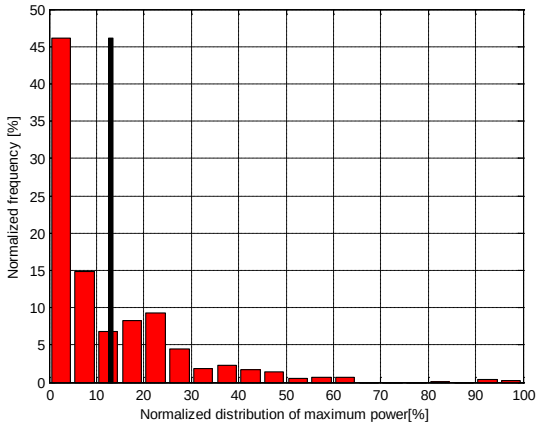

Fig 5.177: Maximum power distribution for driving cycle shown in Fig 5.1

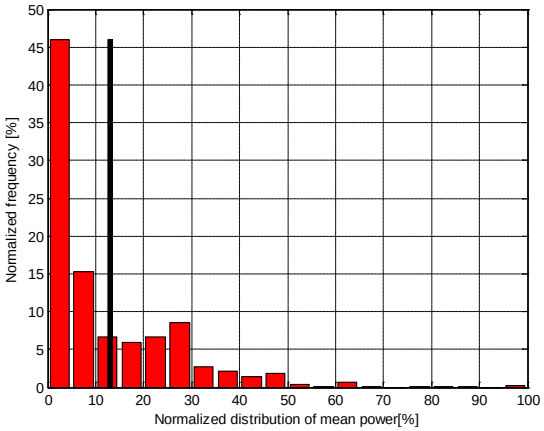

Fig 5.178: Mean power distribution for driving cycle shown in Fig 5.1

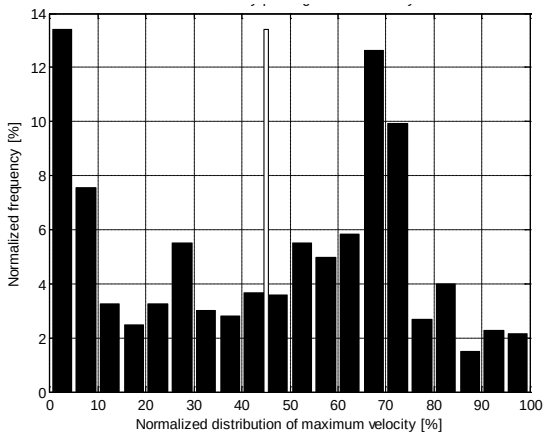

Fig 5.179: Maximum velocity distribution for driving cycle shown in Fig 5.1

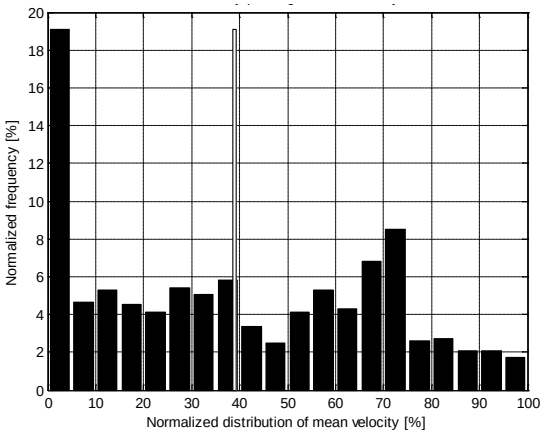

Fig 5.180: Mean velocity distribution for driving cycle shown in Fig 5.1

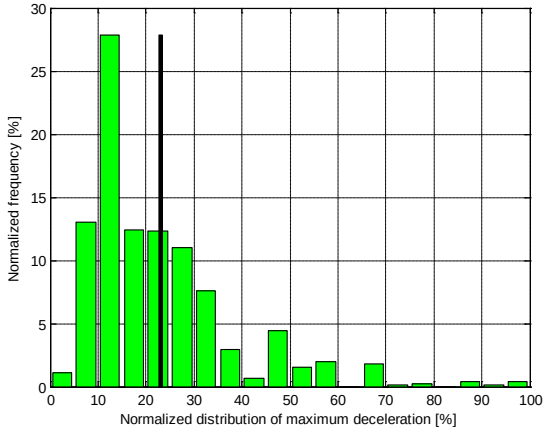

Fig 5.181: Maximum deceleration distribution for driving cycle shown in Fig 5.1

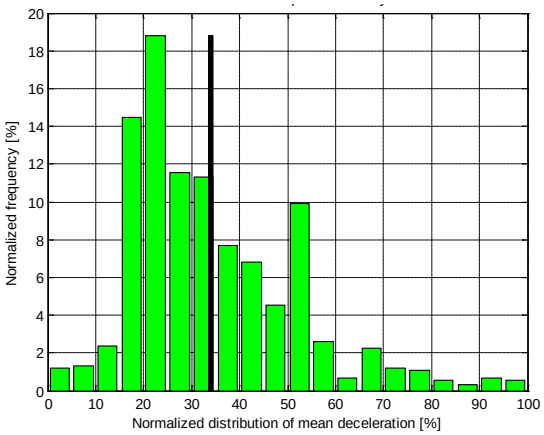

Fig 5.182: Mean deceleration distribution for driving cycle shown in Fig 5.1

Table 5.57: normalization values

Metric	Normalization value
Energy [kJ]	512.92
Maximum power [kW]	89.96
Mean power [kW]	45.31
Maximum deceleration [m/s^2]	-4.16
Mean deceleration [m/s^2]	-1.50
Mean velocity [m/s]	28.31
Max velocity [m/s]	28.50

Analyzing Fig 5.4 it is possible to notice that for this specific driving schedule, a large portion of the braking events are characterized by a small amount of energy. In fact, more than 65% of the total number of negative events has a corresponding energy below the 5% of the maximum value. Similar observations can be done for the braking average power and the maximum power, in particular more than 45% of the negative events has a corresponding average and maximum power value below the 5% of the maximum value.

The same trend is found in the braking events maximum power and energy values, as shown in Fig 5.11. The maximum points density is for very small energy and maximum power values.

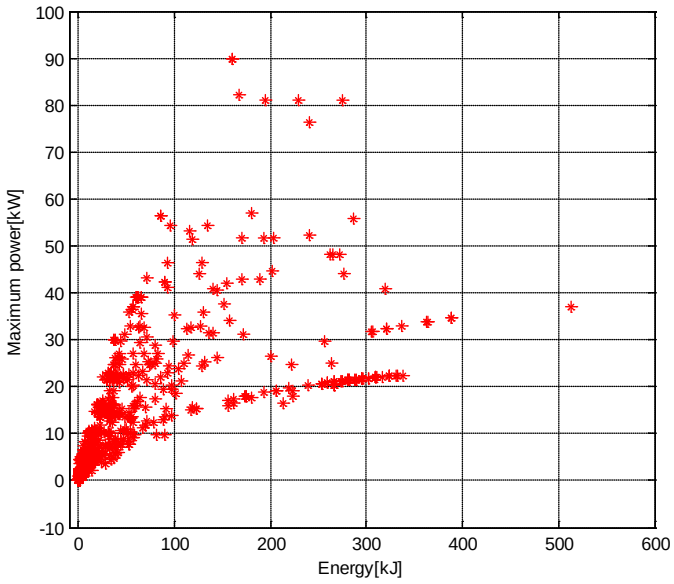

Fig 5.183: Braking events for driving cycle shown in Fig 1

The next step is provide a synthesis of the information contained in the negative events distributions. The goal is to define a representative braking event characterized by statistically relevant values of the variables shown from Fig 5.4 to Fig 5.10. Four different definitions for the representative event variables values are given, which will affect the design requiremements for the energy storage system sizing procedure:

- Weighted average of the variables of each cycle event by using as weights their normalized frequency over the cycle;
- Weighted average of the variables performed with a maximum power distribution of weights;
- Average value of the variables within events;
- Maximum value of the variables within events.

A summary of the representative cycle events is reported in Table 5.4

Table 5.58: Representative braking events of the driving cycle using different definitions

Representative events of the driving cycle				
	Weighted average method	**Mean value method**	**Maximum values method**	**Weighted average method with maximum power distribution**
Energy [kJ]	61.54	45.96	512.92	71.80
Maximum power [kW]	12.59	10.90	89.96	12.59
Mean power [kW]	6.19	5.24	44.19	6.18
Mean deceleration [m/s^2]	-0.53	-0.53	-1.52	-0.21
Max deceleration [m/s^2]	-0.96	-0.95	-4.16	-0.58
Mean velocity [m/s]	11.30	11.09	28.25	3.95
Maximum velocity [m/s]	13.11	12.97	28.50	3.99

5.2.1. Hydraulic Energy Storage System Design

In the previous section, four different definitions of the driving cycle representative event were given. Each one can be used as input for the hydraulic energy storage system design. Since they differ from one another then also the ESS components will have different characteristics and size. In order to conduct a comparative study, the four representative event definitions will be applied to the AESS design process, resulting into four different hydraulic systems. The design procedure considered was presented in detail in Chapter 4.

The hydraulic energy storage system consists of an accumulator, reservoir, variable displacement pump/motor and gears. Fig 5.12 presents a flowchart showing the basic procedure for sizing the system.

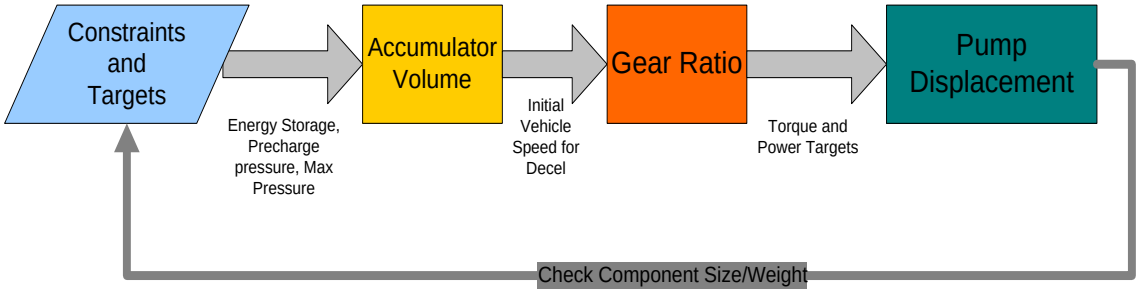

Fig 5.184 Hydraulic ESS Design Flowchart

Step 1: Determine Design Targets and Constraints

By applying the representative event definitions, four sets of design requirements are obtained, as shown in Table 5.5, based on the procedure described in Chapter 4.

Table 5.59: design requirements for system sizing using the four characteristic event definition

	Design target			
	Weighted average method	**Mean value method**	**Maximum value method**	**Weighted average method with Maximum power distribution**
Energy [kJ]	61.54	45.96	512.92	71.80
Maximum power [kW]	12.59	10.90	89.96	12.59

The constraints of the hydraulic energy storage system are typically related to accumulator and pump.

Table 5.60: design constraints for hydraulic system

Design Constraints	
Maximum accumulator pressure	350 bar
Accumulator pre-charge pressure	*Step 2*
Accumulator pressure ratio limitation	4:1
Maximum pump speed	*Step 3*

The listed constraints are average values based on commercial products characteristics. The constraints shown in Table 5.6 are given by the components manufacturers, which mandate specific limitations on the maximum system pressure and on the pump speed [27], [29].

Step 2: Determine Accumulator Size and Pre-charge Pressure

The maximum energy $E_{accumulator}$ for a range of accumulator sizes (V_{acc}) can be calculated for a range of pre-charge pressures p_0. The pre-charge pressure has to be chosen to maximize the storable energy. The accumulator has to satisfy the energy target and should be chosen in order to minimize size and weight penalties.

$$E_{accumulator} = p_0 \int_{V_{min}}^{V_{max}} \left(1 - \frac{V}{V_{acc}}\right)^{-\gamma} dV \tag{5.2}$$

Step 3: Determine Gear Ratio between Pump and Driveshaft

The gear ratio between the pump and the driveshaft determines the speed range at which the pump can operate. Assuming the final drive ratio equal to 1.9:1, based on initial vehicle speed V_{veh} for a typical braking event, as defined in step 1, the gear ratio g_{pump}can be calculated:

$$g_{pump} = \frac{\omega_{pump,max} * r_w}{V_{veh} * g_{FD}} \tag{5.3}$$

In this step, the maximum pump speed $\omega_{pump,max}$ can be defined considering commercial products and in accordance with the equation above.

Step 4: Determine Required Displacement for Desired Torque

The desired pump torque for a given condition is given by the following equation:

$$T_{pump,des} = \frac{M_{eff} * \frac{dV_{veh}}{dt} * r_w}{g_{FD} * g_{pump}} \quad (5.4)$$

By means of this equation it is possible to know the desired torque. Then, the necessary pump displacement required to provide this torque can be calculated as :

$$D_{max,pump} = \frac{T_{pump,avail}}{\Delta p_{pump}} \quad (5.5)$$

The worst case scenario for Δp_{pump} is pre-charge pressure minus the reservoir pressure. For this case we will assume the reservoir pressure is small and Δp_{pump} is equal to the pre-charge pressure.

Step 5: Determine Components Weights and Sizes

After the determination of the main parameters of the design components, it is necessary to calculate the mass and volume. This process is realized using the parametric models of the components calibrated on commercial products, as shown in Chapter 4.The results of the design procedure applied to the four definitions of representative event are summarized in Table 7.

Table 5.61:summary of final hydraulic ESS design attributes considering the four definitions of representative event

Summary of final hydraulic ESS designs				
	Weighted average method	**Mean values method**	**Maximum values method**	**Weighted average method with Maximum power distribution**
(g_{pump}) Pump gearing	4.19	4.85	1.45	3.88
(V_{acc}) Accumulator volume [m^3]	6.00	4.50	47.50	7.00

($T_{pump,des}$) Desired torque [Nm]	48.05	41.60	343.36	48.05
($D_{max,pump}$) Maximum pump displacement [cc/rev]	30.19	26.14	215.74	30.19
System total volume[m^3]	23.66	19.46	148.79	26.14
System total mass [Kg]	65.84	56.63	353.70	70.77

As expected, the ESS design based on the representative event created with the cycle maximum values shows the biggest volume and mass values. This is because this method represents the cycle worst-case scenario criteria that lead to maximize the dimensions of the components.

5.3 Definition of Real-world Driving Cycles for Design Validation

In order to realize a meaningful design procedure validation process, it is necessary to create different driving cycles on which the energy storage system designs attributes can be evaluated. In order to do so, two real-world driving cycles have been created as follows:

- Cycle-A: driving cycle based on the same distribution of driving segments as used for the design cycle;
- Cycle-B: driving cycle based on different distribution of driving segments;

5.3.1. Cycle-A

This driving cycle is based on the same driving segments distribution used to create the system design driving cycle. It means that they are composed by the same number of urban, highway and freeway driving segments. However the two driving velocity profiles are not same. In fact each driving pattern typology has the same maximum velocity, average velocity and number of stop. However, the pattern velocity trend is obtained by means of a stochastic process based real-world data acquisition.
In Fig 5.13 below, the driving cycle velocity profile is shown. Using the same vehicle parameters reported in Table 5.2, the cycle power profile can be obtained in Fig 5.14.

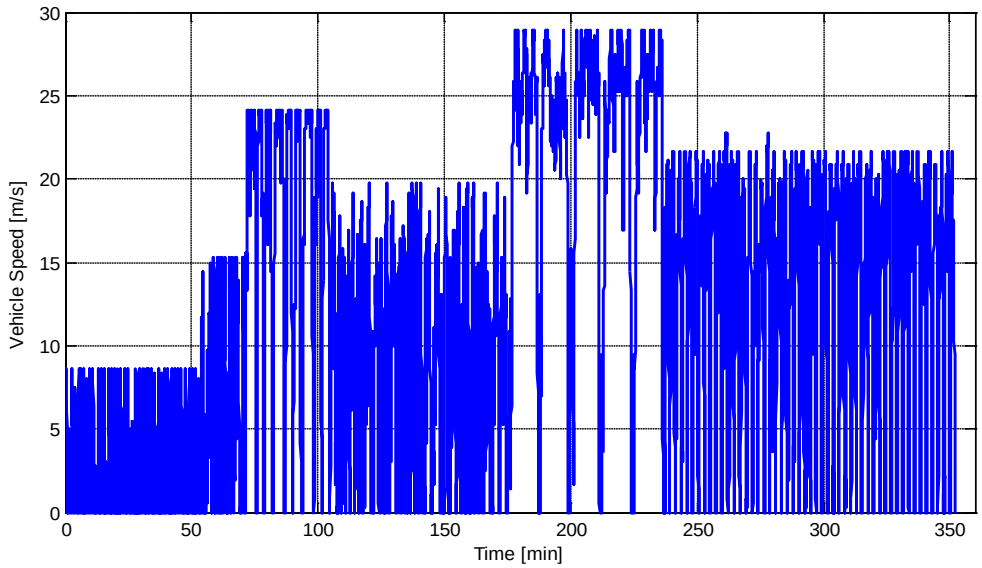

Fig 5.185: Cycle-A velocity profile

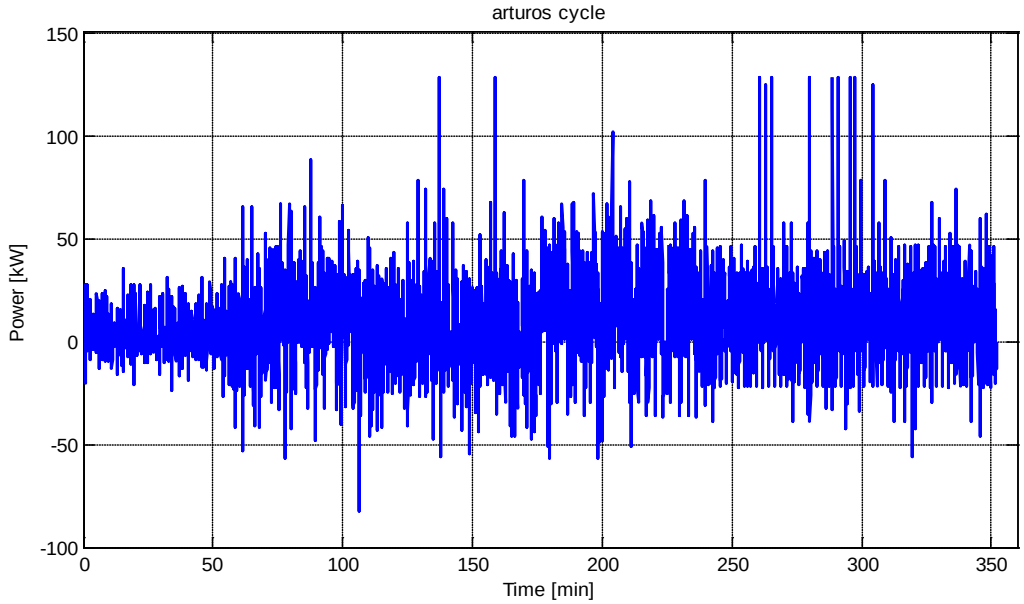

Fig 5.186: vehicle power demand at the wheel for Cycle-A

After the definition of the vehicle power demand profile, the negative and positive power events are identified. For each power event, the following characteristic metrics are evaluated, specifically the total energy, maximum power, average power, maximum deceleration, average deceleration, maximum velocity and average velocity.

By means of these variables, positive and negative power events are classified with the aim to define their statistical distributions. From Fig 5.15 to Fig 5.21 the distributions in the driving cycle of the variables above are shown for negative power events. The y-axis shows the frequency of the variable in the x-axis as observed in the cycle,

normalized with respect to the total number of occurrences per cycle. The normalization values are listed in Table 5.8.

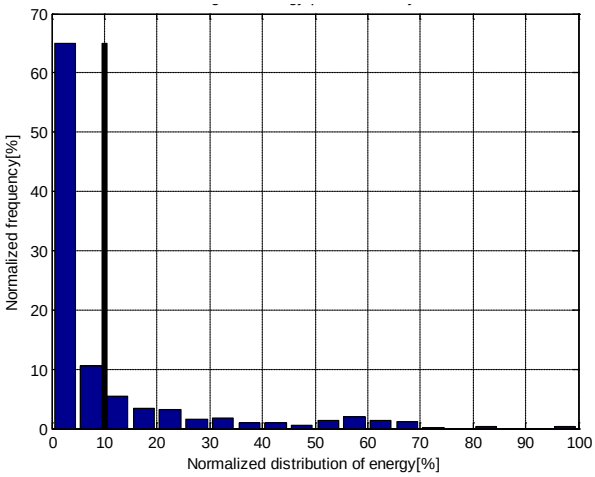

Fig 5.187: Energy distribution for Cycle-A

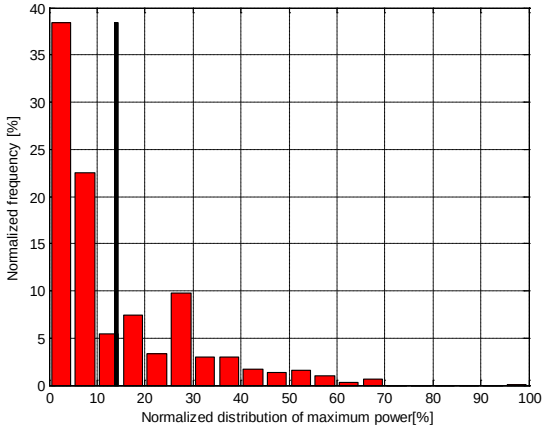

Fig 5.188: Maximum power distribution for Cycle-A

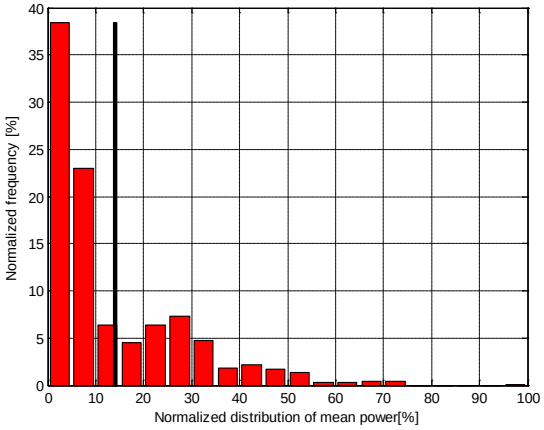

Fig 5.189: Mean power distribution for Cycle-A

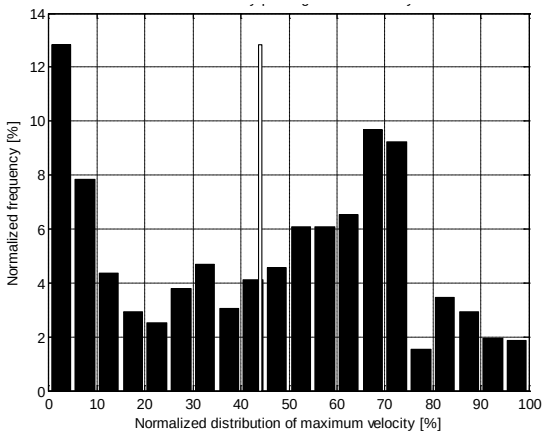

Fig 5.190: Maximum velocity distribution for Cycle-A

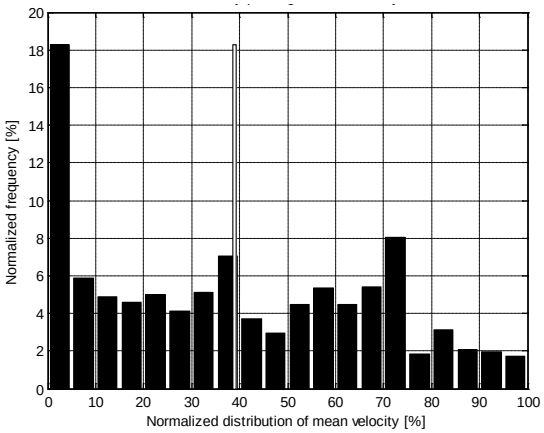

Fig 5.191: Mean velocity distribution for Cycle-A

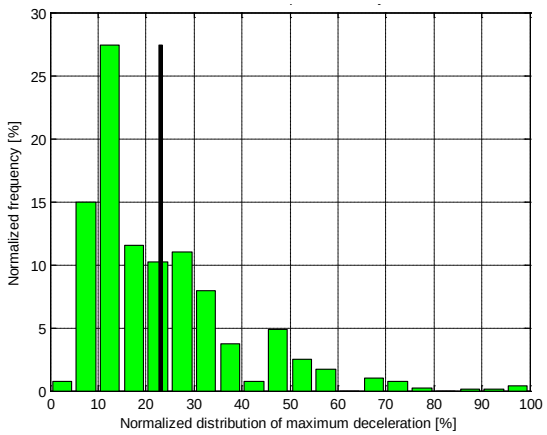

Fig 5.192: Maximum deceleration distribution for Cycle-A

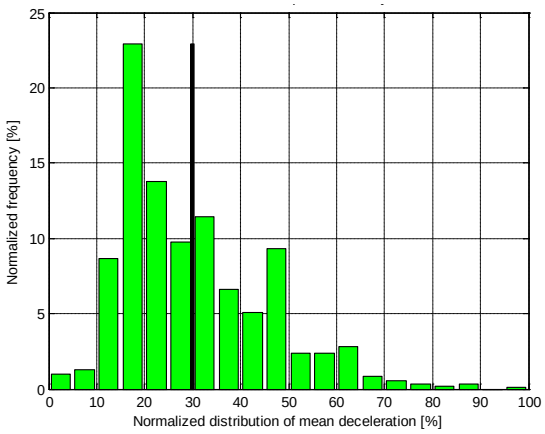

Fig 5.193: Mean deceleration distribution for Cycle-A

Table 5.62: normalization values for the previous distributions

Metric	Normalization value
Energy [kJ]	503.84
Maximum power [kW]	82.20
Mean power [kW]	41.12
Maximum deceleration [m/s^2]	-4.16
Mean deceleration [m/s^2]	-1.71
Mean velocity [m/s]	28.02
Max velocity [m/s]	28.60

The Cycle-A and the driving cycle on which the system has been designed have the same pattern segments composition. This can be noticed by analyzing the metrics distributions. In Fig 5.15 of Cycle-A, a large portion of the braking events is characterized by a small amount of braking energy, around 65%, as in Fig 5.4 for the system design cycle. In both the cycles, a large percentage of the braking events are characterized by a negative maximum and average power concentrate close to small power values. About 60% of events have an average and maximum power value below 10% of the maximum value. From Fig 5.18 to Fig 5.21 velocity and deceleration variables distributions are shown and they are very similar to distributions from Fig 5.7 to Fig 5.10 for the system design cycle.

5.3.2. Cycle-B

This driving cycle is composed by a different distribution of driving patterns. In this case only real-world urban and highway driving segments have been included following the composition in Table 5.9. Moreover, every pattern typology is composed by two subgroups related to the presence or not of traffic.

Table 5.63: Cycle-B real-world driving pattern composition

Total distance	Composition
10 miles	2 UT + 3 HT + 3 HNT + 2UNT

In the Fig 5.22 below, the driving cycle velocity profile is shown. Using the same vehicle parameters reported in Table 5.2, the cycle power profile can be obtained, as shown in Fig 5.23.

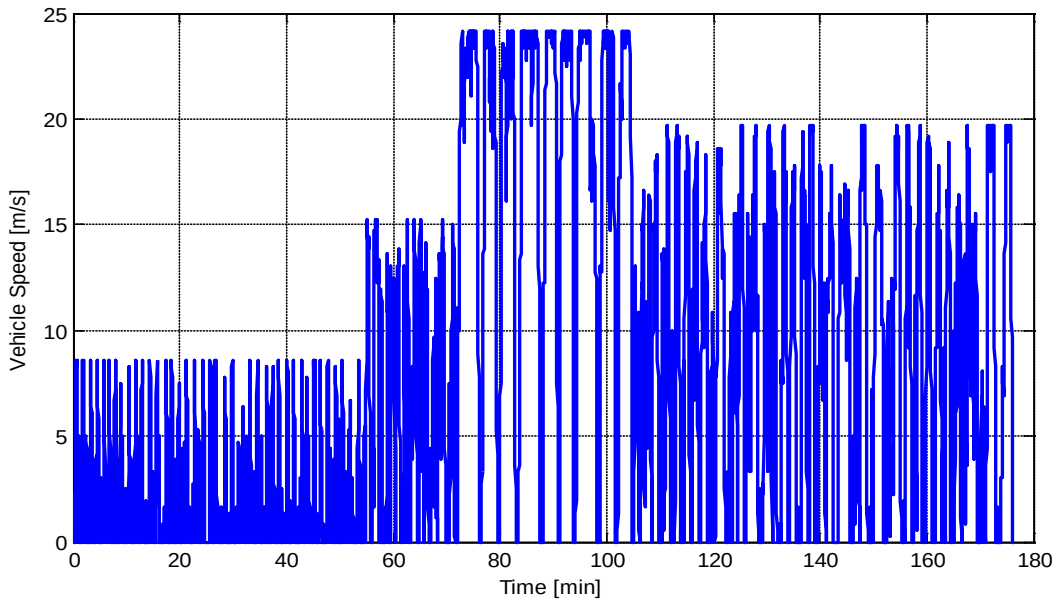

Fig 5.194: Cycle-B velocity profile

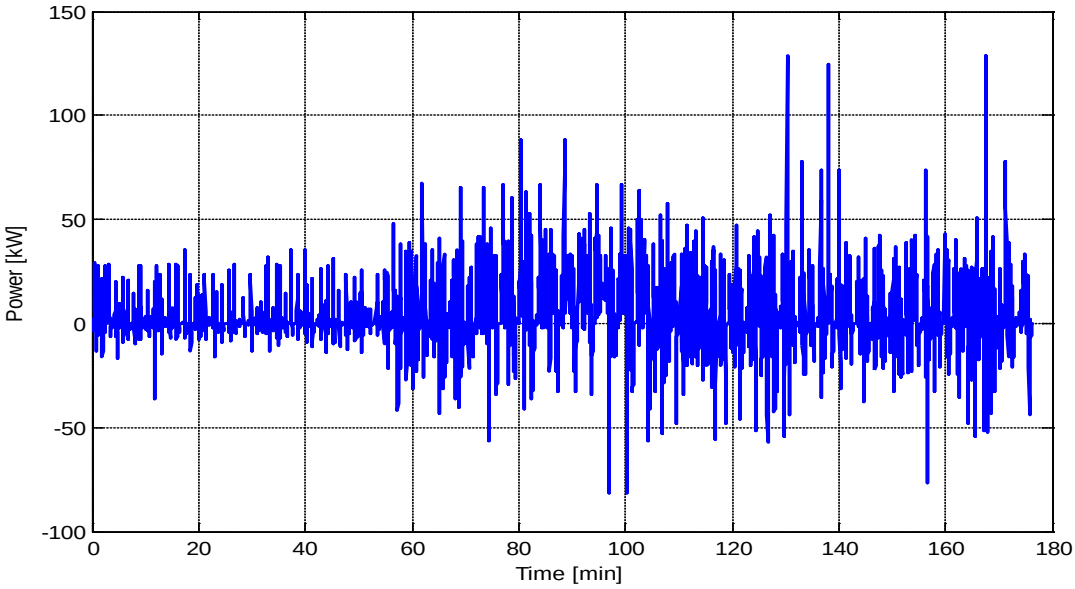

Fig 5.195: vehicle power demand at the wheel for Cycle-B

By using the same procedure, the distributions of the total energy, maximum power, average power, maximum deceleration, average deceleration, maximum velocity and average velocity are shown from Fig 5.24 to Fig 5.30. The normalization values are listed in Table 5.10.

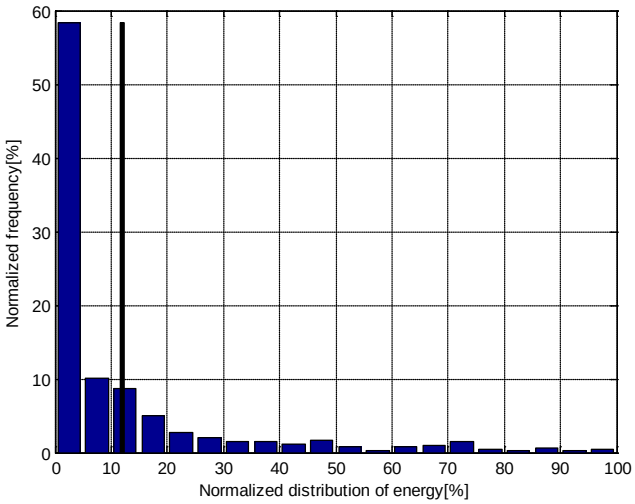

Fig 5.196: Energy distribution

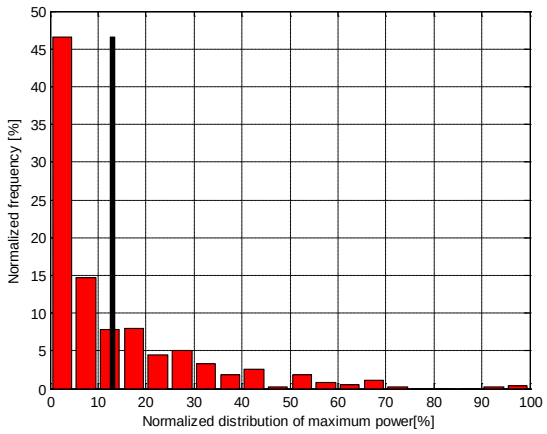

Fig 5.197:Maximum power distribution

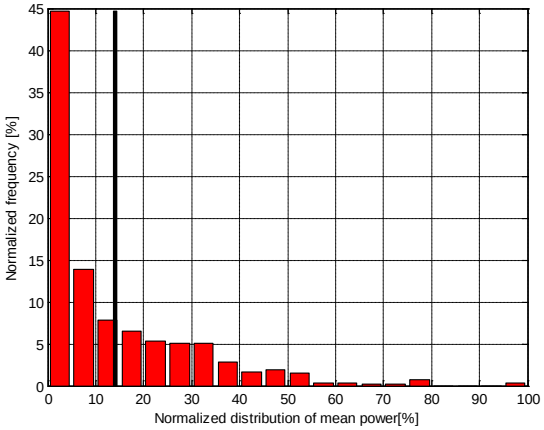

Fig 5.198:Mean power distribution

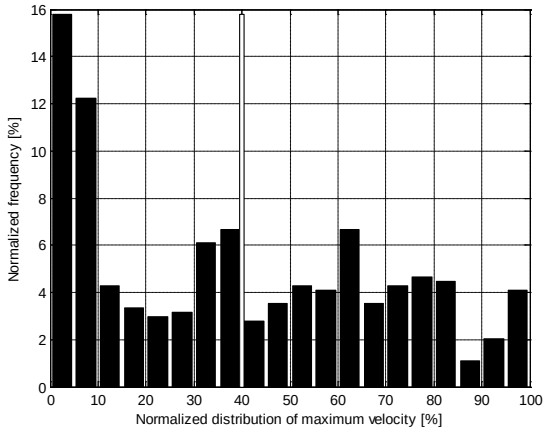

Fig5. 199:Maximum velocity distribution

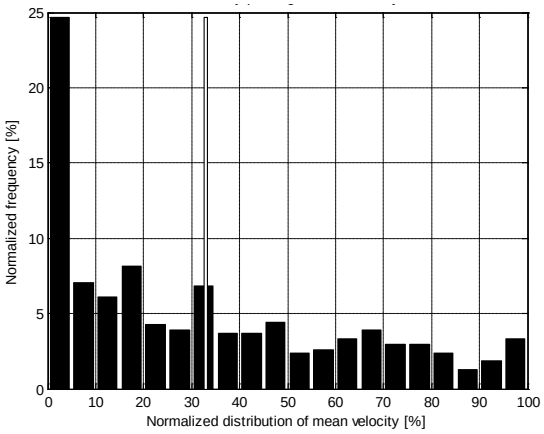

Fig 5.200:Mean velocity distribution

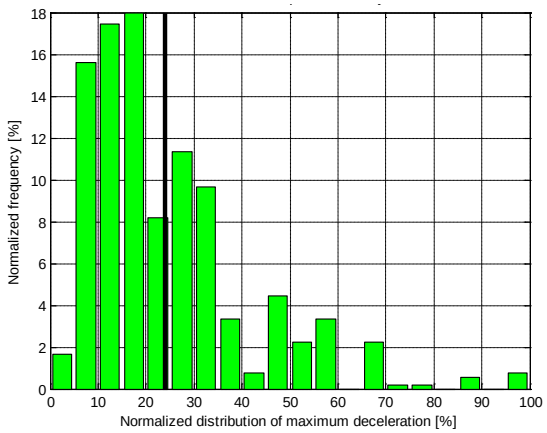

Fig 5.201:Maximum deceleration distribution

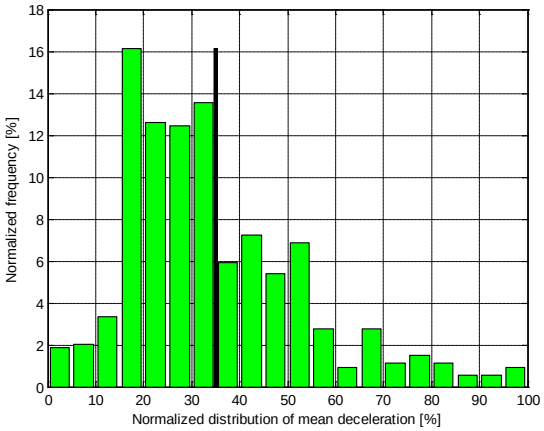

Fig 5.202:Mean deceleration distribution

Table 5.64: normalization values for the previous distributions

Metric	Normalization value
Energy [kJ]	363.85
Maximum power [kW]	81.22
Mean power [kW]	37.06
Maximum deceleration [m/s^2]	-4.16
Mean deceleration [m/s^2]	-1.48
Mean velocity [m/s]	28.81
Max velocity [m/s]	24.16

Comparing Cycle-A with Cycle-B it is possible to notice how the different driving segments composition influences the characteristic distribution of the variable. The main considerations are related to energy and power variables. In Cycle-B the amount of events with low energy value is smaller than Cycle-A, while the amount of events with low average and maximum power is bigger than Cycle-B. An explanation can be found in the absence of freeway driving segments in the second cycle. In fact they are usually characterized by big energy and small power braking events, since the vehicle speed usually is high and there is no need for rapid deceleration phases.

5.4 Definition of Simulation Methodology

5.4.1. Methodology to Determine Testing Events

In the previous paragraph two real-world driving cycles have been determined. These cycles are meant to be used for the hydraulic energy storage system designs validation process. In this specific case Cycle-A is composed by 20 miles of urban, highway and freeway patterns and Cycle-B by 10 miles of urban and highway patterns. This choice was done in order to obtain meaningful driving patterns representing possible real storage system uses. However, in a general driving cycle generation case it is possible to create very long driving patterns on which performing the energy storage system designs validation. A way to validate the designs could be evaluate the energy storage system performances for each braking event in the testing cycle. However, this methodology could cause very long simulation time and require full vehicle simulation (with control strategy). A different methodology is necessary in order to assure a reasonable computation time regardless of the cycle length. In the driving cycle analysis, all the braking events of the cycle are characterized by some metrics. For each metric it is possible to obtain a normalized distribution respect to the maximum metric value. In the distribution the cycle braking events are grouped in 20 categories

depending on the event metric value. Then, choosing a meaningful metric distribution It is possible to derive 20 testing events by means of a statistical process based on these categories. In this validation process methodology, the testing events need to be determined by a power value and an energy value. In this case the normalized distribution of the maximum power has been chosen. This choice is based on the working principle of the short-term energy storage system. Since it is designed to store energy during vehicle braking phases, a fundamental property of this system is the power density. In the light of what said, the testing driving cycle can be meaningfully analyzed starting from the power distribution individuation. In the power distribution each testing event will have the power value corresponding to the value of the category. To determine the energy value of each event, a statistical process is necessary. In each category it possible to apply the weighted average method to the energy values of the events within the category. In this way a unique meaningful energy value is determined for each distribution category. By coupling theses energy values with the power values, 20 testing events are obtained.

An example of this process, the Cycle-A and the maximum power distribution shown in Fig 5.16 are considered. From the latter, it is possible to get the maximum power distribution with respect to the representative value of each distribution category, as in Fig 5.31. In each category the energy values distribution is evaluated and the energy weighted average value is calculated. In Fig 5.32 and Fig 5.33, the third and sixth maximum power distribution categories are shown as exemplification of the statistical process application and the weighted average value is represented by a red line.

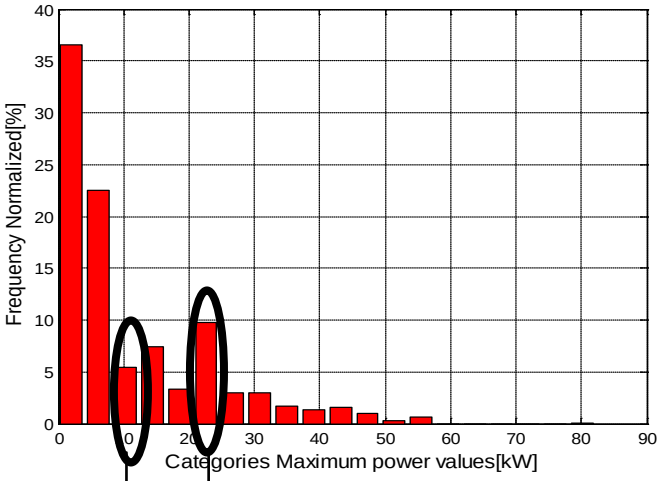

Fig 5.203: maximum power distribution respect to the representative value of each distribution category

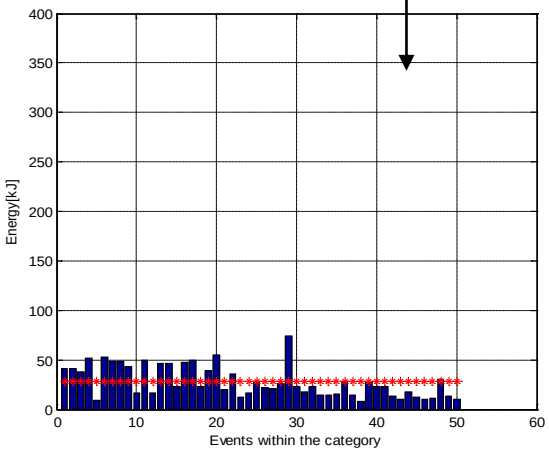

Fig 5.204: Energy values from the third distribution category

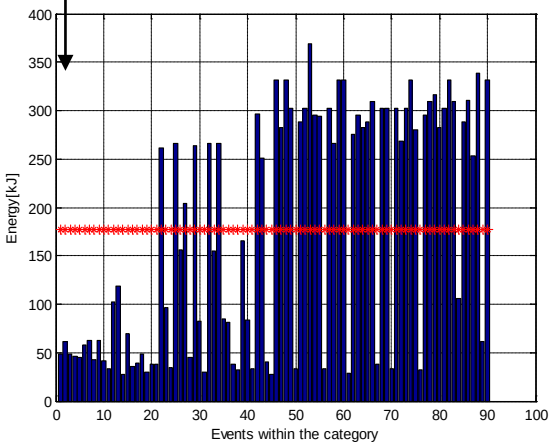

Fig 5.205: Energy values from the sixth distribution category

By applying this statistical process to the events within all the categories maximum power distribution, 20 cycle representative events are obtained. This methodology permits to have a number of events that does not depend on the cycle length.

In Fig 5.34, the testing events characterized by a maximum power value and energy value are shown. It is possible to notice that four events have zero energy value. The motivation can be found by analyzing Fig 5.31. In fact there are some distribution categories, four in this case, in which the number of events occurrences is zero. It means that no events have a maximum power value within the categories minimum and maximum values. Therefore, as explained in detail in the design efficiencies calculation paragraph, these energy-maximum power events will not be considered for the system designs performance evaluation

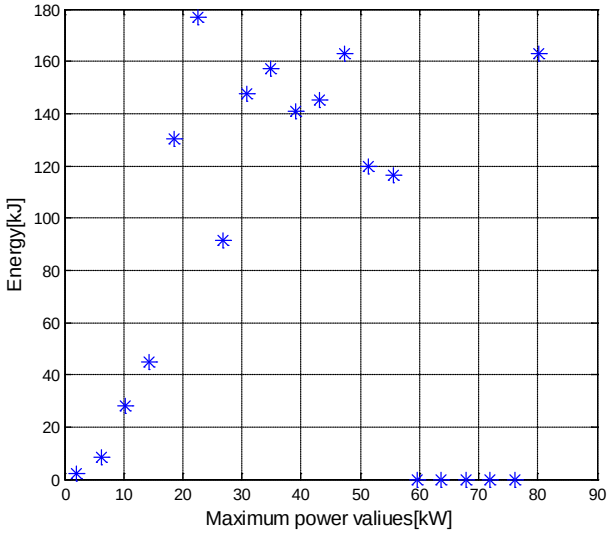

Fig 5.206: testing events energy and maximum power values

5.4.2. Methodology to Simulate the Short-Term ESS Use

In the previous paragraph the methodology aimed to obtain 20 testing events for the energy storage system design validation process has been shown. In the validation process is necessary to simulate the working conditions of the short-term energy storage system.

The short-term energy storage system application is aimed at recovering energy during braking phase to release it during the following acceleration phase. In each phase, the amount of energy that can be released respect to that stored depends on the driving cycle profile characteristics. It can happen that two different braking phases, separated by a traction phase, are so close to not permit to release during the accelerating phase all the energy accumulated during the first braking phase. It means that the trend of the storage system state of charge (SoC) depends on the particular driving cycle profile.

In this simulation, it is assumed that for each testing braking event an acceleration phase follows. This acceleration phase is assumed to be long enough to assure a complete discharge of the energy storage system. In this way it is possible to represent a generalized short-term energy storage system use. In Fig 5.35 is shown an example of state of charge trend, representing a charging phase followed by a fully discharging phase as assumed for the simulation. The maximum charge level depends on the braking event characteristics and on the storage system design. From every representing

design cycle event derives an energy storage system design characterized by an own capability to store energy and by its own state of charge trend for each braking event.

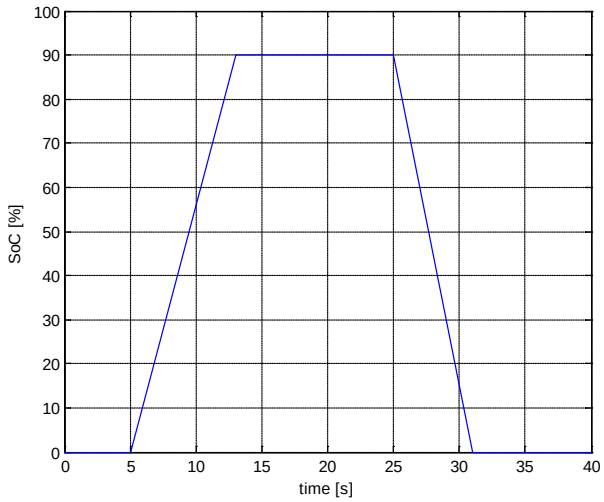

Fig 5.207:example short-term ESS State of Charge variation during a deceleration/acceleration event

In this designs validation process, the tested short-term energy storage systems are assumed to be installed on a vehicle. Hence, for the simulation of the storage system use in each predetermined testing event, a vehicle transient of speed has to be calculated. In order to do this, it is necessary to start from the braking events characteristics and to relate the events energetic quantities to kinematic quantities of the vehicle.

5.4.2.1 Transient of Speed Calculation

In the previous section the braking events to validate the designs have been determined from an exemplary driving cycle, Cycle-A. Each of them is characterized by two metrics: energy and maximum power. These quantities can be used to determine the transient of speed during braking phase. This is the speed of the vehicle on which it is assumed the tested energy storage system is installed. In particular it is necessary to obtain the values of vehicle initial velocity value and deceleration value to simulate the braking phase. The equations to relate the energy E and maximum power P_M to initial vehicle velocity V_i and deceleration a are:

$$E = \frac{1}{2} M_v {V_i}^2 \tag{5.6}$$

$$P_M = M_v V_i a \tag{5.7}$$

By assuming that the vehicle has an energy E during the braking phase start and that the braking power is P_M, it is possible to calculate from (5.6) and(5.7):

$$V_i = \sqrt{\frac{2E}{M_v}} \tag{5.8}$$

$$a = \frac{P_M}{M_v V_i} \tag{5.9}$$

In this case we are assuming that the deceleration is constant and that the braking phase causes the vehicle stop. After the vehicle stop, a following accelerating phase is necessary to test the energy releasing capability of the system. The accelerating phase characteristics depend on the amount of energy stored by system, on the system efficiency and the mechanical components sizes. By using this methodology, it is possible to obtain from each braking event a stop/start event. A theoretical dimensionless vehicle velocity profile during stop/start event is shown in Fig 5.36.

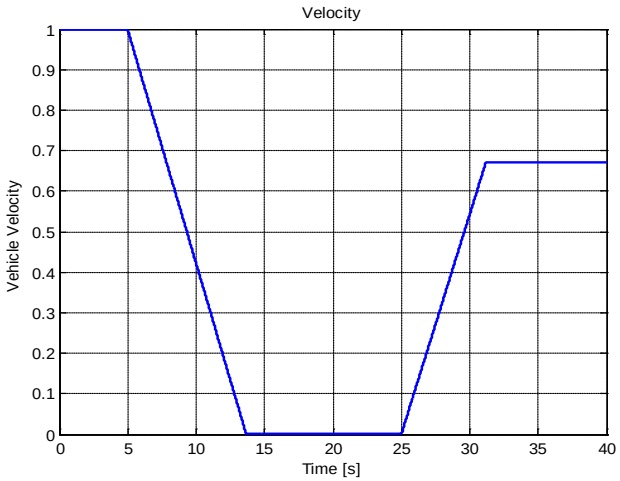

Fig 5.208: dimensionless theoretical velocity profile during stop/start event

5.4.3. Simulation Model

In this simulation it is necessary to use a model to simulate the vehicle. Since the testing events velocity profile has only a decelerating phase, stop phase and an accelerating phase, it is possible to replace a full vehicle model with a simplified one. The behavior of the vehicle is modeled by an equivalent rotating mass with one degree of freedom whose moment of inertia was sized to provide the same initial kinetic energy for

recovery as the vehicle. This assumption has no influence on the validation process and simplifies the procedure.

5.4.4. Definition of AESS Efficiency

In order to complete the design verification, a specific metric related to the energy conversion efficiency must be introduced.

During the system simulation process, each testing event is characterized by available energy that can be stored and maximum power. The capability of the energy to storage system to store as much available energy as possible, depends on its design targets. Therefore, it is possible to define an efficiency calculation for each braking events that takes into account the effective stored energy, E_{stored} and the event available energy in the braking phase, $E_{available}$.:

$$\eta_{1-way} = \frac{E_{stored}}{E_{available}} * 100 \tag{5.10}$$

The simulation methodology provides the presence of a inertial mass model representing the vehicle mass. This mass is subject to a decelerating phase till stop and to a following acceleration phase. The first one is related to braking testing events, while the second on depends on the capability of the storage system to release the energy stored in the previous phase. Therefore It is necessary to introduce a second efficiency calculation related to the inertial mass initial kinetic energy, E_{veh-i}, and to final kinetic energy, E_{veh-f}. This is defined also as round-trip efficiency or2-way efficiency:

$$\eta_{2-way} = \frac{E_{veh-f}}{E_{veh-i}} * 100 \tag{5.11}$$

By mean of the equations (5.10) (5.11) the 1-way efficiency and round-trip efficiency can be calculated by simulating the energy storage use in each cycle testing event. The testing events for Cycle-A are shown in Fig 34. In this figure it is possible to notice the presence of events with zero energy because no cycle braking event is included in these maximum power categories. Hence, it is obvious that the evaluation of the efficiencies for these events is meaningless and they do not have to be taken into account.

In order to evaluate the energy conversion efficiency of the system design on the tested driving cycle, a “statistically representative” efficiency can be defined. This definition is

based on the principle that each efficiency value has to be related to the corresponding testing event frequency on cycle. In this analysis, the statistically relevant efficiency is evaluated by means of the weighted average method. Since the testing events derive from the testing cycle the maximum power distribution, the adopted weights are related to that distribution.

5.5 Evaluation of Energy Storage System Performances by Simulation

In the previous paragraph the methodology to create the simulation for the design procedure validation process has been presented. In this section simulations are done and the results reported.

5.5.1. Sizing Results

By applying the driving cycle analysis to the cycle for hydraulic energy storage system sizing, four representative braking events are extracted and reported in Table 5.4. These are the inputs for the following design procedure. Each of them can be the used to apply the design procedure that is explained in the section before, to size all the systems components. In Table 5.11 the parameters values of the hydraulic energy storage system are listed.

Table 5.65: hydraulic ESS designs components sized depending on the four methods

Hydraulic ESS designs components				
	Weighted average method	**Mean values method**	**Maximum values method**	**Weighted average method with maximum power distribution**
(g_{pump}) Pump gearing	4.19	4.85	1.45	3.88
(V_{acc}) Accumulator volume [m^3]	6.00	4.50	47.50	7.00
($T_{pump,des}$) Desired torque [Nm]	48.05	41.60	343.36	48.05
($D_{max,pump}$) Maximum pump displacement [cc/rev]	30.19	26.14	215.74	30.19

By means of the creation of parametric components models it is possible to correlate the components parameters to physical properties to estimate their attributes. In Table 5.12 the components attribute, mass and volume, are listed.

Table 5.66: ESS components attributes depending on the four methods

ESS components attributes					
	Weighted average method	**Mean values method**	**Maximum values method**	**Weighted average method with Maximum power distribution**	
Pump	15.92	15.07	100.38	15.92	*Mass (Kg)*
	6.26	6.04	28.78	6.26	*Volume(L)*
Accumulator	40.22	36.1	209.48	44.25	*Mass (Kg)*
	11.36	9.7	80.83	13.02	*Volume(L)*
Reservoir	2.30	2.12	9.55	2.47	*Mass (Kg)*
	4.53	3.71	39.17	5.36	*Volume(L)*
Fluid	3.96	3.24	34.27	4.69	*Mass (Kg)*
Total mass [Kg]	62.41	56.64	353.70	67.33	
Total volume[L]	22.17	19.46	148.79	24.64	

The same calculations can be done considering relative values respect to the case with minimum components size. In this case the reference design is the design based on the mean values method. The relative values V_r are obtained by means of:

$$V_r = \frac{x - x_0}{x_0} \tag{5.12}$$

where x is the design attribute value and x_0 is the reference design attribute value.

Table 5.67: ESS components attributes depending on the four methods in relative values

ESS components attributes-relative mass and volume values					
	Weighted average method	**Mean values method**	**Maximum values method**	**Weighted average method with Maximum power distribution**	
Pump	0.06	-	5.66	0.06	*Mass*
	0.04	-	3.76	0.04	*Volume*
Accumulator	0.11	-	4.80	0.23	*Mass*
	0.17	-	7.33	0.34	*Volume*
Reservoir	0.08	-	3.50	0.17	*Mass*
	0.22	-	9.56	0.44	*Volume*
Fluid	0.22	-	9.58	0.45	*Mass*
Total mass [Kg]	0.10	-	5.24	0.19	
Total volume[L]	0.14	-	6.65	0.27	

Below, in Fig 5.37 and Fig 5.38, the total system mass and volume are graphically reported and compared. From Fig 5.39 to Fig 5.45, all the components attributes listed in Table 5.12 are graphically compared.

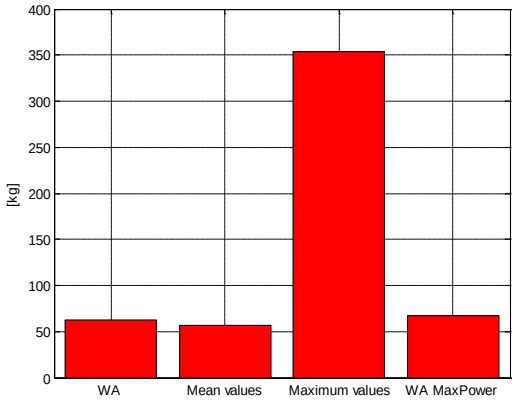

Fig 5.209: Total system mass for the hydraulic system designs

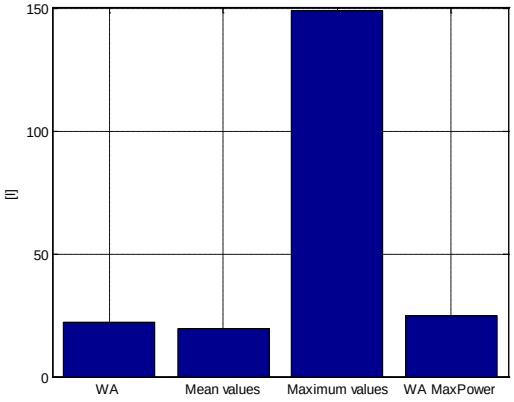

Fig 5.210: Total system volume for the hydraulic system designs

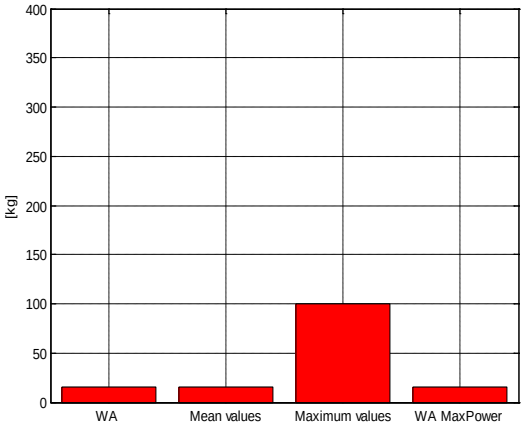

Fig 5.211:Pump mass value for the hydraulic system designs

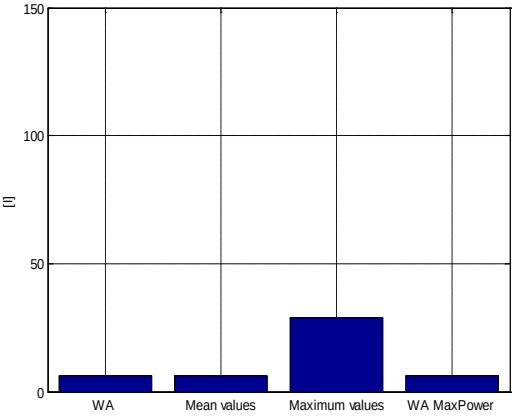

Fig 5.212:Pump volume value for the hydraulic system designs

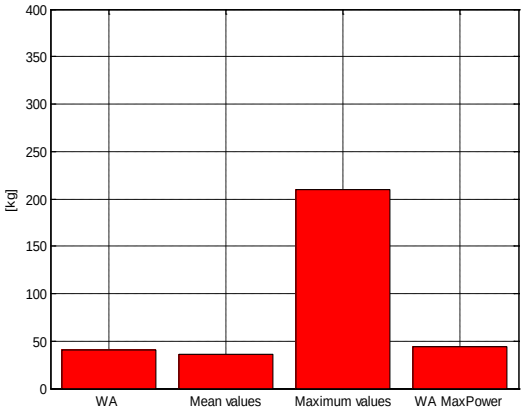

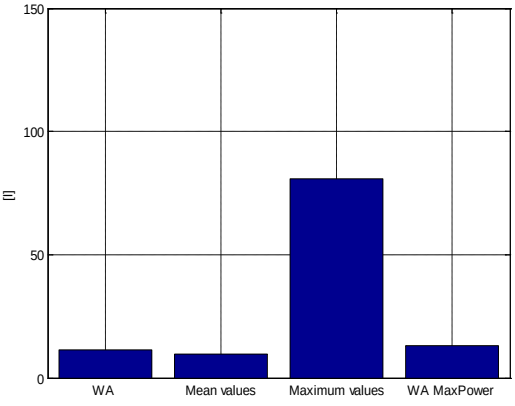

Fig 5.213: Accumulator mass value for the hydraulic system designs

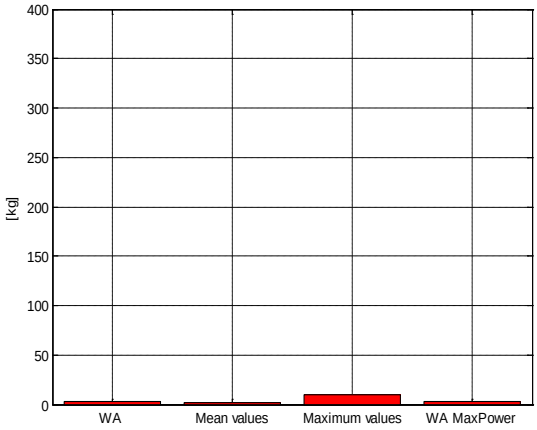

Fig 5. 214: Accumulator volume value for the hydraulic system designs

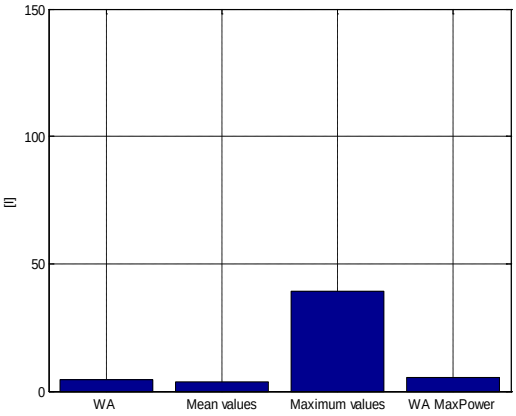

Fig 5.215: Reservoir mass value for the hydraulic system designs

Fig 5.216: Reservoir volume value for the hydraulic system designs

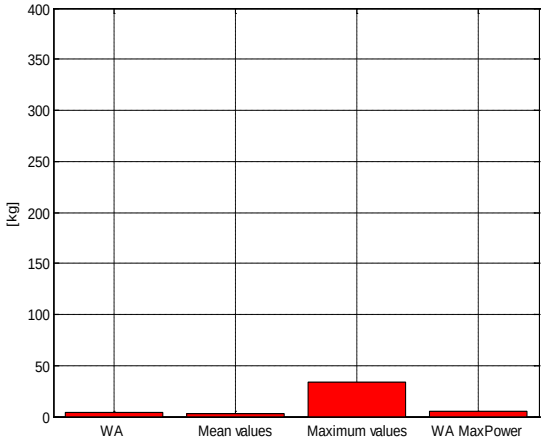

Fig 5.217: Fluid mass value for the hydraulic system designs

All the components attributes defined with the proposed methods are very similar, except for the components based on the maximum values principle. In fact, for this design the total mass is five times bigger than the smallest total mass design.

5.5.2. Simulation Results

The driving cycles used for validation are two, representing different driving scenarios. While Cycle-A has the same distribution of urban highway and freeway driving segments as the design cycle, the Cycle-B is based only on freeway and urban driving portions. Using the design procedure four hydraulic energy storage systems were sized

and based on the simulation methodology presented above, testing events for both Cycle-A and Cycle-B have been obtained. The aim of this section is to provide a validation of the presented design procedure and to compare the performance of the four different systems, based on the efficiency metrics described above.

5.5.2.1 Test Cycle-A

The process to create testing events to evaluate the energy storage system designs is based on the cycle maximum power distribution reported in Fig 5.46. In this figure the distribution of vehicle power reported in absolute value. Each category has a reference power value and an amount of events shown as normalized frequency respect to the total number of events in the cycle.

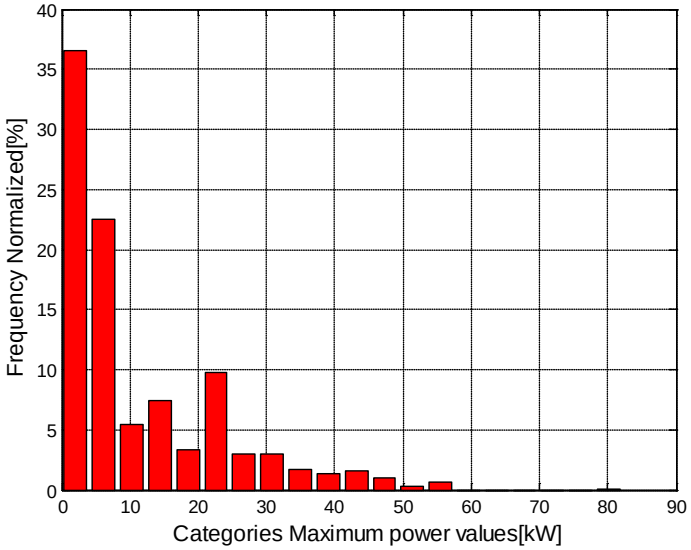

Fig 5.218: Cycle-A maximum power distribution

By means of the testing events creation procedure developed in this Chapter , an energy value can be determined for each maximum power category, as the weighted average of the energy values associated to all of the events which have the same value of the maximum power. A graphic al representation of the maximum power and energy for the 20 testing events of Cycle-A are shown in Fig 5.47.

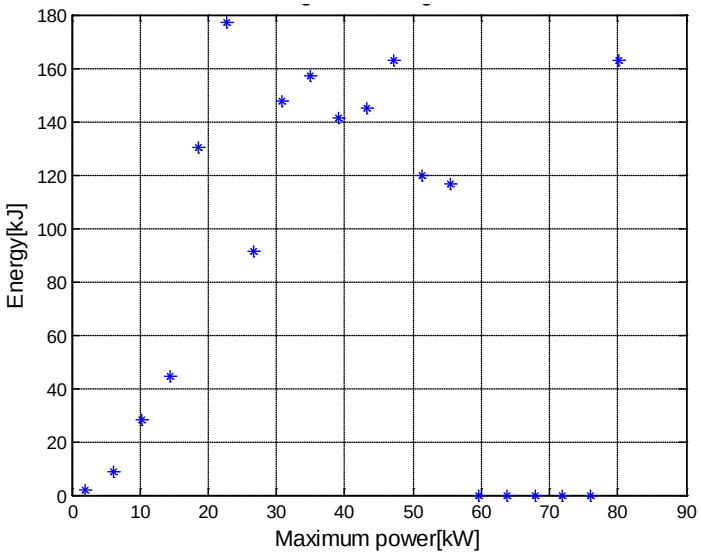

Fig 5.219: testing events for cycle-A

Some observations can be made from Fig 5.47:

- the testing events values show an expected trend between the maximum power and the energy : as the power value increases, also the average energy value of the events increases. Moreover, it is possible to notice that for small power values there is a linear trend, while the points dispersion increases for larger power values, due to the heterogeneity of the driving segments that form the cycle.
- It is possible to notice the presence of testing events characterized by zero energy values. This is due to the presence of five empty maximum power distribution categories, as can be seen in Fig 5.46. In order to evaluate the system efficiency, these events will not be considered.

In Table 5.14, the testing events for Cycle-A are listed with their characteristic metrics: maximum power and energy. Moreover, for each of them, the normalized frequency of occurrence within the category referring to maximum power distribution is reported from Fig 5.46. These values are important in order to evaluate the a final system efficiency through of the weighted average method, since they are used as weights in the equation (3.16)

Table 5.68: testing events characteristic quantities

#	1	2	3	4	5	6	7	8
Events frequency normalized[%]	36.5	22.5	5.4	7.4	3.4	9.8	2.9	2.9
Maximum Power[kW]	2.06	6.17	10.28	14.39	18.50	22.61	26.72	30.83
Energy[kJ]	1.94	8.47	28.27	44.65	130.33	176.95	91.57	147.60
#	9	10	11	12	13	14	15	
Events frequency normalized[%]	1.7	1.3	1.6	1.0	0.3	0.7	0.1	
Maximum Power[kW]	34.94	39.05	43.16	47.27	51.38	55.49	80.15	
Energy[kJ]	157.33	141.06	145.24	162.85	119.84	116.34	162.90	

Analyzing Table 5.14 above, it is also possible to notice that the first six testing events concentrate the 85% of the total number of driving cycle events. This implies that efficiency calculations in the first six testing events are extremely important in the final efficiency evaluation. The efficiencies calculated in the remaining fourteen testing events will have a total weight equal to 15% on the final system efficiency. In this table the five events with zero energy values are excluded.

Each energy storage system design is based on the same driving cycle(similar to Cycle-A), but using different methods to synthesize the metrics, in particular the cycle mean values method, cycle maximum value method and cycle weighted average method with variable own distribution and with maximum power distribution. On these synthetic data the design targets are extracted for the system design procedure. In Table 5.15 the four design targets for system sizing are listed. They have to be taken into account since each system performance strictly depends on the values for which it has been designed.

Table 5.69: design targets

Design targets				
	Weighted average method	**Mean values method**	**Maximum values method**	**Weighted ave. method with maximum power distribution**
Maximum power [kW]	12.59	10.90	89.96	12.59
Energy [kJ]	61.54	45.96	512.92	71.80

5.5.2.2 Design Procedure Validation

In order to validate the design procedure, the hydraulic energy storage system design obtained by applying the weighted average method will be considered. The efficiency will be calculated for each testing event with equations (5.10) and (5.11). Then two final efficiency values will be determined as performance indicators of this system over the testing cycle.

Fig 5.48 and Fig 5.49 show the efficiencies for the hydraulic energy storage system based on design targets obtained by means of the weighted average method. In the graphs the stars represent the efficiency results in each testing event listed in Table 5.14. Moreover, the maximum power distribution of the system design driving cycle is shown coupled to the maximum power value assumed as design target.

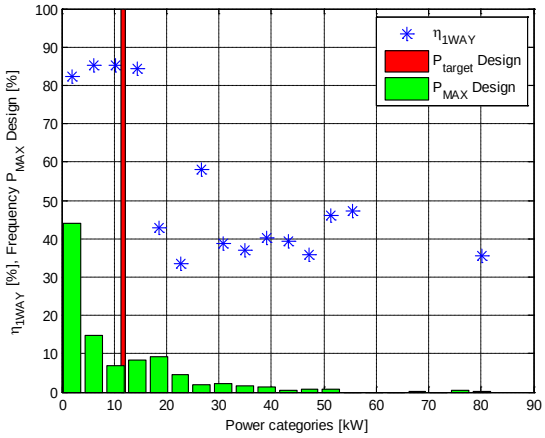

Fig 5.220: 1way efficiency evaluation of design based on weighted method

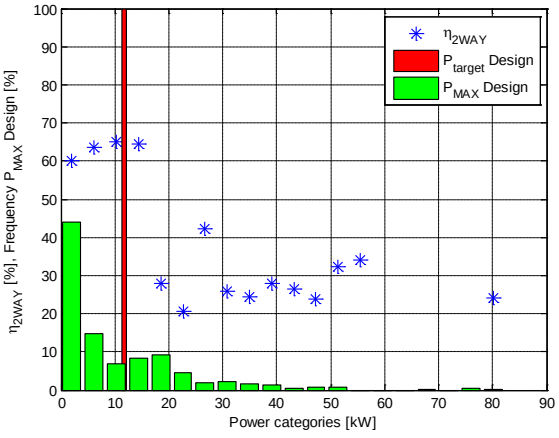

Fig 5.221: 2way efficiency evaluation of design based on weighted method

Fig 5.48 can be analyzed in the light of Fig 5.47 in which the testing events for this cycle are shown in term of energy and maximum power. The energy storage system

design has a better efficiency in the first 4 testing events. As expected, the maximum efficiency is achieved for the design conditions (3^{th}event). Moreover, also the energy design target has a fundamental role: in fact the accumulator, as the energy storage device, has been sized to recover more energy than that one available during this event. This means that during this event the energy storage system maximizes the recovered energy. Similar result occur for the fourth testing event: the available energy is still lower than the maximum storable energy, but the maximum power event exceeds the system design target.

As the testing events assume larger maximum power values, the efficiency drastically decrease, mostly due to the corresponding event available energy. For example, the fifth testing event energy value diverges considerably from the target design, because the energy that could be recovered in this event is more than double the energy that the accumulator can store. It is interesting to observe that the lowest efficiency value is relative to the sixth event, not to the maximum power event as one would expected. In fact, the sixth event is characterized by the maximum energy value within the testing event set. In light of the previous consideration, the relevant efficiency values dispersion can be traced back to the testing events energy values dispersions, which improves the efficiency when these values are closer to the design target. The results for the round-trip efficiency are shown in Fig 5.49. The efficiency trend is here very similar to the one shown in the Fig 5.48. The round-trip efficiency also accounts for the energy losses during the power releasing process.

Since the efficiency evaluation is basically an energy balance, it is meaningful to evaluate the performance considering the energy storing and releasing process. To this end, two testing events have been chosen, namely the event characterized by the highest efficiency (third) and the maximum power event (fifteenth). These events are detailed in Table 5.16.

Table 5.70: representative testing events compared to design targets: the best efficiency event and maximum power event

#	3	15	Design Targets
Maximum Power[kW]	10.28	80.15	12.59
Energy[kJ]	28.27	162.90	61.54

In Fig 5.50 and Fig 5.51 the energy losses are shown during the simulations of the two tested events. The energy losses are mostly concentrated in pump and gears, and they are variable during the transient. In Fig 5.52 and Fig 5.53 the system energy trends are

shown, in particular the energy related to the vehicle, as the first energy provider and ultimate energy receiver, and the one related to the accumulator. In Fig 5.54 and Fig 5.55 two important metrics are shown: the accumulator pressure and pump flow. The first is an indicator of the accumulator energy and the second one an indicator of the system power.

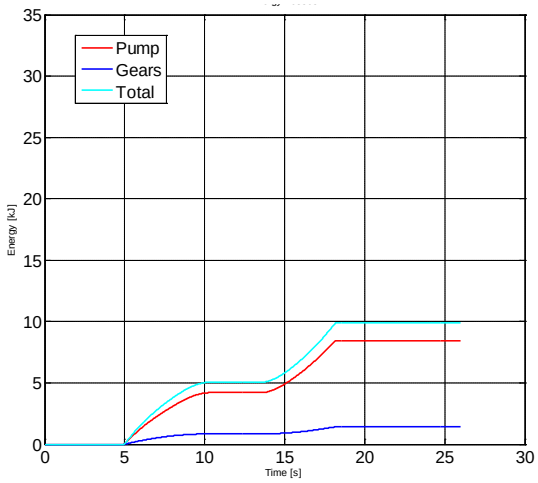

Fig 5.222: Energy losses during the simulation of the event with the greatest efficiency(third event)

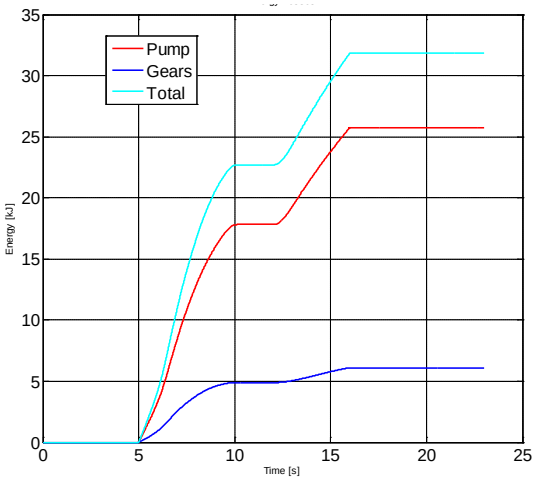

Fig 5.223: Energy losses during the maximum power event simulation

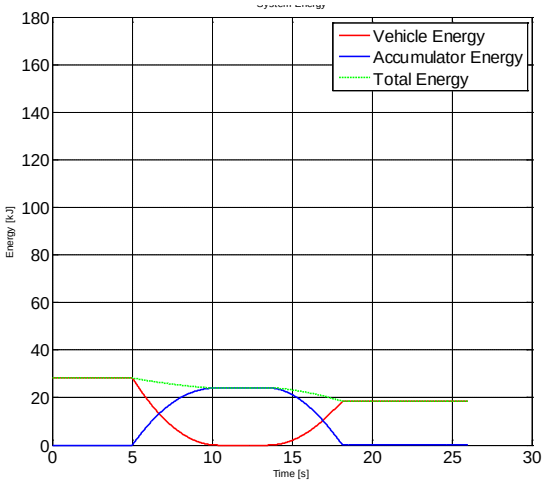

Fig 5.224: System energy trends during the simulation of the event with the greatest efficiency(third event)

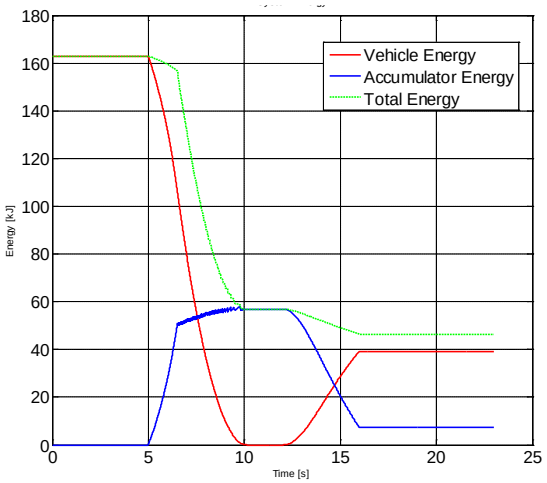

Fig 5.225: System energy trends during the maximum power event simulation

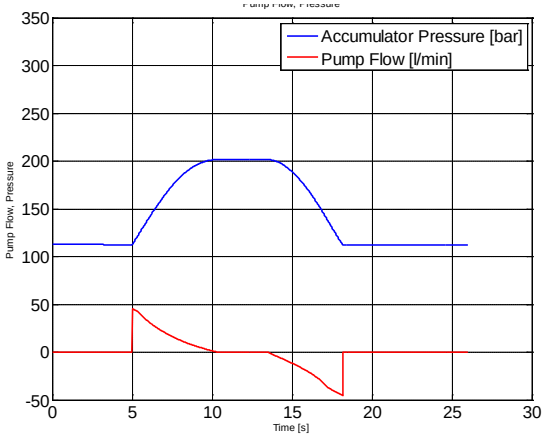

Fig 5.226: Accumulator pressure and pump flow trends during the simulation of the event with the greatest efficiency(third event)

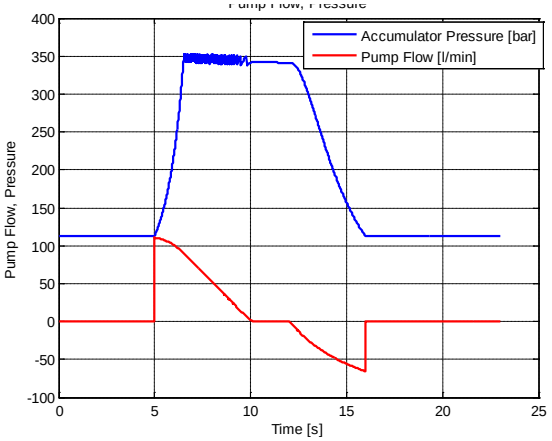

Fig 5.227: Accumulator pressure and pump flow trends during the maximum power event simulation

Comparing the figures above some observations can be made. During the simulation, the hydraulic energy storage system is subject to energy losses mainly concentrated in the pump and gears. While the gear losses contribution is quite moderate also during extreme working conditions (as for the maximum power event) that the pump is the source of the largest losses. This is due to the fact that an axial variable displacement pump was considered, and its efficiency is strictly depending on the working displacement value, torque and angular velocity. For the cases shown above for the maximum power event, although the pump works better when the displacement is close to the maximum value, the losses are still high because of the necessary big torque and high rotational speed. In the event characterized by the greatest efficiency, the system total energy variation is caused mostly by the components losses. In fact, all the available braking energy is stored in the accumulator. This can be understood looking at the pressure trend in Fig 5.54, where the pressure is far from the maximum admissible value, 350 bar. But in the maximum power event, the biggest losses are not due to components but to the inability of the system to store the available energy. In Fig 5.55, despite of the duration of the event braking phase, the pressure limit is immediately reached, causing pressure oscillation in the accumulator due to the relief valve engagement. Hence a large part of the event braking energy is not stored but lost. This can be noticed in Fig 5.53, where the total energy drops drastically and the accumulated energy is a small part of that one owned by the vehicle as kinetic energy at the beginning of the simulation.

Starting from the efficiency metrics calculated per event, the last step is to determine a final value to summarize the hydraulic energy storage system design performance over a

complete cycle. As explained in a previous section of this chapter, this evaluation is obtained by means of the weighted average equation (3.16). The cycle maximum power distribution provides the weights for the mentioned calculation. The weights values are reported in Table 5.14. In Table 5.17 the final efficiencies values are reported.

Table 5.71: efficiencies values for weighted average method design

Efficiencies Cycle-A	
	Values
1way efficiency[%]	73.43
2way efficiency[%]	53.83

The one way-efficiency is related to the capability to store the available energy. Although there are losses due to components working, its value is mainly due to available braking energy lost because of components size. The round-trip efficiency considers also the energy releasing process. In this case the pump/motor is further penalizing the energy efficiency of the system, adding considerable losses.

5.5.2.3 Hydraulic Energy Storage System Designs Comparison

In the previous paragraph the design procedure has been validated by means of the simulations run of the hydraulic energy storage system based on design targets obtained with the weighted average method. Three more system designs can be tested on this cycle to achieve their performance evaluation. The final step of this paragraph is the comparison of the designs efficiency and attributes.

a) <u>Weighted Average Method with Maximum Power Distribution</u>

Fig 5.56 and Fig 5.57 show the efficiency results for the hydraulic energy storage system based on design targets obtained from the weighted average method with maximum power distribution. In the graphs the stars represent the simulation results in each testing event listed in Table 5.14. The maximum power distribution of the driving cycle for system sizing is shown coupled to the maximum power value assumed as design target.

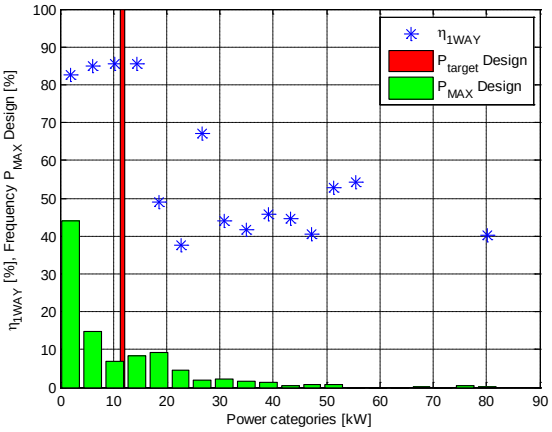

Fig 5.228: 1way efficiency evaluation of design based on weighted average method with maximum power distribution

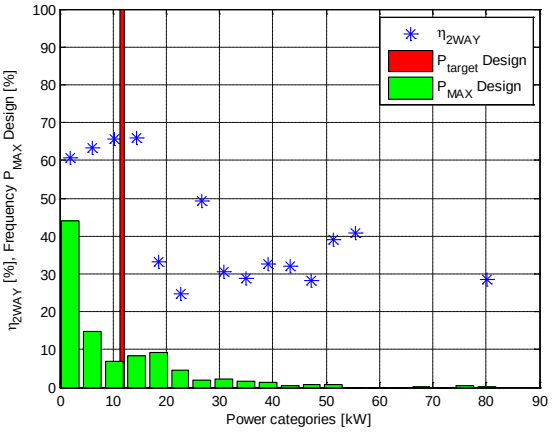

Fig 5.229: 2way efficiency evaluation of design based on weighted average method with maximum power distribution

From the figures above it is possible to notice that the efficiency values trends are similar to the ones observed in Fig 5.48 and Fig 5.49. Referring to Table 5.18, the maximum efficiency value corresponds to the testing event characterized by a maximum power value similar to the system design target value. This is the fourth testing event. The large efficiency values dispersion is due to the great energy variability caused by the statistical approach during their determination. In both efficiency graphs, it is possible to observe that the smallest efficiency value is related to the sixth event, not to the maximum power event. In fact, the sixth event is characterized by the maximum energy value within the testing event set. This is due, as mentioned before, to the accumulator maximum storable energy limit.

In order to evaluate the energy storing and releasing process, two completely different system working conditions are analyzed, namely the event characterized by the highest efficiency (fourth) and the maximum power event (fifteenth). These are detailed in Table 5.18.

Table 5.72: representative testing events compared to design targets: the best efficiency event and maximum power event

#	4	15	Design Targets
Maximum Power[kW]	14.39	80.15	12.59
Energy[kJ]	44.65	162.90	71.80

In Fig 5.58 and Fig 5.59 the energy losses are shown during the simulations of the two tested events and listed in Table 18. The energy losses are mostly concentrated in the pump and gears, and they are variable during the transient. In Fig 5.60 and Fig 5.61the

system energy trends are shown, in particular it is shown the energy related to the vehicle, as the first energy provider and ultimate energy receiver, and the one related to the accumulator. In Fig 5.62 and Fig 5.63 two important metrics are shown: the accumulator pressure and pump flow. The first is an indicator of the accumulator energy and the second one an indicator of the system power.

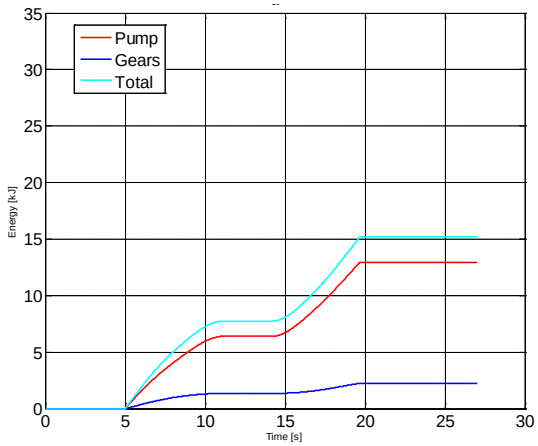

Fig 5.230: Energy losses during the simulation of the event with the greatest efficiency(fourth event)

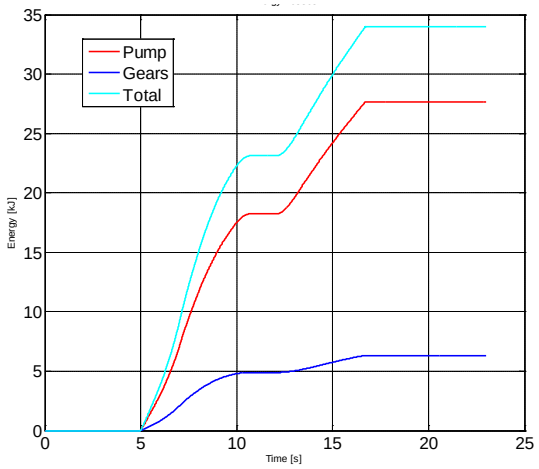

Fig 5.231: Energy losses during the maximum power event simulation

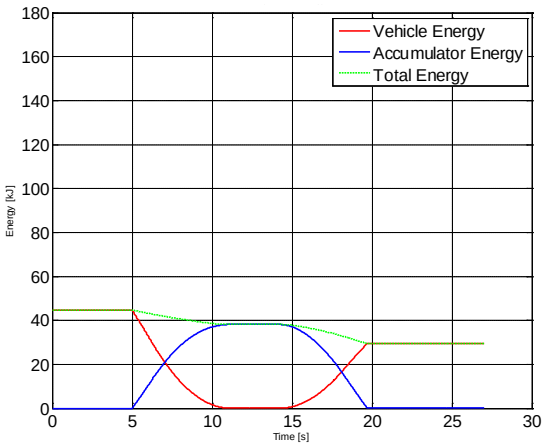

Fig 5.232: System energy trends during the simulation of the event with the greatest efficiency(fourth event)

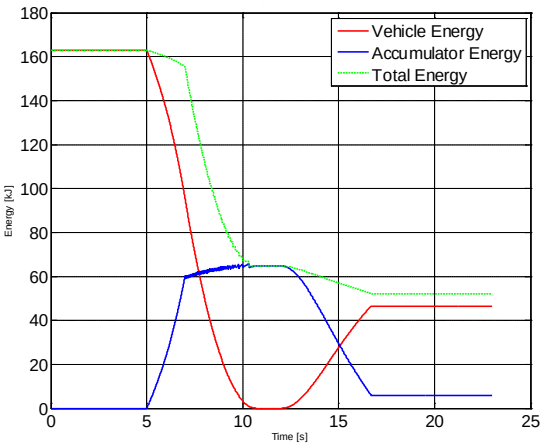

Fig 5.233: System energy trends during the maximum power event simulation

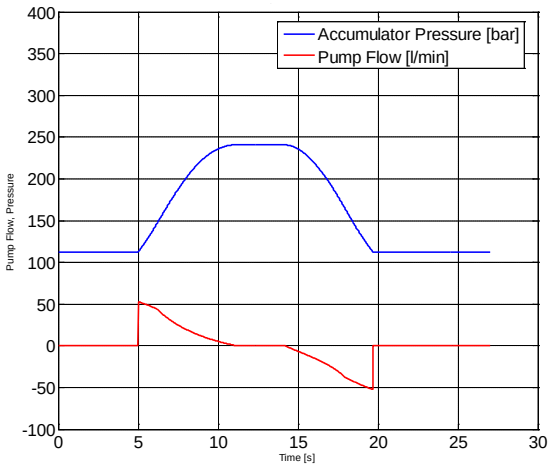

Fig 5.234: Accumulator pressure and pump flow trends during the simulation of the event with the greatest efficiency(fourth event)

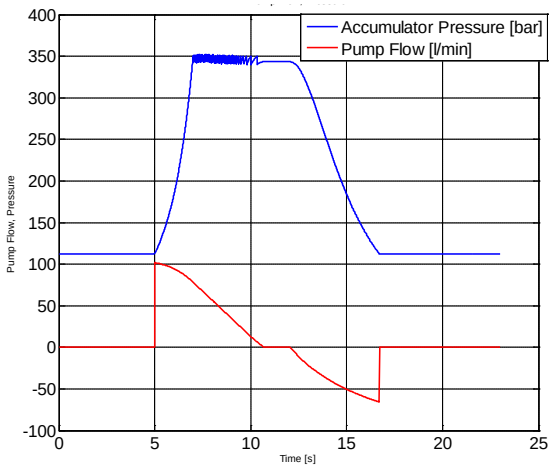

Fig 5.235: Accumulator pressure and pump flow trends during the maximum power event simulation

In the figure above, it is possible to notice the different total system energy trends and energy losses. These are due to the different amount of energy and maximum power owned by the two represented events. In particular it is possible to compare the best efficiency event in this case, with the best efficiency event in the previous design in Fig 5.52 and Fig 5.54. In the present case the maximum efficiency event is the fourth while in the previous it was the third, so it has a bigger amount of energy. Hence, as it is possible to notice in Fig 5.62, the maximum pressure value during the simulation reaches almost 250 bar respect to the 200 bar in the previous case.

Starting from the efficiency metrics calculated per event, the last step is to determine a final value to summarize the hydraulic energy storage system design performance over a complete cycle. This evaluation is obtained by means of the weighted average equation (3.16). The cycle maximum power distribution provides the weights for the mentioned calculation. The weights values are reported in Table 5.14. In Table 5.19 the final efficiencies values are reported.

Table 5.73: efficiencies values for weighted average method with maximum power distribution design

Efficiencies Cycle-A	
	Values
1way efficiency[%]	73.64
2way efficiency[%]	54.18

b) <u>Mean Value Method</u>

Fig 5.64 and Fig 5.65 show the efficiencies results for the hydraulic energy storage system based on design targets obtained by means of the mean value method. In the graphs the stars represent the efficiency results in each testing event listed in Table 5.14. Beside these values, the maximum power distribution of the system design driving cycle is shown coupled to the maximum power value assumed as design target.

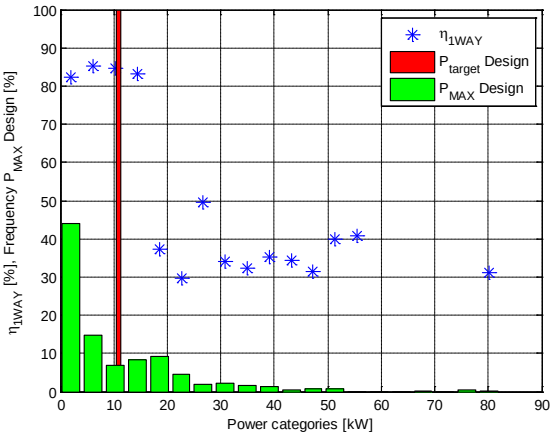

Fig 5.236: 1way efficiency evaluation of design based on mean value method

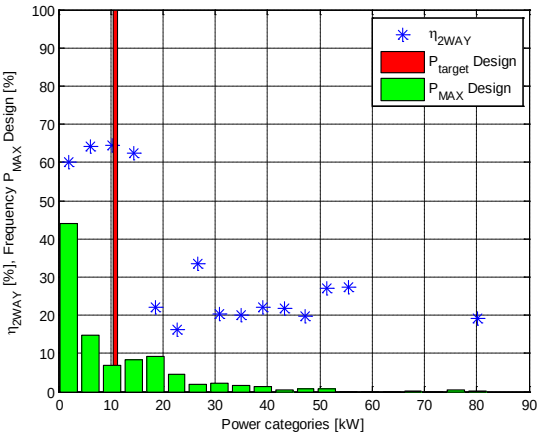

Fig 5.237: 2way efficiency evaluation of design based on mean value method

From the figures above it is possible to notice that the efficiency values trends are similar to that ones observed in the two previous cases. The testing event with the maximum round-trip efficiency is the third one. As it can notice in Table 20, the event maximum power value is very similar to the maximum power design target. However, in the 1way-efficency analysis, the maximum efficiency value does not correspond to the same testing event but to the second one. This due to the different contribution of losses during energy releasing phase. In particular, as shown previously, the loss caused by the variable displacement pump/motor is as bigger as the displacement working value is far from the maximum displacement value. Since the energy-related characteristics of the second event are very moderate, then the efficiency of the pump is lower than in correspondence of the third event. The efficiencies values dispersion is due to the great testing events energy variability. The smaller efficiency value is related to the sixth event , that is the one with maximum energy. This is due as mentioned before to the accumulator maximum storable energy limit.

For this design, two completely different system working conditions are analyzed, namely the event characterized by the highest efficiency(third) and the maximum power event (fifteenth). These are detailed in Table 5.20.

Table 5.74: representative testing events compared to design targets: the best efficiency event and maximum power event

#	3	15	Design Targets
Maximum Power[kW]	10.28	80.15	10.90
Energy[kJ]	28.27	162.90	45.96

In Fig 5.66 and Fig 5.67 the energy losses are shown during the simulations of the two tested events and listed in Table 5.20. In Fig 5.68 and Fig 5.69 the system energy trends are shown.. In Fig 5.70 and Fig 5.71 two important metrics are shown: the accumulator pressure and pump flow.

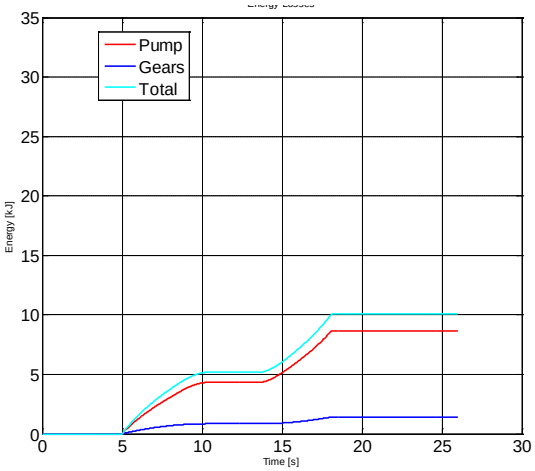

Fig 5.238: Energy losses during the simulation of the event with the greatest efficiency(third event)

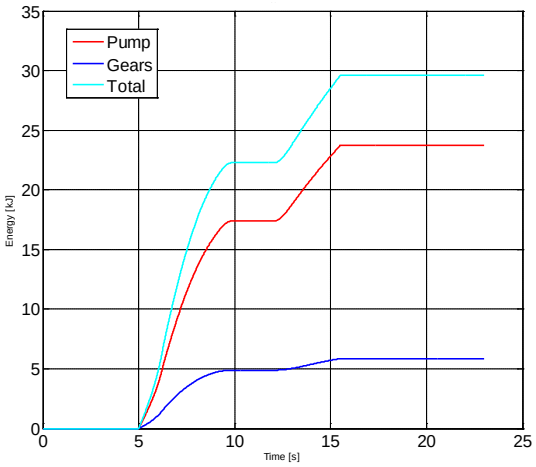

Fig 5.239: Energy losses during the maximum power event simulation

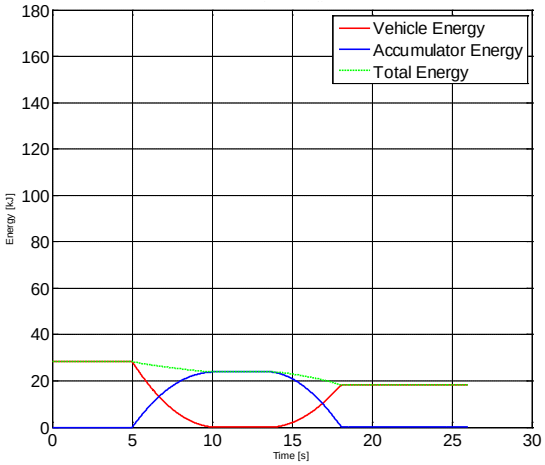

Fig 5.240: System energy trends during the simulation of the event with the greatest efficiency(third event)

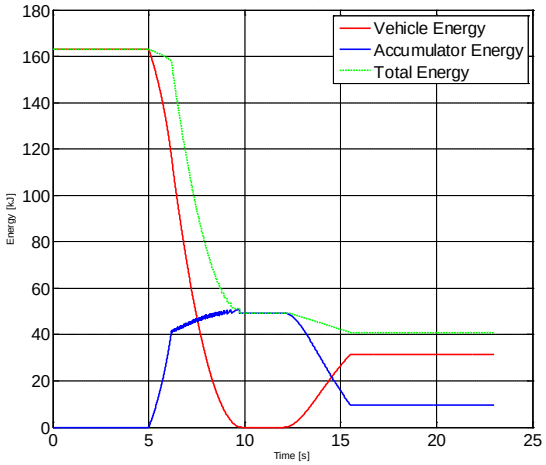

Fig 5.241: System energy trends during the maximum power event simulation

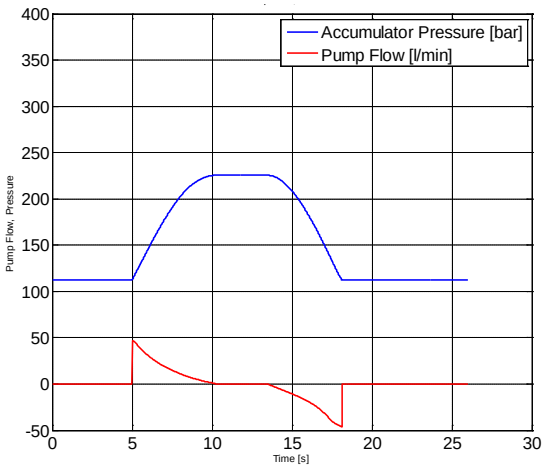

Fig 5.242: Accumulator pressure and pump flow trends during the simulation of the event with the greatest efficiency(third event)

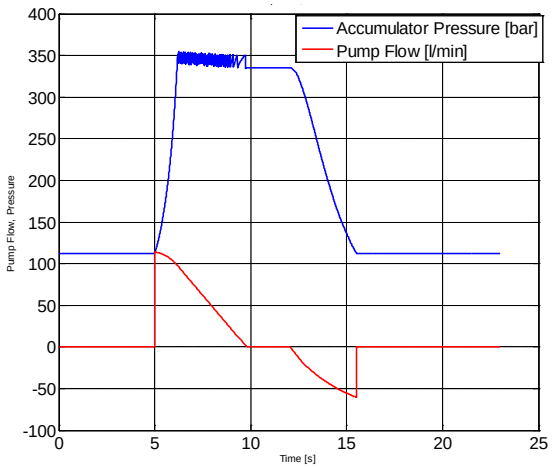

Fig 5.243: Accumulator pressure and pump flow trends during the maximum power event simulation

In the third event, the energy losses are equally distributed between the system storing phase and releasing phase. These are mainly caused by the pump, since the accumulator size does not limit the storable energy. In the maximum power event simulation, although the energy losses due to pump and gears are relevant, the biggest loss is related to the limitation of the storing device to accumulate all the available energy. Observing Fig 5.69, it is possible to notice that the energy stored is almost a fourth of initial vehicle kinetic energy.

Starting from the efficiency metrics calculated per event, the last step is to determine a final value to summarize the hydraulic energy storage system design performance over a complete cycle. In Table 5.21 the final efficiencies values are reported.

Table 5.75: efficiencies values for mean values method distribution design

Efficiencies Cycle-A	
	Values
1way efficiency[%]	70.62
2way efficiency[%]	51.10

c) Maximum Values Method

In this section, the hydraulic energy storage system based on design targets obtained by means of the maximum values method is analyzed. The design components size differs a lot from the previous systems. Then, it is expected to have simulation results not similar to the previous cases.

Fig 5.72 and Fig 5.73 show the efficiencies results. In the graphs the stars represent the efficiency results in each testing event listed in Table 14. Beside these values, the maximum power distribution of the system design driving cycle is shown coupled to the maximum power value assumed as design target.

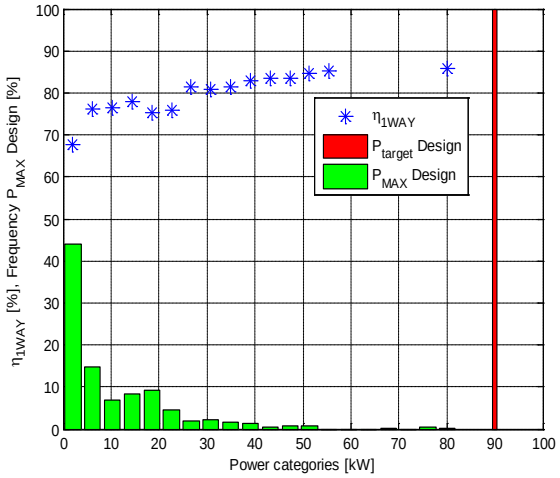

Fig 5.244: : 1way efficiency evaluation of design based on maximum values method

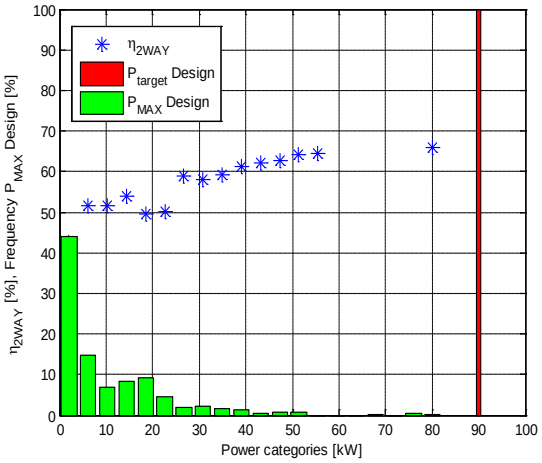

Fig 5.245: 2way efficiency evaluation of design based on maximum values method

By analyzing the figures above, the different efficiencies values trend respect to the previous designs has to be explained. This hydraulic energy storage system design is based on the design cycle maximum values. It means that the design is based on cycle worst-case scenario. As shown in system components sizing process, this design has mass and volume attributes five times bigger than the average previous design sizes. In

Fig 5.72 the best efficiency event is that one characterized by the maximum values of energy and power. Its characteristics are reported in Table 5.22 and compared to the system design targets. The worst efficiencies values are related to the events with the most moderate energetic characteristics instead, despite the large accumulator volume. This phenomenon is due to the losses caused by the pump/motor. In fact as the testing event power decrease as the working displacement value of the pump is far from the maximum displacement value. This working condition causes very small efficiency value of this component, due to the axial variable displacement pump design. Moreover in both efficiency plots, the values dispersion is moderate respect to the other system designs and there is a smooth values trend. This is due to the big accumulator size that gives the opportunity to store all the available energy in each event.

In this case it corresponds to the maximum power event (fifteenth). Its characteristics are reported in Table 5.22.

Table 5.76: representative testing events compared to design targets: the best efficiency event is also the maximum power event

#	15	Design Targets
Maximum Power[kW]	80.15	89.96
Energy[kJ]	162.90	512.92

In Fig 5.74 the energy losses are shown during the simulations of the tested event and listed in Table 5.22. In Fig 5.75 the system energy trends are shown.. In Fig 5.75 two important metrics are shown: the accumulator pressure and pump flow.

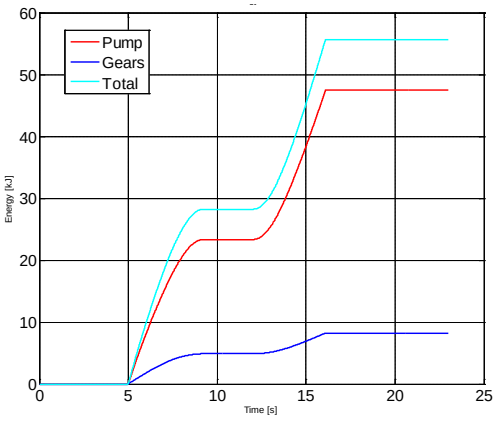

Fig 5.246: Energy losses during the simulation of the maximum power event simulation

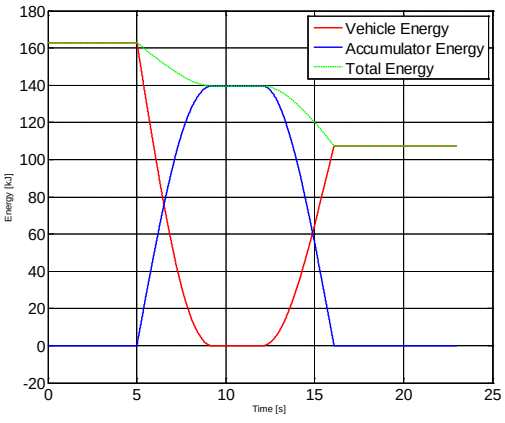

Fig 5.247: System energy trends during the maximum power event simulation

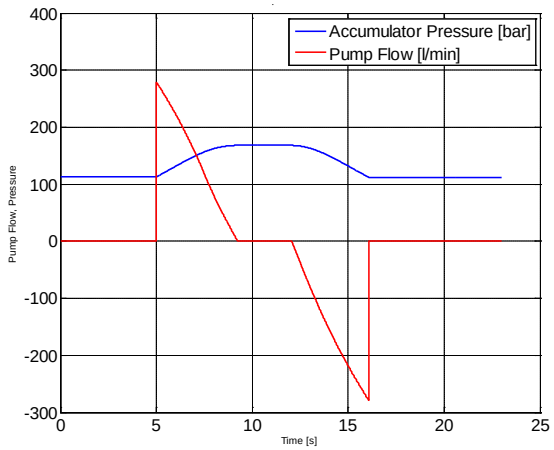

Fig 5.248: Accumulator pressure and pump flow trends during the maximum power event simulation

In this case the maximum efficiency event is that one characterized by the maximum power and energy values. In this case, the maximum power design target value is close to the testing event power, while the event storable energy is one third of the energy-related design target. Therefore, the accumulator is oversized and it is possible to notice in Fig 5.76 that the maximum pressure during the transient is almost half the maximum accumulator pressure value. Similarly to the previous designs, the main energy losses are caused by the pump, as it is possible to observe in Fig 5.74. However, this pump design brings to have a hydraulic fluid flow that is almost three times larger than the previous design shown in Fig 5.71.

Starting from the efficiency metrics calculated per event, the last step is to determine a final value to summarize the hydraulic energy storage system design performance over a complete cycle. In Table 5.23 the final efficiencies values are reported

Table 5.77: representative testing events compared to design targets: the best efficiency event and maximum power event

Efficiencies Cycle-A	
	Values
1way efficiency[%]	70.62
2way efficiency[%]	51.10

d) <u>Hydraulic Energy Storage Systems Comparison</u>

The final simulations result obtained from the four criteria consists in two efficiencies values for each design method. These efficiencies are performance indicators, together with the designs attributes, such as the system mass and volume. The summary of attributes and efficiency is reported in Table 5.24.

Table 5.78: Designs Efficiencies and Attributes comparison

Designs Efficiencies and Attributes comparison				
	Weighted average method	**Mean value method**	**Maximum values method**	**Weighted average method with maximum power distribution**
1-way efficiency[%]	73.43	70.62	73.86	73.64
Round-trip efficiency[%]	53.83	51.10	49.31	54.18
Total mass [Kg]	62.41	56.64	353.70	67.33
Total volume[L]	22.17	19.46	148.79	24.64

In the figures below, Fig 5.77 and Fig 5.78, the efficiencies results for the simulated design methods are reported for a performance comparison.

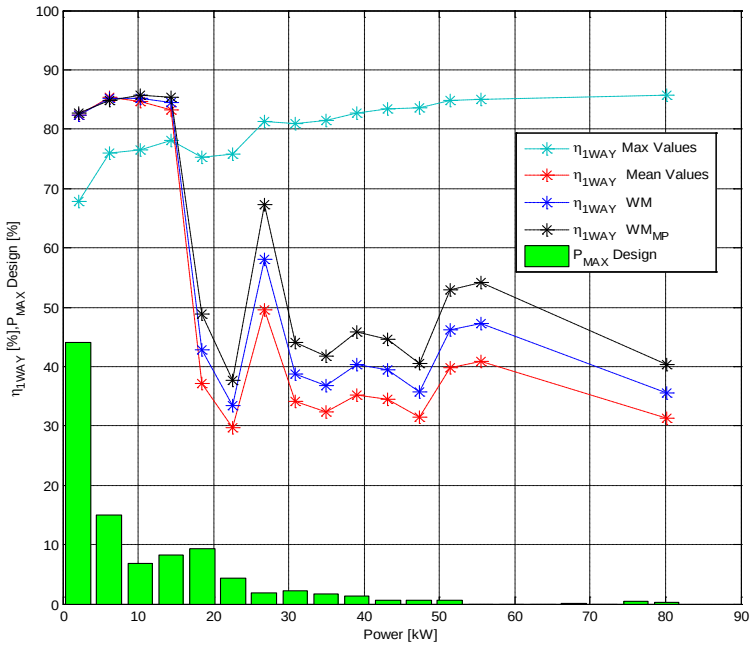

Fig 5.249: 1way-efficency designs comparison

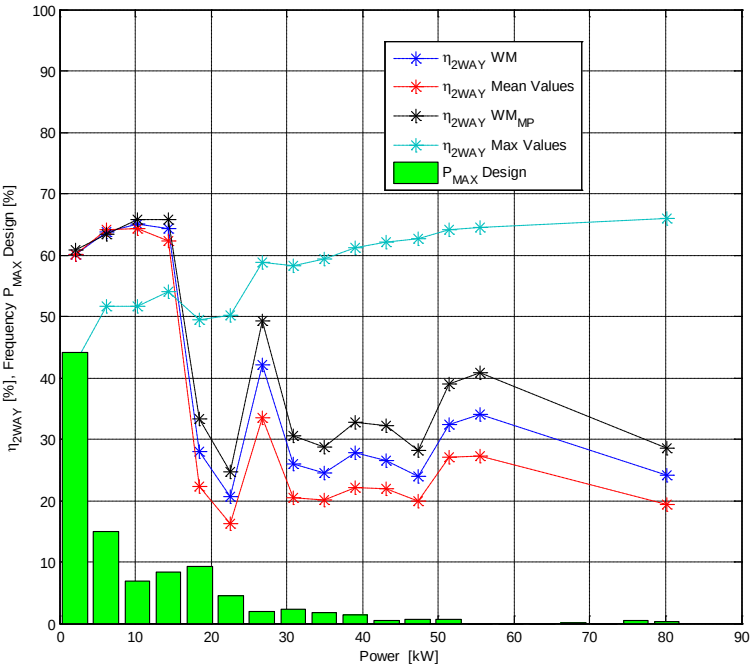

Fig 5.250: Round-trip efficiency designs comparison

In the designs performance and attributes comparison some considerations can be done considering the most relevant results aspects:

- *Maximum efficiency condition:* analyzing the figures above it is possible to observe that the maximum value design method leads to a complete different efficiency profile. This is due to design targets based on the extreme values of driving cycle. Therefore, the most efficient condition occurs in the event with maximum power and energy values. The other three design cases are based on very similar power design targets (between 10.90 kW and 12.59 kW). In fact the testing events with the maximum efficiencies are the third and fourth respectively characterized by 10.28 kW and 14.39 kW as maximum power values. On the contrary, the designs are characterized by different energy design targets (between 45.96 kJ and 71.80 KJ), which influence the accumulator size and the maximum stored energy. Despite this difference, their accumulator capability allows one to store the maximum amount of available energy until the fourth event (44.65 kJ). In correspondence of the fifth event, (130.33 kJ) the accumulator designs become a limitation, causing the efficiency value to decrease.
- *Efficiency profiles:* the efficiency profiles of the maximum values design are the smoothest with an increasing trend with the event power. This is due to the high power capacity of the pump, sized to meet the maximum power design target (89.96 kW), and to the large accumulator, sized to meet the peak energy design target (512.92 kJ). Since the highest energy event is 176.95 kJ, the accumulator is capable to store all the available energy from the cycle. In other terms, it does not have negative effects on the system efficiencies and it does not limit the maximum stored energy. Moreover the pump can always provide the required power because the maximum event power is 80.15 kW. Different conclusions can be drawn for the other three designs. Because of their moderate pump size (maximum power target 12.59 kW) they perform at their best in the third event; however they become limited for the following events, requiring higher pump power. Moreover larger efficiency values dispersion can be noticed, due to the testing events dispersion in Fig 47. For all the systems the lowest efficiency event is the sixth characterized by the maximum energy value within the events. Although their general profiles trends are very similar, the profiles seem to be shifted depending on the accumulator size. In fact, the design based on the weighted average method with maximum power distribution has the largest accumulator capability among them and it follows that it has the highest efficiency values.

- *Efficiency evaluation*: the final efficiency evaluation is based on the weighted average calculation with maximum power distribution. In this distribution the 85% of the weight is concentrated into the first sixth events. Despite the highest efficiency values for the maximum values method design for eleven events simulations, the final efficiency is the lowest among all the methods. This is due to the very low importance, in terms of occurrence, of these events in the cycle. The weighted average method with maximum power distribution has the highest final efficiency values because it performs better during the most recurrent events thanks to a properly sized accumulator.

5.5.2.4 Test Cycle-B

In the previous paragraph, the hydraulic energy storage system designs have compared on a driving cycle with real-world driving patterns composition similar to the cycle used to size the systems. In this paragraph the analysis is processed on the Cycle-B, which has different driving patterns composed only by urban and highway segments (freeway patterns are not included in this scenario).

The process to create testing events to evaluate the energy storage system designs is based on the cycle maximum power distribution reported in Fig 5.46. In this figure the distribution categories power values are not referred to a maximum power normalization value but are reported in absolute values. Each category has a reference power value and an amount of events shown as normalized frequency respect to the total number of events in the cycle.

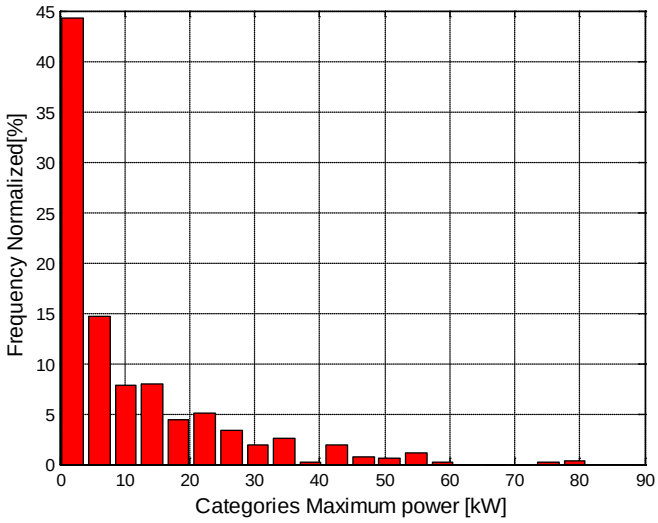

Fig 5.251: Cycle-B maximum power distribution

Following the same procedure applied for Cycle-A, 20 testing events are extracted from Cycle-B. These events are shown in Fig 5.80.

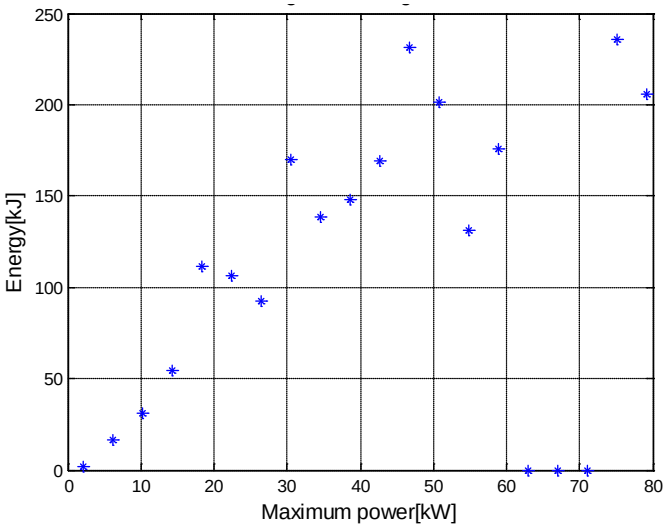

Fig 5.252: testing events for cycle-B

The figure above can be compared to testing events in Fig 5.47. They show similar maximum power and energy trend, characterized by a linear trend for small power values, while the points dispersion increases for larger power values. Moreover, in both the cases some testing events characterized by zero energy values are present, specifically three events in this cycle.

In Table 5.25 Cycle-B testing events are listed with their characteristic quantities: maximum power and energy. Moreover, for each of them, the normalized frequency of events within the category referring to maximum power distribution is reported from Fig 5.79.

Table 5.79: testing events characteristic quantities

#	1	2	3	4	5	6	7	8	9
Events frequency normalized[%]	44.3	14.7	7.8	8.0	4.5	5.0	3.3	1.9	2.6
Maximum Power[kW]	2.03	6.09	10.15	14.21	18.27	22.34	26.40	30.46	34.52
Energy[kJ]	2.19	16.46	31.22	54.71	111.59	106.39	92.31	169.95	138.25
#	10	11	12	13	14	15	16	17	
Events frequency normalized[%]	0.2	1.9	0.7	0.6	1.1	0.2	0.2	0.4	
Maximum Power[kW]	38.58	42.64	46.70	50.76	54.82	58.89	75.13	79.19	
Energy[kJ]	148.31	169.19	231.71	201.56	131.40	175.70	235.52	206.08	

Analyzing the table above, it is also possible to notice that the first six testing events concentrate almost the 85% of the total number of driving cycle events. It means that efficiency calculation in the first six testing events are extremely important in the final efficiency evaluation by means of the weighted average. In particular, in this cycle the first testing event it is very relevant: in fact it statistically occurs almost one time on two.

Each energy storage system design is based on the same driving cycle representing a typical use, but on different criteria to synthesize the driving cycle data. In this analysis are used the same criteria as in the Cycle-A. In Table 15 the four design targets for system sizing have been reported.

a) <u>Hydraulic Energy Storage Systems Designs Comparison</u>

The four aforementioned hydraulic energy storage system designs are evaluated by means of the same simulation procedure adopted over Cycle-A. The summary of attributes and efficiency is reported in Table 5.26

Table 5.80: Designs Efficiencies and Attributes comparison over Cycle-B

Designs Statistically Representative Efficiency and Attributes Comparison				
	Weighted average method	**Mean value method**	**Maximum values method**	**Weighted average method with maximum power distribution**
1-way efficiency[%]	74.02	71.99	71.67	75.97
Round-trip efficiency[%]	54.07	52.05	46.85	55.99
Total mass [kg]	62.41	56.64	353.70	67.33
Total volume[l]	22.17	19.46	148.79	24.64

In the figures below, Fig 5.81 and Fig 5.82, the efficiencies results for the simulated design methods are reported for a performance comparison.

In the designs performance and attributes comparison in Cycle-B, some considerations can be done considering the most relevant results aspects. It is possible to observe that the maximum value design method leads to a completely different efficiency profiles trends. This is due to design targets based on system design cycle extreme values. The other three design cases are based on very similar maximum power design targets (between 10.90 kW and 12.59 kW) and, for these designs, the most efficient condition occurs in the third event. This event is characterized by a maximum power value of 10.15 kW, that is very similar to the design targets. On the contrary, the designs are characterized by different accumulator size, causing a different efficiency values in correspondence of the fourth event (54.71 kJ). The efficiency profiles of the maximum values design has an increasing trend with the event power. This is due to the pump high power capacity and to the large accumulator size. For the other three designs, different conclusions can be drawn.

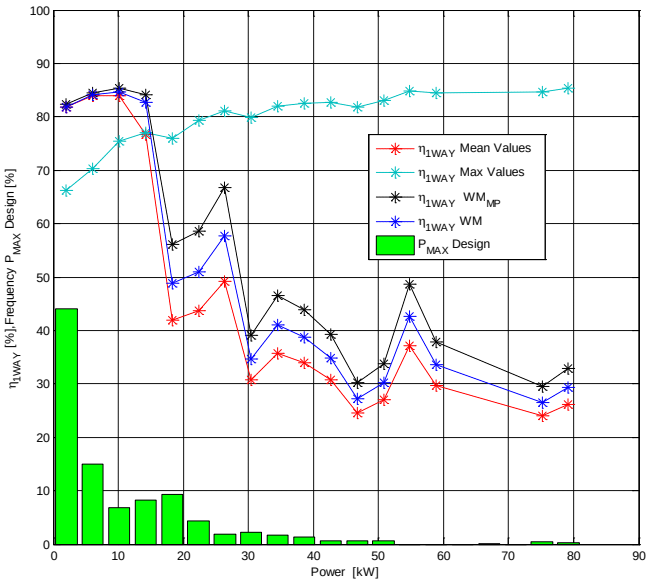

Fig 5.253: 1way-efficency designs comparison over Cycle-B

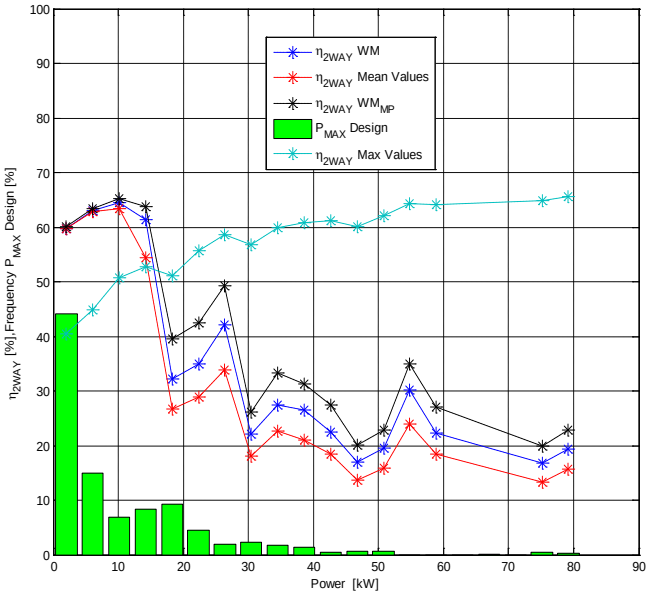

Fig 5.254: Round-trip efficiency designs comparison over Cycle-B

They perform at their best in the third event because of their moderate pump size. However, they become limited from that for events with larger power value. The efficiency profiles trends are very similar, but depending on the accumulator size it is possible to observe different capabilities to store and reuse energy. In fact, the highest efficiency values belong to the design based on the weighted average method with maximum power distribution, that has the biggest accumulator capability among them.

By observing Table 5.26, it is possible to observe that the design based on maximum values criteria has the lowest statistically representative round-trip efficiency although the very large accumulator and pump. This is due to the low energy conversion efficiency in correspondence of the most recurrent events, namely the first six cycle testing events. On the contrary, the other three designs bring to lighter systems and more performing on the aforementioned events. Among them, the design based on the weighted average calculation with maximum power distribution has the best statistically representative round-trip efficiency due to the slightly larger accumulator size.

5.5.3. Comparison of Designs Efficiency over the Tested Cycles

In the previous paragraph four hydraulic energy storage system designs have been tested on two real-world driving cycles. This paragraph focuses on the designs comparison over these cycles. Cycle-A has a driving pattern composition similar to the cycle used to size the systems, reported in Table 1. The Cycle-B driving pattern composition differs from the previous instead, and it is reported in Table 9. Because of their different patterns composition, testing events extracted by means of the statistical procedure explained in the simulation methodology show different energy and maximum power values. In Fig 5.83, the testing events are compared.

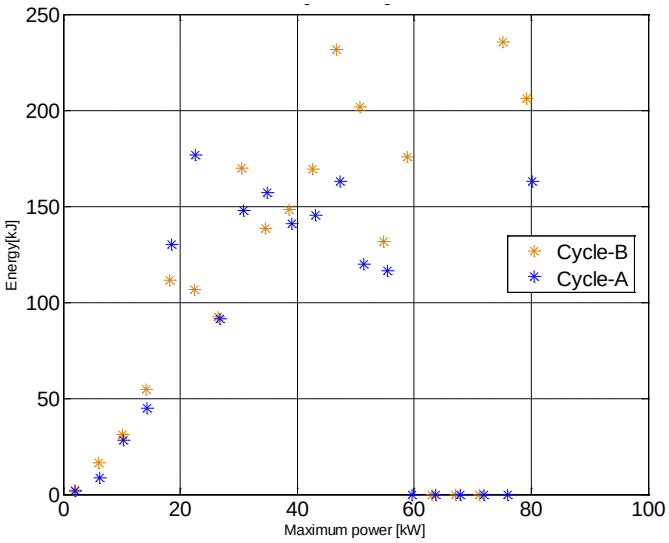

Fig 5.255: Cycle-A and Cycle-B testing events

By analyzing the figure above it is possible to notice how the different cycles composition influences the extracted testing events. It is important to notice that the

zero energy events correspond to maximum power distribution categories with no events: it means they are not considered. The first four events have very similar power and energy characteristics, while from the fifth it is possible to assist to different trends. Cycle-A, since the patterns composition is more heterogeneous present a big events dispersion and an maximum event energy below 200 kJ. Cycle-B events present a more linear trend and its last six events have larger energy values than Cycle-A corresponding events. From Table 14 and Table 25, it is possible to observe that for both the cycles the most recurrent events are the first six events. The first four events are characterized by similar power and energy values, while the fifth and sixth events show relevant energy differences depending on the cycle.

The aforementioned events are used in the one way efficiency and round-trip efficiency calculation. While the first one is related to the capability to store energy, the second one accounts for the losses of both the energy storing and releasing phase. Below, in Fig 5.84 and Fig 5.85, the designs round-trip efficiency on Cycle-A and on Cycle-B is shown, together with the cycle characteristic maximum power distribution.

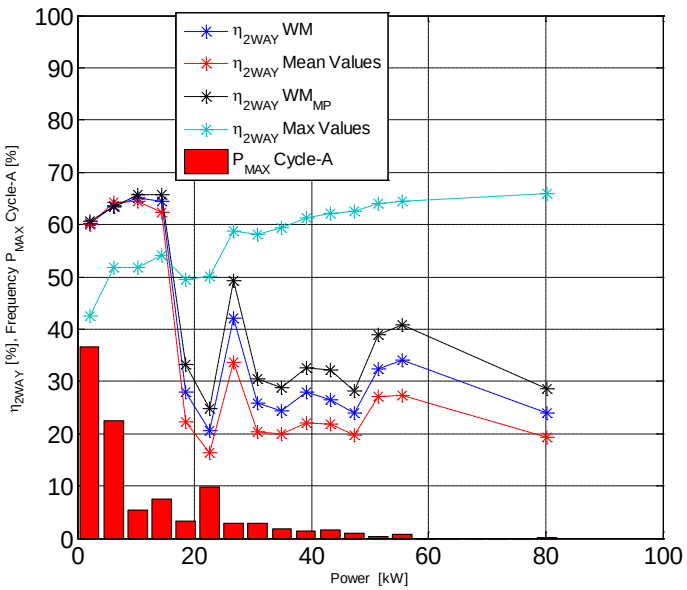

Fig 5.256: Round-trip efficiency designs comparison over Cycle-A

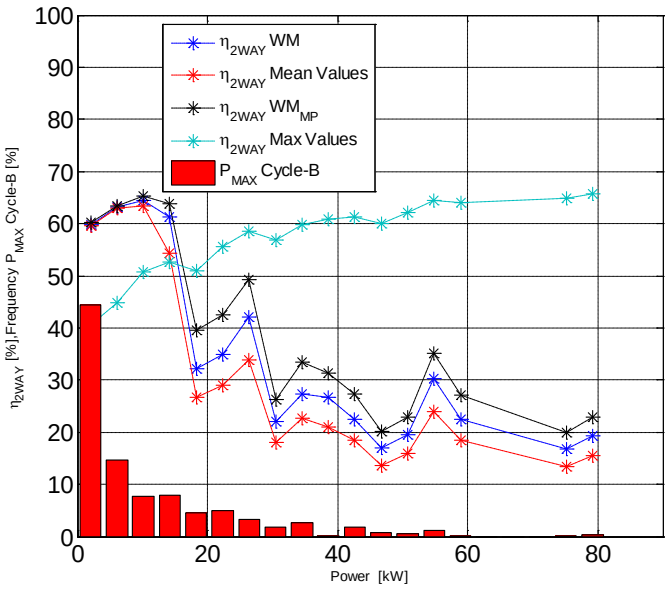

Fig 5.257: Round-trip efficiency designs comparison over Cycle-B

The figures above can be analyzed in order to determine hydraulic energy storage system designs performance over different driving cycles. In both the cycles, the design obtained using the maximum values criteria shows completely different performance respect to the other three designs. In fact, the maximum efficiency value is achieved in correspondence of the event characterized by the closest energy and power values to the design targets. Moreover, although the testing events in the two cycles are subject to energy dispersion, this design shows no considerable sensitivity. This is due to the large accumulator size. The other three designs are based on similar design targets values, that defines the power and energy range in which they perform at their best, showing no dependence on the testing driving cycle change. In both the cycles the efficiency drastically decreases as the testing events assume larger maximum power values. However, they present a different efficiency dispersion due to the testing events energy dispersion, shown in Fig 5.83. In fact, since these systems accumulator is smaller than the first considered design, the events energy variation in the cycles considerably affects the efficiency values. As example, it is possible to observe the sixth testing event for both the cycle. Its characteristic energy value in Cycle-A (almost 180 kJ) is larger than in Cycle-B (about 100kJ), so in the first cycle the designs efficiency is considerably lower than in the second one. A final evaluation can be made accounting for the statistically representative round-trip efficiency values reported in Table 5.27.

Table 5.81: Designs round-trip efficiency and attributes comparison over Cycle-A and Cycle-B

Designs Round-trip Efficiency and Attributes Comparison				
	Weighted average method	**Mean value method**	**Maximum values method**	**Weighted average method with maximum power distribution**
Cycle-A Round-trip efficiency[%]	53.83	51.10	49.31	54.18
Cycle-B Round-trip efficiency[%]	54.07	52.05	46.85	55.99
Total mass [kg]	62.41	56.64	353.70	67.33
Total volume[l]	22.17	19.46	148.79	24.64

Referring to Table 5.82, in both the cycles, the most performing system design is the that one based on the weighted average method with maximum power distribution. However, the results show that it performs at its best in Cycle-B. The reason is related to the cycles testing events. By observing the figures above, it is possible to notice that for this design, the efficiency drops in correspondence of the fifth and sixth event. In these events, the system has better efficiency in Cycle-B than in Cycle-A. The system is sized for a energy target value (71.80 kJ), but the events energy is superior to the accumulator capacity. In the fifth and sixth event, though the power values are very similar in Cycle-A and Cycle-B, the energy values are not. In Cycle-A the energy values (130.33 kJ and 176.95 kJ) are larger than in Cycle-B (111.59kJ and 106.39 kJ). Hence the efficiencies for these events are smaller in Cycle-A. These two efficiencies values make the main difference in order to get the statistically representative efficiency values, reported in Table 38. In fact, it is obtained by means of weighted average method with maximum power distribution and, in this calculation, the first six events are considerably important, since they are the most recurrent.

6. Conclusions

In this work, a methodology for the analysis of driving cycles by means of a statistical approach has been proposed as a key component of the design methodology for Alternative Energy Storage Systems (AESS), developed at The Ohio State University. In this context, the analysis methodology was developed with the aim of extracting information on the most relevant dynamic and energy-related variables of a driving schedule. The information were then processed in order to define statistically relevant data. These data were adopted by the AESS design methodology as design targets of the system sizing procedure.

The driving cycle analysis methodology has been applied to a cycle representing a typical commuting scenario, and four methods were used to retrieve cycle representative data. The energy storage system designs, obtained from them, were tested in simulation on two different driving cycles in order to evaluate their efficiency together with system weight and volume. The results show that three statistical methods yield system designs characterized by volume and mass values compatible with the primary target of the project, namely the realization of light and compact systems for mild-hybrid vehicles. On the contrary, the fourth statistical method yields a oversized system with respect to the most significant use on the cycles. This method represents the conventional ESS design methodology that targets the cycle worst-case scenario. Although the large components size, its statistically representative efficiency is the lowest on both the tested cycles, because this design criteria does not account for the actual recurrence of that scenario. The efficiency results of the three aforementioned designs on the two cycles, show that the identification of the typical vehicle use allows to properly size the energy storage system components, making them work in correspondence of good efficiency operating points during the cycle most recurrent events.

The results show that from the integration of the developed driving cycle analysis methodology with the Alternative Energy Storage System design methodology, an effective tool, Matlab based, has been defined. It allows to automate the driving data statistical analysis and synthesis process. Moreover it allows to evaluate in simulation the system designs over testing driving cycles. The simulation results show that this design procedure is more suitable for AESS, in terms of efficiency results and design attributes, than the conventional design methodology for ESS. The cycle analysis methodology based on the statistical approach has been proven to be valid, since it allows to properly size the AESS components starting from the vehicle use definition.

The proposed driving cycle analysis methodology is a good starting point for future work. Improvements can concern the definition of alternative methods to extract statistically relevant information from the driving cycle for the design procedure. Moreover, it is possible to define alternative representative commuting scenarios for system sizing in order to evaluate which design has the best performance on several testing cycles.

Bibliography

[1] Guzzella, L., & Sciaretta, A. (2007). Vehicle Propulsion Systems-Introduction to Modeling and Optimization.

[2] Beachley, N. H. (1978). Improving Vehicle Fuel Economy with Hybrid Power Systems.

[3] Li, Q. (1998). Development and refinement of a hybrid electric vehicle simulator and its application in design space exploration.

[4] Burke M, Briffet G, Fuller J, Heumann H, Newall J; "Powertrain efficiency optimization of the Torotrak Infinitely Variable Transmission (IVT)". SAE 2002 World Congress, Detroit, USA.

[5] CARS-UK. (s.d.). Jaguar XF Flywheel Hybrid. From CARS UK: http://www.carsuk.net/jaguar-xf-flywheel-hybrid/

[6] EPA. (s.d.). Hydraulic Hybrid - The Most Efficient Lowest Cost Hybrids. From U.S EPA: http://www.epa.gov/oms/technology/420f06043.htm

[7] Joseph E. Shigley, C. R. Mechanical engineering design.

[8] Beachley, N. H. (s.d.). Minimization of Energy Storage Requirements for Internal Combustion Engine Hybrid vehicles.

[9] z. Rahman, K. L. (1999). A Study of Design Issues on Electrically Peaking Hybrid Electric Vehicle for Diverse Urban Driving Patterns.

[10] Tony Markel, M. Z. (s.d.). Energy Storage System Requirements for Hybrid Fuel Cell Vehicles.

[11] Yimin Gao, L. C. (s.d.). Design and Control Principles of Hybrid Braking.

[12] J. Kwon, J. K. (s.d.). Impact of Drive Cycles on PHEV Component Requirements.

[13] D. Cross, J. H. (s.d.). High Speed Flywheel Based Hybrid Systems For Low Carbon Vehicles.

[14] Yazhou, J. (s.d.). Fatigue load and reliability design of machine-tool components.

[15] Doebelin, E. (s.d.). System Dynamics.

[16] A. Pourmovahed, N. B. (s.d.). Modeling of a Hydraulic Energy Regeneration System – Part I: Analytical Treatment.

[17] Y. J. Kim, Z. F. (s.d.). Simulation Study of a Series Hydraulic Hybrid Propulsion System for a Light Truck.

[18] Y. J. Kim, Z. F. (s.d.). Series Hydraulic Hybrid Propulsion for a Light Truck – Optimizing the Thermostatic Power Management.

[19] P.Y. Li, J. V. (s.d.). Open Accumulator Concept for Compact Fluid Power Energy Storage.

[20] Toulson, E. (s.d.). Evaluation of a Hybrid Hydraulic Launch Assist System for use in Small Road Vehicles.

[21] Z. Sun, H.-C. M. (s.d.). Hydraulic Assist Power System.

[22] Kwon, J., Kim, J., Fallas, E., Pagerit, S., & Rousseau, A. (2008). Impact of Drive Cycles on PHEV Component Requirements.

[23] Gong, Q., Midlam-Mohler, S., Marano, V., & Rizzoni, G. (2009). Statistical Analysis Based PHEV Fleet Data Study.

[24] Guzzella, L., & Sciaretta, A. (2007). Vehicle Propulsion Systems-Introduction to Modeling and Optimization.

[25] Hucho, W. (1998). Aerodynamics of road vehicles.

[26] Markel, T., Zolot, M., Wipke, K. B., & Pesaran, A. A. (s.d.). Energy Storage System Requirements for Hybrid Fuel Cell Vehicles.

[27] Rexroth. (s.d.). HAB Series 5X Bladder Accumulator Data Sheet.

[28] Mobley, R. K. (1999). Fluid Power Dynamics.

[29] Parker, H. (2010). P1/PD Series Medium Duty Axial Piston Pumps. Catalog HY28-2665-01/P1/EN.